AN ABSTRACT OF THE DISSERTATION OF

Curtis B. Edson for the degree of Doctor of Philosophy in Forest Resources presented on April 26, 2011.
Title: Light Detection and Ranging (LiDAR): What We Can and Cannot See in the Forest for the Trees.

Abstract approved:

_____

Michael G. Wing

Recently concerns over anthropogenic carbon pollution have received increased global attention and research in forest biomass and carbon sequestration has gained momentum. Light Detection and Ranging (LiDAR) remote sensing has in the last decade demonstrated forest measurement and biomass estimation potential. The project objective was to compare LiDAR forest biomass estimates to traditional field biomass estimates in a conifer predominant forest located in the Pacific Northwest region of the United States.

Chapter 2 of this dissertation investigated mapping-grade GPS accuracy in determining tree locations. Results indicated that post processing of coded pseudorange satellite signals is the most accurate of those we tested for GPS surveying under a conifer dominant forest canopy. Chapter 3 compared LiDAR, total station, and GPS receiver discrete point elevations and DEMs across a range of forest settings. Average total station plot elevation differences ranged from -0.06 m (SD 0.40) to -0.59 m (SD 0.23) indicating that LiDAR elevations are higher than actual elevations. Average plot GPS

elevation differences ranged from 0.24 (SD 1.55) to 2.82 m (SD 4.58), and from 0.27 (SD 2.33) to 2.69 m (SD 5.06) for LiDAR DEMs.

Chapter 4 assessed LiDAR's ability to measure three-dimensional forest structure and estimate biomass using single stem (trees and shrubs) remote sensing. The LiDAR data tree extraction computer software programs FUSION, TreeVaW, and watershed segmentation were compared. LiDAR spatial accuracy assessment resulted in overall average error and standard deviation (SD) for FUSION, TreeVaW, and watershed segmentation of 2.05 m (SD 1.67 m), 2.19 m (SD 1.83 m), and 2.31 m (SD 1.94 m) respectively. Overall average LiDAR tree height error and standard deviations (SD) respectively for FUSION, TreeVaW and watershed segmentation were -0.09 m (SD 2.43 m), 0.28 m (SD 1.86 m), and 0.22 m (2.45 m) in even-age, uneven-age, and old growth plots combined; and for one clearcut plot 0.56 m (SD 1.07 m), 0.28 m (SD 1.69 m), and 1.17 m (SD 0.68 m), respectively. Biomass comparisons included feature totals per plot, mean biomass per feature by plot, and total biomass by plot for each extraction method. Overall LiDAR biomass estimations resulted in FUSION and TreeVaW underestimating by 25 and 31% respectively, and watershed segmentation overestimating by approximately 10%. LiDAR biomass underestimation occurred in 66% and overestimation occurred in 34% of the plot comparisons.

Light Detection and Ranging (LiDAR): What We Can and Cannot See in the Forest for the Trees

by
Curtis B. Edson

A DISSERTATION

submitted to

Oregon State University

in partial fulfillment of
the requirements for the
degree of

Doctor of Philosophy

Presented April 26, 2011
Commencement June 2011

Doctor of Philosophy dissertation of Curtis B. Edson presented on April 26, 2011.

APPROVED:

_____

Major Professor, representing Forest Resources

_____

Head of the Department of Forest Engineering, Resources and Management

_____

Dean of the Graduate School

I understand that my dissertation will become part of the permanent collection of Oregon State University libraries. My signature below authorizes release of my dissertation to any reader upon request.

_____

Curtis B. Edson, Author

ACKNOWLEDGEMENTS

I knew that the pursuit of a doctoral dissertation would be a difficult task however it has been far more demanding than I imagined. Although the burden was on my shoulders, and in some days the weight felt like a herd of elephants, I owe a great deal of thanks to a select few; admiration of the many that have passed before me in similar challenges; and respect to those that have dealt with much greater burdens than this.

I must first acknowledge my brothers and sisters in arms that have dealt with and are dealing with far greater difficulties than a doctoral dissertation. Whenever I had a difficult day in this arduous pursuit, I could always think of my fellow service members and realize that things could be far more difficult. From my drill sergeants through my most recent commanders in the U.S. Army organization I owe a great deal. The confidence that I have built has helped complete this and many difficult tasks. To Dr. John Brockhaus and COL Gene Palka I owe a great deal of gratitude for having the confidence in me to provide for this opportunity.

Thanks to my father Donald Curtis Edson (rest his soul), whom in one perspective I curse and in another love for instilling in me the importance of an education. Life may have been simpler had he not instilled the passion for learning, but it surely would have been less fulfilling. He has missed so much…but I know he would be proud.

I owe the greatest thanks to my wife Katie and sons Forrest, Josh, and Spencer for supporting me in this endeavor. My wife had a choice and my boys have not. Thanks for sticking with me. Although this degree will count as a success in my career

aspirations, one of my early goals in life was to be a good father and husband. I have failed miserably at this goal over the last couple of years. I hope to make it up.

I have been motivated by two small groups that have come in contact with me over the years on two ends of the spectrum. One small group has loved me and the other has doubted me for my faults. To both groups I owe a great deal of thanks. The positive few, most of whom know who they are, gave me the confidence and aspiration to achieve my many successes in life. To the negative few, I have been motivated and inspired to prove you wrong.

Finally, thanks to my supporters at Oregon State University. Thanks to my major professor Dr. Michael Wing for pulling my application out of the illusory cylindrical file and inviting me to study in a field for which he is passionate. It has been difficult for each of us, and in the end the mutual support has paid off. Professor Robert Schultz is the epitome of a career educator. I am sincerely grateful for his passion in the geomatics discipline, care for his students, and willingness to share his knowledge, expertise and equipment. I am proud to consider him one of my few mentors. I am thankful for the willingness of Anne Nolin, Dave Shaw and Lisa Ganio to serve on my multidisciplinary committee. Special thanks to the field crew that helped me collect an amazingly large field database. The “mules and goats” that trekked through the woods with me and in support of this research are David McClung, Thomas Fisher, Stephen LeDuc, Travis Lebow, Kate Faulkner, Melissa Stone, Claire Rogan, Alec Mac, and Jeremy Mitchell. Finally, thanks to Michael Reisner and his family and Josh Baur for the mutual support in getting through this process.

TABLE OF CONTENTS

TABLE OF CONTENTS (Continued)

Page

TABLE OF CONTENTS (Continued)

Page

TABLE OF CONTENTS (Continued)

Page

LIST OF FIGURES

Figure Page

LIST OF TABLES

LIST OF TABLES (Continued)

Table Page

LIST OF TABLES(Continued)

Table Page

Light Detection and Ranging (LiDAR):
What We Can and Cannot See in the Forest for the Trees

CHAPTER 1 – INTRODUCTION

The two main goals of this doctoral endeavor were to further prepare to teach geospatial information sciences and to contribute scientifically to the field of forest engineering and forest resource management.

LiDAR, also known as airborne laser scanning, is a state of the art remote sensing tool widely used for acquiring topographic data and generating digital elevation models. Research in topographic mapping with LiDAR began in the early 1980s (Krabill et al. 1984) with the first commercial LiDAR sensor fielded in 1993 (NOAA 2010). In the last ten years LiDAR has seen increased interest in many activities including forest management, urban planning, natural resource modeling, ice sheet mapping, road design (Lim et al. 2003; Aguilar and Mills 2008), and others. Forest terrain mapping (Reutebuch et al. 2003) and forest inventory (Reutebuch et al. 2005) are some of the primary LiDAR applications within natural resources.

As they are dominant features in the global carbon budget, forests perform a critical role in the terrestrial carbon cycle (Hoen and Solberg 1994; Dong et al. 2003; Hudiburg et al. 2009). Forests are carbon sinks and their net ecosystem production (NEP), which is the net forest carbon balance, is positive. In general forest CO_2 uptake by assimilation is greater than CO_2 losses through vegetation and soil respiration (Hoen and Solberg 1994; Luyssaert et al. 2008). Forests contain the greatest amount of biomass and generally occur in temperate, boreal, and tropical regions (Lefsky et al.

1999a; Lefsky et al. 2005b). They are estimated to account for up to 80% of the earth's total biomass (Dixon et al. 1994) in spanning 3952 million ha of land, but cover only 30% of the land surface (Barker et al. 2007).

Due to the scope of global biomass and its constant state of flux, it is infeasible to measure biomass in its entirety and to maintain a current database (Law et al. 2006). The United States Department of Agriculture (USDA) Forest Service uses the Forest Inventory and Analysis program (FIA) to assess wood resources, monitor forest resource sustainability, and support management decisions that lead to desired forest conditions (Bechtold and Patterson 2005). The inventory is conducted in subsections on a by state basis in periodic increments taking approximately 10-12 years to complete. Since 2001, portions are completed on an annual basis. State and private forest land managers make use of similar methods for inventorying and analyzing forest resources. In some areas, FIA plots cross over onto considerable areas of state and private forest land. The status of the nation's forests and several long-term, chronic forest issues including increasing global wood demand, decreasing forest productivity, land fragmentation, and the impact of growing global populations on resources all strongly influence the FIA program (Smith 2002). Meeting the constrained resource challenges through accurate and reliable resource inventory information is a FIA priority and a difficult goal to accomplish. The FIA has faced obstacles from a variety of circumstances, including sampling system reliability, inventory measurement cycle, and uncertain funding (AFPA 2001; McRoberts et al.

2005; Grotefendt and Schreuder 2006). Remote sensing technology has the potential to strengthening the FIA through rapid data collection across broad landscapes.

One potential method for strengthening the FIA would be to apply new geo-positioning technology (i.e., global positioning system and inertial navigation units) that have made Light Detection and Ranging (LiDAR) applications practical for forest inventory and monitoring. LiDAR measurements are collected remotely by laser pulses from an airborne sensor. LiDAR provide information about landscape feature locations and measurements, and also include a spectral reflectance that results in a near-infrared image. LiDAR data make it possible to remotely measure individual trees and to provide highly detailed information about landscape cover and topography. Previous research suggests that LiDAR imagery could be used to replace field data collection of timber inventory and ecosystem data particularly for capturing individual tree measurements (Andersen et al. 2005; Reutebuch et al. 2005). Renslow et al. (2000) found a 0.9 m root-mean-square-error (RMSE) for horizontal accuracies of individual trees within various forested sites. Lim et al. (2001) reported that 39% of their field-measured tree positions fell within 0.5 m of LiDAR-derived horizontal measurements. Dorren et al. (2006) found a difference between 0.4 and 3.5 m in horizontal error of 30 tree positions between LiDAR-derived and GPS positions. In addition, previous studies have investigated vertical accuracies of tree heights with LiDAR. Dorren et al. (2006) found that LiDAR-derived heights of 30 trees differed from field-measured heights by a range of -4.8 m to 5.2 m. Farid et al. (2006)

determined differences between 0.1 and 2.0 m between LiDAR-derived and field-based tree height measurements.

Forester land managers are responsible for regeneration activities and must ensure that wood resources are being efficiently replenished following forest operations. In addition to accounting for numerous environmental factors that influence regeneration success, economic factors must also be considered in support of inventory and monitoring activities. LiDAR has demonstrated at least partial utility for measuring forest topography and mature conifer stands. Detailed assessments of stand characteristics, growth, and biomass could be provided for entire forests if LiDAR can accurately assess tree regeneration. In addition, LIDAR can offer significant time savings in creating inventory databases, lead to less reliance on ground-based methods, and lead to safer monitoring approaches. The implementation of LiDAR technology for forest regeneration inventory and analysis can be applied to help meet the increasing wood needs of the U.S. and global economies.

Background

LiDAR forest inventory methods may be broken into two broad categories: area based methods done at the plot and stand level, and individual tree based methods (Hyyppa et al. 2004). An example of area based methods are height percentiles from canopy height distributions, which are used for regression or non-parametric models, e.g. ranks, to estimate mean tree height, basal area, and volume (Hyyppa et al. 2008). Individual tree approaches locate individual tree canopy, measure height, and use individual tree based statistics to determine the volume estimates (Bortolot and Wynne

2005). The two primary types of LiDAR systems used in previous studies to estimate forest inventory are large footprint waveform (Means et al. 1999; Lefsky et al. 1999a; Lefsky et al. 1999b; Lefsky et al. 2002), which collect and record a continuous wave of intensity data (Bortolot and Wynne 2005), and small footprint discrete return which records the height and intensity of strong individual laser return signals (Bortolot and Wynne 2005). Once the LiDAR is collected the challenge then becomes to detect and delineate tree information from the data. Three sources of data have historically been used to extract tree feature data (Hyyppa et al. 2008) including the raw point data, known as point clouds (Reutebuch et al. 2005; Andersen et al. 2006; McGaughey 2007); a raster canopy height model (CHM) (Hyyppa et al. 2001; Popescu et al. 2002; Popescu 2010), derived from a digital surface model (DSM) interpolated from individual point returns from trees similar to a digital elevation model (DEM) interpolated from ground returns; and a hybrid approach derived from combining LiDAR data with either airborne or space-borne imagery (Brandtberg et al. 2003; Popescu et al. 2004; Chen 2007; Lucas et al. 2008). Tree feature extraction from LiDAR data is either accomplished manually or through automated means. One example of manual extraction is the United States Department of Agriculture Forest Service (USDA Forest Service) software program FUSION (McGaughey 2007), which uses LiDAR point clouds to visualize and manually extract tree data. Various automated methods have been developed to delineate and measure individual trees from remotely sensed data including feature matching, object based methods (Falkowski et al. 2008), local maximum filters (Brandtberg et al. 2003), variable

window filters (Popescu et al. 2002; Popescu et al. 2004; Popescu and Wynne 2004), image segmentation (Hyyppa et al. 2001; Leckie et al. 2003; Chen 2007), and spatial wavelet analysis (Falkowski et al. 2008).

Objectives Overview

Few studies have characterized large enough amounts of the entire forest canopy structure to give a good depiction of LiDAR detection and delineation accuracy (Brandtberg et al. 2003). The prevalent research in LiDAR forest measurement has focused on the canopy including dominant and co-dominant trees. This has been primarily based on the hypothesis that the canopy would eclipse understory vegetation and prevent airborne laser pulses from penetrating to lower vegetation and returning enough strong signals to differentiate smaller trees and shrubs. Other aforementioned studies have shown that LiDAR can successfully measure relatively small samples of large trees in the dominant and co-dominant canopy. Following the premise that LiDAR successfully measures large trees but may miss much of the understory vegetation, the primary objective of this research is to further analyze the accuracy of LiDAR measurements in trees. Accuracy involves assessing not only successfully detected and delineated vegetation but also what is missed by LiDAR in order to determine what degree LiDAR can estimate temperate coniferous forest biomass in the Pacific Northwest. In other words, we seek not only to further research what trees LiDAR can “see”, but also determine “what we cannot see in the forest with LiDAR for the trees”. The two key components to achieve this objective include how well LiDAR data can be used to find and delineate individual trees and shrubs throughout

the three-dimensional forest structure, and the accuracy of vegetation height measurements. As suggested by these objectives, we were interested in a holistic approach where knowing not only the accuracy of tree measurements in the primary, dominant canopy structure, but also the accuracy of measuring vegetation in co-dominant, sub-canopy, and understory vegetation.

Methods Overview

To accomplish the study objectives, our study design focused on individual feature detection (trees and shrubs) in large area plots (one hectare) consisting of four randomly selected treatments including recently harvested (within 7 years of the LiDAR acquisition) clearcut, even age (under 20 years old), uneven age, and mature/old growth. The study site was in Oregon State University's McDonald-Dunn Research Forest located in the Oregon Coast Range. LiDAR has been applied to measuring mature trees. The clearcut allowed us to evaluate how well LiDAR detects small vegetation without overstory obscuration, and rigorously inventory forest regeneration to assess seedling growth. The remaining treatments enabled the investigation of LiDAR performance in a variety of canopy opening scenarios and three dimensional structures. To sufficiently characterize the plots in detail, all trees ≥ 0.61 m tall? on clearcut plots and ≥ 1.0 m on all other plots, and shrubs ≥ 0.61 m tall and with a crown width of at least 1.0 m on all plots were measured. Measurements included species, height, crown width, stem diameter, and spatial location. Based on the scope of the study, we chose to measure feature locations using mapping-grade Global Positioning System (GPS) receivers to speed up data collection. Several plots

were redundantly sampled using a total station to test both the LiDAR and GPS spatial location accuracy under forest canopy.

The LiDAR was acquired during leaf-off conditions on April 2, 2008 by Watershed Sciences, Inc., Corvallis, Oregon using a Leica ALS50 Phase II scanner. Data provided included tiled raw .LAS files and with all returns, ground returns and a DEM for the entire McDonald-Dunn Forest.

Based on the many computer software programs and algorithms designed for LiDAR forest measurement applications, we compared three commonly applied software methods to delineate and measure the forest in our study including USDA Forest Service FUSION (McGaughey 2007), TreeVaW (Popescu 2010), and inverse watershed segmentation applied using ESRI software ArcGIS version 9.3. FUSION analyzes LiDAR point clouds. TreeVaW and watershed segmentation analyze CHMs.

The end state of this research is to equate the accuracy of forest biomass estimations using LiDAR data compared to forest biomass estimations made using field-measured data. There are three components to comparing the LiDAR data to the field-measured data in this study. Since we are basing our biomass estimations on individual feature locations of trees and shrubs, the accurate location of each feature must be known so that we can ensure that LiDAR features are coincident with field-measured trees and accurately compared. Thus Chapter 2? is an evaluation of GPS spatial accuracy under forest canopy. Next LiDAR tree height accuracy must be assessed as it relates to regression biomass estimations on tree height. Tree and shrub heights are based on the height above ground. In LiDAR feature height measurements,

the ground elevation is based on a LiDAR derived digital elevation model (DEM), thus Chapter 3 evaluates the accuracy of the LiDAR DEM compared to DEMs derived from total station trigonometric leveling. Finally, the dissertation culminates in Chapter 4 by comparing three different LiDAR tree delineation computer software algorithms (FUSION, TreeVaW, and watershed segmentation) in their ability to detect, delineate, and measure forest vegetation. Using the three different tree delineation software algorithm results, LiDAR biomass estimation is calculated using allometric equations by plot and compared to field-measured biomass estimations.

Literature Cited

AFPA (2001). Status report on the US Forest Service Forest Inventory and Analysis Program: Update to the findings of the 1998 Blue Ribbon Panel. Washington, D.C., American Forest and Paper Association.

Aguilar, F. J. and J. P. Mills (2008). Accuracy assessment of LiDAR-derived digital elevation models. The Photogrammetric Record 23(122): 148-169.

Andersen, H.-E., R. J. McGaughey and S. E. Reutebuch (2005). Estimating forest canopy fuel parameters using LiDAR data. Remote Sensing of Environment 94(4): 441-449.

Andersen, H.-E., S. E. Reutebuch and R. J. McGaughey (2006). A rigorous assessment of tree height measurements obtained using airborne LiDAR and conventional field methods. Canadian Journal of Remote Sensing 32(5): 355-366.

Barker, T., I. Bashmakov, L. Bernstein, J. E. Bogner, P. Bosch, D. Rutu, D. Ogunlade, B. S. Fisher, S. Gupta, K. Halsnaes, B. Heij, S. Kahn, S. Kobayashi, M. D. Levine, D. L. Martino, O. Masera, B. Metz, L. Meyer, G.-J. Nabuurs, A. Najam, N. Nebojsa, H.-H. Rogner, J. Roy, J. Sathaye, R. Schock, P. Shukla, R. E. H. Sims, P. Smith, D. A. Tirpak, D. Urge-Vorsatz and D. Zhou (2007). Technical summary. in: Climate Change 2007: Mitigation. Contribution of Working Group III to the Fourth Assessment
Report of the Intergovernmental Panel on Climate Change. Cambridge, United Kingdom and New York, NY, USA.

Bechtold, W. A. and P. L. Patterson (2005). The enhanced Forest Inventory and Analysis program, national sampling design and estimation procedures. General Technical Report. Ashville, NC, U.S. Department of Agriculture, Forest Service, Southern Research Station. SRS-80**:** 85.

Bortolot, Z. J. and R. H. Wynne (2005). Estimating forest biomass using small footprint LiDAR data: An individual tree-based approach that incorporates training data. ISPRS Journal of Photogrammetry and Remote Sensing 59(6): 342-360.

Brandtberg, T., T. A. Warner, R. E. Landenberger and J. B. McGraw (2003). Detection and analysis of individual leaf-off tree crowns in small footprint, high sampling density lidar data from the eastern deciduous forest in North America. Remote Sensing of Environment 85(3): 290-303.

Chen, Q. (2007). Airborne LiDAR data processing and information extraction. Photogrammetric Engineering and Remote Sensing 73: 175-185.

Dixon, R. K., R. A. Houghton, A. M. Solomon, M. C. Trexler and J. Wisniewski (1994). Carbon pools and flux of global forest ecosystems. Science 263: 185-190.

Dong, J., R. K. Kaufmann, R. B. Myneni, C. J. Tucker, P. E. Kauppi, J. Liski, W. Buermann, V. Alexeyev and M. K. Hughes (2003). Remote sensing estimates of boreal and temperate forest woody biomass: carbon pools, sources, and sinks. Remote Sensing of Environment 84(3): 393-410.

Dorren, L., B. Maier and F. Berger (2006). Assessing protection forest structure with Airborne Laser Scanning in steep mountainous terrain. Proceedings from Workshop on 3D Remote Sensing in Forestry, Vienna, Austria.

Falkowski, M. J., A. M. S. Smith, P. E. Gessler, A. T. Hudak, L. A. Vierling and J. S. Evans (2008). The influence of conifer forest canopy cover on the accuracy of two individual tree measurement algorithms using LiDAR data. Canadian Journal of Remote Sensing 34(Suppl. 2): S1-S13.

Farid, A., D. C. Goodrich and S. Sorooshian (2006). Using airborne LiDAR to discern age classes of cottonwood trees in a riparian area. Western Journal of Applied Forestry 21(3): 149-158.

Grotefendt, R. A. and H. T. Schreuder (2006). A new FIA-type srategic inventory (NFI). Monitoring Science and Technology Symposium: Unifying Knowledge for Sustainability in the Western Hemisphere, Fort Collins, CO, U.S. Department of Agriculture, Forest Service, Rocky Mountain Research Station.

Hoen, H. F. and B. Solberg (1994). Potential and economic efficiency of carbon sequestration in forest biomass through silvicultural management. Forest Science 40: 429-451.

Hudiburg, T., B. Law, D. P. Turner, J. Campbell, D. Donato and M. Duane (2009). Carbon dynamics of Oregon and Northern California forests and potential land-based carbon storage. Ecological Applications 19(1): 163-180.

Hyyppa, J., H. Hyyppa, D. Leckie, F. Gougeon, X. Yu and M. Maltamo (2008). Review of methods of small-footprint Airborne Laser Scanning for extracting forest inventory data in boreal forests. International Journal of Remote Sensing 29(5): 1339-1366.

Hyyppa, J., H. Hyyppa, P. Litkey, X. Yu, H. Haggren, P. Ronnholm, U. Pyysalo, J. Pitkanen and M. Maltamo (2004). Algorithms and methods of Airborne Laser

Scanning for forest measurements. International Archives of Photogrammetry, Remote Sensing and Spatial Information Sciences XXXVI(8/W2): 82-89.

Hyyppa, J., O. Kelle, M. Lehikoinen and M. Inkinen (2001). A segmentation-based method to retrieve stem volume estimates from 3-D tree height models produced by laser scanners. Geoscience and Remote Sensing, IEEE Transactions on 39(5): 969-975.

Krabill, W. B., J. G. Collins, L. E. Link, R. N. Swift and M. L. Butler (1984). Airborne laser topographic mapping results. Photogrammetric Engineering and Remote Sensing 50: 685-694.

Law, B., D. Turner, J. Campbell, M. Lefsky, M. Guzy, O. Sun, S. Tuyl and W. Cohen (2006). Carbon fluxes across regions: observationoal constraints at multiple scales. Scaling and uncertainty analysis in ecology J. Wu, K. B. Jones, H. Li and O. L. Loucks, Springer Netherlands**:** 167-190.

Leckie, D., F. Gougeon, D. Hill, R. Quinn, L. Armstrong and R. Shreenan (2003). Combined high-density LiDAR and multispectral imagery for individual tree crown analysis. Canadian Journal of Remote Sensing 29(5): 633-649.

Lefsky, M. A., W. B. Cohen, S. A. Acker, G. G. Parker, T. A. Spies and D. Harding (1999a). LiDAR remote sensing of the canopy structure and biophysical properties of Douglas-fir western hemlock forests. Remote Sensing of Environment 70(3): 339-361.

Lefsky, M. A., W. B. Cohen, G. G. Parker and D. J. Harding (2002). LiDAR remote sensing for ecosystem studies. BioScience 52(1): 19-30.

Lefsky, M. A., D. Harding, W. B. Cohen, G. Parker and H. H. Shugart (1999b). Surface LiDAR remote sensing of basal area and biomass in deciduous forests of Eastern Maryland, USA. Remote Sensing of Environment 67(1): 83-98.

Lefsky, M. A., A. T. Hudak, W. B. Cohen and S. A. Acker (2005b). Geographic variability in lidar predictions of forest stand structure in the Pacific Northwest. Remote Sensing of Environment 95(4): 532-548.

Lim, K., P. Treitz, A. Groot and B. St.-Onge (2001). Estimation of individual tree heights using LiDAR remote sensing. Proceedings of the 23rd Annual Canadian Symposium on Remote Sensing. Quebec, Canada, CASI**:** 243-250.

Lim, K., P. Treitz, M. Wulder, B. St-Onge and M. Flood (2003). LiDAR remote sensing of forest structure. Progress in Physical Geography 27(1): 88-106.

Lucas, R. M., A. C. Lee and P. J. Bunting (2008). Retrieving forest biomass through integration of CASI and LiDAR data. International Journal of Remote Sensing 29(5): 1553-1577.

Luyssaert, S., E. D. Schulze, A. Borner, A. Knohl, D. Hessenmoller, B. E. Law, P. Ciais and J. Grace (2008). Old-growth forests as global carbon sinks. Nature 455(7210): 213-215.

McGaughey, R. (2007). FUSION/LDV: Software for LIDAR data analysis and visualization, United States Department of Agriculture Forest Service, Pacific Northwest Research Station**:** Users Manual.

McRoberts, R. E., W. A. Bechtold, P. L. Patterson, C. T. Scott and G. A. Reams (2005). The enhanced forest inventory and analysis program of the USDA Forest Service: historical perspective and announcement of statistical documentation. Journal of Forestry 103(6): 304-308.

Means, J. E., S. A. Acker, D. J. Harding, J. B. Blair, M. A. Lefsky, W. B. Cohen, M. E. Harmon and W. A. McKee (1999). Use of large-footprint Scanning Airborne LiDAR to estimate forest stand characteristics in the Western Cascades of Oregon. Remote Sensing of Environment 67(3): 298-308.

NOAA. (2010). Remote sensing for coastal management. Retrieved May 1, 2010, from http://www.csc.noaa.gov/crs/rs_apps/sensors/lidar.htm.

Popescu, S. C. (2010). TreeVaW, tree variable window. Retrieved December 11, 2010, from http://ssl.tamu.edu/personnel/s_popescu/TreeVaW/download.htm.

Popescu, S. C., H. W. Randolph and A. S. John (2004). Fusion of small-footprint LiDAR and multispectral data to estimate plot- level volume and biomass in deciduous and pine forests in Virginia, USA. Forest Science 50: 551-565.

Popescu, S. C. and R. H. Wynne (2004). Seeing the trees in the forest: using LiDAR and multispectral data fusion with local filtering and variable window size for estimating tree height. Photogrammetric Engineering and Remote Sensing 70(5): 589-604.

Popescu, S. C., R. H. Wynne and R. F. Nelson (2002). Estimating plot-level tree heights with LiDAR: local filtering with a canopy-height based variable window size. Computers and Electronics in Agriculture 37: 71-95.

Renslow, M., P. Greenfield and T. Guay (2000). Evaluation of multi-return LiDAR for forestry applications, US Department of Agriculture, Forest Service-Engineering, Remote Sensing Applications Center. RSAC-2060/4180-LSP-001-RPT1.

Reutebuch, S. E., H.-E. Andersen and R. J. McGaughey (2005). Light Detection and Ranging (LiDAR): an emerging tool for multiple resource inventory. Journal of Forestry 103: 286-292.

Reutebuch, S. E., R. J. McGaughey, H.-E. Andersen and W. W. Carson (2003). Accuracy of a high-resolution LiDAR terrain model under a conifer forest canopy. Canadian Journal of Remote Sensing 29(5): 527-535.

Smith, W. B. (2002). Forest inventory and analysis: a national inventory and monitoring program. Environmental Pollution 116: 233-242.

Light Detection and Ranging (LiDAR):
What We Can and Cannot See in the Forest for the Trees

CHAPTER 2 – TOTAL STATION AND GPS HORIZONTAL COORDINATE DIFFERENCES UNDER FOREST CANOPY

Curtis B. Edson

Michael G. Wing

Submitted to Forest Science

Abstract

We evaluated the accuracy of mapping-grade GPS receivers in determining tree locations within two temperate conifer forest stands representing moderate and extreme terrain slope conditions. GPS receiver measurement accuracy was compared based on autonomous GPS measurements, post processing of code satellite signals, and post processing of both carrier and code based signals. The locations of 337 trees within the two stands were measured using a digital total station and subsequent tree measurements were collected by a mapping-grade GPS receiver. Average GPS receiver tree position horizontal error was least for the code only differential corrections of tree positions (2.57 m and 2.70 m in the two plots), higher for autonomous measurements (2.86 m and 3.28 m), and greatest for differential corrections that applied both carrier and code signals (2.94 m and 3.46 m). The code only differential corrections for tree locations were significantly different, or nearly statistically significant, from the autonomous measurements as well as the carrier and code corrections. Based on these results, it appears that post processing of coded pseudorange satellite signals is the most accurate and recommended method among those that we tested for mapping-grade GPS surveying of tree locations under a conifer dominant forest canopy.

Introduction

The global positioning system (GPS) has become an effective and reliable tool for resource managers and surveyors alike for obtaining accurate geographic coordinates. There is a growing reliance on GPS in forest management measurement applications

ranging from timber harvesting to fighting fires (Zheng et al. 2005; Zengin and Yeşil 2006). Recent studies have researched the accuracy of GPS in a forest setting (Deckert and Bolstad 1996; Sigrist et al. 1999; Yoshimura and Hasegawa 2003; Johnson and Barton 2004; Bolstad et al. 2005; Wing et al. 2005; Zheng et al. 2005; Wing and Karsky 2006; Zengin and Yeşil 2006; Wing et al. 2008; Andersen et al. 2009) These studies use varying methods, but all demonstrate that GPS is capable of determining geographic positions under canopy with varying degrees of accuracy depending on conditions and equipment used.

To obtain the highest accuracies (within a centimeter of true position) survey grade receivers are used, however this equipment requires a generally unobstructed path between the receiver and the satellite. To obtain highly accurate positions, the GPS receiver must also remain stationary and collect data positions ranging from 20 minutes to up to two hours for rapid-static, or at least four hours for reliable static solutions. In general, the longer the GPS is stationary, the higher the accuracy. These requirements make survey grade GPS unattractive or unusable to foresters, and in many cases foresters do not require the accuracy of a high order survey provided by high precision measurement tools, such as a total station or survey-grade GPS (Bolstad et al. 2005). In addition, the expense involved in purchasing and operating high precision digital measurement tools may not be justified by accuracy requirements (Sigrist et al. 1999; Johnson and Barton 2004; Wing et al. 2005)

Many studies have concluded that mapping-grade GPS receivers are cost effective and sufficiently accurate for forestry applications. Mapping grade receivers achieve

accuracies that are appropriate for many natural resource management applications where allowable error can be as high as 10 meters (Deckert and Bolstad 1996; Wing et al. 2008). Due to the varying nature and topography of forest conditions, however, GPS accuracies vary (Zheng et al. 2005).

Currently there is a great deal of interest and research in using LiDAR (Light Detection and Ranging) for forest measurement applications. Much of this research involves determining individual tree attributes. This requires that LiDAR determined locations of forest features reflect actual on the ground locations, a condition that can only be ensured by comparing LiDAR measurements to reference conditions. In terms of verifying tree stem locations, the two most common approaches are traditional survey methods using a total station or by GPS. We found that some studies mapped individual tree stems using a total station (Andersen et al. 2006; Kato et al. 2009), while most use a GPS to determine the coordinates of the plot center and then determine the specific stem location by direction and distance from the plot center (Means et al. 1999; Næsset et al. 2004; Popescu 2007; Falkowski et al. 2008).

In order to determine a location on the earth's surface, a GPS receiver must receive a signal from at least four GPS satellites at the same time (Van Sickle 2008). This procedure is relatively straight forward and quick in open terrain, but under forest canopy becomes unpredictable. To aid in predicting satellite availability, most GPS come with mission planning software to determine optimal collection times (Wing 2008), however unless one is collecting a small number of data points and/or is not constrained by time, optimal collection windows come seldom under forest canopy,

especially when steep topography is a consideration. Restricted view of the sky with satellites in constant motion is problematic and jeopardize GPS accuracy (Sigrist et al. 1999). There are several techniques for collecting GPS measurements in a forest setting, including real time kinematic (RTK), differential GPS (DGPS), or autonomous GPS with post processing. In addition, there are receiver configuration and measurement processing considerations that can affect GPS accuracies including horizon mask, position dilution of precision (PDOP), multipath, point averaging and occupation period, signal to noise ratio, and code versus carrier differential correction.

Studies have demonstrated that RTK GPS and DGPS techniques can improve horizontal accuracy (Deckert and Bolstad 1996; Yoshimura and Hasegawa 2003; Piedallu and Gegout 2005; Zengin and Yeşil 2006). The RTK method uses carrier phases and DGPS uses course acquisition (C/A) codes in processing satellite communications, and both broadcast real time corrections from the base station to the rover at the time of collection without the need for differential correction (Van Sickle 2008). The advantage to both is that they typically provide more accurate coordinates at the time of collection than what can be achieved with an autonomous GPS. These corrections are theoretically not the most accurate coordinates as they are based on the satellite broadcast ephemeris, which is where the space vehicle is estimated to be by the NAVSTAR control segment. The most accurate coordinates can be achieved by using post-processing differential correction using the satellite precise ephemeris (Karsky 2004). The precise ephemeris is based on the satellites actual orbital path, and

is not available until approximately 12 days after the time of acquisition (Van Sickle 2008).

Under normal circumstances if one has a GPS receiver that is both C/A code and carrier phase capable, using carrier phase may lead to more accurate measurements. Carrier phase is most often associated with GPS measurements using the carrier signals L1 (1575.42 MHz) and L2 (1227.60), whereas C/A codes are modulated onto the carrier wave. An oversimplified explanation is that in code processing both the satellite and the receiver produce the same unique C/A codes with a time stamp. Based on this time stamp, the receiver calculates the time between when the code was produced and when it is received. Using this calculated interval, the receiver can derive the distance from a satellites known location at the time the code was produced. Since this distance is calculated it is known as a pseudorange, as opposed to a range which is actually measured. On the other hand, the basis of the carrier phase measurement is reception of the unmodulated carrier wave from the satellite by the receiver, which produces a replica of the carrier wave and consists of three parts. First, as soon as a receiver and satellite codes are correlated, the satellite is sometimes referred to as locked-on. Once the code correlation occurs, the receiver begins tracking the difference in the *phase* of the wave. The phase difference between the two correlated waves indicates the initial time/distance measurement based on the fraction of the phase. Second, following code correlation, the receiver begins to compare synchronization with the satellite signal and counts the number of full phase *cycles* between the receiver and the satellite. Counts occur from initial lock-on with the

satellite and continue until the observation ends. Third, the *cycle ambiguity* is the number of full cycles between the satellite and the receiver at the instant of lock-on. Using more than one carrier wave allows for a better accounting for atmospheric effects, leading to a more accurate position solution. The only thing that changes among the three parts is the number of cycles in the second part above, unless lock between the receiver and the satellite is lost. If lock is lost, a cycle slip occurs, thus the cycle ambiguity is lost resulting in inaccurate measurements (Van Sickle 2008). Loss of lock can be a common occurrence in the forest as the satellites are in constant movement and at risk of trees or other obstacles blocking signals. Code processing is not susceptible to loss of lock and should be considered in forestry applications.

Horizon-masks are used to prevent the use of satellites that are low on the horizontal plane relative to the GPS receiver. Generally, one should avoid the use of satellites that are low on the horizon because this is where the satellite signal is most degraded due to particulate matter such as smog and water vapor (Hofmann-Wellenhof et al. 2001; Van Sickle 2008). All signals are affected by this particulate matter, however when a satellite is low on the horizon it must pass horizontally through the particles instead of vertically, thus increasing the time distance factor of the satellite signal and greatly reducing the chances for accurate coordinate calculation. In a forest this mask is often irrelevant because instead of minute particulate matter degrading the signal, tree stems and vegetation completely block the satellite from communicating with a receiver.

The PDOP is a measure of the satellite geometry relative to the GPS receiver. Typically a lower PDOP indicates preferred satellite geometry (Piedallu and Gegout 2005). Theoretically, preferred satellite geometry results in greater variation in the known point locations relative to the unknown point location (the GPS receiver), leading to improved solution accuracy. The wait time for improved PDOP in open terrain may be seconds to a few moments, whereas minutes to hours may be required in the forest. This may translate to adding days to field collection tasks depending on the data collection requirements.

Positioning the GPS receiver for preferred satellite geometry can be difficult and time consuming. Accuracy is still not guaranteed, however, even if the receiver is in position to receive sufficient satellite communication for a position fix, signal multipath is another significant issue in forest position determination (Zheng et al. 2005). As the name implies, instead of taking the shortest straight line distance from the satellite receiver, a signal may bounce off one or many objects, therefore taking a longer time to get to the receiver. This longer path may be incorrectly considered by the receiver to be a longer straight line distance, thus creating a scenario where point location determination is inaccurate. Many newer receivers and antennas are designed to recognize this and reject the multipath signal. A GPS signal is transmitted from the satellite in a right hand circular polar wave. When the signal bounces off an object, such as a tree, the signal is reversed to left hand circular polar, thus if it bounces off an object one time the signal may be rejected (Trimble 2005; Van Sickle 2008). If a signal bounces off an object several times, the multipath signal could miss being

detected depending on its polarization and have a significant impact on a solution. A commonly applied method to avoid multipath and improve the view of the sky is to use an offset distance from the desired point location, but lack of precision in maintaining and accurately measuring offsets can negatively impact accuracy (Sigrist et al. 1999).

Generally the longer a GPS remains stationary, in a static position, the higher the accuracy (Deckert and Bolstad 1996; Piedallu and Gegout 2005). This method is known as point averaging, where several readings are taken at a single location, and the *X*, *Y* coordinates are averaged to accept a mean value for the point (Wing 2008). For an accuracy between 1/100,000 to 1/5,000,000, a survey grade GPS must maintain an observation time of one to two hours (Van Sickle 2008). However, for short-term forest data collection using mapping grade GPS receivers, a longer occupation time does not necessarily equate to higher accuracy. In a study comparing five mapping grade GPS receivers, Wing et al (2007) found that doubling the collection from 30 to 60 points did not improve the accuracy, and their horizontal error average remained 1.3 m.

Background

A number of studies have researched GPS accuracies in various forest settings using different equipment configurations and experimenting with collection settings and modes. These studies typically use relatively few ground truth locations to assess GPS accuracies (under 30, and most cases under 10). We know of no peer-reviewed

studies where location coordinates of hundreds of trees were collected and compared using total station versus GPS.

Mapping-Grade Accuracy under Canopy

Deckert and Bolstad (1996) reported a mean error of 6.6 m after collecting 60 point readings per site and differentially correcting measurements. Study sites included coniferous canopy in western and southwestern Virginia visited between May 1993 and January 1994 and the GPS receiver was a mapping grade Trimble Pathfinder Professional GPS. Error improved to 4.4 m when 500 point readings were collected and averaged. These errors were based on locations that had been surveyed by a total station traverse originating from either National Geodetic Survey (NGS) markers or points established in the open from carrier phase GPS.

Sigrist et al. (1999) used a Trimble ProXL and DGPS Trimble Community Base Station and post processed measurements collected under canopy. The study was conducted on flat terrain in north-central Indiana under mixed broadleaf forest with pine and larch plantations smaller than one ha. True locations were established by traverse with electronic survey equipment from control points collected in the open using survey grade GPS. Mixed forest leaf-on and leaf-off horizontal root mean squared error (RMSE) was 4.49 m and 2.96 m respectively. RMSE was 5.06 m and 2.72 m in pine plantations respectively. RMSE in an open control site was 0.46 m.

In a case study using an autonomous +96 Federal Precision Lightweight GPS Receiver (PLGR), Johnson and Barton (2004) reported under-canopy errors based on a single test point within 5 m or less for 47% of the measurements. Reported errors were

within 10 m for 74% of northing measurements and within 10 m for 85% of easting measurements. The receivers were set up on known points and collected at 30 second intervals for six to eight hours.

Yoshimura and Hasegawa (2003) studied GPS accuracy under various canopy conditions including forest road, cedar plantation and natural broadleaf forest with autonomous and DGPS using a Trimble ProXR. The true location coordinates were determined using a dual-frequency GPS static surveying using a Trimble 4600LS. Their reported accuracies for autonomous and DGPS respectively by location were: forest road 5.26 m (SD 1.56 m), 1.67 (SD 2.24 m); cedar plantation 4.85 m (SD 1.21 m), 1.31 m (SD 0.48 m); and natural broadleaf forest 4.66 m (SD 1.75 m), 0.92 m(SD 0.30 m).

Piedallu and Gégout (2005) tested four different GPS receivers and many GPS parameters in northeastern France. The GPS parameters tested included eleven modes of recording period, seven modes of PDOP thresholds, four modes of collection intervals, and autonomous and differentially corrected. They tested various environmental effects including open grassland, coppice forest and deciduous high forest in summer and winter. Differentially corrected GPS measurements from a single location under deciduous high forest in leaf-on and leaf conditions resulted in overall average error of 6.1 m, 7.2 m and 2.2 m for Trimble GeoExplorer1, GeoExplorer2, and ProXR receivers respectively. Autonomous GPS measurements respective of the same GPS receivers resulted in average errors of 6.6 m, 9.7 m and 3.9 m. The fourth GPS model tested was a Garmin 12 MAP whose data were not differentially corrected,

and had an average under deciduous high forest error of 10.3 m. Counter-intuitively they found that accuracy improved during the summer months by a mean of 0.8 m. The ground truth point was established by theodolite traverse from a known triangulated point.

Bolstad et al. (2005) tested GPS accuracies of several mapping grade receivers in open skies and under forest canopy in southern Minnesota. Three locations under canopy were collected repeatedly to test autonomous, differential location using Wide Area Augmentation System (WAAS) and Coast Guard Beacon, and post processing differential correction. The accuracy was based on true point locations determined either directly from NGS control points; or through differentially corrected carrier phase GPS measurements. Canopy closure was at least 70% in all three sites. Considering only the Trimble GeoXT autonomous and differentially corrected accuracy, the mean error was 2.96 m (1.49 m SD) and 2.50 m (1.37 m SD) respectively.

Wing and Ecklund (2007) tested the accuracy of a SXBlue mapping grade GPS receiver under forest canopy on hilly terrain in western Oregon on the Clackamas GPS test course. Canopy closure was stated to be nearly 100% through-out the test course. The average error in autonomous and differential GPS was determined to be 7.2 m (3.9 m SD) and 7.8 m (4.0 m SD) respectively, a statistically insignificant, but slightly more accurate result in autonomous mode.

Wing et al. (2008) tested five different Trimble mapping grade GPS receivers with different configurations in western Oregon in May 2006 under a variety of forest

settings. Significant differences occurred in accuracy based on site and canopy type. Before post processing the average error in open sky, young Douglas-fir forest, and 40 year old Douglas-fir closed canopy forest was 0.8 m (SD 0.3 m), 1.3 m (SD 0.7 m), and 2.2 m (SD 1.5 m) respectively. After post processing, the average was 0.5 m (SD 0.2 m), 0.6 m (SD 0.4 m), and 1.7 m (SD 1.4 m) respectively.

Survey-Grade Accuracy under Canopy

Meyer et al. (2002) tested survey grade GPS receivers under suburban forest broadleaf canopy in central Connecticut using three different receivers: Trimble 4000SSE, Javad Regency and Javad Legacy. They measured fourteen permanent brass benchmarks in varying canopy conditions ranging in canopy closure from 1.2 to 98.6 percent. Results depicted a trend in decreasing accuracy with increased canopy closure at a rate of 2.32 mm for each percent of increase in canopy closure with an R^2 value of 0.82.

Hasegawa and Yoshimura (2003) studied the accuracy of a Leica SR530 geodetic GPS in conditions ranging from open terrain to closed canopy in the Kamigamo Experimental Forest, Kyoto University, Japan. The true position of each collection point was established using GPS static surveying and a total station closed traverse. Each site was occupied for four hours and the measurements were post processed using carrier phase data. Reported measurement errors were 0.014 m in open canopy conditions with few surrounding trees; 0.059 m in large canopy opening; 0.014 m in small canopy opening; and 1.715 m in closed canopy. Code corrected only data were also recorded. Only the closed canopy site had code only corrected error that was less

than the carrier phase. This error was recorded as 0.332 m on L1 frequency and 0.397 m on the L2 frequency.

Anderson et al. (2009) tested a Javad Maxor GGD survey grade GPS in Alaska under mixed and conifer forests on hilly terrain during summer of 2007. They established ground truth coordinates with a total station closed traverse originating from high accuracy control points established with a survey grade GPS. Collection times of 20 minutes were recorded twice for baseline distances of 0-10km and 10-50km. Reported RMSE for the two baseline distances was 0.0770 m and 0.3620 m for an initial mixed forest site, 0.0476 m and 0.4742 m for a second mixed forest site, and 0.0383 m and 0.4628 m for a black spruce site.

Objectives

The overall objective of this research was to evaluate the accuracy of mapping grade GPS receivers in determining tree locations with respect to their true location under temperate conifer forest conditions. More specifically, the objectives of this study were to examine the accuracy of GPS measurements of tree locations for two stands representing moderate and extreme slopes. GPS measurement accuracy was compared based on autonomous GPS measurements, post processing of code signals, and post processing of both code and carrier based signals.

Materials and methods

Study Site

We conducted this study on two 1ha (100 m^2) plots located in the Oregon State University McDonald-Dunn Forest. The two plots were chosen from previous

stratified random sampling used for a larger study. The first plot, named “U8”in this research, is uneven-aged consisting of a mixture of grand-fir (*Abies grandis*) and Douglas-fir (*Pseudotsuga menziesii*) , density 63 and 30 trees per acre respectively with the oldest trees being approximately 85 years and the last selective cut harvest conducted in 1994. Other common understory broadleaf trees include bigleaf maple (*Acer macrophyllum*) and Oregon white oak (*Quercus garryana*); with the primary shrub species being California Hazel (*Corylus cornuta*). The plot is divided by an intermittent stream channel, has a southeast aspect and a 32 percent average slope. The second plot is named “O69” is an old-growth plot dominated by Douglas-fir with some grand-fir, density 52 and 13 trees per acre respectively. The oldest trees are approximately 130 years old. A few Pacific yew (*Taxus brevifolia*) also exist on the plot. Bigleaf maple trees are common, as are California hazel shrubs. The plot is located on a very steep north aspect slope averaging 53 percent. It is on the side of a ridgeline with the top adjacent to a clearcut, which contributed to some historical tree blow-down near the top of the plot.

Total Station Survey

The coordinates for each tree in this study were originally collected by a two person survey crew during summer 2008 using a Nikon DTM 310 total station. Prior to surveying the trees, a radial traverse was conducted using local coordinates collected at stations established with wooden hubs placed such that all trees in the plot could be sighted for measurement. While offering efficiencies in data collection and decreasing the probability for error due to instrument set up variation and blunders, the

disadvantage of this method is that each point is independent of all others, thus there are no checks on individual positions. A closure check was performed on the initial back site point that supported the radial survey, thus assuring minimal instrument set-up error.

All tree coordinate data were collected using the total station sighted on the rod-man who positioned the reflector directly at the tree stem for small trees or using a two meter offset (rarely further) for large trees. Offsets were established using a rod with metric indicator with the base placed approximately 1.37 meters up the stem, then a two m horizontal distance was sighted. The established protocol called for offsets to the cardinal direction south if unobstructed. The offset cardinal direction was then verified and corrected if necessary using a magnetic compass. The offset distance error was periodically checked by using a metric tape instead of the rod. The average error was 0.07 m (SD = 0.07 m). Coordinates, species, health, diameter at breast height (DBH), and height were determined and recorded. The number of trees measured at plot O69 and plot U8 was 257 and 367 respectively.

The project map coordinate system and datum were Universal Transverse Mercator (UTM) and North American Datum 1983 (NAD83). In order to transform the tree coordinates by total station measurement from a local to project coordinate system, a control survey was conducted. A Topcon Hyper-Plus survey-grade GPS was used to establish control. Several attempts were made to establish control within or very close to plot U8. Stations U8h7 and U8h10 (Table 2.1) were established on locations that were used for control for the total station traverse. These were on sloping terrain

typical of the plot and under canopy with many large openings. The remaining attempts were set up on a small hill-top, with even greater canopy opening. The coordinates were differentially corrected using the National Geodetic Survey (NGS) Online Positioning User Service (OPUS). None of these were accurate enough solutions for the purposes of the study. The OPUS solution errors are shown in Table 2.1. These are peak-to-peak errors, or error ranges, and are the differences between the maximum and minimum coordinate values attained from three independent Continually Operating Reference Station (CORS) baseline solutions (NGS 2009).

Table 2.1. NGS OPUS solution peak-to-peak error summary.

Reference Frame: NAD83 (CORS96)

Hub	Date	Duration (hours)	X (m)	Error (m)	Y(m)	Error (m)
U8h7	07/11/09	7.04	-2499891.281	5.277	-3799721.443	6.988
U8h10	07/11/09	6.83	-2499909.218	4.390	-3799726.511	2.096
U8ba	07/20/09	6.20	-2499961.029	0.806	-3799769.750	0.248
U8rv	07/20/09	6.07	-2499943.216	1.072	-3799775.299	0.905
U8ba	07/21/09	7.85	-2499945.286	0.425	-3799783.633	0.322
U8rv	07/21/09	7.87	-2499942.794	0.731	-3799774.950	1.704

After finding that accurate solutions could not be determined under canopy, two control stations were established in larger forest openings as close as possible to the plots. For plot U8 this was on the edge of a forest road with the most 360 degree sky opening available within 100 m. Plot O69 was established on an old forest road on top of the ridge adjacent to the plot with a clearcut also adjacent and to the south. The significance of the adjacent clearcut plot is that the southern boundary of plot O69 is on the top of a ridge. Because the clearcut plot is adjacent, this allowed for a much greater area of unobstructed satellite view by the GPS receiver, thus improving the

accuracy because the survey grade receiver was able to maintain a constant lock on satellites. Table 2.2 shows the final control station coordinates with respective errors.

Table 2.2. NGS OPUS solution for control survey in plots O69 and U8.

Reference Frame: NAD_83 (CORS96)					
Plot	Duration (hours)	X (m)	Error (m)	Y(m)	Error (m)
O69b	6.20	-2492760.316	0.010	-3797630.434	0.107
O69r	6.05	-2492795.790	0.091	-3797611.744	0.025
U8b	5.83	-2499983.556	0.045	-3799800.785	0.823
U8r	5.43	-2500015.920	0.448	-3799750.685	0.176

After two control stations were established near each plot, a closed traverse was conducted using a robotic Leica SmartStation total station to two previously established stations from the radial traverse that established the tree coordinates. Plot U8 involved fourteen traverse points with twelve instrument setups and plot O69 used eight traverse points with ten setups. The closure error is shown in Table2.3. These coordinates were adjusted using the “Compass Rule” (Wolf and Ghilani 2002).

Table 2.3. Control survey closure error.

Plot	Horizontal Error (m)	Northing	Easting Error
U8	0.036	0.020	-0.030
O69	0.150	0.150	0.010

The final processing step in the total station measurement was to transform the local coordinates by translating and rotating those measured for each tree established during the radial traverse into UTM North Zone 10 coordinates, NAD83 datum. Traverse PC software was used for this transformation.

GPS Survey

Two to three person field crews collected the GPS data for each plot between November 2009 and January 2010. Crews used a Trimble ProXH with a Zephyr external antenna connected to a Trimble data collector for plot O69 and Trimble

GeoXH with a Zephyr external antenna for plot U8. The receivers have identical manufacturer specifications but come in different casings. We determined that the accuracy capabilities for the two receivers are virtually identical with respect to this study and any differences in accuracy capabilities in the two were negligible (Table 2.4) (Trimble 2006-2009; Trimble 2008-2009; Lahm 2009). We chose to collect coordinates using autonomous GPS, as this is the most accurate method when the data is postprocessed using the satellites precise ephemeris information (Karsky 2004; Van Sickle 2008).

Table 2.4. Trimble ProXH and GeoXH specifications.

	Trimble ProXH	Trimble GeoXH
Channels	12 (L1 code and carrier/L2 carrier	26 (12 L1code and carrier, 12 L2carrier)
Accuracy		
H-star postprocessed		
With internal antenna	0.30 m	0.30 m
With external Zephyr ant.	0.20 m	0.20 m
Code postprocessed	0.50 m	0.50 m
Carrier postprocessed		
Tracking Satellites 20 min	0.10 m	Information not provided
Tracking Satellites 45 min	0.01 m	0.01 m

Table adapted from Trimble (2006-2009; 2006b; 2008-2009)

We used the GPS data collection software Trimble TerraSync with consistent configuration settings throughout the survey. The receivers were set to collect UTM zone 10 north coordinates and datum World Geodetic System 1984 (WGS84). To avoid using satellites at risk of errors associated with ionospheric and tropospheric attenuation we used a 15 degree horizon mask. Lower PDOP values promote higher GPS accuracies and we chose a PDOP mask of 6, which Van Sickle (2008) describes as typical. As previously discussed, multipath can degrade GPS accuracy. Both GPS receivers in this study were equipped with Trimble H-star technology, which is

designed to aid in the detection and removal of multipath signals. We also used the Trimble TerraSync default SNR value of 39 dBHz (4.0 amu), which is recommended by the manufacturer and in the middle of available settings between 33 dBHz and 43 dBHz (Trimble 2006a).

Field crews were provided with a plot map displaying a tree number overlayed with a 10 m UTM coordinate grid to identify trees previously located by total station. Once a tree was identified and matched to a field mapped tree, the crew recorded the tree number, species and DBH to the nearest cm using a diameter tape. This information was later used for correct tree number identification confirmation. The GPS and antenna were attached to a pole with the antenna mounted 2.2 meters above the ground to avoid multipath and/or signal attenuation from the ground and operator. To measure a tree location, the operator first measured an offset distance (usually two m but sometimes farther if other objects interfered with a two meter offset) in a southern direction (other cardinal directions were used if objects interfered with the southern direction) using the protocol discussed in the total station measurement, and then held the GPS pole vertical and collected GPS readings until a minimum of 30 data points were collected per location. The average number of points collected per position at plot O69 and U8 were 48 and 37 respectively. The ratio of tree location measurements made with GPS to those actually used in error calculation in plot O69 was 196 to 192 and U8 was 200 to 145. Most of the trees that were culled from the database could not be positively matched, and the remainders were a result of trees measured outside the plot boundary. A total of 257 and 367 trees were measured by total station at plots

O69 and U8 respectively. The difference between the number sampled by total station versus collected by GPS is due to difficulty in positively matching trees smaller than 3 m tall.

Each plot involved two to three different crews who collected on several different dates. Once the plot was completed, the GPS files were downloaded and differentially corrected using Trimble Pathfinder Office version 4.10. Each file was differentially corrected using automatic carrier and code processing and code only processing using H-Star corrections with multiple base providers. When the automatic carrier and code processing option is chosen in Trimble Pathfinder Office, the program analyzes the average code processed position, and average carrier processed position and selects the position with the least amount of error. When using the multiple base provider option with H-Star processing, Pathfinder Office averages the coordinate data from each provider in the group weighting the closer base provider higher to determine a single position solution (Trimble 1995-2008). Table 2.5 displays the base providers used and the base line distance from the plot. The integrity index value for each site was in the high 90's for each provider. The integrity index value ranges from 0 to 100 and indicates the reliability of the provider and its likelihood of providing quality results. The higher the value is, the better the integrity value (Trimble 1995-2008).

Table 2.5. GPS correction providers and baseline distance from each plot.

Provider	Distance from O69	Distance from U8
CORS, Corvallis (CORV), OR	11km	4km
UNAVCO, Philomath, OR	12km	11km
UNAVCP, Lebanon, OR	32km	34km

Because WGS84 is the reference ellipsoid for GPS (Van Sickle 2008), and because this study is a portion of a larger study that involves variations in NAD83, we chose to collect positions using WGS84 in UTM zone 10 north. At their original inception WGS84 and NAD83 only differed by one to two centimeters depending on location, however NAD83 (CORS96) differs by up to two meters (Van Sickle 2008). The OPUS solutions used for the total station solutions in this project are based on NAD83 (CORS96). We used Trimble Pathfinder Office software to convert from WGS84 to NAD83 (CORS96), and then combine the separate GPS files into one by exporting to an Environmental Systems Research Institute (ESRI) shapefile for later analysis in the ESRI ArcGIS software.

Geographic Information System (GIS) Processing

Based on our method of matching field mapped trees collected by total station, some risk of tree mismatch existed. The field crews had various experience levels, thus discrepancies exist in matching the total station data to the GPS data with respect to species and DBH, the least important of which were the conifer species. The common discrepancy in species data exists between what one crew identified as Douglas-fir the other a grand-fir. Another potential cause for the mismatch is that the default species setting in the GPS data dictionary was Douglas fir, thus if the crew failed to enter a species, then the GPS automatically filled in Douglas fir based on the

data dictionary. We made the decision to ignore species discrepancies if the DBH matched. There were also discrepancies in the DBH. If the DBH discrepancy was greater than 0.10 m the tree was removed from the analysis database. If the discrepancy was a broadleaf matched to a conifer, then it was removed. The average difference in matching DBH tree by tree was 0.04 m (SD 0.03 m), and 0.03 m (SD 0.04 m) for plot O69 and U8 respectively noting that the protocol for GPS crews to measure the DBH was not put into effect until plot 069 was nearly complete, thus only 10% of the trees were DBH verified, whereas 90% of plot U8 trees were verified. After confirming tree matches, tree coordinates were shifted for the GPS and total station files based on offset distance and half the stem diameter to the theoretical stem center.

Analysis

Each coordinate determined by GPS measurement was subtracted from the total station measurement to determine the easting (X), northing (Y) and overall horizontal error on a by tree basis. Using the statistical package S-Plus version 8.0, we conducted a Welch Modified two-sample t-test to determine if significant differences in error existed in autonomous, carrier and code corrected, and code only corrected positions collected by the GPS receivers. The Welch t-test is a modification of the Student t-test, and is used when there is possible unequal variance in two samples (Ramsey and Schafer 2002). Since this possibility existed in our data we used the Welch t-test. The average horizontal error variance is shown in Table 2.6.

Results

Using tree positions collected by total station as the true coordinate, average measurement errors and standard deviations were calculated for GPS for autonomous (named raw in Table 2.6), differential corrected using both carrier and code, and differential corrected using code only coordinates collected on each plot (Table 2.6). Although a few studies have shown horizontal accuracy error of differentially corrected GPS in excess of 10 m (Deckert and Bolstad 1996; Zheng et al. 2005), based on our experience with the GPS receivers used and the study area, 10m horizontal error seemed excessive. Average error and standard deviation are also shown with 10 m error outliers removed, noting that no more than four locations met the removal criteria (Table 2.6).

Table 2.6. Average tree horizontal position error (m) comparison between total station and mapping-grade GPS. autonomous (raw), carrier/code corrected and code only corrected positions.

	*Plot O69 (n=192)			*Plot U8 (n=145)		
Difference Comparison	Avg. Error	SD	Variance	Avg. Error	SD	Variance
TS to GPS Comparison						
TS minus Carrier/Code GPS						
X Difference	-0.95	2.23		0.43	2.64	
Y Difference	1.08	2.25		1.30	3.07	
Horizontal Difference	2.94	1.85	3.41	3.46	2.50	6.23
TS minus Code only GPS						
X Difference	-0.78	2.18		0.41	2.32	
Y Difference	-0.54	2.18		-0.16	2.55	
Horizontal Difference	2.57	1.94	3.78	2.70	2.17	4.72
TS minus Raw GPS						
X Difference	-0.52	2.19		0.41	2.65	
Y Difference	-1.10	2.59		-0.76	3.00	
Horizontal Difference	2.86	2.18	4.75	3.28	2.43	5.93
TS to GPS (no outliers)						
TS minus Carrier/Code GPS (no outliers)	n=191			n=141		
X Difference	-0.91	2.18		0.50	2.44	
Y Difference	1.05	2.22		1.20	2.77	
Horizontal Difference	2.90	1.78		3.24	2.17	
TS minus Code Only GPS (no outliers)	N=191			n=142		
X Difference	-0.70	1.98		0.50	2.14	
Y Difference	-0.49	2.11		-0.03	2.40	
Horizontal Difference	2.48	1.70		2.58	1.98	

*n applies to all comparisons except those shown in (no outliers)

GPS Error

In both study plots the average GPS horizontal error is greatest when differential correction is applied using both carrier and code [plot 069 = 2.94 m (SD 1.85 m), plot U8 = 3.46 m (SD 2.50 m)]; less error occurs using the autonomous GPS [plot 96= 2.86 m (SD 2.18 m), plot U8 = 3.28 m (SD 2.43 m)]; and finally the least amount of error occurs when using code only differential correction [plot O69 = 2.57 m (SD 1.94 m), plot U8 = 2.70 m (SD 2.17 m)] (Table2.6).

If the results of subtracting the GPS coordinate from the total station coordinate results in a negative value, this would indicate that the GPS point is east or north with respect to *X* and *Y* values; and if the subtracted value is positive, then the GPS point is west or south of the total station point (Table 2.6). The autonomous GPS and code corrected *Y* error values indicate consistent average negative values or GPS positions north of the total station points; while the carrier and code corrected values indicate consistent positive *Y* values, or GPS positions south of the total station positions. Although these average values suggest a directional position trend, visual inspection of the points in a GIS map display did not indicate directional error bias, nor did looking at the signs (negative or positive) of each *X*, *Y* and horizontal values of individual points in a spreadsheet.

We found statistically significant error differences when comparing carrier and code to code only differential correction ($P<0.006$) in Plot U8, and marginally significant error differences in plot O69 ($P=0.056$) (Table 2.7). Statistical significance was only evident on plot U8 ($P=0.035$) in comparing code only differential correction to the raw uncorrected GPS measurements. No statistically significant differences were found on either plot between the carrier and code differential correction compared to the uncorrected raw GPS ($P>0.500$).

Table 2.7. Statistical significance of GPS measurement processing results.

Horizontal Error Difference Comparison	Plot O69 *p*-value	Plot U8 *p*-value
(Total Station - Carrier/Code) to (Total Station - Code only)	0.056	0.006
(Total Station - Carrier/Code) to (Total Station - Raw)	0.717	0.534
(Total Station - Code only) to (Total Station - Raw)	0.161	0.035

To help understand the differential correction coordinate shift, the average difference and standard deviation were calculated to compare raw autonomous GPS to carrier and code, and code only differential correction; and code positions were subtracted from carrier and code correction to compare the average point offset between correction methods (Table 2.8). The difference from the autonomous GPS points was greater using carrier and code processing, rather than just code processing. The horizontal difference between autonomous GPS points and differential corrected points using carrier and code on plot O69 was 3.32 m (SD 1.91 m) and for plot U8 was 3.45 m (SD 2.28 m); and using the code only correction the difference was 1.78 m (SD 1.49 m) for plot O69 and 1.98 m (SD 1.35 m) for plot U8.

Table 2.8. Average horizontal shift in differential correction methods.

	***Plot O69 (n=192)**		***Plot U8 (n=145)**	
Difference Comparison	Average Error	SD	Average Error	SD
GPS Correction Comparison				
Carrier/Code minus Raw GPS				
X Difference	0.43	1.80	0.00	2.25
Y Difference	-2.18	2.56	-2.05	2.81
Horizontal Difference	3.32	1.91	3.45	2.28
Code only minus Raw				
X Difference	0.25	1.10	0.00	1.39
Y Difference	-0.56	1.95	-0.60	1.87
Horizontal Difference	1.78	1.49	1.98	1.35
Carrier/Code minus Code GPS				
X Difference	0.18	1.49	-0.00	1.93
Y Difference	-1.62	1.95	-1.45	2.39
Horizontal Difference	2.57	1.43	2.86	1.83

Discussion

Our results, respective of plots O69 and U8 (Table 2.6), indicate the greatest positional GPS error associated with the differentially corrected data using code and carrier processing (2.94 m and 3.46 m); followed by the raw, uncorrected data files

(2.86 m and 3.28 m); and finally the least amount of error was associated with code only processing (2.57 m, and 2.70 m). These errors are within error ranges reported in other studies using mapping-grade GPS receivers under forest canopy. The errors we determined in our study are less than those found in some studies (Deckert and Bolstad 1996; Johnson and Barton 2004), within the range reported by Yoshimura and Hasegawa (2003); similar to others (Bolstad et al. 2005; Piedallu and Gegout 2005); and greater than those found in the same geographic area by Wing et al. (2008).

Our results showed statistical significance in accuracy comparing differential correction methods using code and carrier to code only in plot U8 ($P = 0.006$) and marginally significant on plot O69 ($P = 0.056$) (Table 2.7). This indicates that in similar forest conditions to our research differential correction using code is likely to have better accuracy results than using carrier correction. Regardless of the sample size, this will provide for additional time savings as cycle slips will be avoided since coded pseudorange measurement is immune to this occurrence (Van Sickle 2008). When comparing differential correction using the code to the uncorrected files there was a significant difference in accuracy in plot U8 ($P = 0.035$) but not in plot O69 ($P = 0.161$). There could be several explanations for these plot differences including crew mistakes, e.g. correct tree identification, offset measurement and DBH measurement, etc; or systematic errors caused by GPS control survey precision, GPS receiver differences, canopy cover, etc. There was no significant difference in positional accuracy when comparing the code and carrier corrected data to the autonomous data with P values equal to 0.717 and 0.534 in plots O69 and U8 respectively. Although

statistically insignificant, this is theoretically significant indicating that the forest canopy and tree stems have such an impact on the carrier signal that differential correction cannot significantly improve accuracy when collecting under forest canopy as compared to GPS signals collected in the open. The most important systemic error that accounts for this is the discontinuity in the signal caused by cycle slips, which are the result of tree stems and canopy temporarily blocking signals as the satellite moves in relation to the GPS receiver and the forest. Based on these results, it appears that using coded pseudorange measurement is the most accurate and recommended method among those that we tested for mapping-grade GPS surveying under a conifer dominant forest canopy.

The most noteworthy differences between this study and the aforementioned previous studies are what was sampled and the sample size. Both of these increase the chances for error and potential error spread. We measured individual trees at a relatively close distance from the stem, opposed to other studies which measured ground truth locations, either preexisting or established for the study, and presumably farther from tree stems. The significance of the distance is that in at least one cardinal direction the measured tree stem and foliage blocked the field of view of any satellite in that portion of the sky. The stem of course completely blocks a signal, and the farther away from a stem and foliage, generally the greater likelihood for canopy opening. The close proximity to at least one stem equates to greater risk in multipath, and chances for error. Distances from the closest trees were not reported in the other studies. The total sample size in our study was 337, which was much larger than

previous studies in terms of individual ground truth locations. This sample size meant a greater amount of time spent in the field than other studies. Other studies collected during optimal satellite availability windows. Based on limited crew time availability, GPS availability windows were only marginally considered. The field crew collected data when it best fit their schedule, thus in some cases better geometry and greater number of satellites could have increased the overall accuracy. This larger amount exposure under less than optimum satellite conditions potentially created a greater error range than may have occurred under optimal conditions. The smallest standard deviation associated with horizontal error was 1.85 m and the greatest was 2.50 m, but the smallest and greatest range in error values was 9.66 m and 12.18 m respectively. Longer collection times may have reduced this error spread, but Wing et al. (2008) found that increasing the number of points collected from 30 to 60 did not have a significant impact on error reduction. Based on time available and desired sample size, collecting significantly more than 60 points was not considered but may be an area for future research.

Although horizon masks are important for GPS collection to avoid error caused by increased atmospheric particulate matter attenuation under open sky conditions, this factor is generally irrelevant in the forest because satellite signals coming from low on the horizon are either blocked by topography or by forest stems and foliage. In our site conditions any satellite that was below approximately 30 degrees on the horizon from the receiver was not available. Based on this and our relatively low PDOP mask of 6, the number of satellites available for position calculation was severely limited, thus

increasing the overall field collection time. Satellite availability came in short time spurts causing “feast or famine” GPS collection. Further research is recommended in PDOP settings under forest canopy to determine maximum recommended PDOP to capitalize on as many satellites as possible without jeopardizing accuracy while increasing collection efficiency.

Based on many difficulties associated with collecting GPS coordinates in a forest setting, if a large number of location coordinates are to be collected under canopy we recommend traditional survey methods using a total station. Although GPS technology is sweeping our society, and a total station survey requires some expertise, in the long run GPS surveys may be more time consuming than traditional methods. The GPS appears to be simple to the layman, but there are so many variables to collecting accurate and precise data that greater expertise and training is required to fully understand and collect accurate GPS data in the field. Many factors extend GPS survey field time, e.g. satellite windows, cycle slips, multipath, etc. A total station survey can be potentially quicker, and more accurate if done correctly, even when considering training time. If considering all of the training time it takes to do more than turn on a GPS and set up over a desired station location, GPS training and total station training time are likely similar to achieve equivalent expertise.

Our results demonstrated that GPS horizontal position accuracy is degraded by forest canopy. Dual frequency receivers collecting two carrier signals are known to remove error bias caused by the earth’s atmosphere. However constant, unbroken communication between the receiver and the satellite must be maintained in order to

avoid cycle slips and promote accurate coordinate measurement. Our research demonstrated that cycle slips caused by the forest canopy degraded satellite signals and reduced the overall horizontal accuracy. Differential correction using pseudorange codes, which are not affected by cycle slips, was more accurate compared to carrier phase processing. The error caused by cycle slips is such an important factor that differential correction using carrier and code was not significantly more accurate than using uncorrected autonomous GPS data. The most accurate average horizontal coordinates were achieved with differential correction using pseudorange codes, but the error was still relatively high (>2.5 m).

Literature Cited

Andersen, H.-E., T. Clarkin, K. Winterberger and J. Strunk (2009). An accuracy assessment of positions obtained using survey- and recreational-grade Global Positioning System receivers across a range of forest conditions within the Tanana Valley of interior Alaska. Western Journal of Applied Forestry 24: 128-136.

Andersen, H.-E., S. E. Reutebuch and R. J. McGaughey (2006). A rigorous assessment of tree height measurements obtained using airborne LiDAR and conventional field methods. Canadian Journal of Remote Sensing 32(5): 355-366.

Bolstad, P., A. Jenks, J. Berkin, K. Horne and H. Reading William (2005). A Comparison of autonomous, WAAS, real-time, and post-processed Global Positioning Systems (GPS) accuracies in northern forests. Northern Journal of Applied Forestry 22: 5-11.

Deckert, C. and P. V. Bolstad (1996). Forest canopy, terrain, and distance effects on Global Positioning System point accuracy. Photogrammetric Engineering and Remote Sensing 62(3): 317-321.

Falkowski, M. J., A. M. S. Smith, P. E. Gessler, A. T. Hudak, L. A. Vierling and J. S. Evans (2008). The influence of conifer forest canopy cover on the accuracy of two individual tree measurement algorithms using LiDAR data. Canadian Journal of Remote Sensing 34(Suppl. 2): S1-S13.

Hasegawa, H. and T. Yoshimura (2003). Application of dual-frequency GPS receivers for static surveying under tree canopies. Journal of Forest Research 8(2): 0103-0110.

Hofmann-Wellenhof, B., H. Lichtenegger and J. Collins (2001). GPS theory and practice. New York, Springer-Verlag Wien.

Johnson, C. E. and C. C. Barton (2004). Where in the world are my field plots? Using GPS effectively in environmental field studies. Frontiers in Ecology and the Environment 2(9): 475-482.

Karsky, D. (2004). Comparing four methods of correcting GPS data: DGPS, WAAS, L-band, and postprocessing. Engineering Tech Tips, United States Department of Agriculture Forest Service 0471-3-2307-MTDC: 1-6.

Kato, A., L. M. Moskal, P. Schiess, M. E. Swanson, D. Calhoun and W. Stuetzle (2009). Capturing tree crown formation through implicit surface reconstruction using airborne LiDAR data. Remote Sensing of Environment 113(6): 1148-1162.

Lahm, J. (2009). GeoXH vs. ProXH. C. Edson.

Means, J. E., S. A. Acker, D. J. Harding, J. B. Blair, M. A. Lefsky, W. B. Cohen, M. E. Harmon and W. A. McKee (1999). Use of large-footprint Scanning Airborne LiDAR to estimate forest stand characteristics in the Western Cascades of Oregon. Remote Sensing of Environment 67(3): 298-308.

Meyer, T. H., C. R. Ferguson, J. E. Bean and J. M. Naismith (2002). The effect of broadleaf canopies on survey-grade horizontal GPS/GLONASS measurements. Surveying and Land Information Science 62(4): 215-224.

Næsset, E., T. Gobakken, J. Holmgren, H. Hyyppä, J. Hyyppä, M. Maltamo, M. Nilsson, H. Olsson, Å. Persson and U. Söderman (2004). Laser scanning of forest resources: the nordic experience. Scandinavian Journal of Forest Research 19(6): 482-499.

NGS. (2009). What is OPUS? Retrieved March 17, 2010, from http://www.ngs.noaa.gov/OPUS/about.html#discussion.

Piedallu, C. and J.-C. Gegout (2005). Effects of forest environment and survey protocol on GPS accuracy. Photogrammetric Engineering and Remote Sensing 71(9): 1071-1078.

Popescu, S. C. (2007). Estimating biomass of individual pine trees using airborne LiDAR. Biomass and Bioenergy 31(9): 646-655.

Ramsey, F. L. and D. W. Schafer (2002). The statistical sleuth: a course in methods of data analysis. Pacific Grove, CA, Thompson Learning.

Sigrist, P., P. Coppin and M. Hermy (1999). Impact of forest canopy on quality and accuracy of GPS measurements. International Journal of Remote Sensing 20(18): 3595-3610.

Trimble (1995-2008). GPS Pathfinder Office Help, Trimble Navigation Limited.

Trimble. (2005). Data sheet: H-Star technology explained. Retrieved February, 2009, from http://trl.trimble.com/docushare/dsweb/Get/Document-224437/022501-071_H-Star%20technology%20explained_0805.pdf.

Trimble (2006-2009). GPS Pathfinder ProXH Receiver Datasheet. Westminster, Trimble Navigation Limited**:** 1-2.

Trimble (2006a). TerraSync software reference manual. T. N. Limited. Westminster, CO. Version 2.60**:** 1-248.

Trimble (2006b). Data sheet: GPS Pathfinder ProXH receiver. Trimble. Westminster, CO.

Trimble (2008-2009). Trimble GeoXH Datasheet. Westminster, Trimble Navigation Limited**:** 1-2.

Van Sickle, J. (2008). GPS for land surveyors. Boca Raton, CRC Press, Taylor & Francis Group.

Wing, M. G. (2008). Keeping Pace with Global Positioning System technology in the forest. Journal of Forestry 106: 332-338.

Wing, M. G. and A. Eklund (2007). Elevation measurement capabilities of consumer-grade Global Positioning System (GPS) receivers. Journal of Forestry 105: 91-94.

Wing, M. G., A. Eklund, S. John and K. Richard (2008). Horizontal measurement performance of five mapping-grade Global Positioning System receiver configurations in several forested settings. Western Journal of Applied Forestry 23: 166-171.

Wing, M. G., A. Eklund and L. D. Kellogg (2005). Consumer-grade Global Positioning System (GPS) accuracy and reliability. Journal of Forestry 103: 169-173.

Wing, M. G. and R. Karsky (2006). Standard and real-time accuracy and reliability of a mapping-grade GPS in a coniferous western Oregon forest. Western Journal of Applied Forestry 21: 222-227.

Wolf, P. R. and C. D. Ghilani (2002). Elementary surveying an introduction to geomatics. Upper Saddle River, New Jersey, Prentice Hall.

Yoshimura, T. and H. Hasegawa (2003). Comparing the precision and accuracy of GPS positioning in forested areas. Journal of Forest Research 8(3): 147-152.

Zengin, H. and A. Yeşil (2006). Comparing the performances of real-time kinematic GPS and a handheld GPS receiver under forest cover. Turkish Journal of Agriculture & Forestry 30(2): 101-110.

Zheng, J., Y. Wang and N. L. Nihan (2005). Quantitative evaluation of GPS performance under forest canopies. IEEE Proceedings of Networking, Sensing and Control: 777-782.

CHAPTER 3 – VERTICAL HEIGHT DIFFERENCES IN DIGITAL ELEVATION MODELS (DEM) DERIVED FROM TOTAL STATION, LIDAR, AND GPS MEASUREMENTS IN FORESTED SETTINGS

Curtis B. Edson

Michael G. Wing

Submitted to Photogrammetric Engineering and Remote Sensing

Abstract

Digital elevation models (DEMs) form the basis of LiDAR derived tree height measurements and other topographic modeling needs within natural resource applications. We compared 2873 total station elevations to the closest discrete LiDAR elevation point and DEM raster cell across several forest and topographic settings. We also examined limiting point comparisons to points within 0.5 m and within one meter. Using all nearest LiDAR points, average total station plot elevation differences ranged from -0.06 m (SD 0.40) to -0.59 m (SD 0.23) indicating that LiDAR elevations are higher than actual elevations. LiDAR DEM differences ranged from -0.09 (SD 0.41) to -0.56 m (SD 0.70). We also compared mapping-grade GPS receiver measurements to LiDAR point elevation and DEMs. Average plot GPS elevation differences ranged from 0.24 (SD 1.55) to 2.82 m (SD 4.58) for the nearest LiDAR point, and from 0.27 (SD 2.33) to 2.69 m (SD 5.06) for LiDAR DEMs.

Introduction

Light Detection and Ranging (LiDAR), also known as airborne laser scanning, has emerged since its initial applications in the mid 1980's (Lim et al. 2003) and 1990's (Hodgson and Bresnahan 2004) into many activities including forest management, urban planning, natural resource modeling, ice sheet mapping, road design (Lim et al. 2003; Aguilar and Mills 2008), and others. Forest terrain mapping (Reutebuch et al. 2003) and forest inventory (Reutebuch et al. 2005) are some of the primary LiDAR applications within natural resources. Research in topographic mapping with LiDAR

began in the early 1980s (Krabill et al. 1984) with the first commercial LiDAR sensor fielded in 1993 (NOAA 2010).

In aerial mapping applications, LiDAR is an active sensor that directly measures elevations of objects it contacts between the aircraft and the ground. Forest measurements that can be derived from LiDAR include ground and vegetation surfaces. LiDAR relies on the principle that a laser pulse moves at the speed of light, thus the time it takes for a laser pulse to travel from the sensor to an object and back to the sensor enables the calculation of the distance between the sensor and object. These measurements allow for the calculation of object heights above ground based on an aircraft's altitude (Evans et al. 2009).

There are three categories of LiDAR sensors including profiling, discrete return, and waveform. Profiling LiDAR records only one return of each laser pulse at relatively coarse densities along a narrow linear transect, whereas waveform and discrete return use a scanning mirror that rotates or oscillates capturing a swath of returns (Lefsky et al. 2002).

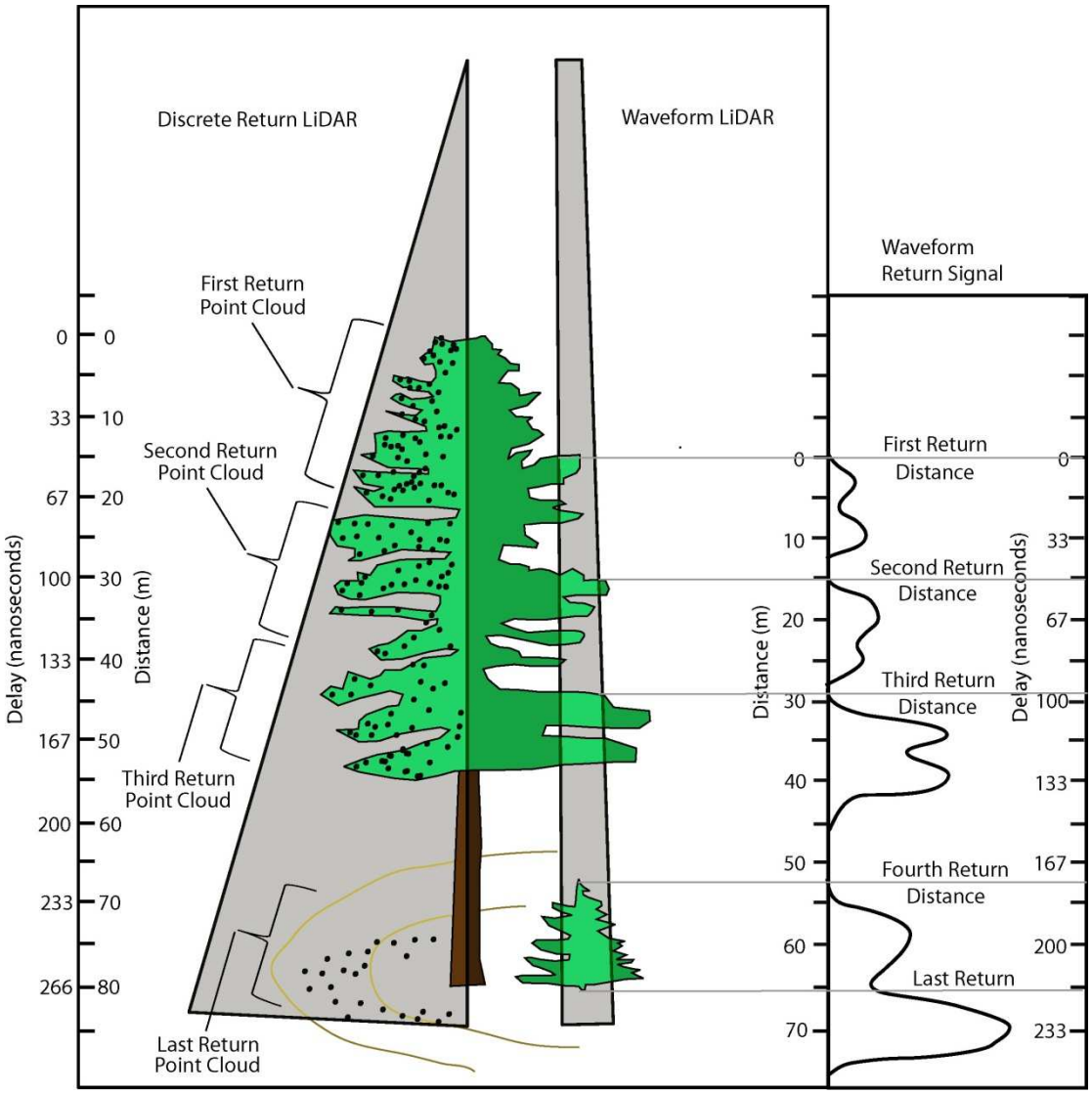

Figure 3.1. Conceptual diagram of discrete return and waveform LiDAR (Lefsky et al. 2002; Penn State Geography 2010).

Basic waveform and discrete return LiDAR system concepts are illustrated in Figure 3.1. Discrete return LiDAR systems record at least one return (typically three to five) per laser pulse and are considered small footprint with typical laser pulse diameters of 0.20-0.80 m. The number of returns that a sensor receives is based on the laser pulse return intensity as influenced by the reflectivity of objects that are targeted.

Waveform LiDAR provides a continuous distribution of laser energy for each laser pulse by capturing the total energy returned to the sensor at fixed distances (Evans et al. 2009). This distance is based on the variation in return time of the full wave of energy returned to the sensor relative to the time the pulse was emitted (Lefsky et al. 2002). In early forestry applications, profiling lasers effectively measured canopy height and timber volume (Nelson et al. 1988). The most common types of LiDAR sensors discussed in current literature are waveform and discrete return. These two types of LiDAR sensors have distinct advantages and disadvantages. Small footprint waveform LiDAR, such as the Experimental Advanced Airborne LiDAR (EAARL) with a 0.20 m diameter footprint when flown at 300 m above the ground (USGS 2009), is beginning to be used more commercially, but they are not used much yet for natural resource applications and can provide quantities of data that overwhelm many computer systems (Evans et al. 2009). Waveform LiDAR have historically been large footprint instruments (3-8 m) that experience low signal to noise ratios relative to discrete return LiDAR, thus increasing the probability of sampling the top of trees or other discrete objects (Lim et al. 2003). Discrete return LiDAR typically capture returns at very high point densities (quantified as the number of returns per unit area) and provide higher resolution of ground and canopy surfaces (Evans et al. 2009), however it is known to underestimate tree heights (Popescu et al. 2002; Andersen et al. 2006; Evans et al. 2009).

An aerial LiDAR system configuration for terrain mapping consists of a laser scanning sensor mounted on an aircraft (either fixed or rotary wing), Inertial

Measurement Unit (IMU), and global positioning system (GPS) (Hodgson et al. 2005; Reutebuch et al. 2005; Pfeifer and Briese 2007; Liu 2008). To obtain accurate ground coordinate measurements, the location of the sensor must be known during the entire data collection period. The aircraft mounted GPS and IMU work in conjunction to continually determine the absolute location of the sensor and the direction that the laser is pointing (Hodgson et al. 2005). Just as in aerial photogrammetry, the aircraft attitude affects the angular orientation of the sensor. The IMU continually measures the attitude of the aircraft for pitch, roll, and yaw (Liu 2008). This information is then used for post processing correction and calibration based on the time indexed position and attitude of the aircraft and on-board instrumentation (Watershed Sciences 2008). The laser sensor consists of a pulse generator, infrared laser in the wavelength range of 0.8 µm to 1.6 µm, and a pulse receiver. The receiver collects the return signals in various intensities after the laser pulse reflects off objects (Hodgson et al. 2005; Pfeifer and Briese 2007; Liu 2008). The return intensity depends on several factors including: the energy of the transmitted laser pulse, the percentage of the pulse intercepted by a feature, feature surface reflectance characteristics based on the laser wavelength, and the fraction of the pulse returned to the sensor versus diffuse reflectance (Lefsky et al. 2002). It takes 4 to 15 ns to emit each pulse, which equates to a pulse length of approximately 2-4 m (Hodgson et al. 2005; Liu 2008). The early systems produced pulses at rates as low as 4 per second (4 kHz) and by the early 2000's as high as 100 per second (100 kHz) (Ramano 2004). As of 2008 pulse rates can reach as high as 400 kHz (Luccio 2008), but most current systems have a

maximum pulse rate of approximately 150 kHz (Chen 2007). Higher pulse rates equate to greater data density. In forestry, thousands of LiDAR points are used per hectare to measure and classify earth features such as vegetation cover or ground terrain. An advantage to LiDAR is that each point from the final output includes measurements in three dimensions (X, Y and Z coordinates) (Liu 2008). Pfeifer and Briese (Pfeifer and Briese 2007) provide a comprehensive review of LiDAR mechanics.

LiDAR has recently emerged as significant technology for forest measurement applications. Many forest attributes can be measured by LiDAR over large areas including canopy height, subcanopy topography, vertical canopy distribution (Lim et al. 2003) and individual tree heights (Andersen et al. 2006). Tree height measurement is a critical component of forest inventory measurements (Husch et al. 1982; Andersen et al. 2006). Tree total height is the linear distance of the tree measured perpendicular from the earth's surface along the stem axis to the apex of the tree (Husch et al. 1982). Historical methods of tree height measurement include indirect techniques using clinometers, laser rangefinders, total station and other survey instruments, photogrammetry; and direct methods with height poles. All of these methods are time consuming and expensive, and potentially suffer from different setbacks (Popescu et al. 2002; Lim et al. 2003; Andersen et al. 2006; Liu 2008). The use of clinometers, range finders, and total station instruments require the ability of the user to see both the tree stem and apex, which is not always possible in a dense forest. Height poles result in inaccuracy caused by parallax (Andersen et al. 2006). Two adjacent aerial

photos (stereo-pairs) are required to measure tree heights accurately. In the photos, only a small portion of the ambient light rays may reach the forest floor and be visible to a photogrammetrist, while the rest of the terrain may be masked by vegetation and shadows.

When measuring tree heights using LiDAR data several factors impact measurement accuracy including: size and reflectivity of the tree, sampling density, LiDAR pulse diameter, and shape of the tree crown. A primary source of error in LiDAR tree height measurement associated with conifer species occurs when laser pulses miss the apex of the tree resulting in a underestimate of tree height (Popescu et al. 2002; Anderson et al. 2006). Another potentially significant impact on height measurement is the terrain height measurement (Andersen et al. 2006). LiDAR tree height estimates are calculated by subtracting the terrain surface as represented by a digital elevation model (DEM) from the highest point associated with an individual tree (Kraus and Pfeifer 1998; Lim et al. 2003). Before any LiDAR forest measurements are made, characterization of terrain elevation and DEM creation should be completed (Popescu et al. 2002). DEMs are important for geographic representation, and the analysis and visualization of topographic features (Li et al. 2005). DEMs are created by interpolating a digital surface model from discrete elevation values that have been collected from across a landscape.

Not all emitted LiDAR pulses penetrate the canopy and strike the ground surface. Kraus and Pfeifer (1998) in previous experiences found that less than 25% of LiDAR pulses reached the ground in “wooded areas”. Means (2000) found that 1-5% of

LiDAR pulses struck the ground when under conifer forest. Creating the DEM first requires eliminating all points classified as non-ground from the three dimensional LiDAR point cloud by automated and manual computer methods. A raster or triangulated irregular network (TIN) DEM is then generated through various interpolation techniques (Popescu et al. 2002; Lim et al. 2003; Hodgson and Bresnahan 2004). The automated method of identifying the ground points that support interpolation is an iterative process using spatial algorithms that identify the lowest points within a search pattern, often referred to as a neighborhood. Identified points are assumed to represent the ground surface and are placed into a set of ground points. The specific neighborhood method applied by LiDAR vendors to identify ground surface points is proprietary. Once the automated method is complete, an analyst will manually refine the ground candidate set, usually by comparing it to orthophotography (Hodgson and Bresnahan 2004) or viewing cross-sections of the ground surface points. The selected set of discrete ground points are then used with any number of interpolation methods to derive a DEM (Popescu et al. 2002). The use of discrete topographic data may seem straight forward, but a wide range of results can occur based on the quality of the input data and the processing algorithm used (Yang et al. 2005). DEMs created from bare earth LiDAR can be interpolated to a vertical precision as fine as 0.1 m (Anderson et al. 2006). The choice of interpolation method is important depending on the desired accuracy, as some methods are considered more exacting than others (Popescu et al. 2002; Chaplot et al. 2006). Some exact methods include distance-weighting, kriging, spline interpolation, triangulation, and finite-

difference methods and radial basis functions, whereas approximate methods include power-series, trend models, Fourier models, distance-weighted least squares, and least squares fitted with splines (Popescu et al. 2002; Chaplot et al. 2006). Regardless of interpolation method, if the distribution of discrete points used for interpolation within uneven terrain are not regularly spaced in the desired resolution of the DEM grid intersections, error can be introduced through interpolation (Fisher and Tate 2006). Laser points used to interpolate an elevation surface are typically irregularly spaced, especially when under dense canopy (Kraus and Pfeifer 1998). A DEM is usually made up of equally-sized grid cells that span an on-the-ground distance in the longitudinal and latitude dimensions, with each grid cell containing an elevation value (Chaplot et al. 2006; Fisher and Tate 2006). The stated resolution of the DEM is the on-the-ground distance that the side of a grid cell covers. The DEM resolution is related to the sampling interval and is a function of the source data and the interpolation method. A 10 m resolution DEM indicates that a 10 m square cell represents one elevation. A 1 m resolution DEM has an elevation representation in a 1 m square cell, and would contain 100 elevation values within the same area represented by a 10 m resolution DEM. The 1 m resolution DEM has a higher resolution than the 10 m DEM. The larger the pixel the lower or coarser the resolution, and the larger the impact of smoothing caused by interpolation (Gaveau and Hill 2003).

The opportunity for error propagation exists in every step of DEM generation. In fact, there is little probability that all elevations in any DEM are correct, thus endemic

error may exist in many DEMs (Fisher and Tate 2006). LiDAR users usually rely on the DEM provider to provide nominal accuracy specifications for the raw data (McGaughey et al. 2004). The majority of accuracy standards to date are based on a finite sample of ground control check points obtained by real time kinematic (RTK) GPS. The elevations obtained by LiDAR are compared to those taken during the ground control check process and the residual error is then presumed to follow a statistically normal distribution. A problem with this presumption is that errors may be prevalent in LiDAR elevations captured over non-open terrain. In a forest, these errors are generally positive in value, in other words the LiDAR derived elevations are usually higher than those on the actual ground surface. These errors are most often a result of false ground samples where the LiDAR returns are actually from low vegetation and logs (Reutebuch et al. 2003; Hodgson and Bresnahan 2004; Aguilar and Mills 2008; Liu 2008).

Canopy cover is defined as “the ground area covered by the crowns of trees or woody vegetation as delineated by the vertical projection of crown perimeters. It is commonly expressed as a percent of total ground area (USDAFS 1998).” Canopy cover may have a significant impact on ground elevation accuracy for two main reasons. First, the percentage of laser pulses that strike the ground surface is directly related to the amount of canopy cover. The greater the canopy cover, the fewer the number of pulses that reach the ground, thus reducing the density of LiDAR points used to interpolate the elevation surface. Additionally the smaller the LiDAR footprint, the better the chances that a laser pulse will pass through breaks in the

canopy. Second, understory vegetation may be mistaken for ground points resulting in overestimation of ground heights (Gaveau and Hill 2003; Leckie et al. 2003; Lim et al. 2003; Andersen et al. 2006; Falkowski et al. 2008)

Background

Chen (2007) argues that discrete-return LiDAR can achieve better tree height accuracy than that gained by field measurement, and that LiDAR may be used as ground truth height information. Previous research has found error in LiDAR tree height measurement. Some of this error can be attributed to the difficulty LiDAR has in hitting the actual apex of the conifer tree species, but LiDAR terrain measurement error may also significantly impact tree height measurement error (Andersen et al. 2006). Leckie et al. (2003) found overall tree height measurement underestimation of 1.56 m (SD 0.77 m) based on the maximum LiDAR elevation hit. To distinguish LiDAR height error measurement caused by missing the tree apex from DEM error they also compared LiDAR heights to ground measured heights to the highest whorl of branches where definite laser pulses strike. After subtracting the mean ground measured height of 0.37 m to the top of the leader (tree apex) from the highest whorl, a tree height error of over one meter remained. They suggest the tree height error was due to two possible causes within their study area. The first potential cause is that dense undergrowth vegetation at a height ranging from 0.5-2.0 m may have caused false ground heights in the DEM. The second potential cause is that the study site's ground truth microrelief around the base of trees varied an estimated 0.5 m compared to the generalized LiDAR height model of the same location.

The relative accuracy of LiDAR for establishing elevations has been studied but little empirical research exists that examines the vertical accuracy of DEMs created from LiDAR data (Leckie et al. 2003; Reutebuch et al. 2003; Hodgson and Bresnahan 2004). LiDAR elevation model accuracies have been found to be as accurate (Kraus and Pfeifer 1998) or better than those generated by photogrammetric means (Carson and Reutebuch 1997; Reutebuch et al. 2003; Fisher and Tate 2006). However, potentially more sources of error exist within LiDAR derived elevations than those produced through photogrammetric means (Fisher and Tate 2006). While typical elevation accuracies stated by LiDAR vendors is around 0.15 m root-mean-squared-error (RMSE), this accuracy is generally only achievable under ideal circumstances such as those found in flat, open terrain (Reutebuch et al. 2003; Hodgson and Bresnahan 2004; Su and Bork 2006). In the last decade, empirical studies have found LiDAR elevation accuracies ranging from 0.26 m to 1.53 m RMSE (Hodgson and Bresnahan 2004)

Kraus and Pfeifer (1998), in a relatively early study of terrain models created from LiDAR data in wooded areas of Vienna Austria, state that DEMs created from LiDAR data in open areas have the same accuracy as DEMs created through photogrammetric techniques. The overall DEM elevation accuracy reported in their pilot study was ± 0.57 m mean square error (MSE). In addition, they found flat terrain accuracies of ± 0.25 m, and that with data processing improvements they estimate that accuracies of ± 0.10 m MSE are possible. They also state that at the time of the study, important geomorphologic features in general such as ditches were often missed by the DEM.

This was primarily attributed to the commercially available scanners at the time having poor data density quality.

Gomes-Pereira and Janssen (1999) in another early study focused on analyzing the suitability for LiDAR DEMs in road planning applications in the Netherlands compared LiDAR derived 1 m post spacing DEM elevations to those determined by photogrammetric measurements. The LiDAR elevation accuracy was determined to range from 0.08-0.15 m RMSE on flat terrain. On sloping terrain the RMSE increased to between 0.25 m and 0.38 m. The overall project RMSE was 0.29 m.

Reutebuch et al. (2003) compared 1.5 m post spacing DEM elevations derived from LiDAR data under forest canopy to checkpoints located by total station traverse initiated from survey grade GPS control points. This comprehensive study was in Western Washington on terrain varying between 140 m and 400 m in elevation. They compared 347 checkpoints located in a four various canopy conditions including clearcut, heavily thinned, lightly thinned, and uncut. The mean error (ME) in elevation between the LiDAR DEM and the checkpoints was 0.22 m (0.24 m Standard Deviation (SD)). The range of these elevation differences was -0.63 m to 1.31 m. The elevation ME for clearcut, heavy thinned, lightly thinned, and uncut canopy classes was 0.16 m (0.23 m SD), 0.18 m (0.14 m SD), 0.18 m (0.18 m SD) and 0.31 m (0.29 m SD) respectively.

Hodgson and Bresnahan (2004) empirically found a DEM elevation error range between 0.17 m and 0.26 m RMSE in different land-cover classes. They compared 2 m post spacing DEM elevations to elevations determined from points surveyed with

either high order horizontal and vertical control or only vertical control. The areas with the lowest elevation error included conifer forest, pavement and high grass, whereas areas of deciduous forest (leaf-off) and brush or low trees had the highest errors. The study area was in central South Carolina in Richland County. Hodgson et al. (2005) conducted a similar study located in the Piedmont area of North Carolina, within terrain described as gently rolling with elevations ranging from 44 m to 136 m above mean sea level. They reported an error range from 0.15 m to 0.36 m RMSE. The highest error occurred in scrub/shrub land cover at 0.36 m RMSE. Errors in pine and leaf-off deciduous forest were approximately the same at 0.28 m and 0.27 m RMSE, respectively, while mixed forest error was lower at 0.24 m RMSE.

Su and Bork (2006) evaluated LiDAR derived DEMs with three main treatment effects of slope, LiDAR off-nadir sampling angle, and four dominant feature types consisting of upland grassland, deciduous forest [leaf-on trembling aspen (*Populus tremuloides*)], shrubland, and riparian meadow. Additionally they evaluated measurement error in three different interpolation methods including kriging, splining, and inverse distance weighting (IDW). The study was conducted at the University of Alberta Kinella Research Station located 150 km SE of Edmonton, Alberta, Canada on a rolling hill, glacial moraine landform. Prior to investigating the treatment effects named above, Su and Bork (2006) assessed interpolation accuracy by comparing discrete LiDAR points to interpolated DEM elevations at the same horizontal location using a jack-knife statistical procedure for all data and again for data collected on slopes exceeding 15º. They reported mean error values of 0.0035 m (RMSE 0.133 m),

0.0028 m (RMSE 0.140 m) and 0.0028 m (RMSE 0.116 m) for kriging, splining, and IDW, respectively. When limiting the data to slopes above 15º, they found mean error values of -0.0063 m (RMSE 0.200 m), -0.0060 m (RMSE 0.205 m) and 0.0018 m (RMSE 0.186 m) for kriging, splining, and IDW respectively. With respect to vegetation types, elevations determined on a DEM interpolated by IDW were compared to those determined by total station survey. ME values of 0.20 and -0.22 m for deciduous forest and lowland meadows, respectively, were reported. The reported overall project average IDW derived DEM elevation error and RMSE was 0.02 m and 0.59 m, respectively, compared to total station surveyed stations.

Objectives

The accuracy of tree heights derived through LiDAR is partly dependent on the accuracy of the DEM that is used as the base datum or ground surface. The primary objective of this study was to determine the accuracy of LiDAR derived DEMs within a range of different forest canopy and topographic conditions. LiDAR derived DEM accuracy is assessed through comparison to elevations (orthometric heights) determined by trigonometric leveling with a digital total station.

To separate errors caused by interpolation, it is important to quantify the absolute elevation error resulting from LiDAR sensor measurements. Our second objective was to compare specific elevations determined by trigonometric leveling to the closest ground elevation determined by the closest discrete LiDAR ground point.

A third objective was to compare elevations measured by a mapping grade GPS receiver under various forested canopy conditions to DEM interpolated elevations created from trigonometric leveling measurements.

A fourth objective resulted from serendipitous discovery. Based on higher elevation accuracies than expected achieved by mapping grade GPS under some forest canopy conditions, we chose to compare elevations determined by mapping grade GPS to the vendor provided DEM interpolated from LiDAR.

Total station data were collected on five of eleven hectare sized plots in the study, thus the first three objectives were met using the five total station plots. The GPS data were collected on all eleven plots. Table 3.1 provides clarification on which instruments were used to collect plot data.

Table 3.1. Field plots and data measurements technologies. An X indicates whether a measurement technology was applied to the plot.

Plot	Total Station	ProXH GPS	GeoXH GPS	GeoXT GPS	LiDAR
C20				X	X
C27				X	X
C61				X	X
C110				X	X
E200	X	X			X
E412				X	X
O16	X	X			X
O69	X	X			X
U8	X		X		X
U13	X	X			X
U56		X			X

Methods

Study Area

The study was conducted in Oregon State University's (OSU) McDonald-Dunn research forest located just north-northwest of Corvallis, Oregon and minutes from the

OSU campus. The forest is approximately 5475 ha (McDonald Forest and Dunn Forest occupying approximately 2930 ha and 2545 ha respectively) ranging in elevation from approximately 75 to 660 m above sea level in the eastern foothills of the Oregon Coast Range. Conifers dominate the forest with Douglas fir (*Pseudotsuga* menziesii) and grand fir (*Abies grandis*) being the apex species. The primary deciduous tree species is bigleaf maple (*Acer macrophyllum*) and shrub species California hazel (*Corylus cornuta var. california*). The forest is intensively managed for research and education, and although the species composition does not vary significantly, there is great variation in stand age, density, and management history.

Figure 3.2. McDonald-Dunn Forest and surrounding communities within Oregon, USA.

Study Design

The original study design called for a total of twenty plots, five from each of four strata, but based on time and resources available eleven total plots were sampled. The plot strata consisted of old growth/mature (referred to as old growth in this study) (two plots), even-aged (two plots), uneven-aged (three plots), and clearcut (four plots). Each plot is hectare (100 m^2) in size and was selected by stratified random sampling using a numbered grid for each stratum and pseudo-random number generator software. Plot statistics are shown in Table 3.2. Plot naming corresponds to the silviculture treatment (C = clearcut; E = even-age; O = old growth; and U = uneven-age) and GIS grid number used for random selection.

The statistics in Table 3.2 are self explanatory with one exception. The "LiDAR Ground Pt/Total Density per m^2" category refers to the density of LiDAR points that were determined to be ground points (see "LiDAR Collection" in the methods section for explanation on ground point evaluation) and subsequently used for the ground file and DEM. The value for the "Total Density per m^2" is the total point density per square meter of all the laser points that reflected off an object in each plot. Vendors provide a system design parameter for the specific LiDAR instrument used to collect the mapping data. These values presented in Table 3.2 are significant for two reasons: 1) the values provided by the vendor are nominal and based on a density in a uniform, open setting, and does not necessarily represent realistic conditions, and 2) LiDAR collection in a forest equates to a truly three-dimensional environment. Regarding the first point, the density of the points that hit the ground is a function of both the system

capability and the density and structure of the vegetation that it must penetrate. The data provided for this project was collected with a “pulse rate designed to yield and average native density (number of pulses emitted by the laser system) of ≥ 8 points per square meter over terrestrial surfaces” (Watershed Sciences 2008). Note the ground point density decreases from clearcut values near 2 points per m^2, which is substantially less than 8 points per m^2 presumably due to the amount of vegetation near the ground and not inflated system capabilities, down to 0.32 points per m^2. This has a potentially significant impact on the accuracy of the DEM. It is also interesting

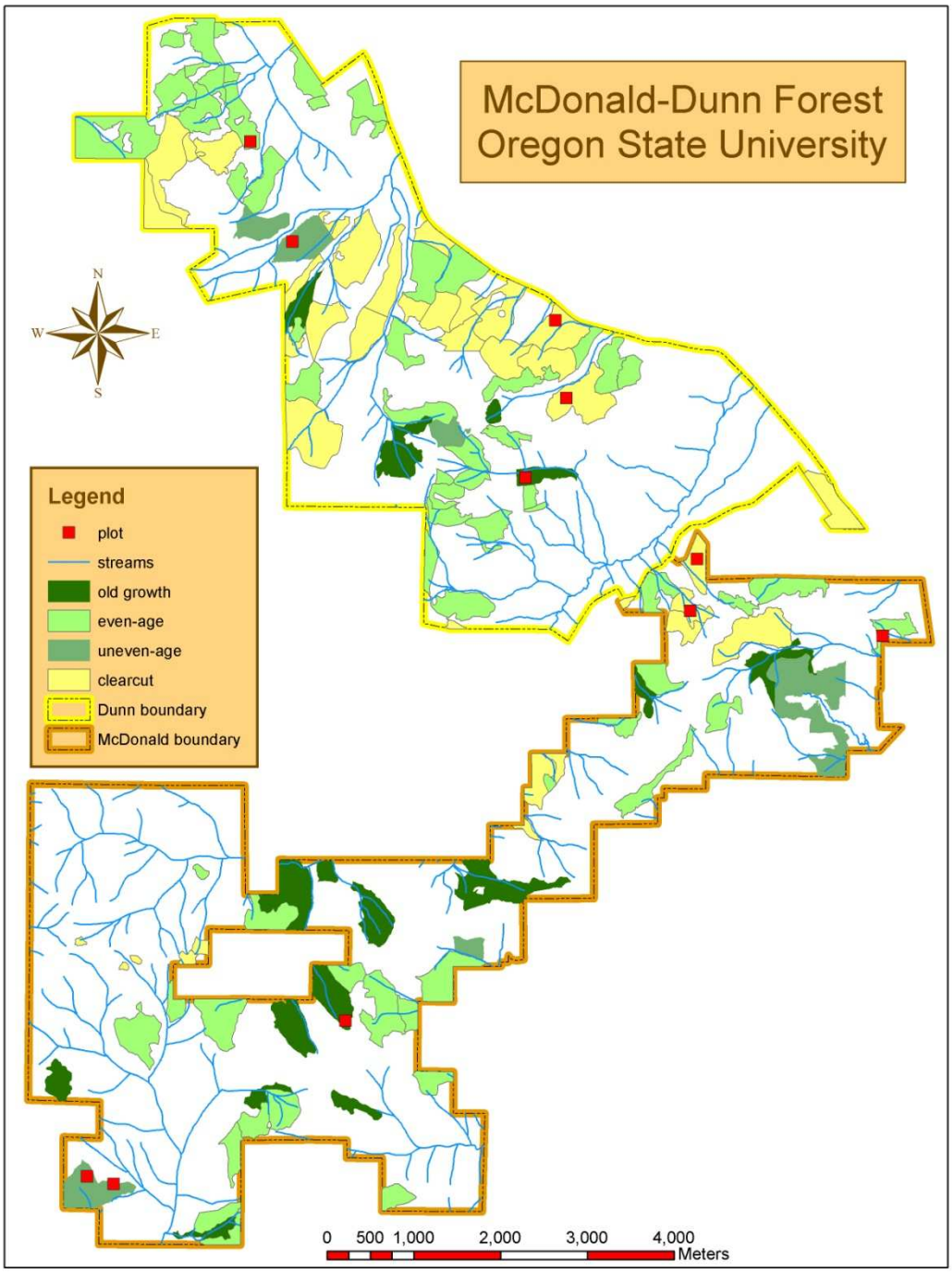

Figure 3.3. Plot locations in McDonald-Dunn Forest.

Table 3.2. Plot statistics for DEM elevation comparison. Total station elevations were collected on five plots while GPS receiver and LiDAR elevations were collected in all.

Plot	C20	C27	C61	C110	E200	E412	O16	O69	U8	U13	U56
Slope Aspect	NW	NW	NE	NE	E	NE	NE	N	E	SE	NE
Slope Degree	24	18	13	9	7	14	17	28	17	14	8
Slope Percent	45	32	22	16	13	25	31	55	32	25	14
GPS Point Count	703	744	538	702	1129	1008	780	238	192	679	1345
GPS Point Density per m^2	0.07	0.07	0.05	0.07	0.11	0.10	0.08	0.02	0.02	0.07	0.13
Total Station Point Count	N/A	N/A	N/A	N/A	1005	N/A	621	516	525	484	N/A
Total Station Point Density per m^2	N/A	N/A	N/A	N/A	0.10	N/A	0.06	0.05	0.05	0.05	N/A
LiDAR Ground Pt. Count	22157	19113	22189	17055	3503	8229	11994	11102	8287	8995	8094
LiDAR Ground Pt Density/Total Density per m^2	2.22/ 11.24	1.91/ 6.36	2.22/ 10.70	1.71/ 7.11	0.35/ 11.44	0.82/ 6.54	1.20/ 14.92	1.11/ 14.55	0.83/ 6.96	0.90/ 5.73	0.781 6.67
Tree Count	691	565	534	575	946	929	363	257	367	498	1255
Conifer	690	556	519	555	775	924	231	189	262	462	1035
Deciduous	1	9	15	20	171	5	132	68	105	36	220
Percent Crown Cover	11	9	10	9	65	27	47	46	43	38	70
*Stand Age yrs.	6	6	6	6	21	13	156	138	85	94	57

* Stand age in years based on oldest trees in the stand at time of LiDAR acquisition.

to hypothetically contemplate the number of points returned in a cubic meter. This of course varies depending on the vegetation attributes such as type, species, size, etc. In this study, the density of the canopy not only impacts the accuracy of the DEM, but also the ability to detect suppressed trees. In the even-aged plots this is not significant because the canopy is uniform and most of the trees should be detected.

The most significant impact is the uneven-aged stands where suppressed trees will likely not be detected when under a dense overstory tree. Increasing the pulse density

capability of a LiDAR system may help improve the accuracy of forest inventories in circumstances where voids are present in the LiDAR data due to the forest canopy. In areas with dense canopy such as triple canopy rain forests, however, the likelihood of penetrating the canopy is significantly decreased.

Reference Datums

There was some initial confusion on whether the LiDAR data were referenced to North American Datum (NAD) 83 (HARN) or NAD 83 (CORS96). The vendor report indicated NAD83 (HARN) but this seemed unlikely given the prevalence of NAD 83 (CORS96) as a standard datum for high precision data projects. It was determined during this research that the horizontal datum used for the LiDAR data were NAD83 (CORS96) (C. Cooper, personal communication, May 28, 2010). The LiDAR point positions were calculated using a smoothed best estimate of trajectory (SBET), which combines postprocessed aircraft position and attitude data. Height above ellipsoid (HAE) elevations were later converted to orthometric heights North American Vertical Datum (NAVD) 88 using a Geoid03 correction (Watershed Sciences 2008). Trimble GPS Pathfinder Office version 4.10 software was used to convert the LiDAR data to NAD83 (CORS96). The total station coordinates were collected using a local coordinate system and later transformed using the National Geodetic Survey (NGS) Online Position User Service (OPUS) solution. OPUS provided the solution for control stations using the NAD83 (CORS96) horizontal datum and NAVD88 vertical datum using a Geoid03 correction. The ground truth GPS data were collected using World Geodetic System (WGS) 84 and postprocessed using Trimble GPS Pathfinder

Office version 4.10 software to convert to NAD83 (CORS96) horizontal datum and NAVD88 vertical datum using a Geoid03 correction.

Applying the correct vertical datum was critical in this research to determine the vertical accuracy of the LiDAR datum. To determine the elevation of a point on the ground, we are concerned with three heights: ellipsoid height (h), orthometric height (H), and geoid height (N). Ellipsoidal height is the vertical distance from the reference ellipsoid to a point on the earth's surface. Elevations determined by GPS are ellipsoidal heights. Orthometric height is the vertical distance from the geoid to a point on the earth's surface. Geoid height is the distance from the reference ellipsoid to the geoid. All distances are measured perpendicular/normal to the reference surface (Wolf and Ghilani 2002; Van Sickle 2008).

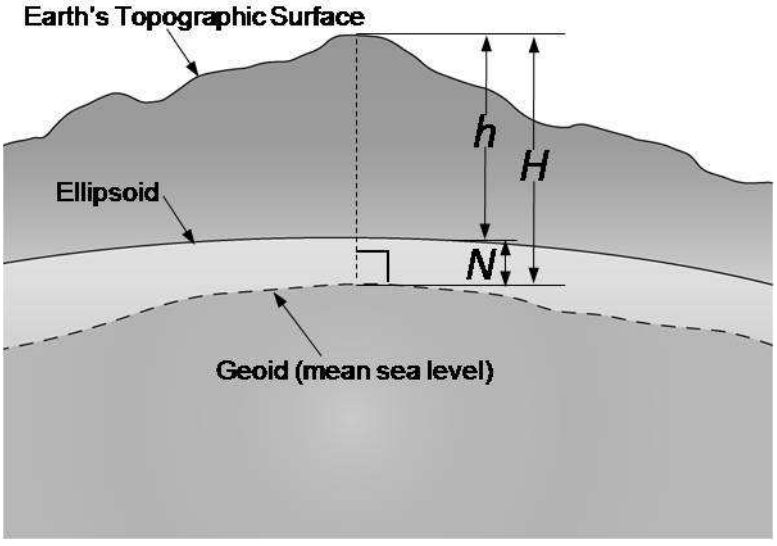

Figure 3.4. Height relationships between orthometric height H, ellipsoid height h, and geoid height N.

To determine the geoid height in our study area we calculated the vertical distance by subtracting the ellipsoid height from the orthometric height using measurements taken in plots within the southwest, eastern, and northwest extremes of the study area. Orthometric, ellipsoid, and geoid heights of these locations are shown in Table3.3.

Table 3.3. McDonald-Dunn Forest orthometric, ellipsoid, and geoid height relationships.

Plot	µOrthometric (H) meters	µ Ellipsoid (h) meters	Geoid Height (-N) meters
E200	132.78	110.58	22.20
E412	114.15	92.33	21.83
U13	268.96	247.02	21.94
		Average	21.99

The earth's gravity field is constantly changing, thus the geoid changes temporally and the vertical datum is updated periodically (Vanicek 1990). Although often referred to only as NAVD88, this vertical datum has various versions based on the geoid model used and is software dependent. Examples of continental United States (CONUS) NAD83 versions include geoids 96, 99, 03, 06, and 09(NGS 2010).

While investigating vertical datums to ensure that correct conversions were being applied by conversion software, we determined that the ArcGIS software version 9.3 uses NAVD88 based on Geoid96, although the metadata for this datum's projection file only specifies NAVD88, (ESRI Technical Support, personal communication, April 22, 2010). Trimble Pathfinder Office converts WGS84 GPS files to NAD83 (CORS96) and NAVD88 using the Geoid03 model. Table 3.4 illustrates the differences in Geoid96, Geoid99, and Geoid03 heights for the study plots measured with the total station in McDonald-Dunn Forest.

Table 3.4. McDonald-Dunn forest geoid model height differences (units are in m).

Plot	Geoid03 minus Geoid 99	Geoid03 minus Geoid 96	Geoid99 minus Geoid 96
E200	-0.08	0.09	0.17
O16	-0.09	0.09	0.17
O69	-0.08	0.09	0.17
U8	-0.09	0.08	0.17
U13	-0.09	0.08	0.17
Average	-0.08	0.09	0.17
SD	0.004	0.006	0.002

Horizontal location of the elevation measurements are also important as previous studies have determined that horizontal displacement can have a major contribution in vertical DEM error (Hodgson and Bresnahan 2004; Su and Bork 2006). Hodgson and Bresnahan (2004) calculated elevation error based on the vendor specification of horizontal error at 1/1000 of the flying altitude. For a flying height of 1207 m above ground level (AGL) this calculates to 1.20 m horizontal error, which they used further to calculate vertical error caused by horizontal displacement based on slope degree. For a mean slope range between 1.67º and 4.15º derived from a triangulated irregular network (TIN) they calculated a vertical error range from 0.025 m to 0.062 m RMSE. Later they estimated observed elevation error for mountainous terrain assuming a 25º slope and determined that the vertical error resulting from horizontal displacement would be substantial, increasing to 0.423 m RMSE. Su and Bork (2006) found vertical errors similar to Hodgson and Bresnahan (2004). Vertical errors associated with horizontal displacement on slopes <10 º were 0.08 m and 0.05 m RMSE for LiDAR and DGPS, respectively (combined LiDAR and DGPS RMSE =0.13 m). On slopes >10 º overall RMSE increased to 0.28 m. At their original inception WGS84 and

NAD83 only differed by one to two centimeters depending on location, however NAD83 (CORS96) differs from WGS84 by up to two meters (Van Sickle 2008), thus using the correct horizontal datum is critical in determining DEM vertical accuracy. Because this project converts GPS receiver data collected in WGS84 to NAD83, the OPUS solution uses NAD83 (CORS96), and the initial LiDAR survey control was thought to use NAD83 (HARN), we thought it necessary to understand the horizontal displacement that could occur if the wrong horizontal datum was used. We chose three plots to compare the original NAD83 datum to NAD83 (HARN) and NAD83 (CORS96). Plots E200, E412 and U13 are in the central east, northwestern and southwestern, portions of the study area respectively. We used Trimble Pathfinder Office 4.10 software to convert the GPS receiver data to NAD83 and NAD 83 (CORS96), and ArcGIS 9.3 software to convert to NAD83 (HARN). The need for two different programs was because ArcGIS had the coordinate file for the HARN conversion and Pathfinder Office did not. We then calculated the coordinate horizontal offsets (Table 3.5) between each point and its representation in the other datums. The average horizontal difference in McDonald-Dunn Forest between NAD83 and NAD83 (HARN), NAD83 (HARN) and NAD83 (CORS96), and NAD83 and NAD83 (CORS96) is 0.91 m, 0.69 m and 1.29 m respectively. The datum shift is illustrated in Figure 3.5, which are the mean center points of all GPS ground points collected in plot E200 shifted based on the respective NAD83 datum. This horizontal displacement could have significant impact on error calculation, thus illustrating the importance of using the correct NAD83 adjustment. Noting that the offsets between NAD83 and

NAD83 (CORS96) were consistent between each plot, and that the shift was inconsistent for each plot between NAD83 (HARN) and the other two datums we conducted further analysis. We used the online program North American Datum Conversion (NADCON) to adjust the same plot points from NAD83 to NAD83 (HARN) and found the same shift values and variation in the plots as those found using ArcGIS. We found no other software program or approach to compare NAD83 (HARN) to NAD83 (CORS96), thus we contacted NGS. According to Dave Doyle, the NGS Chief Geodetic Surveyor (D. Doyle, personal communication, January 20, 2011). NGS has no transformation routine between NAD83 (HARN) and NAD83 (CORS96) for two reasons. One reason is that horizontal shifts between the datums are generally quite small (< 10 cm) across the United States. The average positional difference in Oregon is approximately 6-7 cm, a difference practically impossible to accurately model at the national level with previous attempts resulting in a high standard deviation related to the shift. Secondly, the NADCON transformation from NAD83 to NAD83 (HARN) was restricted to a two-dimensional latitude and longitude shift. The recent NAD83 adjustments are now oriented to three-dimensional shifts. The development of a new adjustment model would require users retain original ellipsoid heights, something that most users do not consider. Finally, Mr. Doyle analyzed Table 3.5 and stated that the reported shifts appear accurate.

Table 3.5. Horizontal datum offset variation between NAD83, NAD83 (HARN) and NAD83 (CORS96) in meters.

Plot	X 83 minus X HARN	Y 83 minus Y HARN	83-HARN hor. diff.	X HARN minus X 96	Y HARN minus Y 96	HARN-96 hor. diff.	X 83 minus X 96	Y 83 minus Y96	83-96 hor. diff
E200	-0.47	0.76	0.89	-0.67	-0.16	0.69	-1.14	0.60	1.29
E412	-0.44	0.78	0.90	-0.70	-0.18	0.73	-1.14	0.60	1.29
U13	-0.51	0.78	0.93	-0.63	-0.18	0.65	-1.14	0.60	1.29
Average	-0.47	0.77	0.91	-0.67	-0.17	0.69	-1.14	0.60	1.29

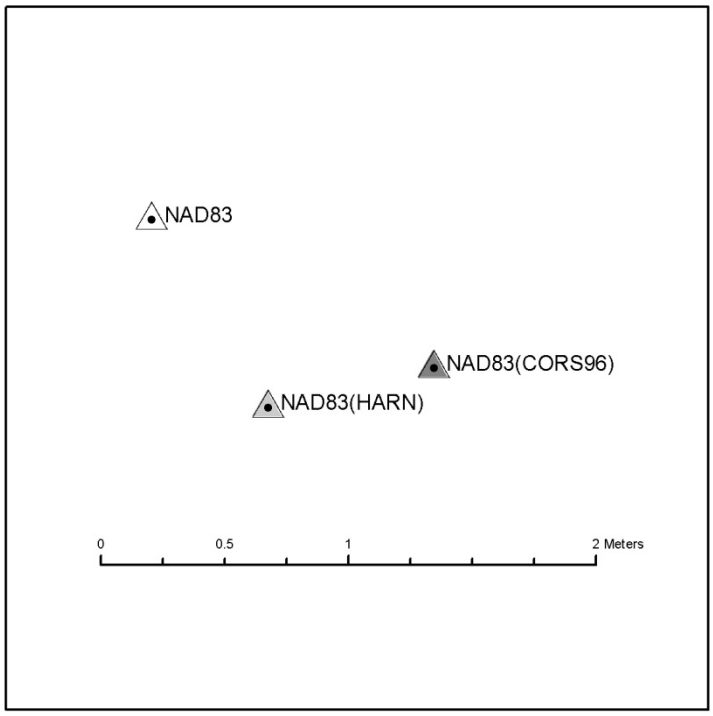

Figure 3.5. Plot NAD83 datum shift.

Total Station Survey

Digital total stations enable accurate measurements of distances, direction, and elevation differences between features. The output from a total station can take the form of coordinates (longitude, latitude, and elevation) that can support accurate DEM generation (Keim et al. 1999). Obtaining topographic elevations using a total station

instrument is known as trigonometric leveling, and involves measuring slope distance and vertical angles from a total station to target points. The elevation difference between two points can then be derived using right triangle relationships (Wolf and Ghilani 2002; Zhang et al. 2005). More accurate measurements are likely when using a fully automated and calibrated high accuracy total station instrument (Zhang et al. 2005). Fully automatic total stations are capable of automatically adjusting for programmed atmospheric conditions, i.e. temperature and barometric pressure, and measurements are made using laser sighting on a prism target, which avoids traditional manual telescopic sighting and associated instrument operator error. According to Zhang et al. (2005) trigonometric leveling still cannot replace first order level surveying in precise leveling in all circumstances but is feasible in some. Trigonometric leveling is certainly adequate for most forest surveying applications where highly accurate measurements are not critical.

A Nikon DTM 310 total station with a rated angular accuracy of five-seconds was used with a Seco single lens reflective prism target mounted on a survey rod to collect all elevation readings. A local coordinate system was used for initial measurements with coordinates being transformed afterwards for analysis. Of the plots surveyed with a total station, three plots were surveyed by closed traverse (plots E200, O16 and U13) while two others used a radial traverse method (plots O69 and U8). While the radial traverse method increases the speed of traverse measurements, no closure error is calculated as the instrument remains stationary throughout all measurements. Closure error is reported in Table 3.6.

Table 3.6. Total station survey closure error. A radial traverse was used for plots O69 and U8 and resulted in no closure statistics.

Plot	Northing Error	Easting Error	Elevation Error	Number of Positions
E200	-0.050	-0.030	-0.020	1104
O16	-0.136	-0.081	-0.020	698
U13	-0.060	0.220	-0.090	560
O69	Radial Traverse			539
U8	Radial Traverse			572

With the exception of the survey stakes used for traverse stations and control stations, the majority of the survey points are based on feature locations, i.e. trees and shrubs measured for a larger, capstone study, thus the method that the survey crew used for the closed traverse was to establish the first traverse station, measure as many features as possible within the plot and then establish the next traverse station, traversing the plot until closing on the first station. Traverse station locations were established using wooden survey stakes and tacks. We had the survey crew change the method to establishing all traverse stations first to ensure closure and then survey the plot features. The crew however missed the intent for closure and conducted a radial traverse. If additional traverse stations were needed, they were established as required. Plot O69 has no closure checks, but in plot U8 the crew made periodic checks on previously established traverse stations with the results shown in Table 3.7).

Table 3.7. Plot U8 traverse station error checks.

Point Number	Traverse station	Northing Error	Easting Error	Elevation Error
106	4	0.006	-0.008	0.005
185	1	-0.036	0.035	0.003
270	7	-0.002	0.026	-0.000
315	1	-0.193	0.231	0.035

Survey control was established to transform the local total station coordinates into a Universal Transverse Mercator (UTM), zone 10 North NAD 1983 horizontal map

coordinate system. A North American Vertical Datum 1988 (NAVD88) using geoid model 2003 (GEOID03) was established for elevations. Two TOPCON Hiper Lite Plus survey grade GPS receivers were used to establish static control for each plot. The National Geodetic Survey (NGS) Online Position User Service was used for postprocessing control station coordinates. The OPUS uses a network of independent single-baseline solutions from three of the closest surrounding Continuously Operating Reference Stations (CORS) to determine average GPS error and correct the user provided GPS coordinates. The peak-to-peak error is provided for each component of a coordinate (X, Y and Z). The peak-to-peak error is the error range between the maximum and minimum value obtained from the three baseline solutions (NGS 2009). Several attempts were made at establishing control over the actual traverse stations but the OPUS peak-to-peak errors were too high for project accuracy requirements. Plot U13 was the only plot with topographic and canopy conditions allowing for satisfactory peak-to-peak errors to establish control over previously existing traverse stations. The four remaining plots required GPS static control establishment outside the plot in an open area to allow for satisfactory peak-to-peak error. Two control stations were established within each plot in order to obtain a backsight and azimuth for a traverse survey. The final OPUS solutions and peak-to-peak errors for the control stations are shown in Table 3.8. The non shaded rows in this table correspond to stations used for closure in the control survey.

Table 3.8. NGS OPUS solution summary.

Reference Frame: NAD_83 (CORS96) UTM Coordinates							
Plot	Duration (hours)	Easting (m)	Error (m)	Northing (m)	Error (m)	*Ortho Height Z(m)	Error (m)
E200b	6.15	482024.719	0.204	4945933.535	0.139	114.094	0.195
E200r	5.93	482018.628	0.018	4945944.978	0.074	114.575	0.052
O16b	6.68	475491.850	0.066	4941412.936	0.004	479.964	0.047
O16r	2.98	475477.745	0.083	4941424.029	0.128	479.393	0.141
O69b	6.20	477742.706	0.010	4947675.503	0.107	259.127	0.063
O69r	6.05	477702.804	0.091	4947673.283	0.025	262.195	0.056
U8b	5.83	472868.793	0.045	4939445.087	0.823	233.164	1.819
U8r	5.43	472814.411	0.448	4939485.507	0.176	239.021	0.151
U13b	9.03	472599.549	0.341	4939711.154	0.667	279.502	0.818
U13r	8.73	472609.562	0.270	4939732.904	0.347	282.088	0.503

In the plot naming convention above “b” stands for base (receiver 1) and “r” for rover (receiver 2).
*Ortho heights are NAVD88 using Geoid 03.

The final processing step in the total station measurement processing was to transform the local coordinates by translating and rotating those measured for each measurement taken during the radial traverse into UTM North Zone 10 coordinates, NAD83 datum. Traverse PC software was used for this transformation.

The GIS software package ArcGIS 9.3 was used to interpolate the point elevation data collected using the total station. The ArcGIS 9.3 spatial analyst tool “Topo-to-Raster” was used, which applies the ANUDEM algorithm for interpolation. This algorithm, developed by the Australian National University, is capable of “burning” drainage channels into the DEM surface based on interpolated values in situations where sufficient ground control may not exist to create a hydrologically correct DEM (Yang et al. 2005). We chose not to enforce this drainage and rely on the interpolated values based on ground control. This was done by choosing NO_ENFORCE in the “drainage enforcement” option of the program. We left the default option of a maximum number of iterations to 40. Andersen et al. (2006) compared DEMs created

from various LiDAR point reduction percentages of a complete LiDAR dataset. They attributed increased elevation overestimation when the LiDAR data set was reduced and speculated that the ANUDEM interpolation algorithm may introduce systematic error in creating DEMs. These over estimations, however, were not statistically significant and limited to <0.03m when compared to a DEM produced from a full LiDAR dataset. ANUDEM may have a similar affect on the DEMs we created from the total station data based on the limited point density. Study site point densities for total station, GPS, and LiDAR measurements for each plot are shown in table 3.2.

GPS Survey

According to Li et al. (2005), GPS elevation points are not likely to match grid height points in any DEM. Although not specifically stated in Li et al. (2005), we interpret that the statement is based on the fact that DEMs are interpolated from relatively few discrete, known elevation points, and GPS receiver measurements are generally not used for DEM generation due to poor elevation precision and accuracy. There are few empirical studies to confirm this suggestion. At a coarse scale (10 m) relative to our research, Li et al. (2005) examined vehicular mounted GPS receivers collecting data on roads in Wales, United Kingdom compared to DTMs (DEMs) created by the British Ordnance Survey (OS) using a contour file. Three different interpolation methods (linear, bilinear, and biquintic) were used to obtain heights from the OS DEM. Several methods of collection were tested including autonomous coarse acquisition C/A code GPS, real-time kinematic (RTK), and post processed GPS using a road reduction filter (RRF). The RRF snaps the horizontal location of the coarse

acquisition (C/A) code GPS height readings to the road center line where the GPS readings were collected. The RRF algorithm first identifies what road the vehicle is traveling on by map matching to a finite set of possible locations in a digital road network and then computes errors based on the trajectory drawn using raw, uncorrected GPS positions received in the moving vehicle and digital road centerlines (Taylor et al. 2001; Blewitt and Taylor 2002). The source of the digital maps is stated in Li et al. (2005) as Ordnance Survey (OS) center line data without resolution specifics however Taylor et al. (2001) in a similar study used OS digital map data with one meter resolution centerline geometry. The RRF method significantly increased the GPS elevation accuracy when compared to autonomous C/A code GPS and real-time kinematic (RTK). The RRF GPS RMSE values ranged from 0.79 m to 0.82 m using the three different DEM interpolation methods.

In another course DEM study, Holmes et al. (2000) compared 252 post processed DGPS points collected using a Trimble 4400 GPS to a 30 m USGS DEMs created by contour digitizing from either photogrammetric sources or existing maps. The study was conducted in Sedgwick Natural Reserve located in the San Rafael Mountains of the California Coast Range. The elevation varied 1000 m within a 2700 ha study area in diverse terrain ranging from floodplain to low foothills and high relief. They calculated the DEM error by subtracting USGS nearest neighbor elevations from the GPS points. The reported error mean was -0.10 m (SD 4.11 m), thus indicating that the USGS overestimated elevation by an average of 0.10 m.

Clark and Lee (1998) investigated the accuracy of elevations for a precision farming study. They created topographic maps with GPS data collected using a Leica Wild SR299E base station with a Leica Wild SR399E rover. Two GPS collection modes were used: 1) In the stop and go mode, stationary GPS readings were collected for 4 seconds before moving to the next collection point, with data post processing occurring following collection; 2) the kinematic mode involved a tractor-mounted roving GPS receiver moving in a gridded pattern conducting a RTK survey. Vertical accuracy was reported using a concept described as “true error points.” The ten randomly placed true error points are control points collected with the base station receiver in rapid static configuration for 3 to 5 minutes. “Mass points” are GPS points collected by the rover GPS and are used to generate the topographic maps. The true error points are not used to create the topographic maps, but are used for the ground truth error calculation. Error is reported as the standard deviation of the difference between the elevation at the true error point compared to the topographic map at the same horizontal location. Stop and go error ranged from 0.02 m to 0.03 m. The error for the kinematic DGPS ranged from 0.03 m to 0.04 m. RTK error ranged from 0.04 m to 0.09 m. In a related precision farming study, Yao and Clark (2000) found that a single frequency GPS receiver rated with sub-meter accuracy can support DEM creation with a vertical accuracy in the range of 0.12-0.14 m. They used a Trimble Pro XRS with integrated GPS-Omnistar antenna mounted on an all terrain vehicle driving at a speed of 6-9 km and making 22 passes across a flat agriculture field located near Watkinsville, Georgia.

Sigrist et al. (1999) studied the impact of forest canopy on vertical GPS measurements using a Trimble ProXL mapping grade GPS in five locations. Canopy cover included an open agriculture field, broadleaf forest, and dense, mature white pine forest all within or near the Martell Experimental Forest located west of Purdue University in north-central Indiana. The mapping grade GPS measurements were compared to ones collected at the same locations surveyed using an Ashtech survey grade GPS. The results of the vertical comparison demonstrated a wide range of RMSE values from 0.77 m in the open to 11.89 m under pine canopy. In another study comparing a mapping grade GPS to a survey grade GPS, Yoshimura and Hasegawa (2003) used a Trimble Pathfinder Pro XR to collect at positions previously collected using a Trimble 4600LS. Autonomous and DGPS positions were compared. The positions were located on a forest landing under open sky, under Japanese cedar plantation canopy averaging 17.0 m in height, on a forest road, and in a natural broad leaf forest. Average autonomous error was calculated as 2.17 m, 4.23 m, 3.65 m, and 3.74 for the landing, plantation, road and natural forest, respectively. Average DGPS error was calculate at 0.44 m, 4.52 m, 4.90 m, and 4.17 m in the same respect.

In our study, three different Trimble mapping grade GPS receivers were used for GPS data collection. These included the GeoXT, GeoXH, and ProXH receivers. Based on funding and procurement time lag of the higher accuracy rated ProXH and GeoXH receivers, we chose to begin the project using the GeoXT receiver for data collection in the clearcut and younger even aged (E412) plots. All but one of the remaining plots were measured using the ProXH, and the final plot data (U8) was collected using the

GeoXH based on project time constraints. The GeoXT was configured using the Trimble Hurricane model external antenna while the GeoXH and ProXH were both configured with the Trimble Zephyr external antenna. Both the GeoXT and GeoXH do not require a data collector (field computer), but the ProXH does. A Trimble Ranger handheld data collector was used with the ProXH. A comparison of GPS receiver specifications is shown in Table3.9.

Table 3.9. Trimble ProXH, GeoXH and GeoXT specifications.

	Trimble ProXH	Trimble GeoXH	Trimble GeoXT
Channels	12 (L1 code and carrier/L2 carrier	26 (12 L1code and carrier, 12 L2 carrier)	14 (12 L1code and carrier, 2 SBAS)
Accuracy			
H-star postprocessed			Not Equipped
With internal antenna	0.30 m	0.30 m	submeter
With external Zephyr ant.	0.20 m	0.20 m	
Code postprocessed	0.50 m	0.50 m	0.50 m
Carrier postprocessed			
Tracking satellites 5 min	info not provided	info not provided	0.30 m
Tracking satellites 10 min	info not provided	info not provided	0.20 m
Tracking satellites 20 min	0.10 m	info not provided	0.10 m
Tracking satellites 45 min	0.01 m	0.01 m	0.01 m

Table adapted from Trimble (2006b; 2007; 2009a; 2009b)

We used the GPS data collection software Trimble TerraSync with consistent configuration settings throughout the survey. The receivers were set to collect UTM zone 10 north coordinates and within theWGS84 datum. To reduce using satellites at risk of errors associated with ionospheric and tropospheric attenuation we used a 15 degree horizon mask. Lower position dilution of precision (PDOP) values promote higher GPS accuracies and we chose a PDOP mask of 6, which Van Sickle (2008) describes as typical. As previously discussed, multipath can degrade GPS accuracy. All three GPS receivers in this study were equipped with multipath rejection

capabilities (GeoXH and ProXH have Trimble H-star ® technology; GeoXT has EVEREST® technology) designed to aid in the detection and removal of multipath signals. We also used the Trimble TerraSync default SNR value of 39 dBHz which is recommended by the manufacturer and in the middle of available settings between 33 dBHz and 43 dBHz (Trimble 2006a).

This study is part of a larger forest mensuration research project, thus each GPS measurement was based on the location of a specific feature, e.g. tree, shrub, log end, etc. The GPS receiver and antenna were attached to a pole with the antenna mounted 2.2 meters above the ground to avoid multipath and/or signal attenuation from the ground and operator. Large tree locations were measured using a two meter offset. All others were generally measured at the feature location. A minimum of thirty and usually not more than sixty points were collected per position. Once the plot data collection was completed, the GPS receiver files were downloaded and differentially corrected using Trimble Pathfinder Office version 4.10. Each file collected using the GeoXT was differentially corrected using course acquisition (C/A) code processing using multiple base station providers selected through proximity to the plot and an integrity index. The original intent was to collect data using dual frequency carrier phase ranging, however when differentially correcting the data, no carrier phase data corrections were possible. The integrity index value ranges from zero to 100 and indicates the reliability of the provider and its likelihood of providing quality results. Higher integrity values are preferred for GPS data collection (Trimble 2008).The closest available base providers were chosen, unless the integrity index was below 80.

We selected this threshold because a priori knowledge indicated that integrity index values above 80 were consistently achievable. Each file collected using the ProXH or GeoXH receiver was differentially corrected with automatic carrier and C/A code processing using multiple base station providers and integrity index. By selecting the automatic carrier and code processing in Trimble Pathfinder Office, the software analyzes the average code processed position and average carrier processed position, and selects the position with the least amount of error. When using the multiple base provider option, Pathfinder Office averages the coordinate data from each base station provider in the group, weighting the closer base provider higher to determine a single position solution. Because WGS84 is the reference ellipsoid for GPS (Van Sickle 2008), we chose to collect positions using WGS84 in UTM zone 10 north. The OPUS solutions used for the total station solutions in this project are based on NAD83 (CORS96). We used Trimble Pathfinder Office software to convert from WGS84 to NAD83 (CORS96), and then combine the separate GPS files into one by exporting to an Environmental Systems Research Institute (ESRI) shapefile for later analysis in the ESRI ArcGIS software.

LiDAR Collection

The LiDAR data were collected on April 2, 2008 under clear, sunny weather conditions. The contractor who flew the LiDAR mission was Watershed Sciences based in Corvallis, Oregon. The contractor used a Leica ALS50 Phase II laser system with a ± 14º scan angle from nadir and pulse rate designed to achieve a point density of ≥ 8 points per square meter. To reduce laser shadows and increase laser coverage,

each flight line had ≥ 50% side-lap, which equates to ≥ 100% overlap throughout the study area. The system is capable of a maximum number of four returns per pulse. Positional coordinates of the airborne sensor and aircraft attitude (pitch, roll, and yaw) were recorded continuously throughout the survey mission to accurately solve for northing, easting, and elevation laser point coordinates. The onboard differential GPS unit measured aircraft position twice per second (2 Hz) and the inertial measurement unit (IMU) measured aircraft attitude 200 times per second (200 Hz) (Watershed Sciences 2008). Ground control was conducted simultaneously with the airborne LiDAR survey using a static GPS located over ground stations with known locations at a rate of one point collected per second (1 Hz) with indexed time. The ground station information provided by the contractor is in Table 3.10. The static GPS data ground control positions were post processed following the airborne survey using CORS and verified using NGS OPUS to quantify daily variance. An additional RTK GPS survey was conducted collecting 510 locations in a limited and open area in the northern portion of the study area (Figure 3.6) for ground truth confirmation of LiDAR point coordinates (Watershed Sciences 2008).

Table 3.10. Base station survey control coordinates for LiDAR survey.

	*Datum: NAD83 (CORS96)		GRS80
Base Station	Latitude	Longitude	Height Above Ellipsoid (m)
McDunn1	44º 42’ 48.40874”	123º 17’ 54.20724”	80.94
McDunn2	44º 42’ 47.73917”	121º 17’ 53.85155”	81.73

*Later determined in this research to be NAD83 (CORS96).

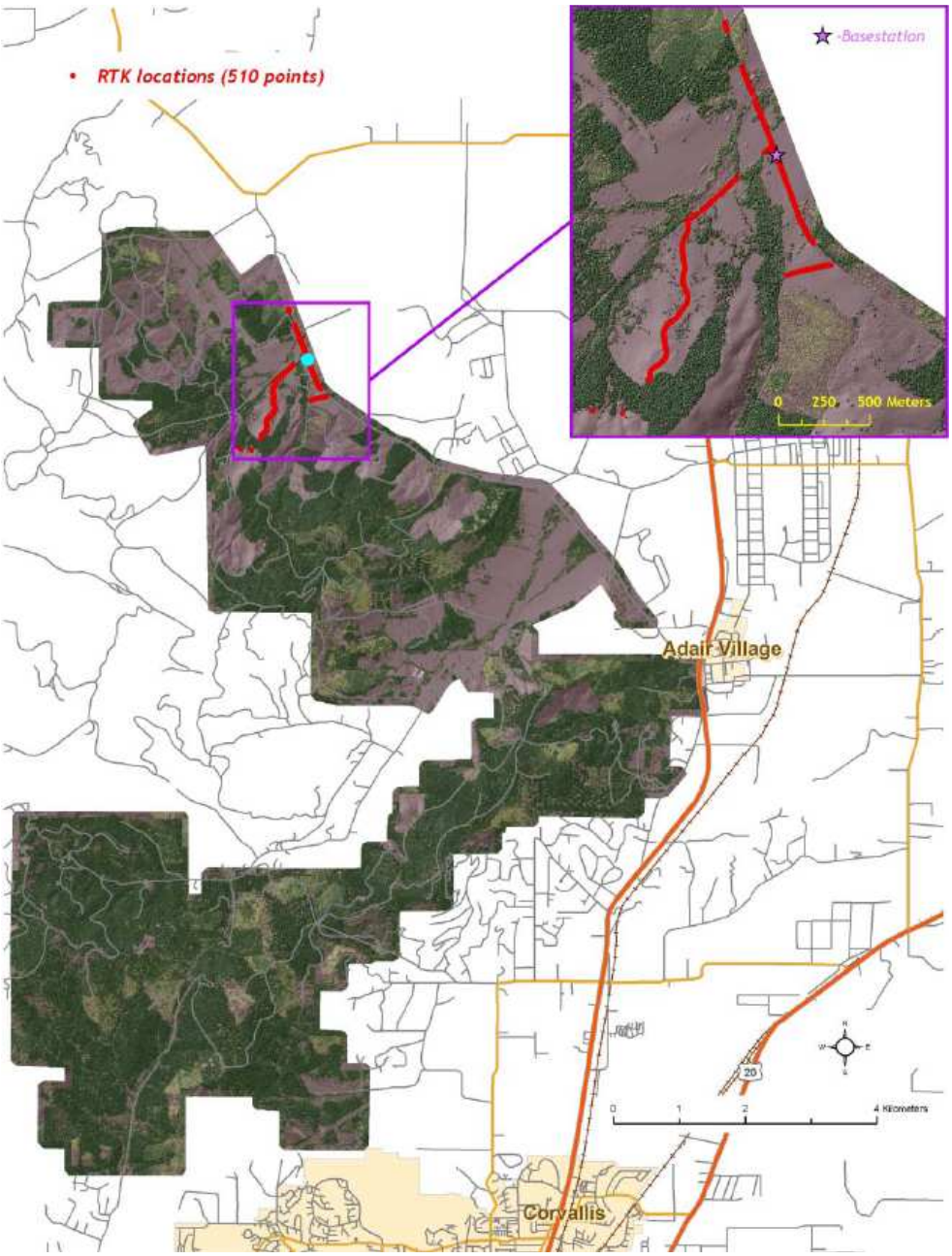

Figure 3.6. Map of LiDAR survey control base stations and RTK positions (Watershed Sciences 2008).

Laser point coordinates were computed with Leica Inertial and Positioning System (IPAS) and Airborne Laser Scanner (ALS) post processing software, then resolved to correct for aircraft pitch, roll, heading, and scale and finally filtered for non-terrestrial

returns caused by birds, vapor, haze, etc. Internal calibration of the LiDAR data were refined using TerraMatch software in which automated sensor attitude and scale corrections yielded 0.03-0.05 m relative accuracy improvements, and then GPS drift was removed per flight line improving relative accuracy by < 0.01 m. TerraScan software was used to classify and model near-ground points, which were then manually inspected and refined for improved ground detail and modeled again (Watershed Sciences 2008). A DEM was generated from a triangulated irregular network (TIN) created from the ground classified LiDAR points with a modeling algorithm within TerraSolid software. Raster tiles were then created and later merged into a DEM mosaic (M. Hey, personal communication, April 20, 2010).

The LiDAR data accuracy was described by the vendor as the mean error and standard deviation of the LiDAR point coordinates compared to RTK surveyed ground point coordinates. Reported laser point density and accuracy are shown in Table 3.11.

Table 3.11. Laser point density and accuracy reported by vendor.

	Target	Reported
Average First Return Point Density	≥ 8 points/m^2	10 points/m^2
Average Ground Point Density		1.12 points/m^2
Vertical Accuracy (1σ)	< 0.13 m	0.02 m
Average Relative Accuracy		0.053 m
Absolute Accuracy		0.026 RMSE
Absolute Z Accuracy		0.007 ME, 0.026 SD

Data provided by the vendor included the following: raw LiDAR point data in .LAS format of ground classified points, first return points, and all four laser returns with X, Y, Z coordinates and intensity values; bare earth DEM and highest hit model in one-meter ESRI grid format; and one-half meter intensity images in GeoTIFF format. No multispectral imagery was acquired for this project. The raw LiDAR file format has a

.LAS extension. This is not an acronym, but is derived from the American Society of Photogrammetry and Remote Sensing (ASPRS) file format stemming from LASer. "The LAS file format is a public file format for the interchange of LIDAR data between vendors and customers" (ASPRS 2009).

Geographic Information System (GIS) Processing

Error in DEMs is most commonly reported by root mean square error (RMSE), and has become standard in map accuracy reporting. Based on this formula error always computes to a positive number, thus it is not necessarily a good illustration of the error distribution because it does not show the direction above or below in the elevation error (Fisher and Tate 2006). The formula for RMSE is

$$RMSE = \sqrt{\frac{\sum(Z_{ref} - Z_{DEM})^2}{n}}$$

where Zref is a measured or derived elevation value, ZDEM is a DEM elevation value, and n is the number of observations. Another commonly used DEM error statistic is mean error (ME). Because ME can either be positive or negative, thus illustrating any bias in the model, some researchers consider it to be a more complete error description when reported with an error standard deviation (S) (Fisher and Tate 2006).

$$ME = \frac{\sum(Z_{DEM} - Z_{Ref})}{n}$$

$$S = \sqrt{\frac{\sum[(Z_{DEM} - Z_{Ref}) - ME]^2}{n - 1}}$$

Because ME illustrates the vertical bias, thus displaying whether the DEM tends to estimate elevations above or below the “true” elevation, we prefer ME, however we use the typical standard deviation, and for comparative results to other studies we have given both ME , sample standard deviation (shown in the tables as SD) and RMSE in our tabular results.

$$SD = \sqrt{\frac{\sum\left(Z_{DEM} - Z_{Ref}\right)^2}{n-1}}$$

To compare ground surveyed elevations determined by total station and GPS to the LiDAR estimated elevations, two methods were applied. First to compare the ground surveyed elevations to the LiDAR DEM, ESRI ArcGIS software was used to overlay the ground surveyed points on the LiDAR DEM and run a “zonal statistics” process. Zonal statistics associate a DEM elevation to the ground surveyed point based on its horizontal location and generates an output database that contains the association. The elevation determined by zonal statistics was then subtracted from each ground surveyed point elevation to determine the error point by point, from which ME, SD, and RMSE were calculated by plot. Second, to compare the ground surveyed elevations to the closest discrete LiDAR point elevation, ArcGIS was used to perform a one-to-one spatial join. The spatial join results in an association of the closest LiDAR elevation point to each ground surveyed elevation. Each matched LiDAR point was subtracted from the ground survey point to calculate the elevation error. Three databases were then created that contained comparative results for all points,

points within one meter of each other, and points within a half meter of each other. The ME, SD, and RMSE were then calculated by plot for all three databases.

Based on the nonparametric characteristics of the plot elevation data, we chose to compare the differences in elevation measurement results and determine the statistical significance in the differences using the Wilcoxon rank-sum test (also referred to as the Wilcoxon-Mann-Whitney test or Mann-Whitney test). The Wilcoxon rank-sum test allows us to ask whether two compared elevation measurement methods (treatments) in each respective plot contain similar mean elevation values. The null hypothesis (H_O) is that there is no difference between elevation means while the alternative hypothesis (H_A) is that elevation mean differences are not equal to 0.

Results

We used three main methods for comparing elevations: 1) discrete point to discrete point, 2) discrete point to DEM, and 3) DEM to DEM. The discrete point to discrete point method compared the ground surveyed elevations from both total station and GPS to the closest discrete LiDAR point elevations. The discrete point to DEM method compared the ground surveyed points collected with total station and GPS to the vendor provided LiDAR DEM. The DEM to DEM method compared our ArcGIS derived DEMs to the vendor provided DEM. Additional comparisons included total station derived DEM to GPS derived DEM and the effect of distance on elevation differences between ground surveyed points to the closest LiDAR elevation point.

ME and SD were calculated for LiDAR and mapping grade GPS derived DEMs compared to total station derived DEMs. Total station elevations are treated as ground

truth. Errors were determined by subtracting the LiDAR DEM and GPS DEM from the total station DEM using ArcGIS software. ME, SD, and RMSE were calculated for LiDAR DEM elevations compared to discrete elevation points collected by total station by calculating zonal statistics in ArcGIS. Zonal statistics assigned the LiDAR DEM elevation to each total station point in an output database, thus allowing for the subtraction of the LiDAR DEM elevation at the discrete total station point from the total station surveyed elevation at the same point. This also enabled manual calculation of RMSE, whereas ArcGIS did not calculate RMSE in the raster subtraction. ME, SD, and RMSE were calculated for LiDAR ground point elevations compared to the closest total station elevations. These result calculations are summarized in Table 3.12. ME, SD, and RMSE were also calculated from the comparison of mapping grade GPS elevations to LiDAR derived DEMs and closest LiDAR ground points. GPS elevations were treated as ground truth. The LiDAR DEM was compared to both GPS discrete elevations and GPS derived DEMs. These error calculations are summarized in Table 3.14.

Total Station and LiDAR Elevation Comparison

Total station data were collected in five of the eleven study plots. LiDAR elevation points compared to total station elevations resulted in ME values ranging from -0.06 m (SD 0.37 m) to -0.60 m (SD 0.17 m) (Table 3.12). All ME values were negative indicating that the LiDAR elevations are above total station elevations on average. Although ME values were as high as -0.60 m, none of the point-to-point comparisons displayed a statistically significant difference in mean values based on Wilcoxon rank-

sum test p-values > 0.18. These statistics are based only on LiDAR points that were within half a meter of a total station point. As discussed in the background section above, horizontal displacement can have an impact on elevation error. Many of the closest LiDAR points to total station points were between 0.5 and 1.0 meter apart and some were further than 1.0 meter apart. We chose 0.5 meters based on half the distance of a one meter resolution DEM used in the study. Table 3.13 displays the statistics for the LiDAR elevation point to total station point one-to-one comparison for all points, points within one meter, and points within one-half meter. Counter to expectations, the mean error did not improve in four of the plots, and only improved by 0.02 m in plot E200 as the comparison data were reduced to only those points within half a meter of each other, and in three of the plots the ME actually increased, but only slightly. In all plots, the SD decreased when limiting the data set from all the closest points to points within half a meter. The plot with the least amount of LiDAR ground points within a half meter of a total station point was E200. The high density of even-aged trees in this plot likely limited the LiDAR canopy penetration to the ground.

Table 3.12. Elevation difference between total station (TS) point and DEM compared to LiDAR DEM and total station DEM compared to GPS DEM.

	Total Station Point minus LiDAR Point		Total Station Point minus LiDAR DEM		Total Station DEM minus LiDAR DEM		Total Station DEM minus GPS DEM	
	Error	*p*-value	Error	*p*-value	Error	*p*-value	Error	*p*-value
E200								
ME	-0.44	0.18	-0.45	0.01	-0.47	0.00	-1.33	0.00
SD	0.09		0.10		0.11		3.12	
RMSE	0.45		0.46					
O16								
ME	-0.36	0.52	-0.45	0.28	-0.35	0.00	-1.84	0.00
SD	0.12		0.18		0.19		5.22	
RMSE	0.38		0.48					
O69								
ME	-0.41	0.69	-0.56	0.53	-0.52	0.01	-1.74	0.00
SD	0.49		0.70		0.63		3.07	
RMSE	0.65		0.90					
U8								
ME	-0.06	0.91	-0.09	0.82	-0.04	0.20	-1.12	0.00
SD	0.37		0.41		0.45		3.38	
RMSE	0.37		0.42					
U13								
ME	-0.60	0.34	-0.50	0.28	-0.56	0.00	0.27	0.35
SD	0.17		0.19		0.23		2.02	
RMSE	0.63		0.54					

*Statistics are based on LiDAR points within 0.5 m of a total station point.

With the exception of plot U8, LiDAR DEM elevations compared to the discrete total station points had a ME around a half meter ranging from -0.45 m (SD 0.10 m) in E200 and O16 (SD 0.18) to -0.56 m (SD 0.70 m) in plot O69 (Table 3.12). Similar errors exist when comparing the LiDAR DEM to the total station DEM with a range in ME of -0.35 m (SD 0.19 m) in plot O16 to -0.56 m (SD 0.23 m) in plot U13. The LiDAR DEM in plot U8 had a low ME of -0.09 m (SD 0.41 m) and -0.04 m (SD 0.45 m) compared to discrete total station points and the total station DEM, respectively. In every comparison involving LiDAR measurements, ME is a negative value and indicates that, on average, LiDAR derived elevations are higher than ground truth elevations. In all but one of the plots, as ME decreases, SD increases. Plot O69 has the

highest ME and SD which stands to reason as this plot is on very steep and rugged terrain under old growth canopy with several downed logs.

Of the three different LiDAR to total station elevation comparisons in table 3.12, the point to point comparisons generally display the least ME values. Two exceptions to this are plots U8 and U13. Plot U8 error decreases from the point to point comparison by 0.02 m with the DEM to DEM comparison, and the plot U13 total station to LiDAR DEM comparison has the smallest ME among LiDAR measurement differences within that plot. The DEM interpolation has an obvious impact on ME. In most cases ME increased with interpolation when comparing the total station point to LiDAR DEM. The highest ME increase is displayed in plot O69 (0.15 m), which is likely due to the steep slopes where slight variation in horizontal distance results in rapid elevation change. ME on plot U13 decreased with interpolation -0.60 to -0.50 m, a 0.10 m difference. While the ME in U13 was consistent with three other plots, it was relatively high (-0.50) in comparison with plot U8. ME in plot U8 was less than 0.10 m for the total station point to LiDAR DEM comparison. Only 300 m separate these two plots with plot U8 having a greater canopy cover and slightly greater slope. There are many potential causes for the larger ME at plot U13, including survey crew error and relatively high peak-to-peak error of control stations (Table 3.8). The only plot that displayed statistically significant error between total station points and LiDAR points is E200 using all matched points (Table 3.13). The error was not significant using only those points within 0.5 m. Curiously this was the plot with the least slope in the study (13%, Table 3.2). Since this was a young even-aged stand with the second

greatest crown cover (65%), this likely had an impact on the accuracy of the DEM because it had the lowest number of LiDAR ground points. An important fact related to this is that this plot had a large area of redundant LiDAR sampling with sidelap in the flight path/LiDAR swath. As table 3.2 shows, the sidelap did not improve the ground point sampling count; the density of points was the least in all the plots due to the density of even-age stems and crown. One would presume that sidelap would improve the canopy penetration, but it is possible that canopy penetration requires an increased pulse rate, thus a greater sampling density. Comparing the total station points to the LiDAR DEM, ME generally increased with the exception of plot U13. The only plot displaying statistically significant ($p = 0.01$) mean elevation differences is plot E200. The error increases when comparing DEM to DEM. Although ME values change little from the total station point and LiDAR DEM comparison to the total station DEM and LiDAR DEM comparison, the mean elevation between the total station and LiDAR DEMs were all significantly different ($p \leq 0.007$) except in plot U8. The increase in error likely reflects error in the interpolation of the DEM because the errors in the total station point to LiDAR point comparison were not necessarily significant ($p > 0.18$). The LiDAR DEM is likely to reflect higher precision and accuracy than the total station DEM due to the far greater density of LiDAR points used in interpolating the DEM.

Table 3.13. Mean elevation error (ME), standard deviation (SD), and root mean square error (RMSE) of the closest LiDAR ground point to a total station point including all closest points, only the closest points within 1 m, and only the closest points within 0.5 m. Measurement units are in meters.

Plot	ME	Rank-Sum Test *p*-value	SD	RMSE	n
E200					
All	-0.46	0.01	0.19	0.49	1005
≤ 1 m	-0.44		0.11	0.46	466
≤ 0.5 m	-0.44	0.18	0.09	0.45	221
O16					
All	-0.35	0.35	0.27	0.44	621
≤ 1 m	-0.34		0.18	0.38	481
≤ 0.5 m	-0.36	0.52	0.12	0.38	304
O69					
All	-0.36	0.66	0.63	0.73	516
≤ 1 m	-0.38		0.54	0.66	441
≤ 0.5 m	-0.41	0.69	0.49	0.65	253
U8					
All	-0.06	0.85	0.40	0.41	525
≤ 1 m	-0.08		0.37	0.38	409
≤ 0.5 m	-0.06	0.91	0.37	0.37	205
U13					
All	-0.59	0.20	0.23	0.64	484
≤ 1 m	-0.59		0.20	0.63	415
≤ 0.5 m	-0.60	0.35	0.17	0.63	254

GPS Receiver and LiDAR Elevation Comparison

GPS receiver measurements were collected in all eleven study plots (Table 3.14). The clear cut plots, and one even-aged plot (E412) were collected with C/A code and the remaining plots were collected using C/A code and carrier phase frequencies. Plot E412 was generally free of GPS signal obstruction from canopy due to the relatively young age of trees within the plot with a few exceptions.

The following discussion relates to the unobstructed C/A code only GPS measurements in table 3.14. The elevation error between GPS points and LiDAR elevation points was relatively low and ranged from -0.50 m to 0.49 m. The plots with the lowest ME were E412 (-0.03 m) and C27 (-0.10 m). These ME values are similar

to the errors in the total station comparison noting that these data were collected under generally open sky conditions with little or no canopy obstruction. In comparing the GPS point data compared to the LiDAR DEM, ME ranged from -0.46 m (SD 0.41 m) to 0.53 m (SD 0.75 m). Although there is no consistency in the LiDAR DEM being above or below the GPS elevations, the ME absolute values are similar to those found when comparing the total station to the LiDAR DEM (Table 3.12). Although the highest error occurred on plot C20 (ME 0.53) where the most rugged terrain occurred with some slash, a similarly high (ME -0.46) occurred on plot C110 which was on relatively flat slope with little terrain variation. Plot C110 did have many perennial shrubs including poison oak (Rhus diversiloba) and Oregon grape (Mahonia aquifolium), which may have contributed to errors in the LiDAR DEM ground classification. The ME was generally improved over the point-to-point analysis when comparing the GPS DEM to the LiDAR DEM elevations plot by plot, although the range in elevation differences was slightly higher with ME values ranging from -0.45 (SD 0.32) to 0.59 (SD 0.64). The improvement is only slight, however, and the error actually increased on plot C20 and E412. In every case, the SD decreased as a result of interpolation smoothing. The least error occurred in plot C27 (ME -0.02 m, SD 0.34), which is surprising given that this plot had many large stumps and small slash piles that could have contributed to false ground identification.

Table 3.14. Elevation error (m) of carrier phase (Φ) with C/A code corrected and C/A code only corrected GPS elevation points and DEM compared to LiDAR.

Plot Statistic	Φ and C/A Code GPS Point minus LiDAR Point		C/A Code only GPS Point minus LiDAR Point		*GPS Point minus LiDAR DEM		*GPS DEM minus LiDAR DEM		TS DEM minus *GPS DEM	
	error	*p*-value	error	*p*-value	error	*p*-value	error	*p*-value	error	*p*-value
C20	Unobstructed GPS Signal (C/A Code Corrected)									
ME			0.49	0.50	0.53	0.42	0.59	0.08		
SD			0.72		0.75		0.64			
RMSE			0.87		0.92					
C27										
ME			-0.10	0.89	-0.04	0.91	-0.02	0.06		
SD			0.46		0.45		0.34			
RMSE			0.47		0.45					
C61										
ME			-0.36	0.38	-0.33	0.41	-0.35	0.08		
SD			0.39		0.40		0.33			
RMSE			0.54		0.51					
C110										
ME			-0.50	0.03	-0.46	0.01	-0.45	0.00		
SD			0.39		0.41		0.32			
RMSE			0.63		0.61					
E412										
ME			-0.03	0.63	0.21	0.39	0.15	0.00		
SD			0.78		0.92		0.65			
RMSE			0.78		1.40					
E200	Canopy Obstructed GPS Signal (C/A code and carrier phase corrected)									
ME	1.71	0.00	1.93	0.00	1.67	0.00	0.87	0.00	-1.33	0.00
SD	2.87		2.66		3.59		3.12		3.12	
RMSE	3.34		3.28		3.96					
O16										
ME	2.82	0.00	2.89	0.00	2.69	0.00	1.43	0.00	-1.84	0.00
SD	4.58		3.57		5.06		5.21		5.22	
RMSE	6.32		4.58		5.73					
O69										
ME	2.13	0.18	4.08	0.02	2.63	0.02	1.22	0.00	-1.74	0.00
SD	3.91		4.99		4.58		3.05		3.07	
RMSE	4.44		6.42		5.27					
U8										
ME	2.46	0.03	2.07	0.13	2.67	0.00	1.26	0.00	-1.12	0.00
SD	3.26		5.71		4.21		3.26		3.38	
RMSE	4.07		6.02		4.97					
U13										
ME	0.24	0.66	0.75	.022	0.27	0.54	-0.29	0.00	0.27	0.35
SD	1.55		1.66		2.33		2.02		2.02	
RMSE	1.56		1.82		2.34					
U56										
ME	1.61	0.00	2.31	0.00	1.79	0.00	1.71	0.00		
SD	3.05		3.46		3.56		2.50			
RMSE	3.45		4.16		4.18					

In comparing measurement differences from obstructed GPS data collected under canopy using carrier phase and C/A code differential corrections the error dramatically increased with the exception of one plot (Table 3.14). The GPS point to closest LiDAR point elevation comparison results in a ME range from 1.61 m to 2.82 m when excluding plot U13. The plot U13 ME of 0.24 m (SD 1.55 m) was low compared to the other plots. The ordinal variation in these plots compared to that of the total station to LiDAR (Table 3.13) does not display the same pattern from low to high error. In these comparisons all of the LiDAR ME's indicate that the LiDAR DEM elevations are below the GPS elevations with one exception. Observing the GPS to LiDAR elevation comparison for all plots (Table 3.15), in seven of the eleven plots when limited to only points within a meter or half-meter distance had little effect on the ME (0.00-0.07m) (Table 3.15). The ME in plot E412 improved by 0.13 m when restricting point comparisons to those within a half-meter. This improvement can be explained by the fact that this plot had a very high density of trees in its SW quadrant that severely restricted the number of LiDAR points that struck the ground. Plots O69 and U8 had the lowest density of GPS points compared to the other plots (Table 3.2). This low point density and relatively steep slopes in comparison to other plots appears to have contributed to the improvements in ME within plots O69 and U8. We cannot explain the error increase of 0.12 m in plot U13.

The comparison between GPS point to LiDAR DEM ME values ranged from 0.27 m (SD 2.33 m) to 2.69 m (SD 5.06 m) for GPS data collected under canopy (Table 3.14). With the exception of plot U13, the ME ranged from 1.67 m to 2.69 m. This

may be attributed mostly to canopy cover and steep slopes. Plot E200 (ME 1.67 m, SD 3.59 m) had a very high crown cover percentage and plot O69 (ME 2.63, SD 4.58 m) was on a very steep slope. Plot O16 was also on a steep slope and based on field measurement experiences it had the greatest slope variation of all study plots. The crown cover percentage was relatively high and included many deciduous trees. Plot U13 had low error values (ME 0.27 m, SD 2.33 m) and, although located on a relatively steep slope with many large canopy openings, had a relatively low tree/canopy density and was the only plot with a SE slope aspect (Table 3.2). In every case except plot U13 the GPS DEM compared to the LiDAR DEM had an improved ME over the GPS point to LiDAR DEM. The ME values ranged from -0.29 m (SD 2.02 m) to 1.71 m (SD 2.50). The SD values also improved in all but one plot (O16). The plot O16 increase in SD may be attributed to the high slope variation in the plot during field observations, which contributed to the high SD values. It appears that the GPS DEM interpolation caused a drop in the overall GPS plot elevation in comparison to the GPS points. The least amount of ME difference occurred in plot U56 (ME decrease = 1.79 m – 1.71m = 0.08) and the greatest amount was plot O69 (ME decrease = 2.63 m – 1.22 m = 1.41 m). This decrease in elevation however resulted in a slightly increased ME, but in the opposite direction on plot U13 (ME decrease = 0.27 m – (-0.29 m) = 0.56 m).

Since the errors dramatically increased in the LiDAR data collected with dual frequency GPS under canopy compared to the C/A code only GPS data collected in the open, we also analyzed whether C/A code only GPS elevations compared to

LiDAR elevation would differ from elevation comparisons from carrier phase and C/A code measurements. We used the point-to-point method and compared GPS elevations to the nearest LiDAR elevation point in plots with canopy cover. In every plot elevation ME increased with C/A code only GPS. With one exception the ME ranged from 0.75 m (SD 1.64 m) to 4.09 m (SD 4.99 m) (Table 3.14). The least amount of error increase occurred on plot O16 where ME only increased 0.07 m. The greatest error increase

Table 3.15. Mean elevation error (ME), standard deviation (SD), and root mean square error (RMSE) of the closest LiDAR ground point to a GPS point*, including all closest points, closest points within 1 m, and closest points within 0.5 m.

Plot	Points Used	ME	Rank-sum *p*-value	SD	RMSE	n	Mean Distance (m) between points	SD Distance (m) between points
Unobstructed GPS Signal								
C20	All	0.49	0.46	0.75	0.90	703	0.37	0.29
	≤ 1 m	0.49		0.74	0.89	687		
	≤ 0.5 m	0.49	0.50	0.72	0.87	568		
C27	All	-0.09	0.85	0.47	0.47	744	0.42	0.47
	≤ 1 m	-0.09		0.46	0.47	720		
	≤ 0.5 m	-0.10	0.89	0.46	0.47	567		
C61	All	-0.32	0.41	0.44	0.54	538	0.52	0.72
	≤ 1 m	-0.36		0.40	0.53	499		
	≤ 0.5 m	-0.36	0.38	0.39	0.54	402		
C110	All	-0.48	0.01	0.41	0.63	702	0.56	0.44
	≤ 1 m	-0.47		0.40	0.62	654		
	≤ 0.5 m	-0.50	0.03	0.39	0.63	379		
E412	All	0.16	0.56	0.94	0.96	1008	1.28	0.80
	≤ 1 m	0.02		0.87	0.87	406		
	≤ 0.5 m	-0.03	0.63	0.78	0.78	151		
Canopy Obstructed GPS Signal								
E200	All	1.72	0.00	3.56	3.95	1129	1.46	1.23
	≤ 1 m	1.71		3.15	3.58	495		
	≤ 0. 5 m	1.71	0.00	2.87	3.34	224		
O16	All	2.87	0.00	5.16	5.90	679	0.71	0.64
	≤ 1 m	3.00		5.30	6.09	527		
	≤ 0.5 m	2.82	0.00	4.58	5.38	326		
O69	All	2.43	0.04	4.63	5.22	238	0.62	0.49
	≤ 1 m	2.17		4.02	4.56	201		
	≤ 0.5 m	2.13	0.18	3.91	4.44	120		
U8	All	2.54	0.00	4.21	4.90	192	0.67	0.48
	≤ 1 m	2.61		3.97	4.75	150		
	≤ 0.5 m	2.46	0.03	3.26	4.07	81		
U13	All	0.12	0.59	2.29	2.29	679	0.94	1.06
	≤ 1 m	0.15		2.33	2.34	519		
	≤ 0.5 m	0.24	0.66	1.55	1.56	274		
U56	All	1.64	0.00	3.40	3.78	1345	0.87	0.82
	≤ 1 m	1.57		3.50	3.84	990		
	≤ 0.5 m	1.61	0.00	3.05	3.45	465		

*The GPS points used in this analysis were C/A code corrected in the unobstructed plots and in the obstructed plots they were C/A code and carrier phase corrected. This also applies to GPS points used to generate respective DEMs.

occurred in plot O69 where ME increased 2.33 m. This does not relate notable information regarding LiDAR elevation accuracy, but demonstrates that GPS elevation accuracy under forest canopy appears to be higher using the combined C/A code and dual frequency carrier phase ranging over C/A code only ranging in mapping grade GPS receivers, however in two of the plots (E200, O16) RMSE values decrease with C/A code only.

Most of the plots with unobstructed GPS reception did not display statistically significant elevation differences except in the GPS DEM to LiDAR DEM comparison. Three of five comparisons resulted in definitive significant differences with *p*-values < 0.00 and the remaining two had *p*-values of 0.08, which is marginally significant. This may be explained by the interpolation of relatively few GPS points compared to LiDAR points. Plot C110 was the only clearcut plot that included a large amount of short, woody ground cover including Oregon grape and poison oak. This likely had an impact on separating the ground points from vegetation. Plots C20 and C27 had a large amount of downed wood and slash piles. We noticed that these features were easily identified and separated from true ground points, thus they were likely removed by the vendor when creating the ground file. Most of the GPS to LiDAR comparisons collected under canopy reflected significant differences. Plot U13 was the only obstructed plot that did not demonstrate significant elevation differences and displayed relatively low ME in the phase and C/A code GPS to LiDAR point comparison. This is likely attributable to the relatively small crown cover (38%, Table 3.2), lack of understory vegetation, and easily identified large downed wood features.

Total Station to Differential Corrected GPS elevation

In comparing the LiDAR DEM to GPS-derived DEM it is important to understand whether the error is coming from the LiDAR DEM or the GPS measurements. For this research we could not compare the discrete elevation obtained by GPS and total station measurements because the coordinates from each were obtained based on tree and shrub locations within each plot. These measurements were also usually taken with a two meter offset at the field crews discretion, thus each GPS point does not necessarily directly match a total station point, even though they may be associated with the same feature. Consequently, we chose to compare the elevations between DEMs derived from total station and GPS measurements rather than pursuing a point to nearest point comparison.

In all but one of the plots the ME values are negative indicating that the mean GPS elevation values are above the mean total station values (Table 3.14). Excluding plot U13, the ME ranges from -1.12 m (SD 3.38 m) to -1.84 m (SD 5.22 m). In plot U13, the ME of 0.27 m (SD 2.02 m) is markedly smaller than the other plots, which coincidently is the same ME between the GPS point and the LiDAR DEM. The average error for the GPS DEM compared to the total station DEM (-1.15 m) is much higher than the average error for the LiDAR DEM compared to the total station DEM (-0.39 m). This indicates that greater elevation error is coming from the GPS than the LiDAR.

Discussion

LiDAR and Total Station Elevation Comparison

Of all the survey methods used in this study, the most trusted method for collecting horizontal and vertical coordinates is trigonometric leveling with a digital total station. We are unaware of a previous study where individual ground survey elevation points were compared to discrete elevations acquired using LiDAR. This may be due to the amount of ground truth points necessary to make a meaningful comparison. In this study we compared 3,151 elevations determined with a total station to the nearest LiDAR elevation point in five plots. We feel that this is the most meaningful comparison for LiDAR vertical measurements since it provides the best measurement of LiDAR absolute elevation accuracy. Using all of the nearest points, the lowest ME was -0.06 m (SD 0.40 m) and the highest was -0.59 m (SD 0.23 m) (Table 3.13). This varies only slightly from a data comparison that included only those nearest LiDAR elevation points that were within 0.5 m of a total station point. The LiDAR elevation accuracy in this comparison is higher in general than in the comparisons that involved DEMs.

A critically important elevation comparison for this investigation was the LiDAR DEM contrasted with elevations determined from the total station data. This is critical because this study is part of a larger forest mensuration study that compares tree heights estimated using LiDAR to those measured in the field. The LiDAR tree heights are based on the LiDAR DEM provided by the vendor. As discussed above, LiDAR tends to underestimate tree heights. Therefore we need to better understand if

this underestimation is due to the laser pulse missing the tree apex, elevation error in the DEM, or some combination of these two components. The LiDAR DEM error ranged from -0.09 m (SD 0.41 m) to -0.56 m (SD 0.70 m) (Table 3.12). The RMSE range in comparing the total station points to the LiDAR DEM was 0.42 m to 0.90 m.

The LiDAR DEM accuracies we determined are consistent with previous studies. Kraus and Pfeifer (1998) found an overall DEM accuracy of 0.57 m RMSE in wooded terrain in Austria. Gomes-Pereira and Janssen (1999) found DEM ME between 0.25 m and 0.38 m on sloping terrain. Hodgson and Bresnahan (2005) reported elevation errors in pine forest and leaf-off deciduous forest that were approximately the same at 0.28 m and 0.27 m RMSE respectively, while mixed forest error was lower at 0.24 m RMSE. The most similar research we found to our study was that conducted by Reutebuch et al. (2003), which was conducted various canopy conditions. The overall project DEM ME, SD, and RMSE were 0.22 m, 0.24 m, and 0.32 m, respectively, with a ME range of 0.16 m (SD 0.23 m) in clearcut stands and 0.31 m (SD 0.29 m) in uncut thick forest canopy. In our study the highest ME (-0.56 m) occurred in plot O69 (Table 3.12), which is located on very steep slopes (55%) in a 138 year old stand. The least amount of error (-0.09 m) occurred in plot U8 which is located on a relatively steep slope (32%) in an 85 year old stand. This further confirms that LiDAR is capable of achieving very high vertical accuracies under forest canopy and steep slopes, but at the same time these environmental characteristics can degrade the accuracy.

LiDAR and GPS Elevation Comparison

The GPS receiver analysis we conducted was similar to the total station comparisons in methods. Although we treated the GPS as the ground truth comparing elevations to the LiDAR, the LiDAR elevations and associated horizontal positions are likely more accurate and precise than mapping grade GPS receiver measurements. This portion of the research was really more of a study in mapping grade GPS elevation accuracy. This portion of the study demonstrates the error of mapping grade GPS elevation data, and that that accuracy is degraded with more severe forest conditions such as topography and canopy. Based on the dramatic overall increase in error in the GPS to LiDAR point comparison over the total station to LiDAR comparison, it appears that much of the elevation error may be attributed to the GPS receiver.

Like the total station comparison, the GPS point to LiDAR closest point comparisons gave us the best indication of LiDAR elevation accuracy because no interpolation is involved as there is with DEM generation. A total of 8,150 elevation locations were compared in eleven plots. In the open, GPS elevation accuracy is surprisingly high when compared to the LiDAR elevations. Using all positions, ME ranged from -0.02 m (SD 0.50 m) to 0.49 m (SD 0.75 m) (Table 3.15). Overall, using all the positions slightly improved the accuracy over limiting the matched points to closer than half meter. Analysis of the plots under canopy reveals that error significantly increases, and the accuracy did not improve using C/A code only, in fact it decreased. Error in the LiDAR points compared to all carrier phase GPS positions resulted in ME ranging

from a low of 0.24 m (SD 1.55 m) in plot U13 to a high of 2.82 m (SD 4.58 m) in plot O16 (Table 3.14). After the lowest ME of 0.24, the next lowest ME is 1.61 m (SD 3.05). Using the total station comparison as the criterion, we believe that these errors are more a reflection of GPS rather than LiDAR measurements. The low error in plot U13 compared to the other plots is likely due to several factors related to canopy cover. Plot U13 is an uneven-aged plot with many large canopy openings of well dispersed large trees. Using plot O16 with the highest ME as an example, although plot O16 had a greater number of ground points (11,994) compared to U13 (8,995) the ME was much higher (2.82 v. 024 m). The overall density is important and considering the spatial relationship of the density is also important. Although the ground point density was higher in plot O16, compared to U13 the gaps in ground points are larger where the canopy did not allow LiDAR to penetrate to the ground (Figure 3.7). These gaps could be responsible for some of the elevation error. The GPS points are also based on tree locations. Plot U13 had a lower average stand age (Table 3.2) and had many more small trees than did O16. These small trees tended to be in the open, and not under forest canopy, thus allowing for potentially more accurate GPS readings. Another observation comparing open plots to plots with canopy cover is that using all the matched GPS points tended to improve the overall accuracy in the clearcut plots as discussed above, but in the plots with canopy cover the opposite occurred. Under canopy conditions, using all the points in the GPS point to LiDAR point elevation comparison increased ME in contrast to limiting the matches to those less than half a meter away.

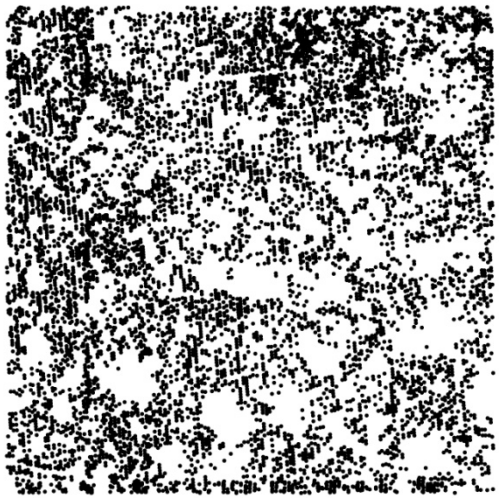

a) Plot U13 LiDAR ground points

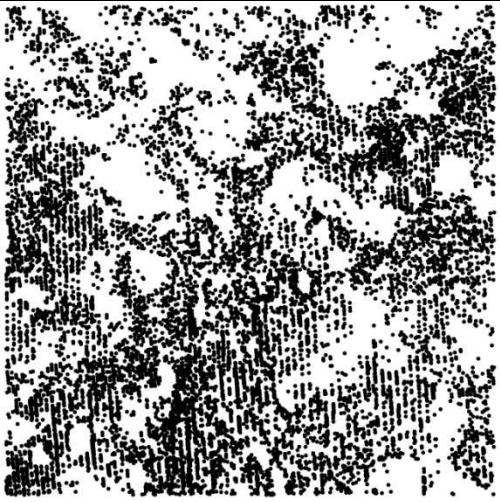

b) Plot O16 LiDAR ground points

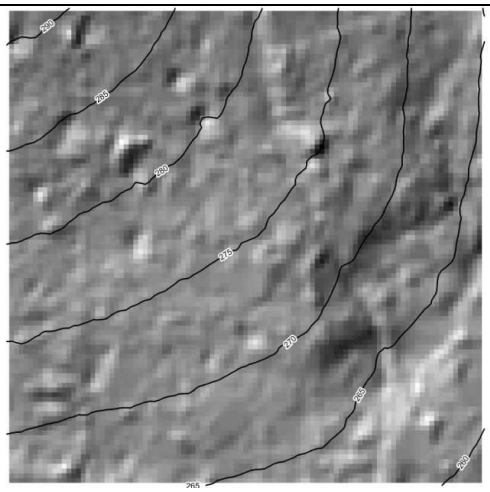

c) Plot U13 shaded relief with 5 m elevation contours

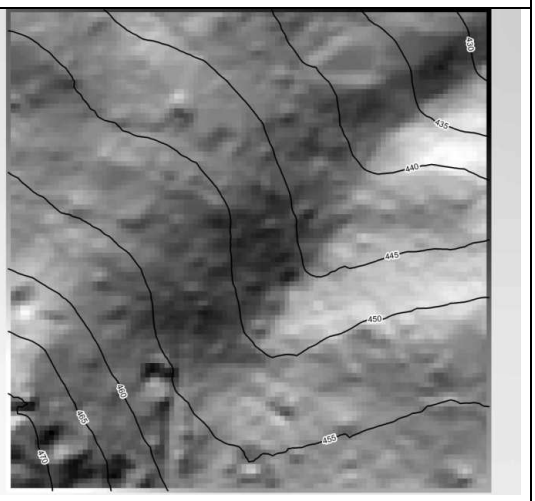

d) Plot O16 shaded relief with 5 m elevation contours

Figure 3.7. U13 and O16 LiDAR ground point density and topography comparison.

Our results differed somewhat from Li et al. (2005), who stated that GPS elevation points are not likely to match grid height points in any DEM. Similar to the point-to-point comparison above, the LiDAR DEM demonstrates surprisingly accurate elevations in open areas when compared to mapping grade GPS elevations; but the DEM analysis further confirms the inaccuracy of GPS acquired elevations when

collected under forest canopy and on steep terrain. The C/A code GPS data collected in the open canopy conditions had ME values that ranged from -0.46 m (SD 0.41 m) to 0.53 m (SD 0.75 m), with the most accurate being -0.04 m (SD 0.45 m) when comparing the GPS point data to the LiDAR DEM (Table 3.14). These values remained relatively consistent when comparing the GPS-derived DEM to the LiDAR DEM with values ranging from -0.45 m (SD 0.32 m) to 0.59 m (SD 0.64 m). Two plots demonstrated accuracy improvement as a result of GPS DEM interpolation and subsequent comparison to the LiDAR DEM. In plot E412, ME improved from 0.21 m (SD 0.92 m) to 0.15 (SD 0.65 m) and plot C27 improved slightly from –0.04 m (SD 0.45m) to -0.02 m (SD0.34). This is notable with respect to C27 as there was significant slash on the plot which could have degraded LiDAR elevation data. Within plot E412, over ninety percent of the trees were taller than the GPS antenna and ranged in height from four meters to eleven meters. The GPS data collected under canopy was collected using dual carrier frequencies and both the C/A code and carrier phase were used in differential correction. The GPS elevation accuracy degraded significantly under canopy with one exception. The exception occurred on plot U13 where the ME of the GPS DEM compared to the total station DEM was 0.27 m (SD 2.02) (Table 3.12), and the carrier phase plus C/A code GPS compared to the LiDAR point elevation ME equaled 0.12 using all comparisons (Table 3.15) Although the ME was surprisingly low, the canopy had an obvious impact on the SD when compared to the GPS data collected in the open. The low error in this plot compared to the other plots with canopy cover is likely a result of many large openings in the canopy and

relatively low density of large trees. As this plot is uneven aged, it had historically been aggressively selective cut. This is also the only plot with a SE slope aspect. We have noticed during this study and during other GPS work in the study area that GPS reception on slopes seems to improve when on south facing slopes. This observation may warrant further research. The remaining plots under canopy demonstrated relatively poor elevation accuracy when compared to the total station elevations. With the exception of U13, average ME ranged from -1.12 m (SD 3.38 m) to -1.84 m (SD 5.22 m). The least accurate occurred on plots with the steepest (plot O69) and most diverse (plot (O16) topography, with ME values of -1.74 m (SD 3.07 m) and -1.84 m (SD 5.22 m) respectively.

The GPS to LiDAR DEM accuracies we found are consistent with other studies and in some examples demonstrate improved accuracies. For studies conducted in open canopy comparing GPS to DEM elevations, Li et al. (2005) found RRF GPS RMSE errors on roads ranging from 0.79 m to 0.82 m compared to 10 m British Ordnance Survey (OS) DEMs, which they refer to as a Digital Terrain Model (DTM). The British OS derives DTM's using digitized contours, which uses all height information contained in a contour file. The results achieved vary depending on the density of the height data contained in the contour file. Holmes et al. (2000) reported an ME of -0.10 m (SD 4.11 m) when comparing DGPS points collected using a Trimble 4400 GPS receiver to a 30 m USGS DEMs created by contour digitizing from either photogrammetric sources or existing maps. Clark and Lee (1998) reported error as the standard deviation of the error between the elevation at the true error point compared

to the topographic map at the same horizontal location. Stop and go error ranged from 0.02 m to 0.03 m, error for kinematic DGPS ranged from 0.03 m to 0.04 m, and RTK error ranged from 0.04 m to 0.09 m. Yao and Clark (2000) found that a single frequency GPS receiver rated with sub-meter accuracy can provide a DEM with vertical accuracy in the range of 0.12-0.14 m. In other studies comparing GPS elevations in forests, Sigrist et al. (1999) compared mapping grade GPS to survey grade GPS measurements. The results of the vertical comparison demonstrated a wide range of RMSE values from 0.77 m in the open to 11.89 m under pine canopy. In another study comparing a mapping grade GPS to a survey grade GPS, Yoshimura and Hasegawa (2003) found average autonomous errors of 2.17 m, 4.23 m, 3.65 m, and 3.74 for forest landing, forest plantation, forest road and natural forest respectively. Average DGPS error was calculated at 0.44 m, 4.52 m, 4.90 m, and 4.17 m respectively.

The total station comparison subtracted LiDAR point and DEM elevations from total station elevations. In all plots the results were negative mean error. This indicates that LiDAR elevations are above true elevations on average. The similar LiDAR elevation comparison to GPS also indicated negative mean error in the open terrain study, although not as consistently. In most cases under canopy, the GPS elevations minus the LiDAR elevations resulted in positive numbers. Subtracting the GPS DEM from the total station DEM, however, resulted in consistently negative values, with one exception where a 0.27 m difference resulted, and thus indicating that the GPS DEM also tends to overestimate ground elevations. We found that LiDAR

overestimates ground elevation in this study, thus when LiDAR is further used to estimate tree heights, the LIDAR DEM error will contribute to underestimating the tree heights.

Based on the number of “ground truth” survey points, this is the most robust study of its kind of which we are aware. Furthermore, we know of no other studies that have matched and compared ground surveyed points to the closest discrete LiDAR ground point. The LiDAR and GPS errors reported in this study are consistent with other studies. The average ME, SD, and RMSE for all five plots with canopy cover where total station data were collected was -0.42 m, 0.39 m, and 0.57 m, respectively, for total station points compared to the LiDAR DEM. The average ME, SD, and RMSE was -0.37 m, 0.39 m. and 0.54 m. respectively for the total station points compared to all of the closest discrete LiDAR points. These average accuracies are surprisingly good considering that five hectare sized plots within a range of canopy and environmental conditions are considered. All plots included Douglas-fir canopy within a mix of dense, young, and even aged stands on relatively flat slopes, mature stands on very steep slopes, and uneven aged stands with various canopy openings. The lowest ME that we found on a single plot with canopy cover was -0.06 m (SD 0.37 m) and -0.09 m (SD 0.41 m) in a total station to LiDAR point and total station to LiDAR DEM comparisons, respectively. While the differences between the LiDAR DEM and the most accurate ground measurement method using a total station survey instrument are statistically insignificant, error significance is truly a judgment call based on the application. In determining tree heights based on a DEM, half a meter is not likely

significant in the resulting amount of milled board feet, however half a meter could be a costly error in many civil engineering projects. This study contains many potential sources of error including those committed by the LiDAR vendor, survey crews, GIS analysis, and statistical analysis. Nevertheless, based on results that demonstrated relatively small measurement differences, we believe that our reported accuracies are conservative, and demonstrate the potential for LiDAR in forestry and natural resource applications.

Literature Cited

Aguilar, F. J. and J. P. Mills (2008). Accuracy assessment of LiDAR-derived digital elevation models. The Photogrammetric Record 23(122): 148-169.

Andersen, H.-E., S. E. Reutebuch and R. J. McGaughey (2006). A rigorous assessment of tree height measurements obtained using airborne LiDAR and conventional field methods. Canadian Journal of Remote Sensing 32(5): 355-366.

Anderson, E. S., J. A. Thompson, D. A. Crouse and R. E. Austin (2006). Horizontal resolution and data density effects on remotely sensed LIDAR-based DEM. Geoderma 132(3-4): 406-415.

ASPRS. (2009). Common LiDAR data exchange format - .LAS industry initiative. Retrieved October 5, 2010, from www.asprs.org/society/committees/lidar/lidar_format.html.

Blewitt, G. and G. Taylor (2002). Mapping Dilution of Precision (MDOP) and map-matched GPS. International Journal of Geographical Information Science 16(1): 55 - 67.

Carson, W. W. and S. E. Reutebuch (1997). A rigorous test of the accuracy of USGS digital elevation models in forested areas of Oregon and Washington. Surveying and cartography: ACSM/ASPRS Annual convention and exposition technical paper 1: 133-143.

Chaplot, V., F. Darboux, H. Bourennane, S. Leguédois, N. Silvera and K. Phachomphon (2006). Accuracy of interpolation techniques for the derivation of digital elevation models in relation to landform types and data density. Geomorphology 77(1-2): 126-141.

Chen, Q. (2007). Airborne LiDAR data processing and information extraction. Photogrammetric Engineering and Remote Sensing 73: 175-185.

Clark, R. L. and R. Lee (1998). Development of topographic maps for precision farming with kinematic GPS. Transactions of the ASAE 41(4): 909-916.

Evans, J. S., A. T. Hudak, R. Faux and A. M. S. Smith (2009). Discrete return LiDAR in natural resources: recommendations for project planning, data processing, and deliverables. Remote Sensing 1: 776-794.

Falkowski, M. J., A. M. S. Smith, P. E. Gessler, A. T. Hudak, L. A. Vierling and J. S. Evans (2008). The influence of conifer forest canopy cover on the accuracy of two individual tree measurement algorithms using LiDAR data. Canadian Journal of Remote Sensing 34(Suppl. 2): S1-S13.

Fisher, P. F. and N. J. Tate (2006). Causes and consequences of error in digital elevation models. Progress in Physical Geography 30(4): 467-489.

Gaveau, D. L. A. and R. A. Hill (2003). Quantifying canopy height underestimation by laser pulse penetration in small-footprint airborne laser scanning data. Canadian Journal of Remote Sensing 29(5): 650-657.

Gomes Pereira, L. M. and L. L. F. Janssen (1999). Suitability of laser data for DTM generation: a case study in the context of road planning and design. ISPRS Journal of Photogrammetry and Remote Sensing 54(4): 244-253.

Hodgson, M. E. and P. Bresnahan (2004). Accuracy of airborne LiDAR-derived elevation: empirical assessment and error budget. Photogrammetric Engineering and Remote Sensing 70(3): 331-339.

Hodgson, M. E., J. Jenson, G. Raber, J. Tullis, B. A. Davis, G. Thompson and K. Schuckman (2005). An evaluation of LiDAR-derived elevation and terrain slope in leaf-off condition. Photogrammetric Engineering and Remote Sensing 62: 415-433.

Holmes, K. W., O. A. Chadwick and P. C. Kyriakidis (2000). Error in a USGS 30-meter digital elevation model and its impact on terrain modeling. Journal of Hydrology 233(1-4): 154-173.

Husch, B., C. I. Miller and T. Beers (1982). Forest mensuration. New York, John Wiley and Sons.

Keim, R. F., A. E. Skaugset and D. S. Bateman (1999). Digital terrain modeling of small stream channels with a total-station theodolite. Advances in Water Resources 23(1): 41-48.

Krabill, W. B., J. G. Collins, L. E. Link, R. N. Swift and M. L. Butler (1984). Airborne laser topographic mapping results. Photogrammetric Engineering and Remote Sensing 50: 685-694.

Kraus, K. and N. Pfeifer (1998). Determination of terrain models in wooded areas with Airborne Laser Scanner data. ISPRS Journal of Photogrammetry and Remote Sensing 53(4): 193-203.

Leckie, D., F. Gougeon, D. Hill, R. Quinn, L. Armstrong and R. Shreenan (2003). Combined high-density LiDAR and multispectral imagery for individual tree crown analysis. Canadian Journal of Remote Sensing 29(5): 633-649.

Lefsky, M. A., W. B. Cohen, G. G. Parker and D. J. Harding (2002). LiDAR remote sensing for ecosystem studies. BioScience 52(1): 19-30.

Li, J., G. Taylor and D. B. Kidner (2005). Accuracy and reliability of map-matched GPS coordinates: the dependence on terrain model resolution and interpolation algorithm. Computers & Geosciences 31(2): 241-251.

Lim, K., P. Treitz, M. Wulder, B. St-Onge and M. Flood (2003). LiDAR remote sensing of forest structure. Progress in Physical Geography 27(1): 88-106.

Liu, X. (2008). Airborne LiDAR for DEM generation: some critical issues. Progress in Physical Geography 32(1): 31-49.

Luccio, M. (2008). Beyond terrain models: LiDAR enters the geospatial mainstream. Retrieved May 1, 2010, from http://www.imagingnotes.com/go/article_free.php?mp_id=204.

McGaughey, R. J., W. W. Carson and S. E. Reutebuch (2004). Direct measurement of individual tree characteristics from LiDAR data. Proceedings of the 2004 Annual ASPRS Conference.

Means, J. E. (2000). Comparison of large-footprint and small-footprint lidar systems: design, capabilities, and uses. Second International Conference on Geospatial Information in Agriculture and Forestry, Lake Buena Vista, Florida.

Nelson, R., R. Swift and W. Krabill (1988). Using airborne lasers to estimate forest canopy and stand characteristics. Journal of Forestry 86: 31-38.

NGS. (2009). What is OPUS? Retrieved March 17, 2010, from http://www.ngs.noaa.gov/OPUS/about.html#discussion.

NGS. (2010). The NGS geoid page. Retrieved May 14, 2010, from http://www.ngs.noaa.gov/GEOID/.

NOAA. (2010). Remote sensing for coastal management. Retrieved May 1, 2010, from http://www.csc.noaa.gov/crs/rs_apps/sensors/lidar.htm.

Penn State Geography. (2010). Lesson 1: LiDAR sensor design. Retrieved October 26, 2010, from https://www.e-education.psu.edu/lidar/l1_p7.html.

Pfeifer, N. and C. Briese (2007). Geometrical aspects of Airborne Laser Scanning and Terrestrial Laser Scanning. International Archives of Photogrammetry, Remote Sensing and Spatial Information Sciences 36(3/W52): 311-319.

Popescu, S. C., R. H. Wynne and R. F. Nelson (2002). Estimating plot-level tree heights with LiDAR: local filtering with a canopy-height based variable window size. Computers and Electronics in Agriculture 37: 71-95.

Ramano, M. E. (2004). Innovation in LiDAR processing technology. Photogrammetric Engineering and Remote Sensing 70: 1202-1206.

Reutebuch, S. E., H.-E. Andersen and R. J. McGaughey (2005). Light Detection and Ranging (LiDAR): an emerging tool for multiple resource inventory. Journal of Forestry 103: 286-292.

Reutebuch, S. E., R. J. McGaughey, H.-E. Andersen and W. W. Carson (2003). Accuracy of a high-resolution LiDAR terrain model under a conifer forest canopy. Canadian Journal of Remote Sensing 29(5): 527-535.

Sigrist, P., P. Coppin and M. Hermy (1999). Impact of forest canopy on quality and accuracy of GPS measurements. International Journal of Remote Sensing 20(18): 3595-3610.

Su, J. and E. Bork (2006). Influence of vegetation, slope, and LiDAR sampling angle on DEM accuracy. Photogrammetric Engineering and Remote Sensing 72(11): 1265-1274.

Taylor, G., G. Blewitt, D. Steup, S. Corbett and A. Car (2001). Road reduction filtering for GPS-GIS navigation. Transactions in GIS 5(3): 193.

Trimble (2006a). TerraSync software reference manual. T. N. Limited. Westminster, CO. Version 2.60**:** 1-248.

Trimble (2006b). Data sheet: GPS Pathfinder ProXH receiver. Trimble. Westminster, CO.

Trimble (2007). Data sheet: GeoXT handheld datasheet. Westminster, CO, Trimble**:** 1-2.

Trimble (2008). GPS Pathfinder Office help, Trimble Navigation Limited.

Trimble (2009a). Data sheet: Trimble GeoXH. Westminster, Trimble Navigation Limited**:** 1-2.

Trimble (2009b). Data sheet: GPS Pathfinder ProXH receiver. Westminster, Trimble Navigation Limited**:** 1-2.

USDAFS. (1998). US Forest Service post-fire conditions glossary. Retrieved August 25, 2010 from http://www.fs.fed.us/postfirevegcondition/glossary.shtml.

USGS. (2009). Experimental Advanced Airborne Research Lidar (EAARL). Retrieved August 23, 2010, from http://ngom.usgs.gov/dsp/tech/eaarl/index.html.

Van Sickle, J. (2008). GPS for land surveyors. Boca Raton, CRC Press, Taylor & Francis Group.

Vanicek, P. (1990). Vertical datum and NAVD 88. Retrieved May 14, 2010, from http://www.ngs.noaa.gov/web/about_ngs/history/Vanicek1.pdf.

Watershed Sciences (2008). LiDAR remote sensing data collection: McDonald-Dunn Research Forest. Corvallis, Oregon, Watershed Sciences Inc.**:** 20.

Wolf, P. R. and C. D. Ghilani (2002). Elementary surveying an introduction to geomatics. Upper Saddle River, New Jersey, Prentice Hall.

Yang, Q., T. G. Van Niel, T. R. McVicar, M. F. Hutchinson and L. Li (2005). Developing a Digital Elevation Model using ANUDEM for the course sandy hilly catchments of the Loess Plateau, China. Canberra, Australia, CSIRO Land and Water**:** 82.

Yao, H. and R. L. Clark (2000). Evaluation of sub-meter and 2 to 5 meter accuracy GPS receivers to develop Digital Elevation Models. Precision Agriculture 2(2): 189-200.

Yoshimura, T. and H. Hasegawa (2003). Comparing the precision and accuracy of GPS positioning in forested areas. Journal of Forest Research 8(3): 147-152.

Zhang, Z., K. Zhang, Y. Deng and C. Luo (2005). Research on precise trigonometric leveling in place of first order leveling. Geo-spatial Information Science (Quarterly) 8(4): 235-239.

Light Detection and Ranging (LiDAR):
What We Can and Cannot See in the Forest for the Trees

CHAPTER 4 – LIDAR FOREST STEM EXTRACTION, HEIGHT MEASUREMENT, AND BIOMASS ESTIMATION METHOD COMPARISON

Curtis B. Edson

Michael G. Wing

Submitted to Remote Sensing

Abstract

Recently forest biomass has received increased attention in the global arena as it relates to anthropogenic carbon emissions and offsetting effects of natural carbon sequestration. A problem is accurate forest biomass accountability. Light Detection and Ranging (LiDAR) remote sensing has demonstrated potential in measuring forest biomass. We assessed the ability of LiDAR to accurately estimate forest biomass on an individual stem basis in a conifer forest in the Pacific Northwest using three different computer software programs compared to traditional field measurement. Software programs included FUSION, TreeVaW and watershed segmentation. To assess the accuracy of LiDAR biomass estimation, two key components were analyzed including stem count and stem height. Pairwise and plot average height differences were assessed. Overall average error and standard deviations (SD) respectively for FUSION, TreeVaW and watershed segmentation were -0.09 m (SD 2.43 m), 0.28 m (SD 1.86 m), and 0.22 m (2.45 m) in even-age, uneven-age, and old growth plots. Average error and SD respectively for FUSION, TreeVaW and watershed segmentation were 0.56 m (SD 1.07 m), 0.28 m (SD 1.69 m) and 1.17 m (SD 0.68 m) in a clearcut plot. The greatest error in one plot was a mean LiDAR stem height of almost three meters shorter than field-measured averages. The most accurate mean height difference was only 0.06 meters shorter in LiDAR than field-measured. The biomass analysis included comparisons of woody plant feature totals in each plot, mean biomass per woody plant feature in each plot, and total biomass by plot for each extraction method. Compared to field-measured biomass overall FUSION and

TreeVaW underestimated by 25 and 31% respectively, and watershed segmentation overestimated by approximately 10%. LiDAR biomass underestimation occurred in 66% and overestimation occurred in 34% of the plot comparisons.

Introduction

Forest attribute inventory information and measurements are critical to forest management (Falkowski et al. 2008). Historically forest inventories have focused on timber production (Hyyppa et al. 2004) and more recently on fuel biomass and carbon stores based on interest in bioenergy and concerns over global climate change and carbon sequestration protocols (Bortolot and Wynne 2005; Lucas et al. 2008; Zhou and Hemstrom 2009). The quantification of biotic carbon stores at various scales and monitoring change in quantity is required for management decisions and policy development related to climate change (Lefsky et al. 2005b; Law et al. 2006; Lucas et al. 2008). Anthropogenic greenhouse gas (CO_2 and others) emissions and land use change are likely to be responsible for a substantial net warming influence since the industrial revolution, while terrestrial and oceanic CO_2 uptake are estimated to remove approximately half of anthropogenic CO_2 emissions (Solomon et al. 2007). The International Panel on Climate Change (IPCC) and others have recommended that all countries devise green house gas reduction strategies, among which is increasing forest biomass (Hoen and Solberg 1994; Hudiburg et al. 2009). The international agreement established in the 1997 Kyoto Protocol and linked to the United Nations Framework Convention on Climate Change set legally binding green house gas emission reduction targets to occur over a five year period from 2008-2012 for thirty

seven industrialized countries and the European community (UNFCC 2010). Internationally, following the Kyoto Protocol, the demand for "carbon credits" is increasing, thus increasing the demand for accurate carbon estimation (Maraseni et al. 2005). A significant problem in monitoring carbon stores in vegetation biomass is the persistent deficiency of accurate biomass estimates (Sessa 2009). Broad based total above ground biomass estimates may be sufficient for some purposes, however the increasing attention on carbon stores has resulted in increasing demand for more refined and detailed assessments of biomass distribution (Lucas et al. 2008).

Biomass is the measurement of plant material mass per unit area. Biomass measurement is sometimes limited to living plant material, but based on the slow deterioration of woody vegetation, the measurement sometimes includes dead material. Above ground biomass is the "mass of live or dead organic matter" (Sessa 2009). The unit of measure is commonly g/m^2 or kg/ha. Biomass is measured via four primary means: a) *in situ* destructive measurement; b) *in situ* non-destructive using equations or conversion; c) derived from remote sensing; and d) modeling (Lucas et al. 2008; Sessa 2009). Allometric equations are then used to statistically infer biomass based on *in situ* field data or remotely sensed data for extrapolation to larger land areas. Allometry assumes that a relationship exists by species based on size or amount of a similar structure. The variable can be applied to one or more measurements, usually height and stem or base diameter (Sessa 2009). Acquiring the data to develop allometric equations is labor intensive and expensive, thus the number of studies and location variation is limited, and therefore users have limited choices. A common

method is to use the most suitable equation based on species and closest regional proximity (Lucas et al. 2008).

As they are dominant features in the global carbon budget, forests perform a critical role in the terrestrial carbon cycle (Hoen and Solberg 1994; Dong et al. 2003; Hudiburg et al. 2009). Forests are carbon sinks and their net ecosystem production (NEP), which is the net forest carbon balance, is positive. In general forest CO_2 uptake by assimilation is greater than CO_2 losses through vegetation and soil respiration (Hoen and Solberg 1994; Luyssaert et al. 2008). Forests contain the greatest amount of biomass and generally occur in temperate, boreal, and tropical regions (Lefsky et al. 1999a; Lefsky et al. 2005b). They are estimated to account for up to 80% of the earth's total biomass (Dixon et al. 1994) in spanning 3952 million ha of land, but cover only approximately 30% of the land surface (Barker et al. 2007).

Due to the scope of global biomass and its constant state of flux, it is infeasible to measure biomass in its entirety and maintain a constant and up to date database (Law et al. 2006). The United States "forest census" (Rapp 2005) have historically been taken by the USDA Forest Service. The inventory is conducted in subsections on a by state basis using the Forest Inventory Analysis (FIA) program in periodic increments taking approximately 10-12 years to complete. FIA inventories have been conducted on an annual basis since 2001. State and private forest land managers make use of similar methods for inventorying and analyzing forest resources. In some areas, FIA plots cross over onto considerable areas of state and private forest land. The status of the nation's forests and several long-term, chronic forest issues including increasing

global wood demand, decreasing forest productivity, land fragmentation, and the impact of growing global populations on resources all strongly influence the FIA program to continue its goal of providing the highest quality information on the extent, condition, and trends of US forest resources (Smith 2002). Meeting the constrained resource challenges through accurate and reliable resource inventory information is a FIA priority and a difficult goal to accomplish. The FIA has faced obstacles from a variety of circumstances including sampling system reliability, inventory measurement cycle, and uncertain funding (AFPA 2001; McRoberts et al. 2005; Grotefendt and Schreuder 2006). Remote sensing technology has the potential for strengthening the FIA through rapid data collection across broad landscapes.

Remote sensing biomass estimates are dependent on the level of detail acquired, which is based on whether the sensor is passive or active and the spatial and spectral resolution capabilities (Lucas et al. 2008). Forest remote sensing focuses on above ground biomass (Dong et al. 2003) and the focus of forest managers is on woody biomass. Above ground woody biomass includes wood in the form of standing and downed tree stems, bark, branches, twigs, stumps, and shrubs (Dong et al. 2003). Landsat Thematic Mapper (TM), Satellite Pour l'Observation de la Terre (SPOT) and other satellite imagery has been used for reliable generalized forest attribute inventories of areas greater than 100 ha in size. In addition, stand level attributes have been manually interpreted using high-resolution aerial images with great time costs and systematic errors (Hyyppa et al. 2001). Multispectral satellite sensors that produce two-dimensional images have significant limitations in estimating above ground

biomass as density increases and are limited in detecting three-dimensional spatial patterns due to their two-dimensional nature (Means et al. 1999; Lefsky et al. 2002). Light Detection and Ranging (LiDAR) remote sensing, also known as airborne laser scanning has demonstrated potential in increasing accuracy of remotely-sensed biophysical measurements while expanding remote sensing capabilities into the third dimension (Lefsky et al. 2002). LiDAR has emerged since its initial applications in the mid 1980's (Lim et al. 2003) and 1990's (Hodgson and Bresnahan 2004) into many activities within forest and natural resources management (Lim et al. 2003; Aguilar and Mills 2008). Forest terrain mapping (Reutebuch et al. 2003) and forest inventory (Reutebuch et al. 2005) are primary LiDAR applications within natural resources. Topographic mapping research with LiDAR in the United States began in the early 1980s (Krabill et al. 1984). During this time, several studies investigated using airborne profiling lasers for forest inventory (Næsset et al. 2004). The first known forest LiDAR study was conducted in the Soviet Union in 1977, in which tree heights derived from LiDAR were compared to photogrammetric estimates with a root mean square error (RMSE) of 0.14 m (Næsset et al. 2004). The first commercial LiDAR sensor was fielded in 1993 (NOAA 2010). The Integrated Global Carbon Observation Strategy (IGCOS) has identified LiDAR as a remote sensing tool that should be developed for remote sensing of forest biomass (Ciais et al. 2010). This relatively new technology is capable of providing biomass estimation accuracies equal or better to other remote sensing technologies (Bortolot and Wynne 2005). Over the last decade LiDAR has demonstrated potential in forest management, however additional rigorous

assessment is required to determine the accuracy of tree height measurements, which is a fundamental forest inventory parameter (Andersen et al. 2006).

LiDAR is unique among remote sensing systems that have traditionally been applied to forest measurement in that it is an active sensor system. Rather than relying on the sun's ambient light, LiDAR emits its own electromagnetic energy in the visible and near infrared range and records the reflecting object's spatial location and return intensity of the reflection. In aerial mapping applications, LiDAR directly measures elevations of objects it contacts between the aircraft sensor and the ground. Based on techniques developed in photogrammetry, forest measurements derived from LiDAR include ground and vegetation surfaces, which are used to assess tree height, volume, and biomass measurements (Popescu et al. 2004). LiDAR relies on the principle that a laser pulse moves at the speed of light, thus the time it takes for a laser pulse to travel from the sensor to an object and back to the sensor enables the calculation of the distance between the sensor and object. These measurements allow for the calculation of an object's height above ground based on an aircraft's altitude at the instant that a pulse was emitted (Evans et al. 2009).

There are three categories of LiDAR sensors including profiling, discrete return, and waveform. Profiling LiDAR records only one return of each laser pulse at relatively coarse densities along a narrow linear transect, whereas waveform and discrete return use a scanning mirror that rotates or oscillates capturing a swath of returns (Lefsky et al. 2002). Discrete return LiDAR systems record at least one return (typically three to five) per laser pulse and are considered small footprint with typical laser pulse

diameters of 0.20-0.80 m. The number of returns that a sensor receives is based on the laser pulse return intensity as influenced by the reflectivity of objects that are targeted (Evans et al. 2009). The intensity of the returned signal compared to the emitted signal is based on several factors including: the energy of the transmitted laser pulse, the percentage of the pulse intercepted by a feature, the feature's surface reflectance characteristics based on the laser wavelength, and the fraction of the pulse returned to the sensor versus diffuse reflectance (Lefsky et al. 2002). Waveform LiDAR provides a continuous distribution of laser energy for each laser pulse by capturing the total energy returned to the sensor at fixed distances (Evans et al. 2009). This distance is based on the variation in return time of the full wave of energy returned to the sensor relative to the time the pulse was emitted (Lefsky et al. 2002). In early forestry applications, profiling lasers effectively measured canopy height and timber volume (Nelson et al. 1988). The most common types of LiDAR sensors discussed in current literature are waveform and discrete return. These two LiDAR sensor types have distinct advantages and disadvantages. Small footprint waveform LiDAR, such as the Experimental Advanced Airborne LiDAR (EAARL) with a 0.20 m diameter footprint when flown at 300 m above the ground (USGS 2009), is beginning to be used more commercially. Small footprint waveform LiDAR is not commonly used for natural resource applications and can sometimes provide quantities of data that overwhelm typical computer systems (Evans et al. 2009). Waveform LiDAR have historically been large footprint instruments (3-15 m) that experience low signal to noise ratios relative to discrete return LiDAR, thus increasing

the probability of sampling the top of trees or other smaller objects (Lim et al. 2003). This capitalizes on digitization of the entire laser return signal which records the vertical distribution of the returned signal coming from all canopy elements (Lefsky et al. 1999b). Discrete return LiDAR typically capture returns at very high point densities (1 to 8 per square meter, or more) and provide higher resolution of ground and canopy surfaces (Evans et al. 2009), however it is known to underestimate tree heights (Popescu et al. 2002; Andersen et al. 2006; Evans et al. 2009).

An aerial LiDAR system configuration for terrain feature mapping consists of a laser scanning sensor mounted on an aircraft (either fixed or rotary wing), Inertial Measurement Unit (IMU), and Global Positioning System (GPS) receiver (Hodgson et al. 2005; Reutebuch et al. 2005; Pfeifer and Briese 2007; Liu 2008). To obtain accurate ground coordinate measurements, the location of the sensor must be known during the entire data collection period. The aircraft mounted GPS and IMU work in conjunction to continually determine the absolute location of the sensor and the direction that the laser is pointing (Hodgson et al. 2005). Just as in aerial photogrammetry, the aircraft attitude affects the angular orientation of the sensor. The IMU continually measures the attitude of the aircraft for pitch, roll, and yaw (Liu 2008). This information is then used for post processing correction and calibration based on the time indexed position and attitude of the aircraft and on-board instrumentation (Watershed Sciences 2008).The laser sensor consists of a pulse generator, infrared laser in the wavelength range of 0.8 µm to 1.6 µm, and a pulse

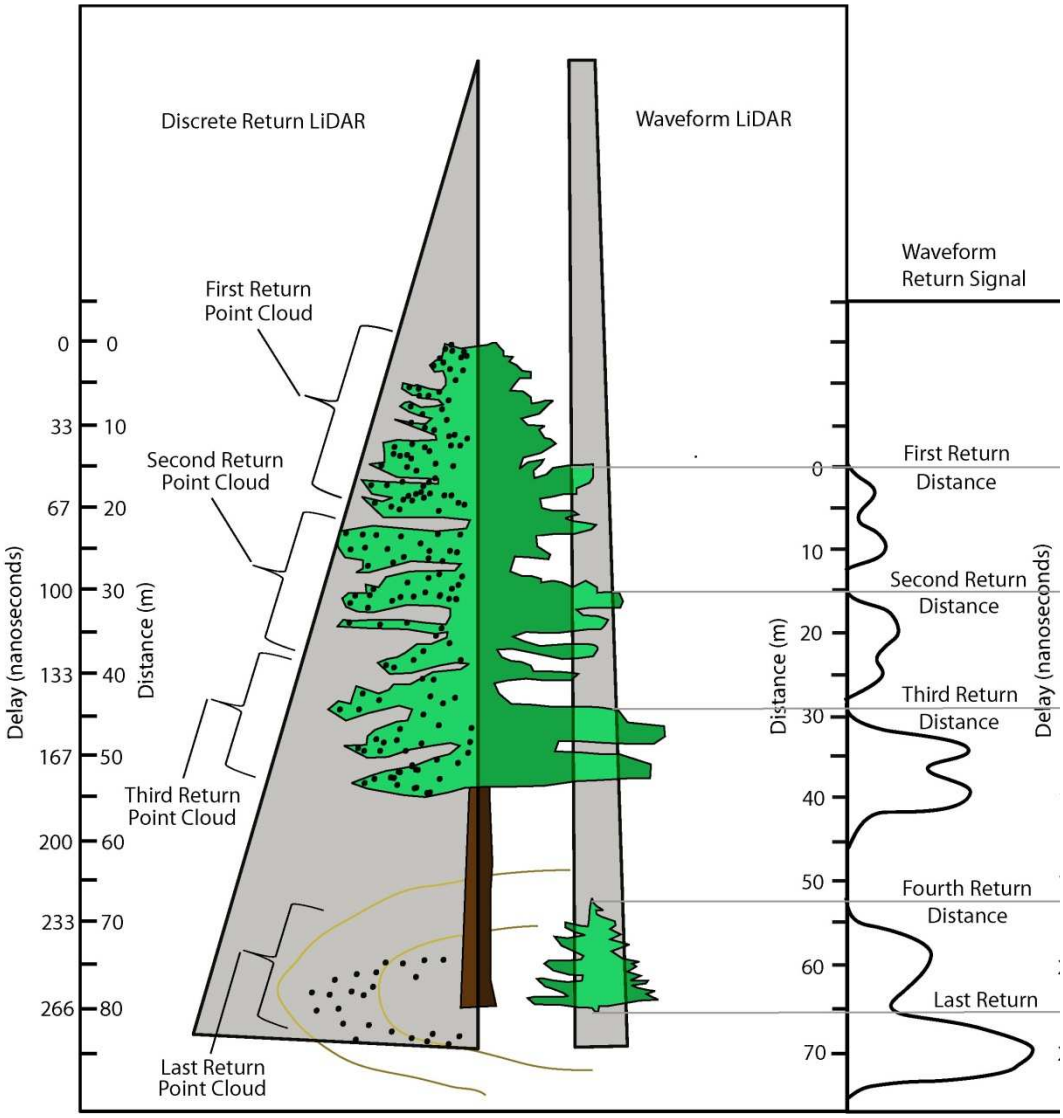

Figure 4.0. Conceptual diagram of discrete return and waveform LiDAR (Lefsky et al. 2002; Penn State Geography 2010).

receiver. The receiver collects the return signals in various intensities after the laser pulse reflects off objects (Hodgson et al. 2005; Pfeifer and Briese 2007; Liu 2008). It takes 4 to 15 ns to emit each pulse, which equates to a pulse length of approximately 2-4 m (Hodgson et al. 2005; Liu 2008). The early systems produced pulses at rates as low as 4 per second (4 kHz) and by the early 2000's as high as 100 per second (100

kHz) (Ramano 2004). Pulse rates can reach as high as 400 kHz (Luccio 2008), but most current systems have a maximum pulse rate of approximately 150 kHz (Chen 2007) to up to 167 kHz (Gatziolis and Andersen 2008). Higher pulse rates equate to greater data density (number of LiDAR returns per unit area). In forestry, thousands of LiDAR points are used per hectare to measure and classify earth features such as vegetation cover or ground terrain. An advantage to LiDAR is that each point from the final output includes measurements in three dimensions (X, Y and Z coordinates) (Liu 2008). Pfeifer and Briese (2007) provide a comprehensive review of LiDAR mechanics.

LiDAR has recently emerged as significant technology for forest measurement applications. Many forest attributes can be measured by LiDAR over large areas including canopy height, subcanopy topography, vertical canopy distribution (Lim et al. 2003), and individual tree heights (Andersen et al. 2006). Tree height measurement is a critical component of forest inventory measurements (Husch et al. 1982; Andersen et al. 2006). Tree total height is the linear distance of the tree measured perpendicular from the earth's surface along the stem axis to the apex of the tree (Husch et al. 1982). Historical methods of tree height measurement include indirect techniques using an Abney level or clinometer, laser rangefinder, total station and other surveying instruments, photogrammetry; and direct methods with a height pole. All of these methods are time consuming and expensive, and potentially suffer from different limitations (Popescu et al. 2002; Lim et al. 2003; Andersen et al. 2006; Liu 2008). The use of clinometers, range finders, and total station instruments require the ability of the

user to see both the tree stem and apex, which is not always possible in a dense forest. Height poles result in inaccuracy caused by parallax (Andersen et al. 2006). Photogrammetry measurements require two adjacent aerial photos (stereo-pairs) to measure tree heights accurately. In the photos, only a small portion of the ambient light rays may reach the forest floor and be visible to a photogrammetrist, while the rest of the terrain may be masked by vegetation and shadows. Many have reported that small-footprint LiDAR tends to underestimate canopy height due to two primary reasons: the failure to detect treetops because of insufficient sampling density (Hyyppa et al. 2001; Lefsky et al. 2002; Gaveau and Hill 2003), and height errors in the DEMs interpolated from LiDAR ground points (Lefsky et al. 2002; Hyyppa et al. 2004; Falkowski et al. 2008), which is the basis for individual tree base heights. The size, shape, and density of tree leaves are very important for both the reflectance and the ability of the laser pulse to penetrate the canopy and strike the ground. However, the geometry and configuration of tree branches is also an important factor in the density of returns. Conifer species tend to have a greater canopy branch density and smaller canopy diameter relative to the main stem compared to a broad, more palmate tree canopy typical of many broadleaf deciduous tree species, e.g. bigleaf maple (*Acer macrophyllum*) and oak (*Quercus spp.*). Thus under leaf off conditions, greater laser penetration to ground is likely to occur in deciduous canopy than with conifers due to the influence of leaves and canopy structure (Rahman and Gorte 2007). On the other hand, greater girth of the branches away from the main stem tends to occur with broadleaf than with conifers, thus broadleaf branches will likely reflect more laser

pulses outward from the main stem than will individual conifer branches. The difficulty in identifying ground points such as a tree crown's apex from the air using LiDAR is compounded in areas with dense canopy and/or understory vegetation (Gaveau and Hill 2003; Hyyppa et al. 2004; Falkowski et al. 2008). Improvements in forest vegetation penetration and ground detection are possible using a LiDAR system with increased pulse transmission numbers (Hyyppa et al. 2001), which is considered to be the key parameter for canopy height model (CHM) accuracy (Hyyppa et al. 2004).

When measuring tree heights using LiDAR accuracy is impacted by several factors including size and reflectivity of the tree, shape of the tree crown, and LiDAR pulse density and footprint (pulse diameter). A primary source of error in LiDAR tree height measurement associated with conifer species occurs when laser pulses miss the sharp apex of the tree resulting in a underestimate of tree height (Popescu et al. 2002; Anderson et al. 2006). Increasing the pulse density may improve the accuracy of LiDAR height measurements by improving the chances of the laser pulse striking at or closer to the tree apex (Gaveau and Hill 2003; Lovell et al. 2005; Lucas et al. 2008). Discrete returns from LiDAR pulses that strike the canopy may be used to estimate tree heights, or canopy elevations may be derived from a CHM (Lovell et al. 2005). A CHM is raster surface model interpolated from points acquired on the upper surface of the canopy. It is similar to a digital elevation model (DEM), however instead of ground points, canopy points are used. Based on the tree structure, errors in LiDAR tree height measurement are also dependant on the algorithm used to create the CHM

(Hyyppa et al. 2004). Stem maps created from a CHM generally only capture the upper primary canopy (Hyyppa et al. 2001). Another potentially significant impact on height measurement is the terrain height measurement (Andersen et al. 2006). Before any LiDAR forest measurements are made, characterization of terrain elevation and DEM creation should be completed (Popescu et al. 2002). DEMs are important for geographic representation, and the analysis and visualization of topographic features (Li et al. 2005). DEMs can be created by interpolating a digital surface model from discrete elevation values that have been collected from across a landscape using LiDAR last returns. LiDAR tree height estimates are calculated by subtracting the terrain surface as represented by DEM from the highest point associated with an individual tree (Kraus and Pfeifer 1998; Lim et al. 2003). LiDAR elevation model accuracies have been found to be as accurate (Kraus and Pfeifer 1998) or better than those generated by photogrammetric means (Carson and Reutebuch 1997; Reutebuch et al. 2003; Fisher and Tate 2006). However, potentially more sources of error exist within LiDAR derived elevations than those produced through photogrammetric means (Fisher and Tate 2006). While typical elevation accuracies stated by LiDAR vendors is around 0.15 m root-mean-squared-error (RMSE), this accuracy is generally only achievable under ideal circumstances such as those found in flat, open terrain (Reutebuch et al. 2003; Hodgson and Bresnahan 2004; Su and Bork 2006). Empirical studies have found LiDAR elevation accuracies ranging from 0.26 m to 1.53 m RMSE (Reutebuch et al. 2003).

Semi-automatic forest inventory methods have been created mainly using aerial photographs and video images with limited stand level accuracy success, thus continued research has focused on the development of improved data sources including LiDAR (Hyyppa et al. 2001). A trend within the commercial sector has been to use LiDAR with moderate sampling density for large area inventories to make stand level estimates such as mean height and stand volume. As long as these measurements meet the inventory accuracy and resolution needs for forest management, this method will suffice (Næsset et al. 2004). However, these broad estimates often do not meet forest management needs, and thus single tree based forest plot inventories that provide more detailed stand information are required in which calculation of stand attributes are based on tree measurements including species, height and crown area (Næsset et al. 2004). Bortolot and Wynne (2005) state that two broad categories of techniques are currently used to detect single tree information using small footprint discrete LiDAR processing. One technique uses distributional statistics, i.e. canopy height and standard deviation taken from a raster CHM or raw returns (Nelson et al. 1988; Means et al. 2000; Næsset and Økland 2002; Lim et al. 2003), which are then used with regression techniques to predict forest properties. The other uses computer visualization techniques to determine the location and measurement properties of individual trees using the CHM (Hyyppa et al. 2001; Popescu et al. 2002). Other processing techniques use discrete LiDAR point clouds to directly measure various individual tree canopy elements (Rapp 2005), while another research area is multi-layered analysis and delineation of suppressed trees, which

requires the use of the original point clouds instead of the CHM as some pulses penetrate under the dominant tree layer (Hyyppa et al. 2004). There are many variations of these LiDAR processing techniques used in research and commercial application.

In this study we compare three individual tree-based methods for deriving forest metrics from LiDAR data including inverse watershed segmentation, TreeVaW, and FUSION. Individual tree-based methods enable parameter estimations at the tree level rather than the plot or stand level (Bortolot and Wynne 2005), which may then be extrapolated to broader levels such as mean stand height and volume (Brandtberg et al. 2003).

Inverse watershed segmentation is the most common method applied to determining locations of individual tree crowns using a CHM by segmenting the inverted raster canopy surface into the equivalent of individual hydrologic drainage basins (Andersen 2009; Goerndt 2010). Following inversion, a watershed segmentation algorithm separates the CHM into distinct tree polygons with raster crown diameter and height values (Goerndt et al. 2010). TreeVaW operates on a CHM using a variable window filter (VWF) that varies its search window size (Popescu and Wynne 2004; Falkowski et al. 2008), otherwise known as a convolution kernel (Jensen 1996), by passing a local maxima (LM) filter over the CHM and determines a tree location based on elevation data contained in individual pixels (Falkowski et al. 2008). Surrounding pixels are assumed to represent laser hits of the same tree crown, and the highest elevation value is taken to indicate the tree apex (Kini and Popescu 2004).

When the filter determines a LM value, a tree x and y coordinate location is identified and then the crown diameter is determined based on the allometric relationship to height (Kini and Popescu 2004; Popescu and Wynne 2004). The Silviculture and Forest Models Team of the United States Department of Agriculture (USDA) Forest Service, Pacific Northwest Research Station in conjunction with the University of Washington Precision Forestry Cooperative has developed a data management and visualization software tool named "FUSION" that is designed specifically for analyzing forest vegetation characteristics using LiDAR data. The program is capable of generating both DEM and CHM surface models, intensity images from the raw LiDAR point files, and analyzing XYZ point data clouds on a plot basis. A three-dimensional cylinder measurement marker is used to manually measure tree dimensions. The cylindrical measurement marker is capable of measuring a feature's horizontal coordinate location, height, crown width, and crown height (McGaughey 2007).

Background

Several key measurements are required to accurately estimate stand height, stem and forest volume, basal area, stem density, biomass (Andersen et al. 2005), carbon sequestration, growth and site productivity (Andersen et al. 2006). Husch et al. (1982) describe the most common forest measurements of stem diameter, crown diameter and height. The standard US diameter measurement is diameter at breast height (DBH), which is measured at 1.3 meters above the ground on the uphill side and 1.4 m when trees are located on level ground. Crown diameter may be used as a predictor variable

for determining DBH and therefore used to estimate tree volume. Tree height may also be used to estimate DBH based on allometric equations (Lucas et al. 2008). The crown is defined as "the part of the tree or woody plant bearing live branches and foliage." Crown cover (*synonym* canopy cover) is defined as "the ground area covered by the crowns of trees or woody vegetation as delimited by the vertical projection of crown perimeters and commonly expressed as a percent of total ground area" (SAF 2008). Arguably the most important crown dimension is the live crown length, which is the portion of the stem that contains all of the live branches (Tappeiner II et al. 2007). Some ambiguity exists in defining crown (canopy) base, however the measurement is valuable for estimating tree growth (Tappeiner II et al. 2007), forest fuels modeling (Andersen et al. 2005), and forest biomass. Andersen et al. (2005) define canopy base height as the lowest height where the canopy fuel density exceeds 0.011 kg/m^3, and the tallest portion of the canopy where the same threshold is exceeded is the canopy height. Fuel density is a measurement of fuel contained within the tree branches and is further delineated by Scott and Reinhardt (2001) as crown bulk density and canopy bulk density, where crown bulk density is "the mass of available fuel per unit crown volume", which is a property of an individual tree, whereas canopy bulk density is "the mass of available canopy fuel per unity canopy volume" measured by stand. One of the critical measurements in forest mensuration for determining volume or mass is tree height (Andersen et al. 2006). Stem volume estimation has traditionally been based exclusively on DBH, but estimates combining height and DBH have proven more accurate if the heights are measured with little or

no bias (Williams and Schreuder 2000; Lovell et al. 2005). Husch (1982) defines three different tree heights that are important to consider in forest measurements including total height, bole height, and merchantable height. These are especially important in considering tree heights measured by LiDAR. Total height is “the distance along the axis of the tree stem between the ground and the tip of the tree”; bole height is “the distance along the axis of the tree stem between the ground and the crown point (crown point is the position of the first crown-forming branch)”; merchantable height is the distance along the axis of the tree stem between the ground and the terminal position of the last usable portion of the tree stem”. These measurements are often summarized and presented as stand level averages. A stand is a forest unit with generally homogeneous tree and landscape characteristics usually one to three ha in area (Hyyppa et al. 2001).

These tree metrics, which result when combined to give three-dimensional values, have historically been measured by field crews using manual means for DBH, crown diameter, and height using the following means respectively: diameter tape or Biltmore stick; projection of the crown vertically to the ground and then measuring the diameter using steel or cloth tape; and clinometers and tape, hypsometer, or height pole. With the exception of small trees measured directly by tape or height pole, DBH is the only direct measurement, and even this method has flaws. The direct measurement using a tape is obtained by measuring at breast height the perimeter of the stem, which is assumed to be the circumference. Diameter tapes are graduated in π units and thus give a direct measurement of the diameter. The obvious flaw is that tree

stems are not perfectly cylindrical, thus the perimeter is not circle. The less circular the perimeter of the stem, the less accurate the diameter measurement (Husch et al. 1982). Measuring tree heights is difficult and subject to measurement error (Williams and Schreuder 2000; Lovell et al. 2005). The use of height poles, although reliable for trees up to approximately twenty-five meters are also subject to error increasing with heights above the user's eyelevel as a result of parallax error (Andersen et al. 2006). The laser range finder is a convenient and commonly used tool for measuring distances and tree heights. They too are subject to some error. In closed stands, the tops of trees are difficult to see, thus the operator must spend a great deal of time and energy searching for a location where he can see the bole, the base and top of the tree at the same time to make the height measurements, therefore measuring tree heights is often a very expensive part of a forest inventory (Andersen et al. 2006; Lucas et al. 2008).

Remote sensing has also historically been used to estimate tree measurements and more recently applied for biomass measurements and carbon estimate. Remote sensing has several advantages over manual ground measurements: it can be used to measure all locations of the forest rather than randomly selected portions; it may be accomplished rapidly relative to ground measurements, thus overall costs may be reduced; and access is not limited by rough terrain in the same respect that ground measurements are (Bortolot and Wynne 2005). Three methods are capable of measuring tree heights and crown properties including automatic image matching of aerial photographs through digital photogrammetry, airborne radar, and LiDAR.

Image matching has resulted in poor tree height accuracy, and radar does not have the same accuracy as traditional manual photogrammetry (Næsset and Økland 2002). Manual photographic interpretation is very time consuming and may be highly subjective, thus limiting the practicality of analog photographic forest measurement applications (Falkowski et al. 2008). In recent years airborne LiDAR has demonstrated great potential in estimating these key forest management parameters (Næsset and Bjerknes 2001; Andersen et al. 2005) and is proving economical and efficient in collecting accurate individual tree heights on a broad scale (Reutebuch et al. 2005; Andersen et al. 2006). This focus on individual tree heights is important in that it renews the focus of traditional surveys to tree numbers, sizes, species and percent canopy cover per unit area or stand (Brandtberg et al. 2003).

Means et al. (2000) compared discrete small footprint LiDAR to ground measured data to predict stand characteristics of height, basal area, and stem wood volume in and near H.J. Andrews Experimental Forest where Douglas-fir dominates in the western Cascades of Oregon. Using ground data that had been collected in 1996 for a previous waveform LiDAR study (Means et al. 1999), and LiDAR data flown October 15, 1999 in a fixed wing aircraft using an AeroScan LiDAR instrument, nineteen 50 m by 50 m plots were selected. Plots were chosen that had a single predominant story or age class including one shrub dominant plot (avg. ht. = 7 m), seven young tree plots (ht. range = 17-28 m), three mature tree plots (ht. range = 30-42 m), and eight old-growth plots (ht. range = 35-52 m). A 10 m DEM was produced using the lowest last return LiDAR and two 10 m grids were created using average mean heights and

average maximum heights. Using Statistical Analysis System software (SAS), ground data and LiDAR measurements were compared using stepwise regression and scatter plots. Stand height, basal area, and stem wood volume were dependent variables and predictor variables were average maximum height, maximum height, and average mean height. Separate comparisons were made using all plots and another without the eight old-growth plots. When all plots were used, basal area and stem wood volume scatter plots demonstrated heteroscedasticity (differing variance). However, when the subset of plots were used without the old-growth plots heteroscedasticity was not apparent, thus the natural logarithm was used for basal area and stem wood volume in the comparison with all plots. The coefficient of determination values in the all plot data for height, basal area natural log, and stem wood volume natural log were 0.93 (RMSE 3.4 m), 0.95, and 0.97, respectively. Regression RMSE was only reported for non transformed values. The coefficient of determination values using eleven plots and omitting the old-growth sites plots for height, basal area, and stem wood volume were 0.98 (RMSE 1.7 m), 0.94 (RMSE 5.4 m^3/ha), and 0.95 (RMSE 73 m^3/ha).

Hyyppa et al.(2001) studied LiDAR capabilities using a high pulse rate laser scanner compared to ground-truth data in a 2 km x 0.5 km (100 ha) boreal forest site located in Kalkkinen, southern Finland, approximately 130 km north of Helsinki. The site was on hilly topography with 1.3 ha average stand size consisting of mainly Norway spruce and Scots pine (*Pinus sylvestris*). The ground data were collected by "conventional standwise forest inventory methods" in August – October 1996 using

sample plots (size not specified) to estimate mean tree height, basal area (m^2/ha), and basal volume (m^3/ha). The LiDAR data were collected on September 2-3, 1998 using a TopoSys-1 sensor flown at an altitude of 400 m above ground level with an approximate average ground density of 10 points per m^2. LiDAR tree extraction and height measurement were completed using a segmentation process developed for aerial photos and adapted for use with LiDAR to create a CHM. A 3 x 3 convolution filter was used to delineate trees from a raster CHM. The filter passes through the CHM iteratively and first finds the local maximum value, which the program delineates as a tree. From this "seed" point, the crown is determined and marked as being associated with the respective seed based on decreasing values away from the seed. Individual trees and associated tree heights and crown widths are then determined. Mean heights were obtained with a standard error of 1.8 and 1.7 m for LiDAR and ground measured field data, respectively. Hyyppa et al. (2001) surmised that height differences were due to field measurement procedural since tree height measurements are among the most difficult tree metrics to accurately measure in the field. Basal area and volume standard error were also estimated at 3.4 m^2/ha and 35.8 m^3/ha for field data and estimated from LiDAR data to be 2.0 m^2/ha and 18.5 m^3/ha. The LiDAR standard error suggested that the segmentation procedure successfully delineated tree crowns and the achieved accuracy was better than field measurement. Large systematic overestimation was attributed to under segmentation, where the number of segmentation iterations is controlled by a scale parameter. If no filtering or too little filtering was applied, the number of tree crowns was exaggerated.

Naesset and Okland (Næsset and Økland 2002) studied the accuracy of LiDAR in measuring tree height and crown length parameters by individual tree and by plot. This two part study was part of a larger study and included two study areas within the boreal forest study site located in southeast Norway consisting primarily of Norway spruce (*Picea abies*). The Ostmarka study area was within a 2.5 ha area and consisted of ten 5 by 10 m rectangular plots selected subjectively by topographic and ecological properties ranging from steep slopes to flat terrain. Tree x and y locations were determined within the plots whose corner coordinates were determined by differential Global Positioning System (GPS) and Global Navigation Satellite System (GLONASS). Plot coordinate accuracies ranged from 0.1 to 1.5 m. Tree height (h) and height to base of crown (h_c) were measured using a Suunto hypsometer. Tree heights ranged from 2.2 to 27.1 m, and the mean height was computed for all trees and reported as Lorey's mean heights. The Valer study area was approximately 1000 ha in size and consisted of 174 plots from an earlier study, from which 27 plots were selected based on study specifications. The heights of all trees greater than 4 cm DBH and the base crown height of all trees greater than 15 cm DBH were measured also using a Suunto hypsometer. Only the Lorey's mean height was reported for the 27 plots and ranged between 13.5 to 25.2 m. Individual tree heights from the Ostmarka study area were regressed against predictor variables determined from the LiDAR canopy height distributions. Only trees which received at least two LiDAR hits were included resulting in 51 of 68 trees being selected. The final regression model had an R^2 value of 0.75. Regressions were then estimated for individual trees including the

crown base height and the relative crown length for trees > 15 cm dbh. The relative crown length is proportion of the distance from the crown base height to the top of the tree and is computed using the equation:

$$R_c = \frac{h - h_c}{h}\ 100$$

This comparison included 45 trees and resulted in a R^2 value of 0.71. The range, mean, and SD of differences respectively between predicted and ground-truth values for Ostmarka were -3.83 to 14.03 m, 0.18 m (SD = 3.15) for individual tree heights (51 trees), -5.08 to 2.97 m, 0.03 m (SD = 2.19) for individual height to crown (45 trees), and -5.08 to 2.97 m, 0.03 m (SD = 2.19) for Lorey's mean height (10 plots).

The Valer study area mean crown base heights were regressed with an R^2 value of 0.61, and the range, mean, and SD of differences were -3.82 to 2.90 m, 0.05 m (SD = 1.52 m), respectively. Cross validation of the selected regression model from Ostmarka determined that the mean difference between predicted and measured tree height was not significant (P > 0,05). The standard deviation in differences between predicted and field-measured values of relative height to base of crown for the Ostmarka and Valer studies were 6.32% and 7.11% respectively compared to 8.8% and 10.9% observed mean values.

Brandtberg et al. (2003) conducted a small footprint, high sampling density leaf-off LiDAR study consisting of over 1500 trees within a 6 ha of the West Virginia Research Forest located 15 km east of Morgantown, West Virginia. The LiDAR data were compared to a Geographic Information System (GIS) tree database compiled

from photo-interpretation and ground survey collected during the year 2000. The study site was located at approximately 600m above sea level and includes deciduous chestnut oaks (*Quercus prinus*) other native oaks (*Quercus*), red maple (*Acer rubrum*) and yellow poplar (*Liriodendron tuliperifera*). The LiDAR data were collected using a Saab TopEye system mounted on a helicopter flying at 100 m above ground level. The system is capable of receiving up to four returns per pulse, but reported only receiving two per pulse, which they presumed to be due to the leaf off conditions of the vegetation and that small branches are opaque and dark to the near infrared laser (1.064 µm) wavelength, thus are not as reflective as leaves. A segmentation algorithm was used to delineate individual trees from a CHM. Forty-eight sample trees were used to compare LiDAR heights to field-measured heights and two-hundred trees from each species group (oak, maple and poplar) were randomly selected for a species classification test using linear discriminant analysis (LDA). The height of tall trees tended to be underestimated and shorter trees overestimated by the LiDAR data. The mean of standard errors was 1.1 m and R^2 was 0.69. The species classification test using LDA had mixed results, the best of which had a classification accuracy of 60% using several first return single variables (Zmean, ZStdDev, ZSkew, ZKurt, RMean, RStdDev, RSkew, RKurt, ZMax and RMax). Brandtberg et al. (2003) also noted that individual small trees were very difficult to detect, especially when next to taller trees, even when separating the data into multiple scales. In this study a scale-selection tool "based on local extrema over scales of different combinations of normalized scale invariant derivatives" was used. Three different scales were chosen based on a scale-

space technique using crown radius. The first and second test intervals were the 5^{th} and 95^{th} percentiles and 25^{th} and 75^{th} percentiles, respectively, chosen from a histogram displaying crown radius on the abscissa and number of individuals on the ordinate. The third interval was chosen at random from either side of the crown radius mode denoted by the histogram peak.

Gaveau and Hill (2003) sought to quantify canopy height underestimation by small-footprint LiDAR data in a broadleaf woodland study conducted in Monks Wood National Nature Reserve in Cambridgeshire, eastern U.K. The study area ranged in elevation from 6 to 46 m [above mean sea level] and tree species consisted primarily of ash (*Fraxinus excelsior*)(most common in the study area), English oak (*Quercus robur*), field maple (*Acer campestre*), silver birch (*Betula pendula*), European aspen (*Populus tremula*), and small-leaf elm (*Ulmus minor*). The primary understory and fringe shrub species were hawthorn (*Crataegus monogyna*), common hazel (*Corylus avellana*), blackthorn (*Prunus spinosa*), dogwood (*Cornus sanguine*), and wild privet (*Ligustrum vulgare*). The objective of this study was not to locate individual trees with LiDAR, but to compare canopy heights accurately measured from the ground to those measured using LiDAR. A total station was referenced to an Ordnance Survey (OS) bench mark and then canopy locations were randomly selected for measurement. To obtain very accurate canopy height measurements, the total station was placed on a 15 m platform sighted on an OS benchmark; a reflecting prism was placed at the top of the tree canopy using an 18 m truck- mounted platform, or 8 m extendable pole for shrub canopy measurements. By using this method for height measurement, error

uncertainty of hypsometers or clinometers was avoided. Four areas were sampled for upper surface sampling including two for shrubs and two for trees. A total of 43 points were sampled along a 220 m transect in shrubs, and 39 points along a 275 m transect in trees. The LiDAR data were acquired on 10 June, 2000 using an ALTM 1210 airborne laser terrain mapper using a 1.047 µm infrared laser. Average point-sample density ranged between one point per 2.80 m^2 to one point per 6.50 m^2. Two general comparisons were made: one compared field collected elevation points to discrete LiDAR points within 0.60 m, which corresponds to the stated LiDAR horizontal positioning accuracy; and the second compared the field canopy height measurements to the CHM derived from LiDAR heights. The discrete point sample comparison included 10 measurements made on man-made features, i.e. parking lots and building tops, 16 shrub canopy points, and 12 tree canopy points. Mean errors were -0.01 m (0.12 m SD) for man-made surfaces, -0.91 m (0.50 SD) for shrub canopy, and -1.27 m (0.94 SD) for tree canopy. The average CHM residual using all ground measured canopy reference points was -1.02 m and -2.21 m for the shrubs and trees, respectively.

Leckie et al. (2003) researched combining multispectral data and LiDAR data for individual tree crown analysis. Only LiDAR results are summarized in this paragraph. The study site was located 30 km northwest of Victoria, British Columbia and evaluated LiDAR with field data collected in three 20 m x 20 m plots from a larger study containing primarily Douglas-fir with other species. Stem densities and average height for each plot were 300 and 26.2 m (2.00 SD), 500 and 25.2 m (1.94 m SD),;

and 725 and 24.4 m (2.42 m SD), respectively. All plot ground truth data had previously been stem mapped with records of species, DBH, sample tree heights, and understory and ground vegetation information. The LiDAR data were acquired on August 19, 2001 with a Lightwave model 110, 1.047 µm wavelength laser mounted on a helicopter. The LiDAR analysis resulted in overall tree height measurement underestimation of 1.56 m (SD 0.77 m) based on the maximum LiDAR elevation hit. To distinguish LiDAR height error measurement caused by missing the tree apex from DEM error Leckie et al. (2003) also compared LiDAR heights to ground measured heights to the highest whorl of branches where definite laser pulses strike. After subtracting the mean ground measured height of 0.37 m to the top of the leader (tree apex) from the highest whorl, a tree height error of over one meter remained. They suggest the tree height error was due to two possible causes within their study area. The first potential cause was that dense undergrowth vegetation at a height ranging from 0.5-2.0 m may have caused false ground heights in the DEM. The second potential cause was that the study site's ground truth microrelief around the base of trees where the field measurement occurred which varied an estimated 0.5 m in either direction from the generalized LiDAR height model of the same location.

Bortolot and Wynne (2005) used a computer vision algorithm with LiDAR data collected in a 4.6 km^2 section of loblolly pine (*Pinus taeda*) in the Appomattox-Buckingham State Forest, Virginia to determine stand biomass. They limited the study to stands between the ages of 11 and 16 years to avoid younger (smaller) trees that the LiDAR would not detect, and older stands where subdominant trees were masked by

larger trees. The ground data were collected between 2002 and 2003 in 25 fixed 15 meter radius plots, using a 0.07 m DBH cutoff. They chose to limit trees to larger than seven centimeters as they believed the smaller trees would not be visible in the CHM. Tree DBH and dominance status were measured to determine above ground biomass using models developed by Naidu et al. (1998). A total of 642 trees were measured with an average of 56 per plot. The biomass estimates were averaged and multiplied by the total number of trees to determine the total above ground biomass. The LiDAR data were collected in 2002 using a Digital Topographic Imaging System II sensor with a maximum of 5 points/m^2. Ground and non-ground returns were separated by the vendor and the CHM was interpolated using the kriging method. To identify trees in the LiDAR data the Nelder Mead simplex algorithm was used, which is similar to the TreeVaW algorithm developed by Popescu et al. (2002), except that it uses more parameters to identify a tree location. The algorithm uses eleven parameters (P) and a polygon shaped window with P+1 vertices. The argument for using eleven parameters is that these increased numbers of parameters enables the program to be more robust in adapting to different forest types. The algorithm was evaluated by using the entire data set which used the same data for testing and training and then again using independent subsets of the data. Stepwise multiple linear regression was used to predict biomass using LiDAR tree counts and heights. Tree heights were ranked from highest to lowest and then extracted at 25^{th}, 50^{th}, and 75^{th} percentiles. These percentiles were chosen because the difference in magnitude of height differences among percentiles should reflect structural differences that may relate to

biomass. The coefficient of determination (R^2) results for the entire dataset were between 0.50 and 0.53 with RMSE values between 13.6 and 13.9 trees/ha. The independent subsets had R^2 values between 0.35 and 0.69 with RMSE values between 15.6 and 140.4 trees per hectare. Stepwise multiple linear regression was used to predict tree counts delineated using LiDAR. The equation used in the study was $B = \beta_0 + \beta_1 (\text{H50})^2$, where B = biomass and H50 is the median height.

Andersen et al. (2006) used high-density, multiple return LiDAR collected in a 5.2 km^2 area in the Washington State, Capitol Forest consisting primarily of Douglas-fir (*Pseudotsuga menziesii*) and western hemlock (*Tsuga heterophylla*) in September 2005 and March 2006 to estimate forest metrics including canopy base height and canopy height. They compared LiDAR measurements to field measurements of trees larger than 14.2 cm DBH collected on 101 fixed area plots ranging in size from 0.02 to 0.2 ha. Tree height and crown base height were measured using an Impulse 100 hand-held laser range finder. Using a program written in IDL (Research Systems Inc. Interactive Data Language) and predictor variable used by Naesset and Bjerknes (2001), LiDAR data were used to predict tree height and stem density at the plot-level, which were then used to estimate several structural measurements including canopy height and canopy base height. The regression analysis used to estimate canopy height and canopy base height resulted in coefficient of determination (R^2) values of 0.98 and 0.77 respectively compared with field based methods. Andersen et al.(2006) continued with this research by comparing Douglas-fir and ponderosa pine (*Pinus ponderosa*) tree heights attained with both wide and narrow beam LiDAR to field measurements

collected with a Topcon ITS-1 total station. Additionally they compared tree heights collected using an Impulse 100 laser range finder to those collected using the total station. The high-density LiDAR (6 points/m2) narrow beam LiDAR proved to achieve greater accuracy than wide beam. A total of seventy-one trees were measured including forty-one Douglas-fir (mean height 25.7 m, 9.8 m SD), and thirty-three ponderosa pine (mean height 16.5 m, 5.6 m SD). Measurements collected from twelve trees were removed from the analysis due to high error (RMSE > 5 cm). LiDAR derived tree height error was reported (mean ± SD) including overall height error, vertical error in treetop measurement and vertical error in tree base measurement respectfully for Douglas-fir (29 trees) -1.05 m (0.41 m SD), -1.09 (0.32 m SD), -0.04 (0.16 m SD); ponderosa pine (30 trees) -0.43 m (0.13 m SD), -0.40 m (0.11 m SD), 0.03 m (0.10 m SD); all trees combined (59 trees) -0.73 m (0.43 m SD), -0.74 m (0.42 m SD), -0.004 (0.14 m SD). The field measurement height error of the laser range finder compared to the total station resulted in -0.37 m (0.29 m SD) for Douglas-fir ,-0.16 m (0.21 m SD) for ponderosa pine , and-0.27 m (0.27 m SD) for all trees,. This indicates that on average, the laser range finder underestimates tree heights. Nominal horizontal accuracy of the trees based on tree-top location was also reported with an error range of 0.50-0.55 m.

Coops et al. (2007) conducted a study in a Douglas-fir and western hemlock forest located in the Oyster River area of Vancouver Island, British Columbia, Canada to determine the capability of discrete return small-footprint LiDAR to estimate and model vertical and horizontal canopy structure. The 5 by 5 km study area ranged in

elevation between 120 and 460 m above mean sea level. Six stands were chosen to measure all trees above 0.10 m DBH within a 20 by 20 m square plot. Field crews used a laser range finder to measure each tree's height, base to live crown, and maximum and minimum crown radius. Compass and laser rangefinder were used to map stem coordinate to plot center points which were determined using a Trimble GeoXT mapping grade GPS. Mean tree height and maximum tree height were reported by for both field-measured and LiDAR measured heights for six plots. Reported mean height measurements in meters for field and LiDAR are shown in Table 4.0. The LiDAR compared to field-measured heights were highly correlated with R^2 for mean plot height of 0.85, $P < 0.001$ (SE = 1.8 m) and R^2 for maximum height of 0.82, $P < 0.05$ (SE = 2.2 m). Many studies have found height errors as high as 3 m. These errors were attributed to three primary factors including missing the tree crown apex, positional errors, and errors in the field measurements. LiDAR tends to underestimate plot heights due to the way LiDAR samples terrain and the likelihood that the LiDAR beam misses the tree apex. Increasing the pulse density that strike earth features could be increased by flying at a lower elevation above the ground, slowing the aircraft speed, or making multiple repeat passes. GPS errors of 1-2 meters associated with establishing plots and LiDAR horizontal location errors of up to one meter can contribute to errors between field and LiDAR heights. Finally, the difficulty in identifying and measuring the tops of trees with a laser range finder can contribute errors up to 2 m in tall trees.

Table 4.0. Mean tree height (m) comparison field-measured by laser range finder (LRF) and LiDAR (Coops et al. 2007).

Stand Number	I	II	III	IV	V	VI
Number of trees/ha (ha^{-1})	1325	1000	700	556	575	800
Mean height (LRF)	19.0	18.2	22.1	22.7	28.7	23.7
Mean height (LiDAR)	13.8	15.6	17.6	22.7	20.3	18.6
Max height (LRF)	24.3	36.5	32.6	38.5	40.6	33.5
Max height (LiDAR)	28.4	33.2	33	35.2	35.2	35.7

McGaughey et al. (2007) compared measurements made using the tree visualization and measurement tool FUSION to the same tree measurement characteristics made on the ground using traditional methods. The study was conducted in the Capitol State Forest in Washington State on mountainous terrain varying in elevation between 150 and 400 meters with slopes ranging from 0 to 45 degrees. The forest was predominantly Douglas-fir and highly varying in silviculture treatments including clearcut, various thinning densities, and plantations ranging in age from newly planted to 70 year old mature forests. Field data were collected for lightly and heavily thinned 0.2 acre (0.81 ha), 16.05 m fixed radius study plots located using differential GPS. In each plot all trees greater than 0.127 m DBH were measured including location, height, height to crown base, and crown diameter. Location of each tree was measured from the plot center point using an Impulse laser rangefinder with a MapStar compass module. Tree and crown base height were also measured with the laser rangefinder. LiDAR data were collected in the spring of 1999 using a Saab TopEye system mounted on a helicopter flying at 200 m above ground at a speed of 25 m per second and collecting a pulse density of four pulses per m^2. A total of 112 trees on ten plots (six lightly thinned and four heavily thinned) identified using FUSION were matched to the closest field-measured trees. The average difference in tree

location was 0.97 m (SD = 0.56 m), and the maximum difference was 2.77 m. The average tree height difference was -0.29 m (SD = 2.23 m), and the range of differences was -8.37 to 6.36 m). This negative height difference indicates that the LiDAR measurement was lower than the field tree height measurement. The average crown base height measurement difference was -3.22 m (SD = 3.97 m), with differences ranging from -14.15 m to 7.94 m. A total of forty-two field-measured small trees could not be identified in the LiDAR data using FUSION due to limited number of LiDAR returns, however some small trees located in openings were easily identified. The major problems encountered in identifying trees in the LiDAR data were identifying trees in areas where tree crowns overlapped or were understory, and identifying the live crown base.

Falkowski et al. (2008) compared two different tree detection and measurement algorithms with LiDAR data collected in the Palouse Range located nine km northeast of Moscow, Idaho. The forest consisted primarily of Douglas-fir, grand-fir (*Abies grandis*), western red cedar (*Thuja plicata*), and western larch (*Larix occidentalis*). The inventory scheme comprised eighty-three 0.04 ha inventory plots stratified by elevation, insolation and leaf area index. All plot locations were determined using a Trimble ProXR GPS and differentially corrected, and then each tree location was determined using distance and azimuth from the plot center. Species and DBH were recorded for each tree and snag $\geq$ 0.027 m DBH . Tree heights and crown diameter were measured using an Impulse 200 laser rangefinder on a subsample of smallest and largest trees within each plot; all other tree heights and crown diameters were

determined using allometric equations. Trees were placed in crown classes based on plot-level canopy position majority. Inventory plots were separated into four different strata including 0-25%, 25%-50%, 50-75%, and 75-100% canopy cover. LiDAR data were collected in summer 2003 using a Leica ALS 40 at a flying height of approximately 2500 m using a 1.064 µm near infrared wavelength laser. Using ground and non-ground returns, a DEM and CHM were created respectively with the DEM having a RMSE of 0.306 m in high canopy cover forest and 0.166 m low canopy forest, and the CHM with a 0.5 m spatial resolution. The two algorithms compared were spatial wavelet analysis (SWA) and TreeVaW. The SWA is multiscale and is capable of detecting and measuring trees across a range of different sizes, and TreeVaW is also capable of determining trees of different sizes based on tailored stand or forest allometric equations, which for this study was $cd = 0.14h + 2.56$ where cd is tree crown diameter, and h is tree height in meters. Two distinct random samples were collected, one to estimate errors of omission and commission, and the other to estimate tree measurement accuracy of SWA and TreeVaW. A total of 120 trees were sampled with 30 being selected from each canopy cover stratification. Sampled tree height and crown diameters ranges were 5.12 – 36.8 m (mean 16.65 m) and 1.60 – 14.55 m (mean 4.69 m), respectively. Field-measured trees were paired with SWA and TreeVaW identified trees; and those field-measured trees identified outside a 2.5 m distance from outside of a LiDAR identified crown edge were recorded as omissions; and if a LiDAR tree was identified where no field-measured tree was located, a commission error was recorded. From the 120 sample tree, SWA detected 96 trees (80%) and

TreeVaW detected 102 trees (85%). By dominant, codominant, and subdominant canopy cohort SWA detected 97%, 62%, and 42% respectively and TreeVaW detected 94%, 79%, and 58% respectively of sampled trees. The Pearson's correlation coefficient (*r*) and RMSE were used to compare LiDAR tree heights compared to field-measured tree heights. The Pearson's correlation coefficient shows the linear degree of association between two sample variables X and Y (Ramsey and Schafer 2002) and is calculated using the following formula:

$$r = \frac{\sum_{i=1}^{n}(X_i - \bar{X})(Y_i - \bar{Y})/(n-1)}{s_X s_Y}$$

where s_X and s_Y are the sample standard deviations. A negative *r* value indicates a negative correlation, or inverse relationship and a positive value vice versa. The higher the value, the greater the correlation. Overall correlation values of LiDAR tree heights compared to field-measured heights were $r = 0.89$ (RMSE = 3.96 m) for SWA and $r = 0.89$ (RMSE = 4.06 m) for TreeVaW. Falkowski et al. (2008) stated that the accuracy of LiDAR height measurements was dependent on LiDAR derived DEMs and that the DEM interpolated from measurements under dense canopy in this study exhibited higher error.

Wing et al. (2010) conducted a LiDAR forest measurement study in a wildfire burned area in southwestern Oregon. Trees were field-measured on three different sites in areas with varying burn severity from minimal to substantial. All sites contained primarily Douglas-fir, Site 2 also contained large amounts of ponderosa pine, and Site 3 had large amounts of golden chinkapin (*Castanopsis chrysophylla*).

The wildfire occurred in 2002 and field measurements were made in September 2006. Field measurements included DBH, height, crown radius, and spatial location of 463 trees. DBH was measured with a diameter tape; height and crown were measured using an Impulse 200 laser range finder. Spatial location of each tree was measured using a Trimble ProXH mapping grade receiver equipped with an external Hurricane antenna. LiDAR data were collected in September 2004 with an Optech ALTM 30/70 Airborne Laser Terrain Mapper mounted in a Cessna 2010 aircraft. The USDAFS FUSION version 2.00 software was used for LiDAR point cloud analysis. FUSION determines tree heights based on the manual identification of each tree, where the operator places an appropriate sized cylinder around the three dimensional point cloud identified as a tree. Tree heights are determined by subtracting DEM ground height from the highest point in the point cloud. Crown diameter is measured based on the diameter of the measurement cylinder. The mean, standard deviation, and RMSE were calculated for field-measured tree heights and subtracted from LiDAR measured tree heights. Field-measured tree heights were compared to LiDAR-derived tree heights through paired *t*-tests. The Wilcoxon rank-sum test was also used to compare trees separated into categories (e.g. killed by fire or alive) and regression was used for examining single parameter influence on tree position and height differences. Eighty-five percent of the field-measured trees were identified in the LiDAR data using FUSION, and the unidentified trees were primarily intermediate and suppressed trees. Paired *t*-test height comparisons resulted in significant differences at Site 3 ($P<0.01$) and with combined data for all sites ($P<0.01$). The Wilcoxon rank-sum test resulted in

significant differences between field and LiDAR heights for tall and short trees at all sites ($P<0.05$); and a significant difference was found between large and small crowns on Site 3 ($P<0.02$). Linear regression analysis resulted in no significant differences in height, DBH, and crown diameter variables at individual sites, When all tree height differences were combined from all sites, tree height ($P < 0.02$), DBH ($P < 0.01$), and crown diameter were significant explanatory variables for height differences. The significant differences at Site 3 were attributed in part to dense live tree canopy, which made measuring tree heights in the LiDAR point clouds difficult, and may have contributed to less accurate GPS field measurements. Other potential tree height errors were partially attributed to laser range finder measurement; topographic slope; low pulse densities; DEM error; and time lapse between the fire, LiDAR measurements, and field measurements. In addition, small shifts in laser rangefinder pivot points and extreme pivot angles have been shown to contribute to height measurement error (Wing et al. 2004). Hyyppa et al. (2000) found that standard error in LiDAR tree height measurement increased with slope (0.15 m at 0% slope and 0.40 m at 40% slope). Site 1 had a slope of 50%, which may have contributed to height measurement error. The higher the pulse density, the greater the likely hood the tree apex will be struck by a LiDAR pulse. The pulse rate between 1.6 and 2.5 pulses m^{-2}, which is relatively low, may have contributed to tree height underestimation by the LiDAR. Finally, the temporal differences between when the fire occurred, LiDAR collection, and field collection may have contributed bias as some branches may have dropped between when the LiDAR was flown and when field data were collected

mostly impacting canopy measurements. Tree growth was believed to be less than 0.25 m per year as the sites were not favorable for rapid growth.

Objectives

The background information above has illustrated that much of the focus on LiDAR research has been on trees occupying a dominant and co-dominant portion of the canopy. Some may consider the necessity of a young-tree inventory as not important or less important than established stands, especially considering a priori knowledge resulting from near term management operations. However, monitoring the status of young stands with trees under ten meters in height is important for growth projections. In addition, stem density is important in planning thinning or planting treatments (Næsset and Bjerknes 2001). Understory vegetation including shrubs and young trees can amount to large amounts of biomass, which is important for estimating carbon stores and monitoring fuels for fire risk mitigation. Thus, this research not only focuses on LiDAR forest mensuration capabilities in dominant and co-dominant canopies, but also in the suppressed sub-canopy. In other words, what vegetation can discrete return LiDAR detect, and what does it miss? Previous research suggests that LiDAR pulses do not strike as much of the suppressed sub-canopy vegetation compared to the dominant and co-dominant canopy and that these suppressed points are not used in generating the CHM (Brandtberg et al. 2003; Hyyppa et al. 2004; McGaughey et al. 2004; Bortolot and Wynne 2005; Hyyppa et al. 2008; Lucas et al. 2008). We are not only interested in the accuracy of LiDAR in measuring detected trees , but we also seek to quantify the woody vegetation that is

missed by LiDAR on an individual tree and area volume basis. Our study had four main objectives related to measuring forest tree and shrub features.

The first objective was to determine the characteristics of individual trees and shrubs that LiDAR detects and misses within a range of forest settings. We believe this is not only a function of tree and shrub size, but is also influenced by the horizontal and vertical density of vegetation and tree species (deciduous or coniferous). The second objective was to determine the accuracy of LiDAR tree and shrub height measurements of detected features compared to ground measured heights. The third objective was to determine the horizontal x and y location accuracy of LiDAR measured trees and shrubs. The fourth objective was to compare hectare volume estimates derived from LiDAR data compared to ground measured estimates. We evaluate our study objectives with three different techniques for delineating individual tree and shrub measurements, thus comparing the results of the different methods is the fifth objective. The techniques include an inverse watershed segmentation algorithm and a variable window algorithm, both of which rely on the use of a CHM. In addition, a visualization program that determines feature locations using raw LiDAR point clouds is also applied. As discussed above, CHM's eliminate much of the suppressed vegetation, whereas characterizing suppressed sub-canopy is possible using original point clouds (Hyyppa et al. 2004).

Methods

Study Site

The study was conducted in Oregon State University's (OSU) McDonald-Dunn research forest located on the northern border of Corvallis, Oregon and minutes from the OSU campus. The forest is approximately 5475 ha (McDonald Forest and Dunn Forest occupying approximately 2930 ha and 2545 ha, respectively) ranging in elevation from approximately 75-660 m above sea level in the eastern foothills of the Oregon Coast Range. Conifers dominate the forest with Douglas fir (*Pseudotsuga* menziesii) and grand fir (*Abies grandis*) being the apex species. The primary deciduous tree species is bigleaf maple (*Acer macrophyllum*) and shrub species California hazel (*Corylus cornuta var. california*). The forest is intensively managed for research and education, and although the species composition does not vary significantly, there is great variation in stand age, density, and management history.

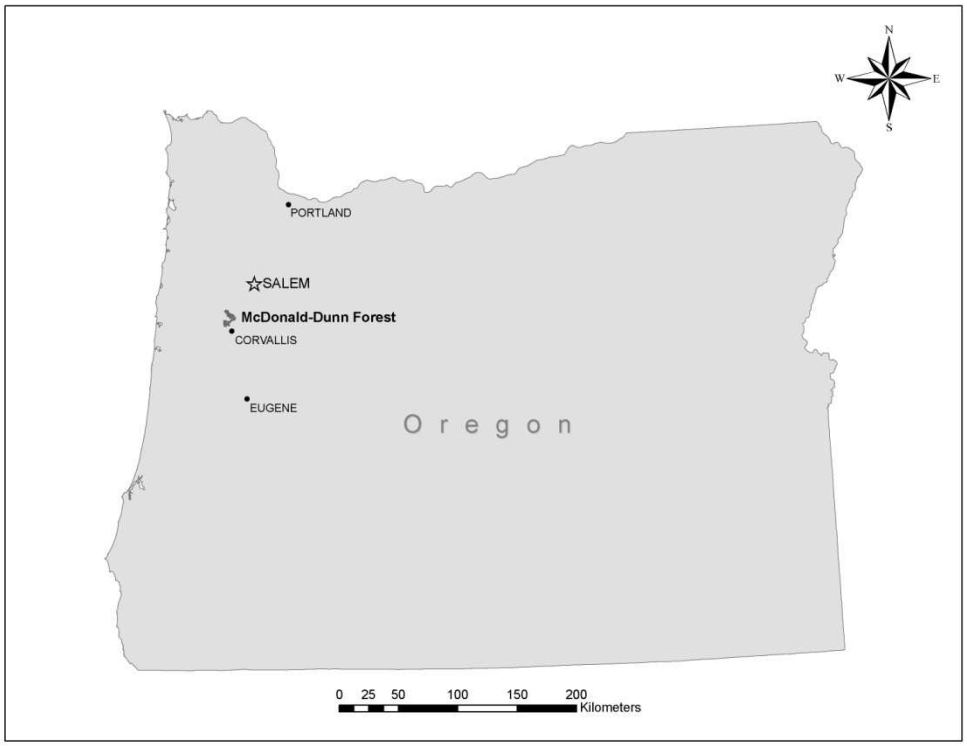

Figure 4.1. McDonald-Dunn Forest and surrounding communities within Oregon, USA.

Study Design

The original study design called for a total of twenty plots, five from each of four strata, but based on time and resources available eleven total plots were sampled. The plot strata consisted of old growth/mature (referred to as old growth in this study) (two plots), even-aged (two plots), uneven-aged (three plots), and clearcut (four plots) treatments. Each plot is hectare (100 m^2) in size and was selected by stratified random sampling using a numbered grid for each stratum and pseudo-random number generator software. Plot statistics are shown in Table 4.1. Plot naming corresponds to

the silviculture treatment (C = clearcut; E = even-age; O = old growth; and U = uneven-age) and GIS grid number used for random selection.

Table 4.1. Plot statistics for tree and shrub measurement comparison. Total station elevations were collected on five plots while GPS receiver and LiDAR elevations were collected in all plots.

Plot	C20	C27	C61	C110	E200	E412	O16	O69	U8	U13	U56
Slope Aspect	NW	NW	NE	NE	E	NE	NE	N	E	SE	NE
Slope Degree	24	18	13	9	7	14	17	28	17	14	8
Slope Percent	45	32	22	16	13	25	31	55	32	25	14
GPS											
Tree Count	691	565	534	575	946	929	363	238	192	498	1255
Shrub Count	8	15	0	118	56	57	140	-	-	47	72
Total Station											
Tree Count	N/A				910	N/A	355	257	367	385	N/A
Shrub Count					78		173	45	153	48	
LiDAR	825	647	632	619	1067	957	210	222	191	311	824
Feature Count											
Percent	11	9	10	9	65	27	47	46	43	38	70
Crown Cover											
*Stand Age yrs.	6	6	6	6	21	13	156	138	85	94	57

* Stand age in years based on oldest trees in the stand at time of LiDAR acquisition. Shrubs were not counted by GPS survey crews on plots O69 and U8.

The majority conifer species within the study plots was Douglas-fir (*Pseudotsuga menziesii*) (Appendix A-1) with a large contingent of grand-fir (*Abies grandis*) in the uneven-aged and old growth plots (Figure 4.2). Ponderosa pine (*Pinus* ponderosa) (35 plot C61, 14 plot C110) and Pacific yew (*Taxus brevifolia*) (20 plot O69) were found in limited circumstances in addition to several other isolated individuals such as silver fir (*Abies alba*) and western hemlock (*Tsuga heterophylla*). Although the forest is dominated by conifers, the primary deciduous tree species occupying the subcanopy is bigleaf maple (*Acer* macrophyllum). Many other broadleaf tree species were inventoried including cascara buckthorn (*Rhamnus* purshiana) (53 plot E200, 19 plot U56), cherry (*Prunus sp.*) (92 plot E200, 148 plot U56), and ocean spray (*Holodiscus*

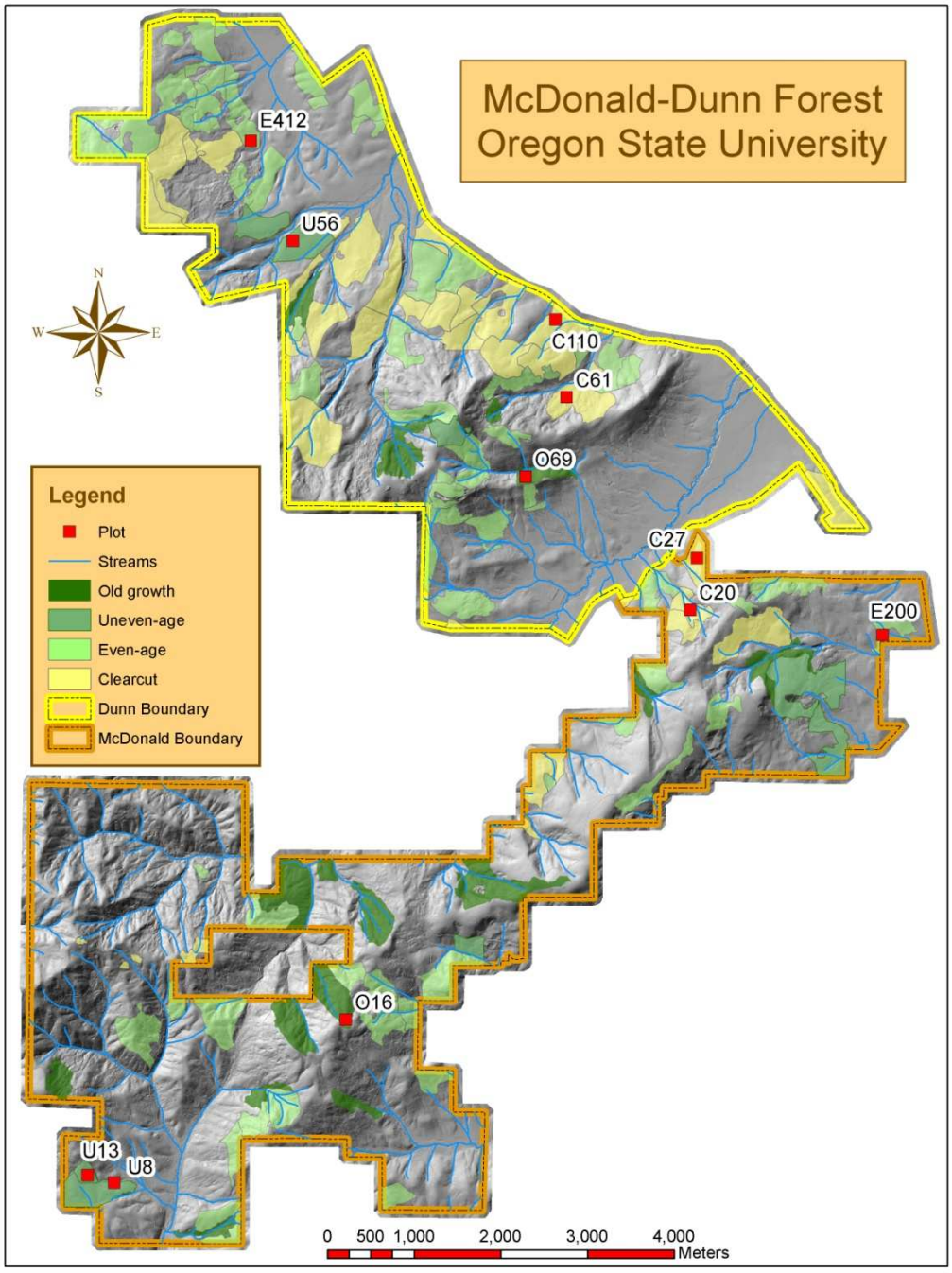

Figure 4.2. Plot locations in McDonald-Dunn Forest.

discolor) (33 plot O69) and many others typical of the region in far fewer numbers. California hazel (*Corylus cornuta*) is prolific in this region and dominated the understory species of all plots except clearcut where it had obviously been managed. Besides bigleaf maple, many other isolated shrubs typical of the region were inventoried, and ocean spray was conspicuous in two plots (33 in plot O16, 29 in plot U56). The densest ground cover was found on C110, which had portions covered in Oregon grape (*Berberis nervosa*) (63 inventoried) and poison oak (*Rhus diversiloba*) (not inventoried).

Plot Layout

After randomly selecting the plots, each was demarcated on the ground using an autonomous Trimble GeoXT GPS receiver prior to beginning the attribute survey. A stake was mounted in each corner and center of four sides of the 1 ha square plot and marked with its respective plot number and relative location within the plot for easy identification. Colored tape was tied to vegetation along the perimeter at easily visible increments to aid in finding the boundary stakes.

Total Station Survey

A Nikon DTM 310 total station with a rated angular accuracy of five-seconds was used with a Seco single lens reflective prism target mounted on a survey rod to collect the coordinate locations for trees and shrubs. All trees at 1 m and greater in height and all shrubs with a crown diameter of 1 m and greater were measured in five of the eleven plots. Additionally each downed tree log end coordinate was collected for those with an approximate dbh greater than 0.30 m and approximate tree sweep location.

Tree sweep was measured for conifer trees that had a noticeable lean angle, thus indicating a different tree apex location compared to its base. A local coordinate system was used for initial measurements with actual coordinates being determined in an office setting for analysis. Of the plots surveyed with a total station, three plots were surveyed by closed traverse (plots E200, O16 and U13) while two others used a radial traverse method (plots O69 and U8). While the radial traverse method increases the speed of traverse measurements, no closure error is calculated as the instrument remains stationary throughout all measurements. Closure error is reported in Table 4.2.

Table 4.2. Total station survey closure error. A radial traverse was used for plots O69 and U8 and resulted in no closure statistics.

Plot	Northing Error	Easting Error	Elevation Error	Number of Positions
E200	-0.050	-0.030	-0.020	1104
O16	-0.136	-0.081	-0.020	698
U13	-0.060	0.220	-0.090	560
O69	Radial Traverse			539
U8	Radial Traverse			572

Traverse station locations were established using wooden survey stakes and tacks. All tree coordinate data were collected using the total station sighted on a rod-person who was positioned directly at the tree stem for small trees or using a two meter offset (rarely further) for large trees. Offsets were established using a metric rod placed approximately 1.37 meters up the stem, and then a two m horizontal offset was sighted. The established protocol called for offsets to the cardinal direction south if unobstructed. The offset cardinal direction was then verified and corrected if necessary using a magnetic compass. The offset distance error was periodically

checked by using a metric tape instead of the rod. The mean error was 0.07 m (SD = 0.07 m). Coordinates, species, health, dbh, and height of all trees and shrubs were determined and recorded.

Survey control was established to transform the local total station coordinates into a Universal Transverse Mercator (UTM), zone 10 North NAD 1983 horizontal map coordinate system. A North American Vertical Datum 1988 (NAVD88) using geoid model 2003 (GEOID03) was applied for elevations. Two TOPCON Hiper Lite Plus survey grade GPS receivers were used to establish static control for each plot. The National Geodetic Survey (NGS) Online Position User Service was used for postprocessing control station coordinates. The OPUS uses a network of independent single-baseline solutions from three of the closest surrounding Continuously Operating Reference Stations (CORS) to determine average GPS error and correct the user provided GPS coordinates. The peak-to-peak error is provided for each component of a coordinate (X, Y, and Z). The peak-to-peak error is the error range between the maximum and minimum value obtained from the three baseline solutions (NGS 2009). Several attempts were made at establishing control over the actual traverse stations but the OPUS peak-to-peak errors were too high for project accuracy requirements. Plot U13 was the only plot with topographic and canopy conditions allowing for satisfactory peak-to-peak errors to establish control over previously existing traverse stations. The four remaining plots required GPS static control establishment outside the plot in an open area to allow for acceptable peak-to-peak error. Two control stations were established within each plot in order to obtain a backsight and azimuth

for a traverse survey. The final OPUS solutions and peak-to-peak errors for the control stations are shown in Table 4.3. The non shaded rows in this table correspond to stations used for closure in the control survey.

Table 4.3. NGS OPUS solution summary.
Reference Frame: NAD_83 (CORS96) UTM Coordinates

Plot	Duration (hours)	Easting (m)	Error (m)	Northing (m)	Error (m)	*Ortho Height Z(m)	Error (m)
E200b	6.15	482024.719	0.204	4945933.535	0.139	114.094	0.195
E200r	5.93	482018.628	0.018	4945944.978	0.074	114.575	0.052
O16b	6.68	475491.850	0.066	4941412.936	0.004	479.964	0.047
O16r	2.98	475477.745	0.083	4941424.029	0.128	479.393	0.141
O69b	6.20	477742.706	0.010	4947675.503	0.107	259.127	0.063
O69r	6.05	477702.804	0.091	4947673.283	0.025	262.195	0.056
U8b	5.83	472868.793	0.045	4939445.087	0.823	233.164	1.819
U8r	5.43	472814.411	0.448	4939485.507	0.176	239.021	0.151
U13b	9.03	472599.549	0.341	4939711.154	0.667	279.502	0.818
U13r	8.73	472609.562	0.270	4939732.904	0.347	282.088	0.503

In the plot naming convention above “b” stands for base (receiver 1) and “r” for rover (receiver 2).. *Ortho heights are NAVD88 using Geoid 03.

The final processing step in the total station measurement processing was to transform the local coordinates by translating and rotating those measured for each feature established during the radial traverse into UTM North Zone 10 coordinates, NAD83 (CORS96) datum. Traverse PC software was used for this transformation.

GPS Survey

In our study, three different Trimble mapping grade GPS receivers were used for GPS data collection in all eleven plots. These included the GeoXT, GeoXH, and ProXH receivers. Based on funding and procurement time lag of the higher accuracy rated ProXH and GeoXH receivers, we chose to begin the project using the GeoXT receiver for data collection in the clearcut and younger even-aged (E412) plots. All but one of the remaining plots was measured using the ProXH, and the final plot data (U8) was collected using the GeoXH based on project time constraints. The GeoXT was

configured using the Trimble Hurricane model external antenna while the GeoXH and ProXH were both configured with the Trimble Zephyr external antenna. Both the GeoXT and GeoXH do not require a data collector (field computer), but the ProXH does. A Trimble Ranger handheld data collector was used with the ProXH. A comparison of GPS receiver specifications is shown in Table 4.4.

Table 4.4. Trimble ProXH, GeoXH and GeoXT specifications.

	Trimble ProXH	Trimble GeoXH	Trimble GeoXT
Channels	12 (L1 code and carrier/L2 carrier	26 (12 L1code and carrier, 12 L2 carrier)	14 (12 L1code and carrier, 2 SBAS)
Accuracy			
H-star postprocessed			Not Equipped
With internal antenna	0.30 m	0.30 m	submeter
With external Zephyr ant.	0.20 m	0.20 m	
Code postprocessed	0.50 m	0.50 m	0.50 m
Carrier postprocessed			
Tracking satellites 5 min	info not provided	info not provided	0.30 m
Tracking satellites 10 min	info not provided	info not provided	0.20 m
Tracking satellites 20 min	0.10 m	info not provided	0.10 m
Tracking satellites 45 min	0.01 m	0.01 m	0.01 m

Table adapted from Trimble (Trimble 2007), Trimble (Trimble 2009a), and Trimble (Trimble 2009b)

We used the GPS data collection software Trimble TerraSync with consistent configuration settings throughout the survey. The receivers were set to collect UTM zone 10 north coordinates within a WGS84 datum. To reduce using satellites at risk of errors associated with ionospheric and tropospheric attenuation we used a 15 degree horizon mask. Lower PDOP values promote higher GPS accuracies and we chose a PDOP mask of 6, which Van Sickle (2008) describes as typical. All three GPS receivers in this study were equipped with multipath rejection capabilities (GeoXH and ProXH have Trimble H-star ® technology; GeoXT has EVEREST® technology) designed to aid in the detection and removal of multipath signals. We also used the

Trimble TerraSync default signal-to-noise ratio (SNR) value of 39 dBHz which is recommended by the manufacturer and in the middle of available settings between 33 dBHz and 43 dBHz (Trimble 2006a).

Similar to the total station survey, each tree, shrub, log end (logs > 0.30 cm diameter), and tree sweep (where applicable) was measured using a GPS. The GPS receiver and antenna were attached to a pole with the antenna mounted 2.2 meters above the ground to avoid multipath and/or signal attenuation from the ground and operator. Large tree locations were measured using a two meter offset. All others were generally measured at the feature location. A minimum of thirty and usually not more than sixty points were collected per position. Once the plot data collection was completed, the GPS receiver files were downloaded and differentially corrected using Trimble Pathfinder Office version 4.10. Each file collected using the GeoXT was differentially corrected using course acquisition (C/A) code processing using multiple base station providers selected through proximity to the plot and an integrity index. The original intent was to collect data using dual frequency carrier phase ranging. However, when differentially correcting the data, no carrier phase data corrections were possible. The integrity index value ranges from zero to one-hundred and indicates the reliability of the provider and its likelihood of providing quality results. The higher the index is, the better the integrity value (Trimble 2008).The closest available base providers were chosen, unless the integrity index was below eighty. We selected eighty because a priori knowledge indicated that integrity index values above 80 were consistently achievable. Each file collected using the ProXH or GeoXH

receiver was differentially corrected with automatic carrier and C/A code processing using multiple base station providers selected with consulting the integrity index. By selecting the automatic carrier and code processing in Trimble Pathfinder Office, the software analyzes the average code processed position and average carrier processed position, and selects the position with the least amount of error. When using the multiple base provider option, Pathfinder Office averages the coordinate data from each base station provider in the group, weighting the closer base provider higher to determine a single position solution. Because WGS84 is the reference ellipsoid for GPS (Van Sickle 2008), we chose to collect positions using WGS84 in UTM zone 10 north. The OPUS solutions used for the total station solutions in this project are based on NAD83 (CORS96). We used Trimble Pathfinder Office software to convert from WGS84 to NAD83 (CORS96), and then combined the separate GPS files into one by exporting to an Environmental Systems Research Institute (ESRI) shapefile for later analysis in the ESRI ArcGIS software.

Tree and Shrub Measurements

The field data collected for trees were species, height, crown width, dbh for stem diameters 13 cm and larger, diameter at ground level (agl) for stem diameters under 13 cm for all trees one meter and taller (0.61 m and taller in clearcut plots). Heights for tall trees were measured using an Impulse 200LR laser range finder. Height poles were used to measure trees shorter than three meters and all shrubs. A diameter tape was used for dbh and a caliper for agl. Crown radii for large trees were measured in one of two ways. One method was to estimate the projection of the crown vertically to

the ground and measure the distance from the tree stem to the ground point using a laser range finder. The other method was to stand at the base of the main stem and measure the angular distance to the end of the crown using the laser range finder, which the laser rangefinder then converted to a horizontal distance. Small trees and shrub crown measurements were made using a tape measure. In all cases two crown measurements were made per feature. The first length was measured at the longest stem in the crown, and the second was taken at 90^{o} around the stem in a clockwise direction. The crown diameter was then estimated by averaging the two crown measurements, multiplying by two, and adding the DBH. Canopy base height was measured using the FUSION software program however it was not measured by field crews. Shrub height and crown diameter was measured using the same method as used for trees for all shrubs with a crown width one meter and larger. Total field-measured vegetation is shown in Table 4.5 and species count by plot are shown in Appendix A-1 (trees) and Appendix A-2 (shrubs).

Table 4.5. Study total tree and shrub counts by species common name.

All Trees	Count	Conifers Only	Count	All Shrubs	Count
SPECIES		SPECIES		SPECIES	
bigleaf maple	371	Douglas-fir	5245	Bigleaf maple	110
California hazel	8	grand fir	876	California hazel	381
cascara buckthorn	76	pacific yew	20	Cascara buckthorn	2
cherry	247	Pacific silver fir	8	cherry	17
cottonwood	1	ponderosa pine	49	Douglas fir	1
Douglas-fir	5245	Total	6198	holly	9
grand fir	876			madrone	1
hawthorne	6	Conifers Minus Snags		mountain mahogany	1
holly	6	SPECIES		oceanspray	73
madrone	10	Douglas-fir	5156	Oregon white oak	5
oceanspray	3	grand fir	866	Oregongrape	64
Oregon white oak	9	Pacific yew	20	other	14
Oregongrape	9	Pacific silver fir	8	Pacific dogwood	6
other	18	Ponderosa pine	48	red elderberry	12
Pacific yew	20			Scoular's willow	2
Pacific dogwood	2	Total	6098	snowberry	1
Pacific silver fir	8			vine maple	12
ponderosa pine	49				
red elderberry	6			Total	711
vine maple	10				
Total	6980				

LiDAR Collection

The LiDAR data were collected on April 2, 2008 under clear, sunny weather conditions. The contractor who flew the LiDAR mission was Watershed Sciences based in Corvallis, Oregon. Watershed Sciences used a Leica ALS50 Phase II laser system with a ± 14º scan angle from nadir and pulse rate designed to achieve a point density of ≥ 8 points per square meter. To reduce laser shadows and increase laser coverage, each flight line had ≥ 50% side-lap, which equates to ≥ 100% overlap throughout the study area. The system is capable of a maximum number of four

returns per pulse. Positional coordinates of the airborne sensor and aircraft attitude (pitch, roll and yaw) were recorded continuously throughout the survey mission to accurately solve for northing, easting, and elevation laser point coordinates. The onboard differential GPS unit measured aircraft position twice per second (2 Hz) and the inertial measurement unit (IMU) measured aircraft attitude 200 times per second (200 Hz) (Watershed Sciences 2008). Ground control was conducted simultaneously with the airborne LiDAR survey using a static GPS located over ground stations with known locations at a rate of one point collected per second (1 Hz) with indexed time. The ground station information provided by the contractor is in Table 4.6. The static GPS data ground control positions were post processed following the airborne survey using CORS stations and verified using the NGS OPUS to quantify daily variance. An additional RTK GPS survey was conducted collecting 510 locations in a limited and open area in the northern portion of the study area (Figure 4.3) for ground truth confirmation of LiDAR point coordinates (Watershed Sciences 2008).

Table 4.6. Base station survey control coordinates for LiDAR survey.

	*Datum: NAD83 (CORS96)		GRS80
Base Station	Latitude	Longitude	Height Above Ellipsoid (m)
McDunn1	44º 42’ 48.40874”	123º 17’ 54.20724”	80.94
McDunn2	44º 42’ 47.73917”	121º 17’ 53.85155”	81.73

*Later determined in this research to be NAD83 (CORS96).

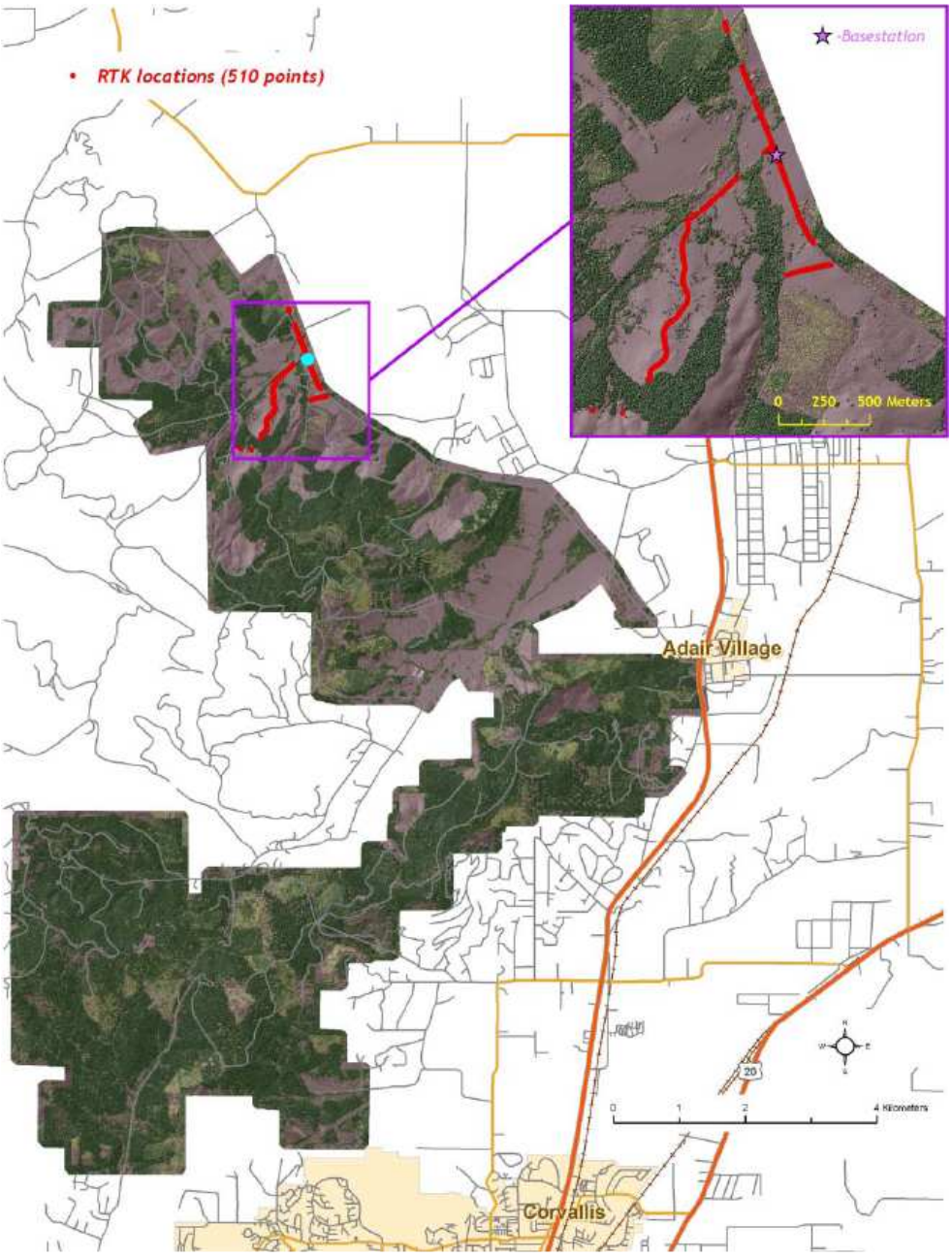

Figure 4.3. Map of LiDAR survey control base stations and RTK positions (figure from Watershed Sciences 2008).

Laser point coordinates were computed with IPAS and ALS post processing software, then resolved to correct for aircraft pitch, roll, heading, and scale and finally filtered for non-terrestrial returns caused by birds, vapor, haze, and other undesired

features. Internal calibration of the LiDAR data were refined using TerraMatch software in which automated sensor attitude and scale corrections yielded 0.03-0.05 m relative accuracy improvements, and then GPS drift was removed per flight line improving relative accuracy by < 0.01m. TerraScan software was used to classify and model near-ground points, which were then manually inspected and refined for improved ground detail and modeled again (Watershed Sciences 2008). A DEM was generated from a triangulated irregular network (TIN) created from the ground classified LiDAR points with a modeling algorithm within TerraSolid software. Raster tiles are then created and later merged into a DEM mosaic (M. Hey, personal communication, April 20, 2010).

The LiDAR data accuracy was described by the vendor as the mean error and standard deviation of the LiDAR point coordinates compared to RTK surveyed ground point coordinates. Reported laser point density and accuracy are shown in Table 4.7.

Table 4.7. Laser point density and accuracy reported by vendor.

	Target	Reported
Average First Return Point Density	≥ 8 points/m^2	10 points/m^2
Average Ground Point Density		1.12 points/m^2
Vertical Accuracy (1σ)	< 0.13 m	0.02 m
Average Relative Accuracy		0.053 m
Absolute Accuracy		0.026 RMSE
Absolute Z Accuracy		0.007 ME, 0.026 SD

Data provided by the vendor included the following: raw LiDAR point data in LAS format of ground classified points, first return points, and all four laser returns with X, Y, and Z coordinates and intensity values; bare earth DEM and highest hit model in one-meter ESRI grid format; and one-half meter intensity images in GeoTIFF format. No multispectral imagery was acquired for this project. The raw LiDAR file format

has a .LAS extension. This is not an acronym, but is derived from the American Society of Photogrammetry and Remote Sensing (ASPRS) file format stemming from LASer. "The LAS file format is a public file format for the interchange of LIDAR data between vendors and customers" (ASPRS 2009).

LiDAR Processing

Several different algorithms have been developed to delineate individual tree crowns and measure tree heights. In this study the three extraction algorithms (methods) compared were WS segmentation, TreeVaW, and FUSION. The WS segmentation and TreeVaW methods automatically delineate and measure features determined to be trees from the CHM (Figure 4.4), whereas FUSION requires manual location and measurement of each tree feature from the LiDAR point cloud and, if needed to aid in extraction, a CHM. We used FUSION to create CHM rasters at spatial resolutions of 0.1, 0.3, and 1 m in order to examine resolution influence on tree determination processes. Additionally, FUSION uses mean and median convolution smoothing filters in creating a CHM. The program preserves the local maxima (peaks) while smoothing the surrounding pixels, forcing the surface to adhere to the tree tops. While preserving the tree top designated by the local maxima the filter smoothes surrounding canopy pixels based on the mean or median value of the pixel values within the filter kernel. Besides the value of the local maxima, which maintains the value as the highest point in each tree neighborhood, the values of the surrounding crown are stepwise smoothed (McGaughey 2007). We experimented with both filter approaches and found that the median filter when compared to the field-measured data

appeared to have increased errors of omission, thus we used the mean filter. Filter options tested were none, 3 x 3, and 5 x 5. After running WS segmentation and TreeVaW iteratively using each CHM resolution, two factors were used to select the model that best matched the field survey data. The first factor was the number of trees and the second was spatial variation. The closest matched sum of trees was selected first, and then the spatial variation of the tree points were observed in a GIS. Spatial variation included two subparts: location and pattern. In many cases the LiDAR generated tree count by plot had similar counts to the field survey count, however when viewing the spatial location of the points in a GIS map, it became obvious that errors of commission occurred, e.g. many points were clustered in a location where only one tree was field-measured; or many single trees were located in locations that trees did not exist and were well outside a reasonable distance from a field-measured tree, thus creating a spatial pattern that did not match the field-measured pattern.

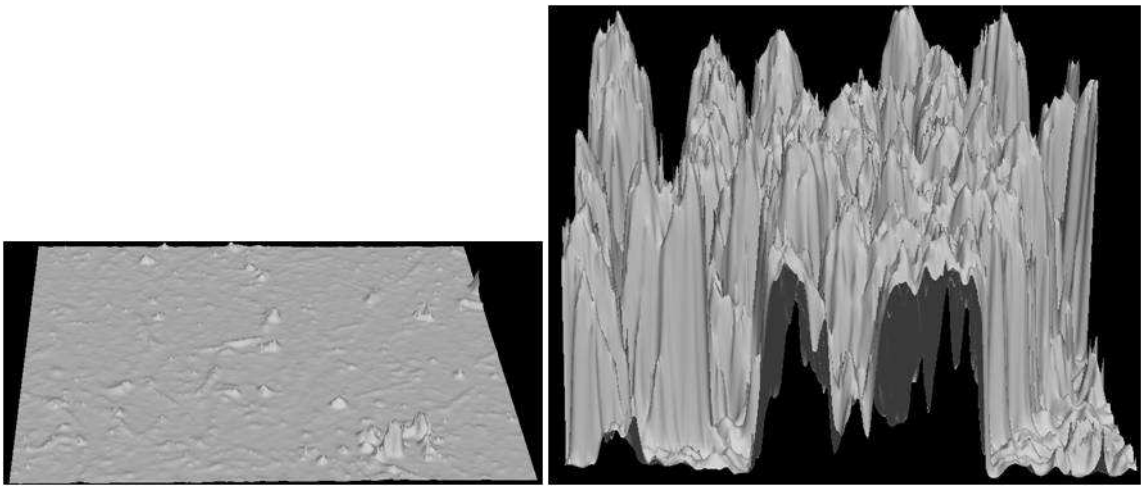

a) CHM – Plot C20 Clearcut b) CHM – Plot O69 Old growth

Figure 4.4. Canopy Height Model (CHM) representing (a) clearcut and (b) old growth plots.

ArcGIS software was used to conduct inverse watershed segmentation. Watershed segmentation determines tree locations and heights by inverting the CHM so that when the model is turned upside down the peaks become depressions (Figure 4.5). When the raster surface is configured as a depression model, watershed segmentation can then be performed to delineate basins (canopy basins). The canopy basin raster model is converted to canopy polygons which delineate a polygon canopy vector file. The model then uses zonal statistics to overlay the canopy basin file on the CHM and assign the highest pixel value per individual tree canopy basin while replacing all other pixels with a no-data value leaving one pixel remaining with a height value per designated canopy. This value becomes the tree height (Z) and tree bole location (X and Y). Two shapefiles are created in the process, one with only a tree X and Y location and another with a tree X and Y location that includes tree height (Z).

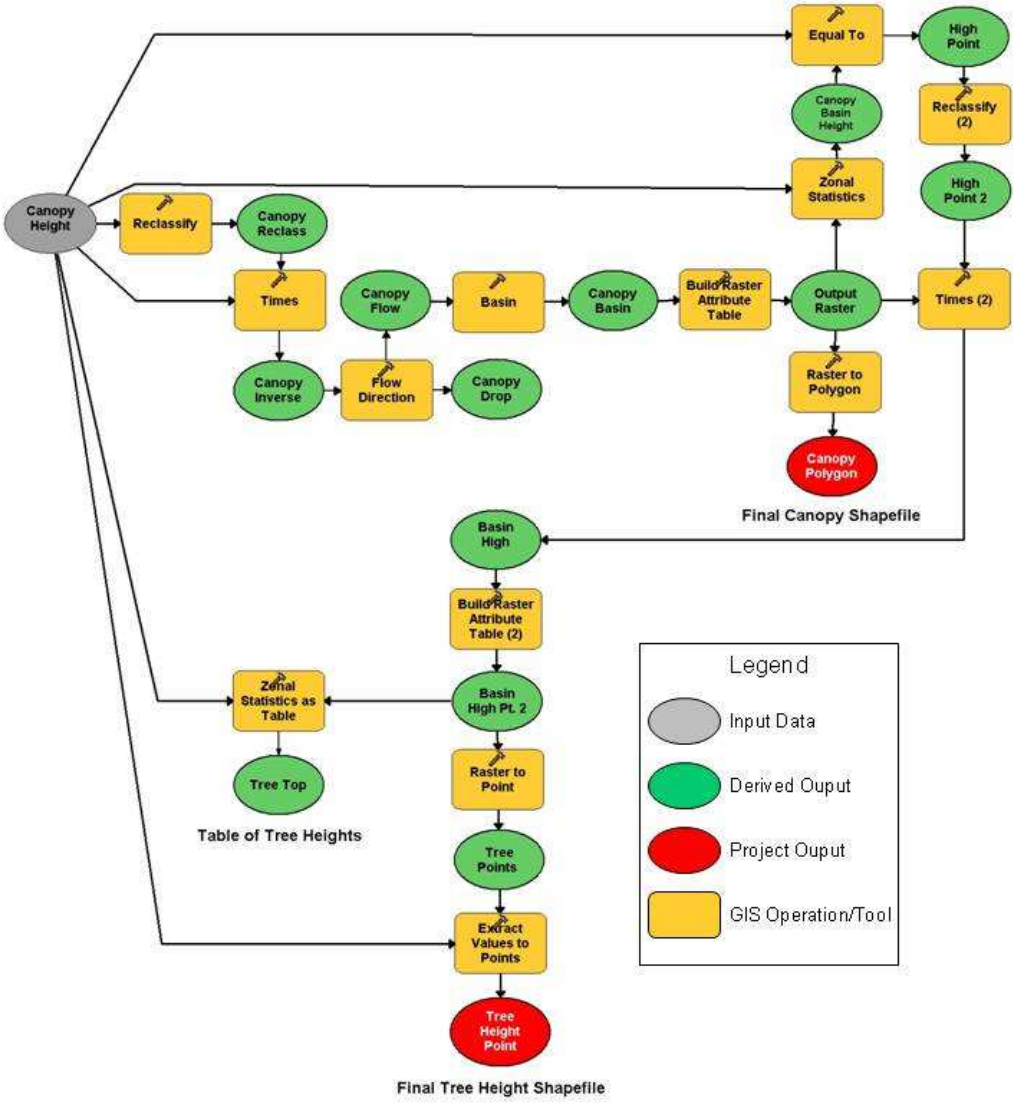

Figure 4.5. Inverse Watershed Segmentation model flow.

We used TreeVaW software version 1.0 (Popescu 2010). TreeVaW implements the CHM processing software in Interface Definition Language (IDL) to locate and

measure trees. TreeVaW uses the CHM in ENVI image format and produces output consisting of tree positions in x and y coordinates, tree heights, and crown radii (Popescu 2010). The "VaW" in TreeVaW is an acronym for variable window. The program delineates trees by deriving an appropriate size circular search window to find tree tops from the CHM based on the relationship between the height of trees and their crown size. As found in nature, the taller the tree, the larger the crown size (Popescu et al. 2002). The program is designed for conifer forest applications and uses a search window based on a default regression relationship of crown diameter as a function of height developed in the southeastern United States, thus the crown diameter relationship was edited using the field collected data for this project. The program's default regression formula is $CW = 2.51503 + 0.012000H^2$ where CW is crown width and H is height. Initial attempts at TreeVaW tree delineation met with poor results in clearcut plots when the regression equation from all field collected trees was used, thus a separate equation was used for the clearcut plots based only on the field database of clearcut plot conifer species. Three attempts were made to determine which regression equation to use for delineating trees in clearcut plots and are further discussed in the results section. For all other plots, the field collected database of all trees except snags having no crown was used for the regression. Dead trees with discernable crowns were included. The input of minimum and maximum crown width and maximum expected tree height parameters are also required before running TreeVaW. We input these values based on our field data.

We applied FUSION software version 2.70 (USDAFS 2008) for tree delineation. The FUSION software consists of two main programs, FUSION and the LiDAR data viewer (LDV). Many component command line programs also come with the FUSION package for preparing and processing raw LiDAR data for analysis in FUSION and LDV. Once pre-processing steps are completed and the LiDAR data are prepared for plot level analysis, trees are manually selected and measured in LDV using the LiDAR point cloud (Figure 4.6a) and measurement marker (Figure 4.6b). Although canopy base height was not measured by field crews in our study, of the three LiDAR software programs used in the study, FUSION is the only one capable of this measurement. In the FUSION generated plots, we measured heights of the upper portion of the point cloud, which in most cases is likely the top of the crown and not the apex of the tree, and measured the lowest discernible portion of the point cloud coincident with what appeared to be the lowest whorl of branches. This was only possible in larger trees in primary canopy where sufficient returns were available to identify the minimum and maximum crown heights. Crown diameter was measured using the measurement marker in either a circular form for a generally round shaped crown, or elliptically where the crown was more oval shaped from an orthogonal perspective. Spatial x and y location was measured based on where the analyst determines the apex and center of the tree to be located. Each set of measurements is added to a Comma Separated Value (CSV) file database of individual trees. These files were then converted to ESRI shapefile format for GIS analysis.

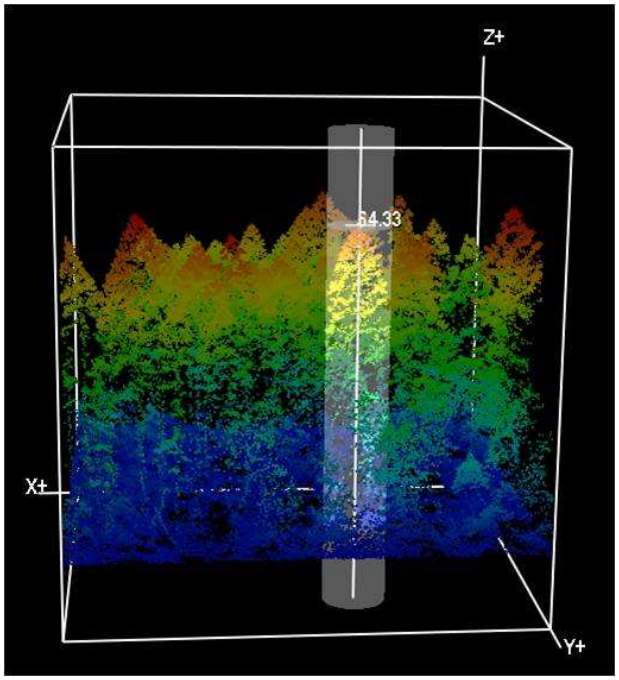

a) LiDAR point cloud and measurement marker

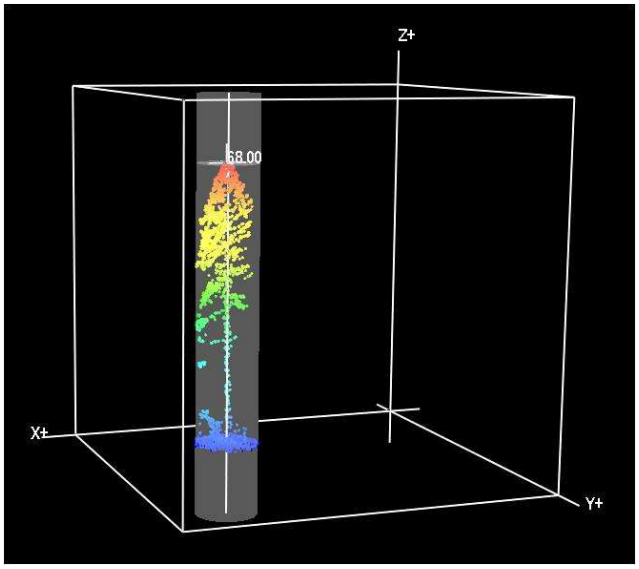

b) LiDAR tree and measurement marker

Figure 4.6. a) FUSION LiDAR Data Viewer (LDV) measurement window displaying tree height measurement capability. Tree X and Y location, height, crown width, crown base height, and elevation at tree base may be measured and saved to file; b) FUSION measurement marker surrounding a single LiDAR tree.

Initial LiDAR data preparation is a relatively time consuming process that includes processing the raw .LAS files, data conversion for respective software requirements, subsetting into areas of interest/plots, creating ground and canopy surface models, and other processing. Once the LiDAR was prepared for each software program used in this study, there were significant differences in time required to delineate trees. Both TreeVaW and watershed segmentation were automated tree delineation programs that processed each hectare sized plot in this study rapidly within seconds. FUSION on the other hand requires the operator to manually measure and save each tree. This process is relatively quick (30-60 seconds per tree) for large trees in the primary canopy, but becomes progressively more difficult to differentiate smaller trees in the sub-canopy. Based on the time required to delineate individual trees using FUSION, and that this project involved thousands of trees, we limited tree delineation using FUSION to six plots (C110, E200, O16, O69, U8, U13). Plots for FUSION analysis were chosen based on the desire to test the capability of the software in each of the four plot treatments within the study. Plots, E200, Ol6, and U13 were originally selected because they were the initial plots surveyed using a total station. Plot C110 was randomly selected. Plots O69 and U8 were added later because they had also been surveyed using total station, and Plot O69 was important to analyze based on its steep topography. The advantage to using TreeVaW and watershed segmentation is the speed of processing. The disadvantage to these two programs is that they are limited by the CHM, which inherently due to interpolation loses tree

information below the upper canopy. The advantage of FUSION is that it uses the LiDAR point cloud, where all points are available to the user.

Field-measured tree x and y locations and tree heights were compared to those determined by each LiDAR extraction method. For this study, the main purpose of comparing the accuracy of each tree's spatial location was to establish confidence that tree height comparisons between ground and LiDAR were based on the same tree. The only confirmation of this was similar spatial location and height. The most accurate method used for determining tree spatial location in this study was by total station survey instrument.

Geographic Information System (GIS) Processing

Tree and shrub locations were measured by total station on five of the eleven plots as discussed above. Only absolute spatial location was measured. Height and species was nominally noted, i.e. tree heights were noted as small, average, large, or extra large for the respective plot. The tree functional type was noted as conifer or broadleaf. GPS measurements were made in all eleven plots. In addition to absolute spatial location, tree height, crown radius, and species were determined and recorded. In the total station surveyed plots, the specific tree data collected in the GPS survey was used to match total station surveyed trees such that the most accurate horizontal coordinates were combined with specific species and height measurements. Total station feature points were matched to those determined by GPS using ArcGIS software. Each tree feature was matched manually based on proximity, height (absolute to nominal), and species (specific to nominal) and assigned the same unique

identification number. Trees were only matched if relative confidence existed that the two represented the same tree. Where there was doubt, features were not matched. The least amount of confidence in matching occurred in the even-aged plot (E200), where most of the trees were a similar height and species (Douglas-fir). In this case proximity was the only matching metric, thus some bias may exist in horizontal error between individual features locations determined by GPS and total station.

Biomass

Biomass was calculated using allometric equations from the biomass computation package BIOPAK (Means et al. 1994) (Table 4.18). Because we measured only height and crown diameters for shrubs, and did not measure stem or basal diameters we chose to use percent crown cover for shrub biomass estimates. We used GIS software to calculate crown cover by creating a polygon layer using the field-measured crown diameter measurements for all shrubs in the plot, clipping the shrub crown polygon layer using the plot perimeter data, and then calculating percent crown cover for the one ha plot. The majority of the shrubs in the study area were California hazel (*Corylus cornuta*) (Appendix A-2), thus we used this species to calculate a general biomass estimate on a by-plot basis. The closest allometric equations using crown cover we could find for our study area were based on destructive sampling of California hazel collected in riparian zones and meadows in the Sierra Nevada range, California. The equation used was BAT = (5.01 * COV) * m^2. BAT is total above ground biomass including foliage and COV is the cover percentage, and m^2 is the plot dimension in square meters (Means et al. 1994). Crown (canopy) cover is the

proportion of vertically projected tree or shrub crown (above ground vegetation) that covers the forest floor measured as the presence or absence of canopy vertically above sample points across an area of forest. The height of the tree or shrub has no impact on this measurement as it is the vertical projection of the crown that is measured. Crown cover may be used to predict volume by species because crown area to trunk (stem) basal area has a near linear relationship (biomass) (Jennings et al. 1999). For trees within this study, all biomass estimates were based on allometric equations related to DBH or DBA, with some equations including height. For trees smaller than 0.13 m DBH, the DBA equations were used. Where weights were calculated in cm^3, weights were converted to kg. All LiDAR biomass estimates were based on Douglas-fir biomass estimates. Two Douglas-fir equations were used, one for trees $\geq$ 0.13 m DBH and trees < 0.13 m (Table 4.17) based on BIOPAK values (Means et al. 1994). BIOPAK provides a Coast Range region equation for small trees whose stem diameter is measured at the base and another based on DBH of larger trees (Table 4.8). We used a cutoff of 0.13 m DBH for large and small trees. If a tree was smaller than 0.13 m DBH, then the stem diameter was measured at ground level (AGL). LiDAR DBH estimates were based on regression analysis from trees measured in this study

Table 4.8. Equations used to determine plot biomass from biomass computation package BIOPAK (Means et al. 1994).

Species	Bio Component Description	Region*	Biomass Equation
Abies amabilis (Pacific silver fir)	BAT = Total aboveground biomass	G	BAT =12800 + 0.1836 * (DBH)2 * HT
Abies grandis (grand fir)	BAT = BAT without dead branches	G	BAT = 30.2 + 146.9 * (DBH)2 * HT
Acer circinatum (vine maple)	BFT = Total foliage biomass	W	ln(BFT) = 1.8820 + 1.9754 * ln(DBA)
Acer circinatum (vine maple)	BST = Total stem biomass	W	ln(BST) = 3.1591 + 2.5335 * ln(DBA)
Acer macrophyllum (bigleaf maple)	VAE = Volume (cm^3) above grd.	C	ln(VAE) = 1.623161 + 2.22462 * ln(DBH) + 0.57561 * ln(HT)
Arbutus menziesii (Pacific madrone)	BAT = Total aboveground biomass	C	BAT = -1080 + 918.92 * DBA^2
Berberis repens (Oregon grape)	BAT = Total aboveground biomass	G	ln(BAT) = 2.976 + 2.092 * ln(DBA)
Cornus nuttallii (Pacific dogwood)	BFT = Total foliage biomass	W	ln(BFT) = 2.7920 + 1.8685 * ln(DBA)
Cornus nuttallii (Pacific dogwood)	BBL = Live branch biomass	W	ln(BBL) = 2.2606 + 2.8737 * ln(DBA)
Cornus nuttallii (Pacific dogwood)	BST = Total stem biomass	W	ln(BST) = 3.2943 + 2.0625 * ln(DBA)
Corylus cornuta californica (Cal. hazel)	Cover	S	BAT = 5.01 * COV
Holodiscus discolor (oceanspray)	BAT = Total aboveground biomass	R	ln(BAT) = 3.769 + 3.033 * ln(DBA)
Pinus ponderosa (ponderosa pine)	BAT = Total aboveground biomass	G	BAT = 1160 + 0.1870 * (DBH)2 * HT
Populus trichocarpa (black cottonwood)	BAT = BAT without dead branches	G	BAT = 7400 + 0.1564 * DBH^2 * HT
Prunus emarginata (bitter cherry)	BAT = Total aboveground biomass	E	ln(BAT) = -9.27455 + 2.8934 * ln(LEN+WID)
Pseudotsuga menziesii (Douglas-fir)	BAT (Large trees) = Biomass aboveground (w/o dead branches)	C	ln(BAT) = 4.7824 + 2.2985 * ln(DBH)
Pseudotsuga menziesii (Douglas fir)	BAT (small trees) = Geometric mean stump dia.above grd biomass.	C	ln(BAT) = 4.59314 + 2.03553 * ln(DBA)
Quercus garryana (Oregon white oak)	VAE = Volume (cm^3), above ground. live+dead wood plus bark	G	ln(VAE) = 0.793195 + 2.14321 * ln(DBH) + 0.7422 * ln(HT)
Thuja plicata (western redcedar)	BAT = Total aboveground biomass	G	BAT = 40400 + 0.0969 * (DBH)2 * HT
Tsuga heterophylla (western hemlock)	BAT = Total aboveground biomass	G	BAT = 29800 + 0.1558 * (DBH)2 * HT
Umbellularia californica (Cal. laurel)	VAE = Volume (cm^3), above grd. live+dead wood plus bark	C	ln(VAE) = 0.2643834 + 1.94553 * ln(DBH) + 0.88389 * ln(HT)

*Region abbreviations: G-General, W- Western Cascades, C- Coast Range, E- Eastern Cascades, R- Rocky Mountains

Results

LiDAR Model Selection

Using two factors of stem count and spatial variation, the LiDAR model results were compared (Tables 4.9 and 4.10). Each method resulted in various errors of omission and commission. For WS segmentation and TreeVaW, we experimented with different resolution CHMs interpolated from the original LiDAR point clouds. When using a CHM, any vegetation below the dominant/co-dominant canopy is likely to fall below the CHM surface, thus we experimented with higher resolutions to determine if smaller trees could be discernible within the LiDAR data. In some cases clustering was observed where errors of commission occurred. One example of this was many tree points clustered around only one field surveyed tree. In some cases this was due to multiple hits on a single broadleaf tree and in others, false tree tops on a conifer tree. Errors of commission were also observed where a tree was delineated in a location where no field surveyed tree existed. This was primarily due to higher resolution CHM interpolation causing errors of commission. The 0.1 m resolution was decisively in error compared to the other, coarser resolutions. The best matching LiDAR designated results also had instances of clustered points around a single field surveyed vegetation point, which in most instances appeared to be multiple hits on a broadleaf tree such as bigleaf maple.

A one meter resolution CHM interpolated without a convolution filter resulted in watershed segmentation tree designations that appeared to best match field-measured trees (Table 4.9). Three exceptions to this were in the even-aged plots and one uneven-aged plot. In plot E412 the 0.3 resolution CHM using 3 x 3 and 5 x 5 filters displayed the spatial pattern obviously created by planting in rows, and the 5 x 5 filter best matched the number of stems to field-measured. The GPS field collected data did not reflect this pattern based on random spatial error caused by the GPS. TreeVaW did not display this pattern either except when using the 0.3 meter resolution canopy height model with a 3 x 3 filter.

Table 4.9. Delineated stem counts resulting from inverse watershed segmentation using various CHM resolutions compared to field-measured vegetation. Checked numbers indicate the resolution and filter method that best matched field count numbers.

	CHM Resolution and Filter Size						
Plot	0.1 m , 5x5 Filter	0.3 m, 3x3 Filter	0.3 m, 5x5 Filter	1 m, No Filter	Field Count Tree/Shrub	Field Count Total	LiDAR/Field Count (%) all/tree only
C20	6780	948	595	825✓	691/8	699	118/119
C27	1249	366	250	647✓	565/15	580	111/115
C61	3969	684	411	632✓	534/0	534	118/118
C110	3535	381	247	619✓	575/118	693	89/108
E200	6848	1067✓	776	476	946/56	1002	107/113
E412	12268	1540	957✓	546	929/57	986	97/103
O16	14728	2049	999	210✓	363/140	503	42/58
O69	14769	1736	974	222✓	257/45	302	73/86
U8	19994	1727	991	191✓	367/153	520	37/52
U13	18312	1623	688	311✓	498/47	545	57/62
U56	17331	1523	824✓	256	1255/72	1327	62/66
Total		1067	1781	3657			
Grand Total		6505 (from ✓ selected values)			6980/711		85/93

*Percent of best matching LiDAR count to field count total and trees only.

Several iterations were run in the clearcut plots to find the best match of TreeVaW delineated trees to field-measured trees (Table 4.10). The two decision factors used to

determine the best match for TreeVaW were numbers of trees and spatial relationship as discussed in methods. The first iteration utilized the crown to tree height relationship from all field-measured trees (minus snags with no crown): CW = 0.0028 + 1.1207 * (H), where CW = crown width and H = tree height (R^2 = 0.74). TreeVaW also requires inputs of expected maximum height and crown widths. We used expected values for the entire project that were based on maximum ground measured heights and crown widths from all plots combined. The second iteration used the same crown to tree height relationship but the required inputs of maximum tree height and crown width were limited to sizes expected only in the clearcut plots, which were determined from the field sampled database of all clearcut plot trees. The third iteration used the crown to tree height relationship found only in clearcut plot conifer trees, CW = 0.09550 + 0.5173 * (H) (R^2 = 0.77), and the required input of tree height and crown width remained limited to sizes expected in clearcut only plots, also determined from the database of field sampled clearcut conifer trees. All other plots besides clearcut plots used the crown to tree height relationship of CW = 0.0028 + 1.1207 * (H). Individual tree measurements are saved in a text file including height, spatial location, and crown radius. Crown radius is used for generation of circular crown buffers in GIS, thus converting the radius into a diameter. Each TreeVaW text file was then converted to an ESRI shapefile for GIS analysis.

GIS point files were generated from field-measured data and each of the three tree extraction software programs used in this study (Figure 4.7). Visual inspection of tree

patterns suggest that all methods compare relatively well to the field-measured points for Plot E200 as little canopy height differentiation existed. In plots O16 and U13 strictly looking at numbers, the watershed segmentation achieves the greatest number of trees, followed by TreeVaW and FUSION (Table 4.11). The most obvious pattern is displayed in plot E200. Tree planting pattern is observed using all methods, the least obvious of which is the field-measured data likely due to the random horizontal error associated with mapping grade GPS. Table 4.11 compares field collected and LiDAR method feature counts.

Table 4.10. TreeVaW LiDAR stem counts compared to GPS and total station field counts. Checked numbers indicate the resolution and filter method that best matched field-measured trees based on count and spatial relationship.

	CHM Resolution and Filter Size						
Plot	0.1m , 5x5 Filter	0.3m, 3x3 Filter	0.3m, 5x5 Filter	1m, No Filter	GPS Field Count Tree/Shrub	Total Station Count Tree/Shrub	Difference (%) / tree n*
C20	98/385/385	102/132/70	✓96/135/52	98/172/98	×691/8	N/A	14/14
C27	16/51/51	95/54/53	65/51/39	58/✓115/58	×565/15	N/A	19/20
C61	776/316/316	120/108/78	193/112/57	✓82/111/62	×534/0	N/A	15/15
C110	281/540/540	165/81/105	✓104/80/58	101/182/101	×575/118	N/A	15/18
E200	973	664	✓704	616	×946/56	910/78	70/74
E412	2507	✓1049	475	664	×929/57	N/A	106/113
O16	822	197	✓218	114	×363/140	355/173	43/60
O69	1129	276	✓197	125	238/-	×257/45	65/77
U8	1243	✓123	118	88	192/-	×367/153	24/34
U13	1987	457	✓285	211	×498/47	385/48	52/57
U56	✓1117	276	187	167	×1255/72	N/A	84/89
Total	1117	1172	1604	197			
Grand Total			4090 (from ✓ selected values)		**6980/711		53/59

Clear cut iterations are listed in order from left to right third, second, and first iteration. *Percent of best matching LiDAR count to field count total and trees only. Field counts used were based on the GPS inventory, with the exception of Plots O69 and U8 where GPS excluded shrubs. **Shaded counts with an × indicate values used to calculate totals.

LiDAR Count Comparison

Comparing each method of LiDAR tree detection shows a great deal of variation in the number of trees detected in each plot with manual detection trees in FUSION consistently delineating fewer (Table 4.11), noting that FUSION was only used on six plots. Based only on field-measured tree counts, tree delineation was best performed by watershed segmentation followed by TreeVaW and FUSION with overall percentages equaling 93%, 59%, and 44% respectively. Watershed segmentation appeared to perform noticeably better on the clearcut and even aged with the exception of plot E412 where TreeVaW had an approximate equal percentage (Tables 4.9 and 4.10). All methods did considerably poorer in uneven aged and old growth treatments due primarily to missing understory trees.

That said, each program was relatively consistent when manually matching trees to field-measured tree points in a GIS (Table 4.12). FUSION again demonstrated the fewest matches, followed by TreeVaW and watershed segmentation. FUSION was within 16% (994) and TreeVaW 14% (994) of the count achieved by watershed segmentation (1151). In this portion of the study, only trees that were within a reasonable distance and similar height were compared. Reasonable distance was based on height. Taller trees were subjectively given greater manual search windows based on having larger crowns that could potentially be struck by LiDAR pulses.

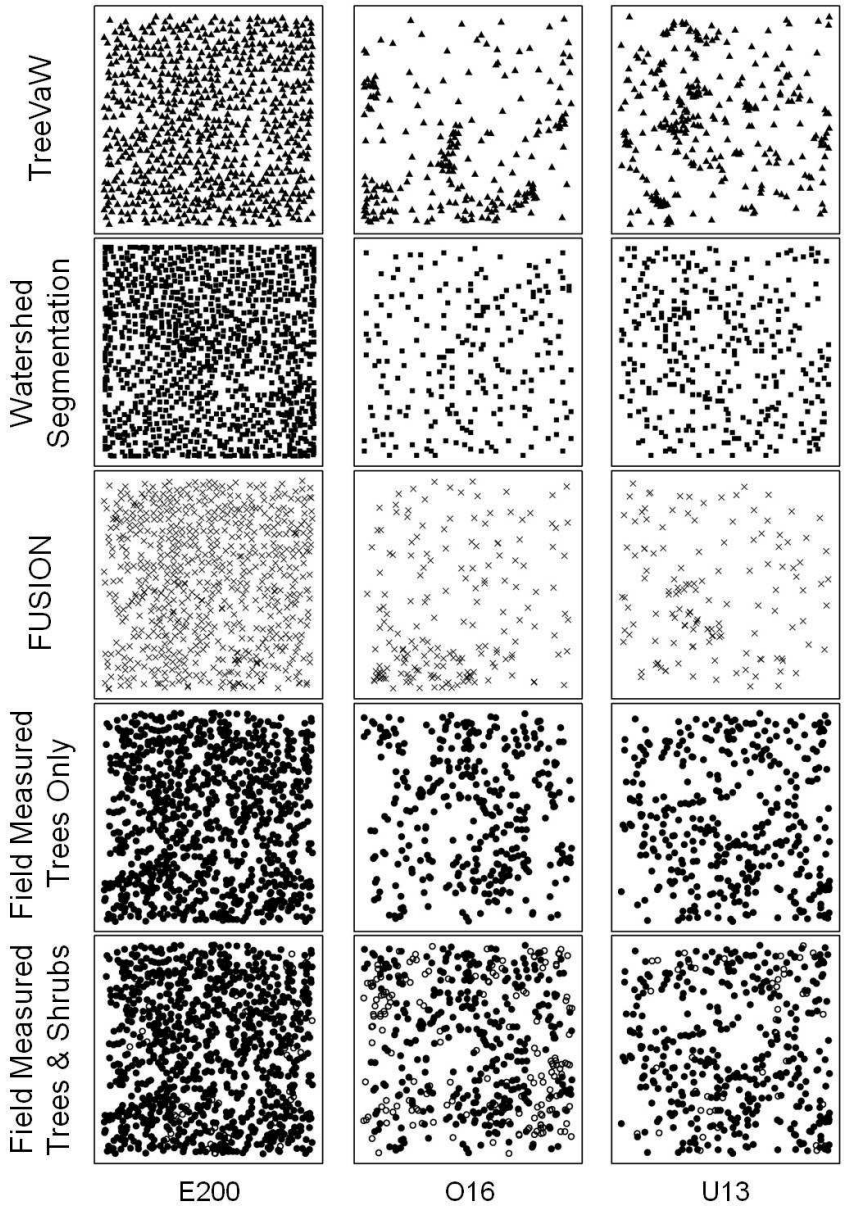

Figure 4.7. LiDAR tree extraction method comparison for plots representing even aged (E200), old growth (O16), and uneven aged (U13) conditions. The figure rows (ordinate) contain images of the plotted tree/vegetation stem locations by method and the columns (abscissa) are the corresponding plots. Field-measured points are displayed with trees (solid dots), shrubs (hollow dots), and with trees only.

Table 4.11. Tree feature count by LiDAR extraction method compared to field count by total station and GPS.

Plot	WS Segment.	TreeVaW	Fusion Count	GPS Tree/Shrub	GPS Field Count Total	Total Station Count Tree/Shrub
C20	825	96	N/A*	691/8	699	N/A*
C27	647	115	N/A	565/15	580	N/A
C61	632	82	N/A	534/0	534	N/A
C110	619	104	184	575/118	693	N/A
E200	1067	704	652	946/56	1002	910/78
E412	957	1049	N/A	929/57	986	N/A
O16	210	218	181	363/140	503	355/173
O69	222	197	86	238/-	238	257/45
U8	191	123	88	192/-	192	367/153
U13	311	285	135	498/47	545	385/47
U56	824	1117	N/A	1255/72	1327	N/A
Total	6505	4090	1326	Field Count 6980/711		
% of Fld Count (all/trees).	85/93	53/59	37/44			

*N/A indicates that FUSION or total station summaries were not performed on this plot.

LiDAR Height Comparison

We compared field-measured and LiDAR derived tree heights using three comparisons. The first comparison was conducted on select plots by matching and pairing individual features as explained in methods. Height errors between the three methods of extracting LiDAR features compared to ground measurements were initially calculated by tree. Average height errors, standard deviations (SD), and root mean square errors (RMSE) were then calculated for five plots (plots E200, O16, O69, U8, and U13) where field total station measurements were made (Table 4.12). Additionally the same height comparison was performed for one clearcut plot (plot C110) where only field GPS measurements were made (Table 4.14). This second height comparison is differentiated from the other by three primary factors: field

spatial location measurement, field height measurement, and silvicultural treatment. The spatial locations were measured by GPS, tree heights were measured using a height pole, and the silvicultural treatment was a clearcut consisting of seedlings. The difference in the clearcut is important because the trees were small, but no overstory existed to prevent the LiDAR pulses from striking the tree. Since overstory was not a factor, then the primary factor impacting whether a tree was detected is LiDAR pulse density. Another factor is that the point matching was completed manually in FUSION. We found it difficult to identify small trees in FUSION and believed this to be primarily due to overstory obscuration. We wanted to determine if small trees could be detected in FUSION when no overstory obscuration existed. Because of these differences, we chose to display this comparison separately. A third comparison evaluated plot averages for all study plots (Table 4.16).

Table 4.12. LiDAR tree extraction method comparing spatial location and average and absolute tree height* error (m) to field measurements.

Plot	Method	Statistic	X_{TS} minus X_{LiDAR}	Y_{TS} minus Y_{LiDAR}	Horizontal Difference	Field Height minus LiDAR Height	Trees
E200	**FUSION**	Avg. (Abs.)	0.29	0.03	1.66	0.41 (0.86)	589
		SD (RMSE)	1.50	1.29	1.10 (1.99)	1.27 (1.33)	
	TreeVaW	Avg. (Abs.)	0.14	0.02	1.70	0.50 (0.91)	620
		SD (RMSE)	1.50	1.34	1.08 (2.02)	1.25 (1.35)	
	WS Seg.	Avg. (Abs.)	-0.35	-0.18	1.73	0.52 (0.96)	691
		SD (RMSE)	1.49	1.32	1.06 (2.03)	1.28 (1.38)	
O16	**FUSION**	Avg. (Abs.)	-0.48	-0.50	2.95	-0.22 (1.33)	119
		SD (RMSE)	2.73	2.45	2.28 (3.72)	2.19 (2.19)	
	TreeVaW	Avg. (Abs.)	-0.89	-0.14	3.59	0.15 (1.79)	86
		SD (RMSE)	3.51	2.29	2.32 (4.27)	2.62 (2.61)	
	WS Seg.	Avg. (Abs.)	-0.63	-0.33	3.52	0.17 (1.74)	104
		SD (RMSE)	3.03	2.97	2.45 (4.28)	2.49 (2.49)	
O69	**FUSION**	Avg. (Abs.)	-0.23	-1.34	2.72	-2.72 (3.79)	70
		SD (RMSE)	2.37	1.97	1.96 (3.35)	4.22 (4.99)	
	TreeVaW	Avg. (Abs.)	-0.17	-0.53	3.36	-1.75 (3.50)	72
		SD (RMSE)	3.92	2.38	3.15 (4.59)	4.52 (4.82)	
	WS Seg.	Avg. (Abs.)	-0.34	-0.73	2.97	-1.97 (3.73)	71
		SD (RMSE)	2.66	2.34	2.06 (3.61)	4.69 (5.05)	
U8	**FUSION**	Avg. (Abs.)	0.36	0.32	1.66	-1.29 (3.44)	83
		SD (RMSE)	1.16	1.65	1.24 (2.06)	4.90 (5.04)	
	TreeVaW	Avg. (Abs.)	0.11	0.01	1.78	-0.02 (2.79)	74
		SD (RMSE)	1.41	1.89	1.53 (2.34)	4.31 (4.29)	
	WS Seg.	Avg. (Abs.)	0.18	0.34	2.19	-0.44 (3.43)	108
		SD (RMSE)	2.19	1.94	1.97 (2.94)	5.02 (5.02)	
U13	**FUSION**	Avg. (Abs.)	-0.12	-0.22	3.04	-0.06 (1.14)	108
		SD (RMSE)	2.86	2.69	2.48 (3.91)	1.52 (1.51)	
	TreeVaW	Avg. (Abs.)	0.07	-0.12	3.14	0.25 (1.22)	142
		SD (RMSE)	3.03	2.42	2.27 (3.87)	2.16 (2.16)	
	WS Seg.	Avg. (Abs.)	0.00	-0.23	3.67	0.34 (1.13)	177
		SD (RMSE)	3.52	3.10	2.91 (4.68)	1.59 (1.62)	
Total	**FUSION**	Avg. (Abs.)	0.12	-0.14	2.05	-0.09 (1.38)	969
		SD (RMSE)	1.94	1.79	1.67 (2.64)	2.43 (2.43)	
	TreeVaW	Avg. (Abs.)	0.02	-0.06	2.19	0.28 (1.23)	994
		SD (RMSE)	2.24	1.76	1.83 (2.85)	1.86 (1.88)	
	WS Seg.	Avg. (Abs.)	-0.27	-0.19	2.31	0.22 (1.46)	1151
		SD (RMSE)	2.23	2.01	1.94 (3.02)	2.45 (2.46)	

* Field-measured tree spatial location and height were determined by total station and laser rangefinder respectively.

In the total station to LiDAR comparisons, three plots (E200, O16, and U13) had mean height errors no greater than 0.52 m (SD 1.28 m). Among these three plots, the largest average mean height error was in plot E200 with the watershed segmentation method and the lowest was in plot U13 at -0.06 m (SD 1.52 m) (Table 4.12). The overall greatest amount of height error occurred in plot O69 (-2.72 m (SD 4.22)) with FUSION. Plot 069 also had the most error when comparing LiDAR approaches across plots. Height errors in O69 may have been impacted by the plot's severe sloping terrain. When comparing the height measurement results using a paired t-test, plots E200 and O69 were significantly different for all LiDAR techniques except one ($p < 0.01$), thus indicating that there is a high probability that mean tree heights measured by LiDAR compared to those measured by laser range finder are generally not the same (Table 4.13). The lone exception occurred in plot E200 for the watershed segmentation results (p=0.19). Statistically significant differences also occurred with FUSION in plots O16 and U8. The significant differences that were determined in plot E200 are noteworthy because this plot is generally a monoculture of Douglas-fir planted at the same time and having a similar mean height. For these reasons, plot E200 is the plot most expected to have similar results when comparing LiDAR results to field measurements.

Table 4.13. Statistical comparison of paired LiDAR-derived tree heights to laser range finder (LRF) tree heights.

Plot	Avg LRF Height*	Avg LiDAR Height	df	t-stat	*p*-value
E200					
FUSION	14.09	13.69	588	4.59	<0.01
TreeVaW	13.85	13.35	619	5.94	<0.01
WS Seg.	13.75	13.24	690	1.30	0.19
O16					
FUSION	34.98	35.19	118	-2.34	0.02
TreeVaW	33.66	33.51	85	1.36	0.18
WS Seg.	37.06	36.89	103	-0.76	0.45
O69					
FUSION	41.53	44.25	69	-5.39	<0.01
TreeVaW	35.04	36.79	71	-3.28	<0.01
WS Seg.	39.45	41.43	70	-3.54	<0.01
U8					
FUSION	44.39	45.68	82	-2.40	0.02
TreeVaW	36.90	36.92	73	-0.04	0.97
WS Seg.	38.37	38.81	107	-0.91	0.36
U13					
FUSION	18.48	18.54	107	-0.13	0.90
TreeVaW	14.15	13.90	141	1.15	0.25
WS Seg.	13.28	12.93	176	0.16	0.88

For the one clearcut plot (C110) where height comparisons were made by tree matching, height measurements were compared between field horizontal measurements determined by mapping grade GPS and height measurements determined mostly by height pole to the same measurements determined by the three LiDAR extraction methods (Table 4.14). In this plot it appeared that shrubs were detected as no canopy existed to prevent LiDAR pulses from reaching shrubs. In all plots besides the clearcut plots it appeared shrubs were not detected due to LiDAR pulse obstruction by canopy. This observation is based on manual observations of point clouds in FUSION, and features delineated in watershed segmentation and TreeVaW that did not correspond to field-measured shrub locations, and LiDAR

heights that indicated trees rather than shrubs. The least amount of error occurred when comparing TreeVaW trees to field-measured, however only 17 trees could be matched. The greatest amount of error was 1.27 m (SD 0.51 m) comparing shrubs detected by watershed segmentation to field measurements. The second least amount of error was 1.17 m with watershed segmentation and FUSION in detecting shrubs and trees, respectively.

Table 4.14. LiDAR tree extraction method comparing spatial location and height (m) of trees and shrubs to field measurement in one clearcut plot.

Plot	Statistic	X_{TS} minus X_{LiDAR}	Y_{TS} minus Y_{LiDAR}	Horizontal Difference	Field Height minus LiDAR Height**	n Paired
C110 Trees						Trees
FUSION	Avg. (Abs.)	-0.93	0.42	1.42	0.56 (1.08)	83
	SD (RMSE)	0.82	0.81	0.59 (1.53)	1.07 (1.36)	
TreeVaW	Avg. (Abs.)	-0.71	1.46	2.63	0.28 (1.30)	16
	SD (RMSE)	1.92	2.33	2.15 (3.35)	1.69 (1.56)	
WS Seg.	Avg. (Abs.)	-1.07	0.42	1.59	1.17 (1.23)	339
	SD (RMSE)	0.85	2.14	2.02 (2.57)	0.68 (1.37)	
C110 Shrubs						Shrubs
FUSION	Avg. (Abs.)	-1.03	0.67	1.30	1.17 (1.17)	44
	SD (RMSE)	0.42	0.40	0.38 (1.36)	0.48 (1.26)	
TreeVaW	Avg. (Abs.)	-0.98	0.60	1.23	0.97 (0.97)	4
	SD (RMSE)	0.49	0.37	0.32 (1.26)	0.59 (1.10)	
WS Seg.	Avg. (Abs.)	-1.13	0.53	1.37	1.27 (1.27)	57
	SD (RMSE)	0.62	0.49	0.56 (1.48)	0.51 (1.37)	

* Field-measured tree spatial location and height were determined by mapping grade GPS and height pole respectively. **Average (avg.) and absolute (abs.) height differences provided.

Statistically significant height errors ($p < 0.01$) (Table 4.15) were observed with all methods in the clearcut plot except with TreeVaW, but only sixteen and four features were compared in trees and shrubs respectively and with this method.

Table 4.15. Statistical comparison of LiDAR-derived tree heights (h) to height pole measured (HP) tree heights in one clearcut plot.

Plot	μ (HP h) – (LiDAR h) (m)	(HP h) – (LiDAR h) 95% CI (m)	df	t-stat	*p*-value
C110 Trees					
FUSION	0.56	0.24-1.46	82	2.93	< 0.01
TreeVaW	0.28	-0.66-1.21	15	-2.00	0.54
WS Seg.	1.17	1.04-1.33	338	22.45	< 0.01
C110 Shrubs					
FUSION	1.17	1.01-1.30	43	16.31	< 0.01
TreeVaW	0.97	-0.16-2.10	3	2.33	0.08
WS Seg.	1.27	0.94-1.59	56	18.72	< 0.01

Comparing all field laser range finder (LRF) height measurements to the three methods of LiDAR height measurements in each plot using a Welch modified two-sample t-test resulted in significant differences ($p < 0.01$) in all comparisons but four (Table 4.16). Results were inconclusive with TreeVaW in plot O16 ($p = 0.68$) and O69 ($p = 0.83$); and with watershed segmentation in plot C61 ($p = 0.95$) and E200 ($p = 0.46$).

LiDAR Horizontal Comparison

The LiDAR detected and delineated tree horizontal location compared to known locations of field-measured trees were similar in each method (Table 4.12). The least horizontal difference between LiDAR measured trees occurred with FUSION software in all plots. The overall mean horizontal difference between field-measured trees and LiDAR measured trees by FUSION, TreeVaW, and watershed segmentation were 2.05, 2.19, and 2.31 m respectively. The horizontal difference by method can be explained by the precision of the measurement method. FUSION utilizes the point

cloud compared to other methods, which use the raster-based CHM. Measurement of the spatial location of a tree in FUSION is based on identifying the single highest discrete point. The only error introduced is by the operator who may not align the measurement marker precisely with the highest point. Methods that rely on a CHM also rely on the highest point however this point is represented by a raster cell (pixel), with a precision that is limited by the resolution of the cell and a coordinate location based on the cell center. The cell resolutions used for this study in most cases for TreeVaw (Table 4.10) and watershed segmentation (Table 4.9) were 0.3 and 1.0 m, respectively.

In many cases it was obvious when the same tree was identified by each program based on spatial location and height. It is also interesting to note that in no case was the same tree identified in the exact same location (Figure 4.8, Table 4.17). Again this may be attributed to differences in spatial resolution and precision of measurement, but some may also be attributed to differences in computer algorithms.

Table 4.16. Statistical comparison of mean LiDAR tree heights (h) to field-measured (FM) tree heights as measured by a laser range finder.

Plot	Method	Average Height (m)	(μ FM h) – (μ LiDAR h) 95% CI (m)	df	t-stat	*p*-value
C20	Field-measured	1.06				
	FUSION		NOT MEASURED			
	TreeVaW	1.20	-1.46-(-1.11)	451	-14.54	<0.01
	WS Seg.	0.87	0.08-0.31	1067	3.34	<0.01
C27	Field-measured	1.04				
	FUSION		NOT MEASURED			
	TreeVaW	2.50	-1.75-(-1.18)	125	-10.05	<0.01
	WS Seg.	0.53	0.16-0.33	1207	5.66	<0.01
C61	Field-measured	1.70				
	FUSION		NOT MEASURED			
	TreeVaW	15.03	-15.57-(-11.09)	189	-11.75	<0.01
	WS Seg.	1.68	-0.49-0.53	1091	0.06	0.95
C110	Field-measured	1.87				
	FUSION	2.06	-0.39-0.00	256	-1.93	0.05
	TreeVaW	3.16	-1.55-(-1.03)	206	-9.79	<0.01
	WS Seg.	0.97	0.78-1.01	1189	15.67	<0.01
E200	Field-measured	12.52				
	FUSION	13.67	-1.37-(-0.94)	1482	-10.67	<0.01
	TreeVaW	13.02	-0.74-(-0.27)	1724	-4.23	<0.01
	WS Seg.	12.43	-0.14-0.31	1807	0.74	0.46
E412	Field-measured	6.56				
	FUSION		NOT MEASURED			
	TreeVaW	4.69	1.74-2.01	1855	27.80	<0.01
	WS Seg.	4.45	1.95-2.28	1819	25.60	<0.01
O16	Field-measured	18.86				
	FUSION	31.16	-15.22-(-9.39)	334	-8.31	<0.01
	TreeVaW	19.46	-3.51-2.30	390	-0.41	0.68
	WS Seg.	35.15	-19.14-(-13.44)	384	-11.23	<0.01
O69	Field-measured	20.22				
	FUSION	43.94	-28.15-(-19.29)	147	-10.58	<0.01
	TreeVaW	19.81	-3.28-4.10	387	0.22	0.83
	WS Seg.	31.49	-14.86-(-7.68)	436	-6.17	<0.01
U8	Field-measured	18.00				
	FUSION	45.65	-29.80-(-25.51)	417	-25.37	<0.01
	TreeVaW	25.97	-11.94-(-4.01)	188	-3.97	<0.01
	WS Seg.	35.56	-20.12-(-15.00)	490	-13.47	<0.01
U13	Field-measured	6.67				
	FUSION	16.66	-12.86-(-7.13)	177	-6.88	<0.01
	TreeVaW	10.53	-5.64-(-2.10)	465	-4.29	<0.01
	WS Seg.	16.18	-11.54-(-7.48)	456	-9.20	<0.01
U56	Field-measured	6.66				
	FUSION		NOT MEASURED			
	TreeVaW	15.18	-10.49-(-6.57)	329	-8.55	<0.01
	WS Seg.	26.69	-21.02-(-19.05)	1615	-39.79	<0.01

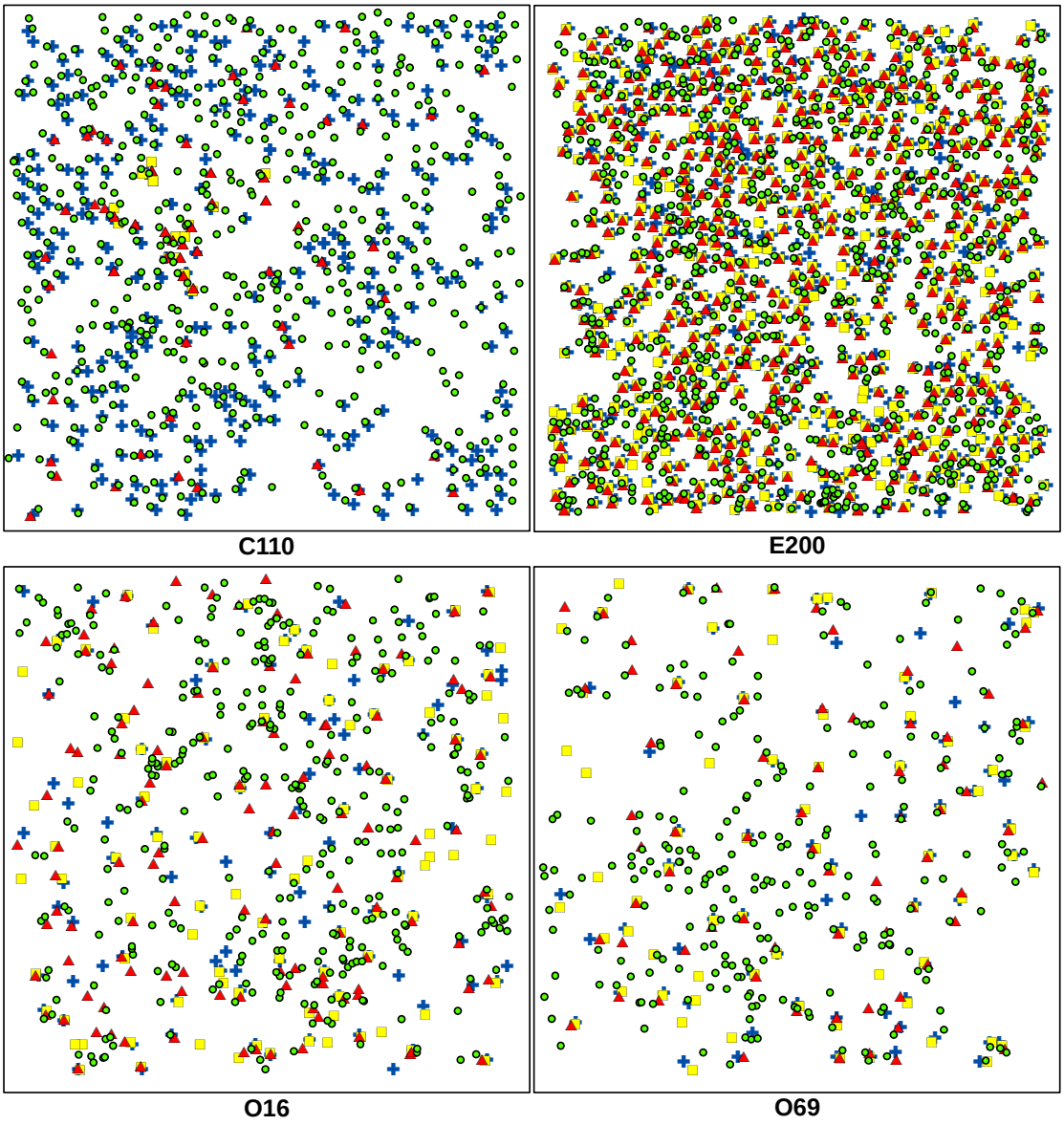

Figure 4.8. Plot maps of trees used for height comparisons of FUSION, TreeVaW and watershed segmentation matched trees and all field-measured trees. Tree locations were measured by GPS in C110 and total station in all others. Plot E200 tree symbols are smaller than others to facilitate point differentiation detail and pattern based on the larger number of trees delineated.

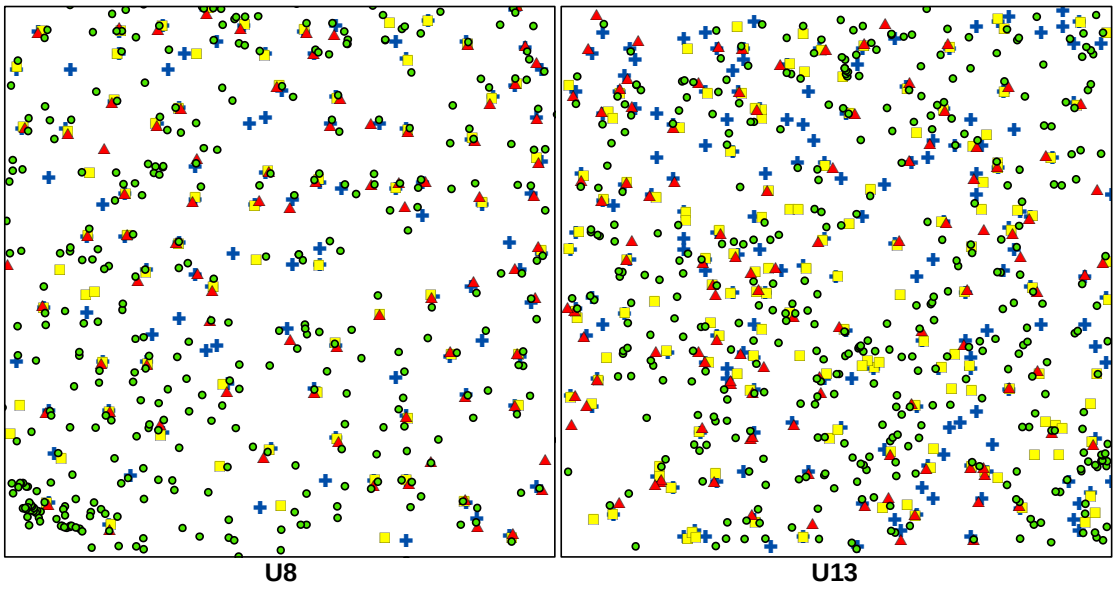

Figure 4.8 (continued). Plot maps of trees used for height comparisons of FUSION, TreeVaW and watershed segmentation matched trees and all field-measured trees. Tree locations were measured by GPS in C110 and total station in all others. Plot E200 tree symbols are smaller than others to facilitate point differentiation detail and pattern based on the larger number of trees delineated.

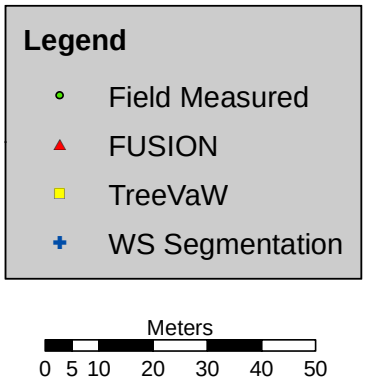

Table 4.17. Comparison of horizontal distance (m) between trees determined to be the same feature. Selection criterion was that the tree was delineated in all four methods (field, FUSION, TreeVaW and watershed segmentation).

Plot/ Statistic	Field to Fusion distance	Field to TreeVaW distance	Field to WS Seg. distance	Fusion to TreeVaW distance	Fusion to WS Seg. distance	TreeVaW to WS Seg. distance	Combined	*n*
C110								9
Average	0.99	1.49	1.51	1.04	0.91	0.65	1.10	
SD	0.87	0.96	1.14	0.62	0.41	0.42	0.81	
E200								534
Average	1.66	1.68	1.75	0.48	0.85	0.61	1.17	
SD	1.11	1.08	1.06	0.45	0.43	0.39	0.98	
O16								62
Average	3.02	3.44	3.18	1.50	1.46	0.98	2.26	
SD	2.50	2.30	2.20	1.64	1.63	1.72	2.24	
O69								46
Average	2.76	3.23	3.18	1.43	1.34	1.46	2.23	
SD	1.75	2.97	2.12	2.55	1.87	3.09	2.57	
U8								55
Average	1.59	1.38	1.42	0.70	0.99	0.68	1.13	
SD	1.17	1.21	0.99	0.45	1.58	1.57	1.27	
U13								75
Average	3.21	3.28	3.49	1.41	1.16	1.15	2.28	
SD	2.61	2.62	2.97	1.41	1.30	1.85	2.44	
Total								781
Average	1.97	2.04	2.09	0.73	0.97	0.75	1.42	
SD	1.62	1.73	1.67	1.05	0.95	1.20	1.53	

Field data for plot C110 was collected using GPS, all other plots by total station.

Biomass Comparison

The biomass comparison includes a by feature comparison total for each plot (Table 4.18), a comparison of mean biomass per feature in each plot (Table 4.19), and a total biomass by plot comparison for each LiDAR extraction method (FUSION, TreeVaW, and watershed segmentation) compared to biomass estimated from field measurements (Table 4.20). Overall FUSION underestimated biomass by 25%, TreeVaW underestimated by 31%, and watershed segmentation overestimated by 53%

of total weight by kg (Table 4.18). The watershed segmentation overestimation was primarily due to an extreme overestimation in one plot (U56, 504%). Excluding plot U56, the watershed segmentation method overestimated biomass by 10%. LiDAR biomass underestimation occurred in 66% of the plot comparisons (19 of 29) and overestimation occurred in 34% of the comparisons. Nine of the 29 comparisons were within 20% (over or under) of the ground estimations. In five out of six comparisons, FUSION underestimated biomass. In plot U8 FUSION overestimated by 10%. TreeVaW underestimated biomass in eight of eleven comparisons. The overestimations occurred in plot C61 (20%), plot U13 (29%), and plot U56 (3%). Watershed segmentation resulted in underestimation in six of eleven plots. The watershed segmentation method overestimations occurred in all plot treatments except clearcut (E200, 25%; O69, 14%; U8, 54%; U13, 35%; U56 504%) (Table 4.18). The anomaly in plot U56 was due to count and height overestimation of trees over 20 m tall. The field survey resulted in 146 trees over 20 m tall however the watershed segmentation method delineated 665 features over 20 m tall. Average tree height for plot U56 was larger than the field-measured data by a factor of four. It was thought that multiple over 20 m tall features were designated where large bigleaf maples occurred, however not enough maples were on this plot to account for such an overage. We evaluated biomass estimates for plot U56 with TreeVaW for 0.3 m resolution CHM using a 3 x 3 filter and a 0.1 m resolution CHM and 5 x 5 filter to illustrate biomass differences caused by errors of commission in the 0.1 m CHM. The

0.1 m resolution CHM resulted in a total biomass estimate (743,438 kg/ha) that was nearly five times that of the 0.3 m resolution CHM. The watershed segmentation method resulted in similarly extreme errors of commission in plot U56. No other explanation accounted for the overestimation.

Plot characteristics in this study were highly variable. The variability in the LiDAR biomass estimation results are a manifestation of the field variability. These results make it difficult to predict biomass on a by plot basis with consistency. That said, many biomass estimates were within 10 to 20% of the field based estimates. If plot U56 watershed segmentation biomass results are removed, the watershed segmentation overall biomass estimation was 13% over field estimates, thus the overall estimation was within just over 30% or better considering the three delineation methods. These overall results indicate promise in using LiDAR for broad, forest level biomass estimation.

Table 4.18. Biomass estimates by plot using BIOPAK. Field measurement data calculated per tree by species. LiDAR calculations by feature based on large Douglas-fir (DBH ≥ 0.13 m) and small Douglas-fir (DBH < 0.13 m).

Plot	Method	Average Tree Height (m)	Min. Tree Height (m)	Max Tree Height (m)	Tree Biomass kg Per Hectare	Shrub Biomass kg Per Hectare	Biomass Total kg/ha	Percent of Field-measured
C20	Field-measured	1.06	0.02	35.00	553	58	611	
	FUSION				NOT MEASURED			
	TreeVaW	1.20	0.03	8.66			442	72.37
	WS Segmentation	0.87	0.35	9.05			478	78.19
C27	Field-measured	1.04	0.54	8.63	357	59	416	
	FUSION				NOT MEASURED			
	TreeVaW	2.50	1.21	9.36			289	69.49
	WS Segmentation	0.53	0.19	20.65			345	83.03
C61	Field-measured	1.70	0.32	44.45	16295	0	16295	
	FUSION				NOT MEASURED			
	TreeVaW	15.03	1.22	41.55			19479	119.54
	WS Segmentation	1.68	0.35	41.85			4731	29.03
C110	Field-measured	1.87	0.32	9.40	987	240	1227	
	FUSION	2.06	0.36	9.69			333	27.12
	TreeVaW	3.16	1.37	9.53			612	49.85
	WS Segmentation	0.97	0.35	9.58			457	37.28
E200	Field-measured	12.52	1.04	18.31	83070	266	83336	
	FUSION	13.67	6.50	17.40			69006	82.80
	TreeVaW	13.02	5.69	17.34			75700	90.84
	WS Segmentation	12.43	1.07	17.34			103913	124.69
E412	Field-measured	6.56	1.21	21.37	15592	239	15831	
	FUSION				NOT MEASURED			
	TreeVaW	4.69	1.76	20.56			6993	44.17
	WS Segmentation	4.45	0.90	20.56			12883	81.38

Table 4.18. Biomass estimates by plot using biomass calculation package BIOPAK (continued).

Plot	Method	Average Tree Height (m)	Min Tree Height (m)	Max Tree Height (m)	Tree Biomass kg Per Hectare	Shrub Biomass kg Per Hectare	Biomass Total kg/ha	Percent of Field-measured
O16	Field-measured	18.86	1.05	64.70	472976	1868	474844	
	FUSION	31.16	4.02	63.88			293328	61.77
	TreeVaW	19.46	3.02	63.57			197288	41.55
	WS Segmentation	35.15	1.38	63.62			416444	87.70
O69	Field-measured	20.22	2.05	69.71	366511	1755	368266	
	FUSION	43.94	1.14	68.70			261929	71.12
	TreeVaW	19.81	2.75	68.20			216549	58.80
	WS Segmentation	31.49	1.13	31.49			421644	114.49
U8	Field-measured	18.00	1.10	57.88	215013	1722	216735	
	FUSION	45.65	16.07	54.03			238278	109.94
	TreeVaW	25.97	1.95	53.91			164559	75.93
	WS Segmentation	35.56	0.97	53.79			332918	153.61
U13	Field-measured	6.67	0.56	52.60	141586	279	141865	
	FUSION	16.66	1.54	53.08			97340	68.61
	TreeVaW	10.53	3.36	52.78			183065	129.04
	WS Segmentation	16.18	0.92	52.87			191971	135.32
U56	Field-measured	6.66	1.00	42.36	146791	208	146999	
	FUSION				NOT MEASURED			
	TreeVaW 0.3/3x3	15.18	1.71	42.52			151046	102.75
	TreeVaW 0.1/5x5	20.92	2.56	42.52			743438	505.74
	WS Segmentation	26.69	0.91	42.52			760674	503.60
						Study Totals		
						Field-measured	146425	
						FUSION Total	960214	74.65
						TreeVaW Total	1016022	69.29
						WS Segmentation	2246459	153.19

Using a Welch modified t-test to examine the differences in mean feature (tree/shrub) biomass by plot (Table 4.19), statistically significant differences ($p \leq 0.03$) were observed in all but one plot and in 17 of 28 LiDAR extraction methods. Potentially equal biomass means could not be ruled out in plot C20. FUSION overestimated mean biomass in all plots, and in 66% of the plots (E200, O69, U8, and U13) this overestimation was statistically significant noting that these were all plots with significant canopy cover. Plot O16 also had significant canopy cover, however 58% of the trees were larger than 10 m tall, and of the 32% below 10 m tall, there were very few seedlings. TreeVaW displayed statistically significant differences in 8 of 11 plots (*p*- values ≤ 0.03). The three plots that did not display significant differences were C20, O69, and U13 and were all within 30% of the field-measured biomass estimate. The watershed segmentation method had inconclusive results in the clearcut plots, but in all other comparisons to field based biomass estimation resulted in statistically significant differences.

Table 4.19. Probability that LiDAR (L) based feature mean biomass estimates by plot are equal to field (F) measurement estimates.

Plot	Avg Field Biomass (kg)	Avg LiDAR Biomass (kg)	(μ F bio) – (μ L bio) 95% CI*	df	t	*p*-value
C20						
FUSION			NOT MEASURED			
TreeVaW	2.40	2.06	3.01	704	0.21	0.58
WS Seg.	2.40	0.57	4.48	695	1.13	0.87
C27						
FUSION			NOT MEASURED			
TreeVaW	0.63	2.51	-1.31	134	-5.47	<0.01
WS Seg.	0.63	0.53	0.27	816	0.90	0.81
C61						
FUSION			NOT MEASURED			
TreeVaW	30.34	105.86	-26.66	655	-2.53	0.01
WS Seg.	30.34	7.49	68.84	540	0.82	0.79
C110						
FUSION	1.73	1.81	0.25	323	-0.41	0.34
TreeVaW	1.73	3.56	-1.35	224	-6.34	<0.01
WS Seg.	1.73	0.74	1.19	947	8.13	1.00
E200						
FUSION	87.81	105.03	-22.29- (-13.15)	1376	-8.29	<0.01
TreeVaW	87.81	107.53	-24.34-(-15.09)	1638	-8.36	<0.01
WS Seg.	87.81	97.38	-13.81-(-5.34)	1578	-4.44	<0.01
E412						
FUSION			NOT MEASURED			
TreeVaW	16.78	6.66	9.04-11.20	1945	18.37	<0.01
WS Seg.	16.78	13.46	1.82-4.82	1589	4.35	<0.01
O16						
FUSION	1288.76	1585.56	-675.48-81.88	504	-1.54	0.12
TreeVaW	1288.76	904.99	30.68-736.87	581	2.13	0.03
WS Seg.	1288.76	1983.07	-1054.76-(-333.84)	566	-3.78	<0.01
O69						
FUSION	1415.10	3045.69	-2182.08—1079.08	201	-5.83	<0.01
TreeVaW	1415.10	1099.23	-118.14-749.87	448	1.43	0.15
WS Seg.	1415.10	1899.30	-909.69-(-58.70)	457	-2.24	0.03
U8						
FUSION	584.27	2707.71	-2302.89-(-1943.97)	202	-23.33	<0.01
TreeVaW	584.27	1337.88	-1027.90-(-479.31)	170	-5.42	<0.01
WS Seg.	584.27	1743.02	-1348.45-(-969.05)	374	-12.01	<0.01
U13						
FUSION	284.31	662.18	-579.28-(-176.45)	218	-3.70	<0.01
TreeVaW	284.31	325.81	-173.56-90.55	658	-0.62	0.54
WS Seg.	284.31	615.29	-466.54-(195.42)	689	-4.79	<0.01
U56						
FUSION			NOT MEASURED			
TreeVaW	117.53	547.27	-523.53-(-335.96)	300	-9.02	<0.01
WS Seg.	117.53	923.15	-847.36-(-763.88)	1273	-37.87	<0.01

* Clearcut plots are one-sided *p* values

Consolidating features (trees/shrubs) together from all plots and determining a feature average resulted in statistically significant differences ($p < 0.01$) between each LiDAR extraction method compared to field measurements (Table 4.20). All LiDAR biomass feature average estimates were larger than field estimates. When combining and analyzing plot total biomass, statistical significance was inconclusive in all cases. Plot average biomass estimated by LiDAR was less than field measurements in both FUSION and TreeVaW but was greater for the watershed segmentation results.

Table 4.20. Probability that LiDAR (L) based mean biomass estimates for all features combined are equal to field (F) measurement estimates.

Plot	Avg Field Biomass (kg)	Avg LiDAR Biomass (kg)	(μ F bio) – (μ L bio) 95% CI*	df	t-stat	*p*-value
Average Feature						
FUSION Plots	425.44	712.85	-376.38-(-198.45)	2751	-6.33	<0.01
TreeVaW Plots	209.41	261.60	-87.47-(-16.34)	8300	-2.84	<0.01
WS Seg Plots.	209.41	345.29	-166.90-(-105.28)	13308	-8.75	<0.01
Average by Plot						
FUSION Plots	214,379	160,035	-145189.80-253876.60	9	0.61	0.55
TreeVaW Plots	133,312	84,046	-68142.39-166673.07	15	0.95	0.38
WS Seg. Plots.	133,312	204,223	-260773.90-118950.2	17	-0.79	0.44

Discussion

We reported LiDAR tree height errors using FUSION, TreeVaW, and watershed segmentation extraction methods in clearcut, even-age, uneven-age, and old growth forest plots. These errors are generally consistent with those reported in other studies of LiDAR height measurements in various forest conditions compared to field measurements, albeit somewhat higher than some in old growth plot O69 and uneven-aged plot U8 (Naesset and Okland 2002, Brandtberg et al. 2003, Gaveau and Hill 2003, Andersen et al. 2005, McGaughey et al. 2007). To illustrate the complexity in measuring individual trees with LiDAR, many factors influencing the accuracy of

LiDAR forest measurement are reviewed below. Some of the key factors that impact LiDAR tree height measurement include survey control, location the LiDAR pulse(s) strike the tree, base measurement datum, differentiating individual trees, position of the tree within the canopy, and use of a raster CHM versus the LiDAR point cloud.

The vendor provided resolution and accuracy summary for this study stated a point resolution specification of ≥ 8 points/m^2 and an achieved resolution of 10 points/ m^2, and a vertical accuracy of better than 0.13 m. This accuracy is based on measurements made in perfect LiDAR ground conditions, such as those found on paved road surfaces with no vertical obstruction. The resolution and accuracy deteriorates markedly with variation in natural terrain conditions including forest canopy, understory vegetation, small scale topography, and other environmental conditions.

Field measurements are subject to systematic and random error propagation. The field survey crew was trained in proper procedures and the design of proper protocols prevented many potential errors. However due to the scope of this study, it is wrought with a myriad of potential accidental errors. The field survey measured thousands of features, thus error is likely to have occurred periodically in tree height measurement with a laser range finder (both systematic and accidental). Laser range finders are known to introduce height error, however we used one that has been shown to have the highest accuracy in comparison to other commonly used models (Wing et al. 2004).

Where and how many LiDAR pulses strike and reflect off the tree impacts tree identification and measurement. In conifer species the odds of a pulse striking a single,

very thin apex are low. These odds decrease further when the tree occurs below the primary canopy where pulses that might strike the tree are intercepted by the upper canopy. In every method of tree extraction used in this study the number of pulses hitting the tree impacts identification and canopy dimension measurements. Without an adequate number of pulses striking a tree in FUSION, tree identification was difficult in both dense and clearcut forest plots. In dense plots, upper tree identification was relatively easy based on the unique shape and canopy of each tree, however as smaller trees were shrouded by larger ones, tree identification was difficult at best. Manually identifying a three dimensional array of dots (the LiDAR point cloud) that belong to a single tree is a tedious process. Differentiating small trees in a clearcut where overstory trees are not a factor was also very difficult. This is strictly a result of LiDAR resolution. Theoretically one would think that a pulse rate of 8-10 pulses per m^2 would be enough to enable the identification of small conifers whose crown is approximately 1 m^2. However, based on the sparseness of young conifer foliage, often only one or two LiDAR points struck a tree making identification difficult to impossible.

TreeVaW and watershed segmentation both rely on a CHM for tree identification and measurement. If points are generated from trees existing below the primary canopy, these points will be eliminated in rendering the CHM surface, thus the tree that exists in the field will be removed from the model.

All LiDAR tree height measurement methods rely on some form of base elevation model. In this study all utilized methods relied on a vendor provided DEM. We chose

to use this DEM instead of creating a new one based on the vendor having the expertise and software necessary to separate ground points from non-ground points such as understory vegetation, stumps, and slash. In certain circumstances when conducting the ground survey it was obvious that a LiDAR pulse would not reach the ground surface. Examples of this are dense blackberry, poison oak, and Oregon grape thickets. It is questionable if computer software or an analyst could always identify these features. Even if positively identified, many thickets in this study occupied 100 m^2 or more. Interpolation of the ground surface under this vegetation likely introduced error in the DEM.

What level of vertical accuracy is good enough for a tree height measurement? What is the impact if LiDAR height estimation is off by 1 m? If the estimate is under or over from a timber management perspective, then tree volume estimates will be wrong. On the other hand, a loss of some of the tree top is expected in felling operations. For illustrative purposes and from a biomass estimation perspective, Table 4.20 quantifies the impact of height errors based on Douglas-fir above ground biomass in small trees of the same height estimated in this study. These calculations are based on small Douglas-fir biomass equations for a single tree (Table 4.8) and multiplied by the number of trees. This small tree equation was used to represent the approximate size of the top of a tree. Volume estimates are highly variable based on the height of the tree used in allometric equations, and the allometric equation itself, thus the estimates in Table 4.21 are conservative. Ground truth confirmation would likely be prudent in economic decisions involving LiDAR volume/biomass estimation.

Table 4.21. Biomass error estimate based on LiDAR height error.

	1.0 m error (kg)	1.5 m error (kg)	2.0 m error (kg)
Single Tree	0.68	1.07	1.62
100 Trees	67.85	106.58	161.67
500 Trees	339.25	532.91	808.35
1000 Trees	678.50	1065.83	1616.71

We found that there are three main factors that influence the accuracy of LiDAR forest biomass estimates: feature (tree/shrub) count, feature height, and species identification. This study illustrates that the effectiveness of using LiDAR with the protocols we used for forest measurement has its limitations, but based on this research and previous studies further investigation is warranted and development of regional protocols could result in LiDAR becoming a very effective forest measurement tool for volume and biomass estimates. Clearly this and previous studies have demonstrated that measuring large trees or a consistent stand of even-age trees is relatively accurate, however measuring all trees and shrubs at the stand or forest level for purposes of estimating biomass is not necessarily accurate compared to field-based estimates. Detecting and measuring small and understory vegetation would likely improve with increased LiDAR resolution (greater pulse density) and warrants further investigation. We also found that the cell resolution of the CHM impacted tree extraction results in TreeVaW and watershed segmentation. Further research is recommended to determine one ideal CHM resolution for stand level tree extraction and biomass estimation, or a potential solution is to use different resolutions per stand treatment. The use of the LiDAR point clouds enable the measurement of all features vertically throughout the canopy structure, however the manual method of feature

extraction in FUSION is tedious and slow relative to automated methods, but automated methods used in this study were limited by the CHM. An automated method of feature extraction using point clouds may be a solution to improved measurement accuracy. This study was also limited in estimating biomass because we did not differentiate species in LiDAR estimations. One method to identify species is to use other imagery, e.g. multispectral aerial photographs or satellite imagery in conjunction with LiDAR. One recommendation is that, if budgets permit, aerial photographs should be taken simultaneously with the LiDAR. The LiDAR system used in this study also acquired return intensity values, which we feel can be used to differentiate conifer from deciduous species, and will be further investigated to improve biomass estimates. Finally, biomass estimates vary widely in their accuracy when relying on allometric equations. Based on many site specific factors and age classes, predicting above ground biomass developed from different sites and ages can raise debate (Saint Clair 1993). A great deal more variation in biomass equation prediction exists than many realize. Variation in equations is likely by at least ± 25-50% (Harmon, M, personal communication, November 30, 2010).

Other Observations

Another component of forest biomass that we would be remiss in not discussing is downed wood and slash. We found that large downed wood and slash piles were relatively easy to manually identify in the LiDAR point clouds (Figure 4.9). Large log features would be easy to manually extract and measure the dimension of in a GIS based on length between each end point and diameter based on height, however

automating the identification and measurement process would be necessary for the application of broad based biomass estimation. Figure 4.9 a) is a point cloud depicting all of Plot O69 from one side showing logs in the lower portion of the image and a larger scale image of the lower left hand corner shown in 4.9 b). A GIS point file displays points from 0.3 to 3.5 m above ground where linear arrays of points depict logs among other points from C27 (Fig. 4.9c), and a GIS point file from Plot O69 displays features, some of which correspond to field-measured logs, which were delineated by conducting a "hotspot" analysis of elevation above ground with a buffer placed around them to aid in locating log features (Fig. 4.9d). The "Hot Spot" analysis tool in ArcGIS calculates the Getis-Ord Gi statistic for each feature in a dataset. The result is a Z score, which can be used to examine spatial clustering. It is a neighborhood analysis tool, which determines if a point has a high Z score and if it is surrounded by other points with a high Z score. The local feature and corresponding neighborhood score is proportionally compared to the sum of all features in the data set, and if random chance is ruled out, a result is a statistically significant Z score indicating that feature clustering is occurring, sometimes referred to as a "hot spot" (ESRI 2011). In many cases, due to the large number of pulses directed off nadir from the aircraft, the bole of the tree reflected enough points to potentially estimate the DBH and further refine biomass estimation. In addition, many (over 10) large squirrel nests were identified by the field survey crew who pondered whether they would be identifiable in LiDAR as a potential wildlife application. We confirmed that none were

identifiable in the LiDAR point clouds. Higher point density would be necessary for this application.

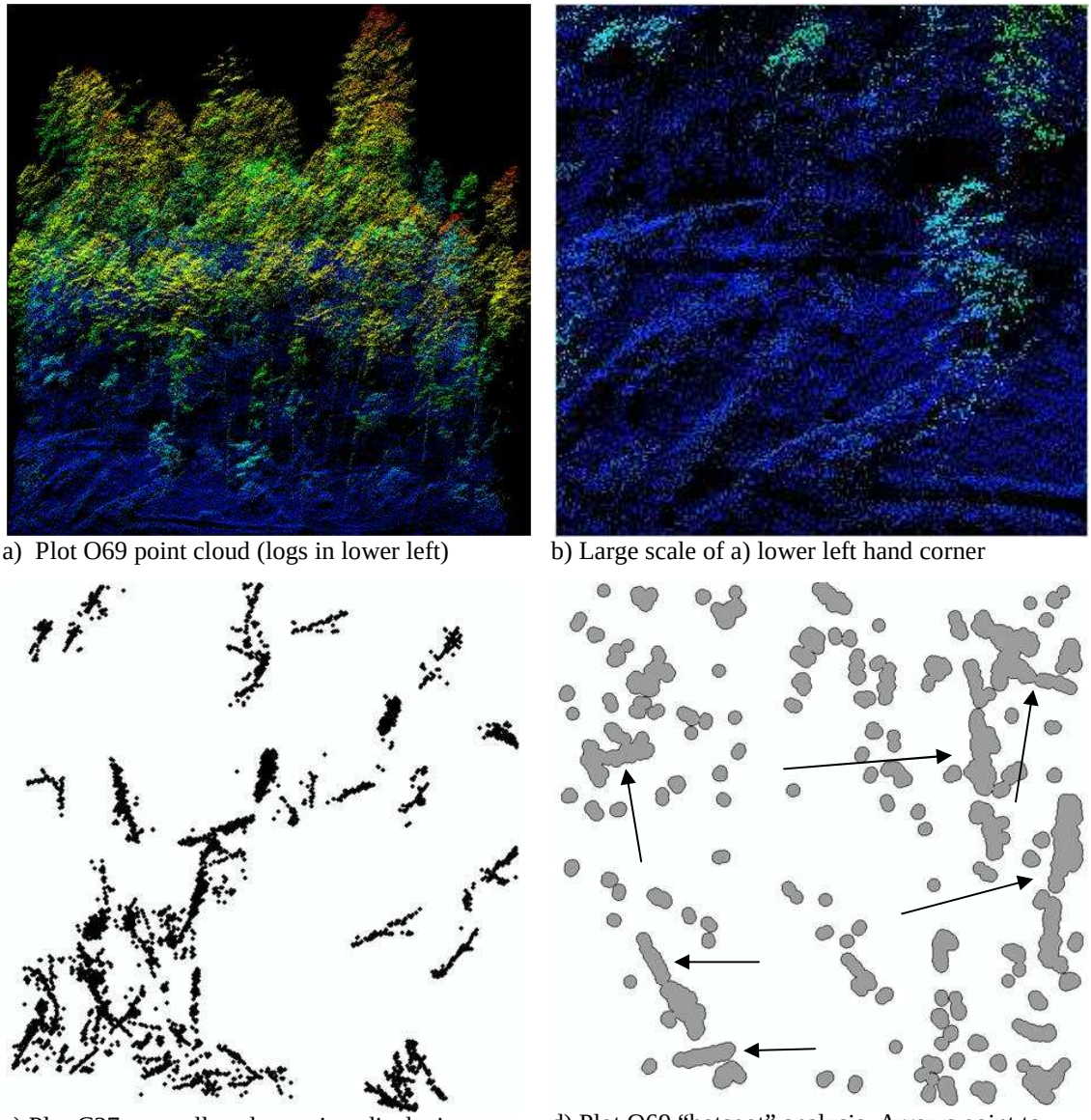

a) Plot O69 point cloud (logs in lower left)

b) Large scale of a) lower left hand corner

c) Plot C27 manually select points displaying mostly downed trees in ArcGIS

d) Plot O69 "hotspot" analysis. Arrows point to corresponding downed trees.

Figure 4.9. Downed trees identified in LiDAR data: a) point cloud of trees and downed trees , b) point cloud from lower left had portion of panel a), c) select linear array of points corresponding to downed trees in GIS, and d) "hotspots" with buffers mostly corresponding to downed trees extracted in GIS.

Literature Cited

AFPA (2001). Status report on the US Forest Service Forest Inventory and Analysis Program: Update to the findings of the 1998 Blue Ribbon Panel. Washington, D.C., American Forest and Paper Association.

Aguilar, F. J. and J. P. Mills (2008). Accuracy assessment of LiDAR-derived digital elevation models. The Photogrammetric Record 23(122): 148-169.

Andersen, H.-E. (2009). Using Airborne Light Detection and Ranging (LIDAR) to characterize forest stand condition on the Kenai Peninsula of Alaska. Western Journal of Applied Forestry 24: 95-102.

Andersen, H.-E., R. J. McGaughey and S. E. Reutebuch (2005). Estimating forest canopy fuel parameters using LiDAR data. Remote Sensing of Environment 94(4): 441-449.

Andersen, H.-E., S. E. Reutebuch and R. J. McGaughey (2006). A rigorous assessment of tree height measurements obtained using airborne LiDAR and conventional field methods. Canadian Journal of Remote Sensing 32(5): 355-366.

Anderson, E. S., J. A. Thompson, D. A. Crouse and R. E. Austin (2006). Horizontal resolution and data density effects on remotely sensed LIDAR-based DEM. Geoderma 132(3-4): 406-415.

ASPRS. (2009). Common LiDAR data exchange format - .LAS industry initiative. Retrieved October 5, 2010, from www.asprs.org/society/committees/lidar/lidar_format.html.

Barker, T., I. Bashmakov, L. Bernstein, J. E. Bogner, P. Bosch, D. Rutu, D. Ogunlade, B. S. Fisher, S. Gupta, K. Halsnaes, B. Heij, S. Kahn, S. Kobayashi, M. D. Levine, D. L. Martino, O. Masera, B. Metz, L. Meyer, G.-J. Nabuurs, A. Najam, N. Nebojsa, H.-H. Rogner, J. Roy, J. Sathaye, R. Schock, P. Shukla, R. E. H. Sims, P. Smith, D. A. Tirpak, D. Urge-Vorsatz and D. Zhou (2007). Technical summary. in: Climate Change 2007: Mitigation. Contribution of Working Group III to the Fourth Assessment
Report of the Intergovernmental Panel on Climate Change. Cambridge, United Kingdom and New York, NY, USA.

Bortolot, Z. J. and R. H. Wynne (2005). Estimating forest biomass using small footprint LiDAR data: An individual tree-based approach that incorporates training data. ISPRS Journal of Photogrammetry and Remote Sensing 59(6): 342-360.

Brandtberg, T., T. A. Warner, R. E. Landenberger and J. B. McGraw (2003). Detection and analysis of individual leaf-off tree crowns in small footprint, high sampling density lidar data from the eastern deciduous forest in North America. Remote Sensing of Environment 85(3): 290-303.

Carson, W. W. and S. E. Reutebuch (1997). A rigorous test of the accuracy of USGS digital elevation models in forested areas of Oregon and Washington.

Surveying and cartography: ACSM/ASPRS Annual convention and exposition technical paper 1: 133-143.

Chen, Q. (2007). Airborne LiDAR data processing and information extraction. Photogrammetric Engineering and Remote Sensing 73: 175-185.

Ciais, P., B. Moore, W. Steffen, M. Hood, S. Quengan, J. Cihlar, M. Raupach, S. Rasool, C. Doney, C. Heinze, C. Sabine, K. Hibbard, D. Schulze, M. Heimann, P. Chedin, P. Monfray, A. Watson, C. LeQuere, P. Tans, H. Dolman, R. Valentini, O. Arino, J. Townshend, G. Seufert, C. Field, T. Igrashi, C. Goodale, A. Nobre, G. Inoue, D. Crisp, D. Baldocchi, J. Tschirley, S. Denning, R. Cramer, R. Francey and D. Wickland (2010). Integrated global carbon observation theme: A strategy to realize a coordinated system of integrated global carbon cycle observations**:** 1-61.

Coops, N., T. Hilker, M. Wulder, B. St-Onge, G. Newnham, A. Siggins and J. Trofymow (2007). Estimating canopy structure of Douglas-fir forest stands from discrete-return LiDAR. Trees - Structure and Function 21(3): 295-310.

Dixon, R. K., R. A. Houghton, A. M. Solomon, M. C. Trexler and J. Wisniewski (1994). Carbon pools and flux of global forest ecosystems. Science 263: 185-190.

Dong, J., R. K. Kaufmann, R. B. Myneni, C. J. Tucker, P. E. Kauppi, J. Liski, W. Buermann, V. Alexeyev and M. K. Hughes (2003). Remote sensing estimates of boreal and temperate forest woody biomass: carbon pools, sources, and sinks. Remote Sensing of Environment 84(3): 393-410.

ESRI (2011). How Hot Spot Analysis: Getis-Ord Gi* (Spatial Statistics) works. ArcToolbox Help.

Evans, J. S., A. T. Hudak, R. Faux and A. M. S. Smith (2009). Discrete return LiDAR in natural resources: recommendations for project planning, data processing, and deliverables. Remote Sensing 1: 776-794.

Falkowski, M. J., A. M. S. Smith, P. E. Gessler, A. T. Hudak, L. A. Vierling and J. S. Evans (2008). The influence of conifer forest canopy cover on the accuracy of two individual tree measurement algorithms using LiDAR data. Canadian Journal of Remote Sensing 34(Suppl. 2): S1-S13.

Fisher, P. F. and N. J. Tate (2006). Causes and consequences of error in digital elevation models. Progress in Physical Geography 30(4): 467-489.

Gatziolis, D. and H.-E. Andersen (2008). A guide to LiDAR data acquisition and processing for the forests of the Pacific Northwest**:** 1-32.

Gaveau, D. L. A. and R. A. Hill (2003). Quantifying canopy height underestimation by laser pulse penetration in small-footprint airborne laser scanning data. Canadian Journal of Remote Sensing 29(5): 650-657.

Goerndt, M. E. (2010). Comparison and analysis of small area estimation methods for improving estimates of selected forest attributes. Forest Engineering Resources and Management. Corvallis, OR, Oregon State University. Ph.D.**:** 149.

Goerndt, M. E., V. J. Monleon and H. Temesgen (2010). Relating forest attributes with area- and tree-based Light Detection and Ranging metrics for Western Oregon. Society of American Foresters.

Grotefendt, R. A. and H. T. Schreuder (2006). A new FIA-type srategic inventory (NFI). Monitoring Science and Technology Symposium: Unifying Knowledge for Sustainability in the Western Hemisphere, Fort Collins, CO, U.S. Department of Agriculture, Forest Service, Rocky Mountain Research Station.

Hodgson, M. E. and P. Bresnahan (2004). Accuracy of airborne LiDAR-derived elevation: empirical assessment and error budget. Photogrammetric Engineering and Remote Sensing 70(3): 331-339.

Hodgson, M. E., J. Jenson, G. Raber, J. Tullis, B. A. Davis, G. Thompson and K. Schuckman (2005). An evaluation of LiDAR-derived elevation and terrain slope in leaf-off condition. Photogrammetric Engineering and Remote Sensing 62: 415-433.

Hoen, H. F. and B. Solberg (1994). Potential and economic efficiency of carbon sequestration in forest biomass through silvicultural management. Forest Science 40: 429-451.

Hudiburg, T., B. Law, D. P. Turner, J. Campbell, D. Donato and M. Duane (2009). Carbon dynamics of Oregon and Northern California forests and potential land-based carbon storage. Ecological Applications 19(1): 163-180.

Husch, B., C. I. Miller and T. Beers (1982). Forest mensuration. New York, John Wiley and Sons.

Hyyppa, J., H. Hyyppa, D. Leckie, F. Gougeon, X. Yu and M. Maltamo (2008). Review of methods of small-footprint Airborne Laser Scanning for extracting forest inventory data in boreal forests. International Journal of Remote Sensing 29(5): 1339-1366.

Hyyppa, J., H. Hyyppa, P. Litkey, X. Yu, H. Haggren, P. Ronnholm, U. Pyysalo, J. Pitkanen and M. Maltamo (2004). Algorithms and methods of Airborne Laser Scanning for forest measurements. International Archives of Photogrammetry, Remote Sensing and Spatial Information Sciences XXXVI(8/W2): 82-89.

Hyyppa, J., O. Kelle, M. Lehikoinen and M. Inkinen (2001). A segmentation-based method to retrieve stem volume estimates from 3-D tree height models produced by laser scanners. Geoscience and Remote Sensing, IEEE Transactions on 39(5): 969-975.

Hyyppa, J., U. Pyysalo, H. Hyyppa and A. Samberg (2000). Elevation accuracy of laser scanning-derived digital terrain and target models in forest environment. In Proceedings of EARSeL-SIG Workshop LIDAR, Dresden, Germany, European Association of Remote Sensing Laboratores.

Jennings, S., N. Brown and D. Sheil (1999). Assessing forest canopies and understorey illumination: canopy closure, canopy cover and other measures. Forestry 72(1): 59-74.

Jensen, J. R., Ed. (1996). Introductory digital image processing. Prentice Hall Series in Geographic Information Science. Upper Saddle River, New Jersey, Prentice Hall.

Kini, A. U. and S. C. Popescu (2004). TreeVaW: a versatile tool for analyzing forest canopy LiDAR data - a preview with an eye towards future. ASPRS Images Decision: Remote Sensing Foundation for GIS Applications: 1-10.

Krabill, W. B., J. G. Collins, L. E. Link, R. N. Swift and M. L. Butler (1984). Airborne laser topographic mapping results. Photogrammetric Engineering and Remote Sensing 50: 685-694.

Kraus, K. and N. Pfeifer (1998). Determination of terrain models in wooded areas with Airborne Laser Scanner data. ISPRS Journal of Photogrammetry and Remote Sensing 53(4): 193-203.

Law, B., D. Turner, J. Campbell, M. Lefsky, M. Guzy, O. Sun, S. Tuyl and W. Cohen (2006). Carbon fluxes across regions: observationoal constraints at multiple scales. Scaling and uncertainty analysis in ecology J. Wu, K. B. Jones, H. Li and O. L. Loucks, Springer Netherlands**:** 167-190.

Leckie, D., F. Gougeon, D. Hill, R. Quinn, L. Armstrong and R. Shreenan (2003). Combined high-density LiDAR and multispectral imagery for individual tree crown analysis. Canadian Journal of Remote Sensing 29(5): 633-649.

Lefsky, M. A., W. B. Cohen, S. A. Acker, G. G. Parker, T. A. Spies and D. Harding (1999a). LiDAR remote sensing of the canopy structure and biophysical properties of Douglas-fir western hemlock forests. Remote Sensing of Environment 70(3): 339-361.

Lefsky, M. A., W. B. Cohen, G. G. Parker and D. J. Harding (2002). LiDAR remote sensing for ecosystem studies. BioScience 52(1): 19-30.

Lefsky, M. A., D. Harding, W. B. Cohen, G. Parker and H. H. Shugart (1999b). Surface LiDAR remote sensing of basal area and biomass in deciduous forests of Eastern Maryland, USA. Remote Sensing of Environment 67(1): 83-98.

Lefsky, M. A., A. T. Hudak, W. B. Cohen and S. A. Acker (2005b). Geographic variability in lidar predictions of forest stand structure in the Pacific Northwest. Remote Sensing of Environment 95(4): 532-548.

Li, J., G. Taylor and D. B. Kidner (2005). Accuracy and reliability of map-matched GPS coordinates: the dependence on terrain model resolution and interpolation algorithm. Computers & Geosciences 31(2): 241-251.

Lim, K., P. Treitz, M. Wulder, B. St-Onge and M. Flood (2003). LiDAR remote sensing of forest structure. Progress in Physical Geography 27(1): 88-106.

Liu, X. (2008). Airborne LiDAR for DEM generation: some critical issues. Progress in Physical Geography 32(1): 31-49.

Lovell, J. L., D. L. B. Jupp, G. J. Newnham, N. C. Coops and D. S. Culvenor (2005). Simulation study for finding optimal lidar acquisition parameters for forest height retrieval. Forest Ecology and Management 214(1-3): 398-412.

Lucas, R. M., A. C. Lee and P. J. Bunting (2008). Retrieving forest biomass through integration of CASI and LiDAR data. International Journal of Remote Sensing 29(5): 1553-1577.

Luccio, M. (2008). Beyond terrain models: LiDAR enters the geospatial mainstream. Retrieved May 1, 2010, from http://www.imagingnotes.com/go/article_free.php?mp_id=204.

Luyssaert, S., E. D. Schulze, A. Borner, A. Knohl, D. Hessenmoller, B. E. Law, P. Ciais and J. Grace (2008). Old-growth forests as global carbon sinks. Nature 455(7210): 213-215.

Maraseni, T. N., G. Cockfield, A. Apan and N. Mather (2005). Estimation of shrub biomass: development and evaluation of allometric models leading to innovative teaching methods. International Journal of Business & Management Education Special Issue: Postgraduate Research in Innovative Methods of Teaching and Learning: 17-32.

McGaughey, R. (2007). FUSION/LDV: Software for LIDAR data analysis and visualization, United States Department of Agriculture Forest Service, Pacific Northwest Research Station**:** Users Manual.

McGaughey, R. J., W. W. Carson and S. E. Reutebuch (2004). Direct measurement of individual tree characteristics from LiDAR data. Proceedings of the 2004 Annual ASPRS Conference.

McRoberts, R. E., W. A. Bechtold, P. L. Patterson, C. T. Scott and G. A. Reams (2005). The enhanced forest inventory and analysis program of the USDA Forest Service: historical perspective and announcement of statistical documentation. Journal of Forestry 103(6): 304-308.

Means, J. E., S. A. Acker, B. J. Fitt, M. Renslow, L. Emerson and C. J. Hendrix (2000). Predicting forest stand characteristics with Airborn Scanning LiDAR. Photogrammetric Engineering and Remote Sensing 66(11): 1367-1371.

Means, J. E., S. A. Acker, D. J. Harding, J. B. Blair, M. A. Lefsky, W. B. Cohen, M. E. Harmon and W. A. McKee (1999). Use of large-footprint Scanning Airborne LiDAR to estimate forest stand characteristics in the Western Cascades of Oregon. Remote Sensing of Environment 67(3): 298-308.

Means, J. E., H. A. Hanson, G. J. Koerper, P. B. Alaback and M. W. Klopsch (1994). Software for computing plant biomass-BIOPAK users guide. Portland, OR, United States Department of Agriculture Forest Service**:** 194.

Næsset, E. and K.-O. Bjerknes (2001). Estimating tree heights and number of stems in young forest stands using Airborne Laser Scanner data. Remote Sensing of Environment 78(3): 328-340.

Næsset, E., T. Gobakken, J. Holmgren, H. Hyyppä, J. Hyyppä, M. Maltamo, M. Nilsson, H. Olsson, Å. Persson and U. Söderman (2004). Laser scanning of forest resources: the nordic experience. Scandinavian Journal of Forest Research 19(6): 482-499.

Næsset, E. and T. Økland (2002). Estimating tree height and tree crown properties using Airborne Scanning Laser in a boreal nature reserve. Remote Sensing of Environment 79(1): 105-115.

Naidu, S. L., E. H. Delucia and R. B. Thomas (1998). Contrasting patterns of biomass allocation in dominant and suppressed loblolly pine. Canadian Journal of Forest Research 28(8): 1116-1124.

Nelson, R., R. Swift and W. Krabill (1988). Using airborne lasers to estimate forest canopy and stand characteristics. Journal of Forestry 86: 31-38.

NGS. (2009). What is OPUS? Retrieved March 17, 2010, from http://www.ngs.noaa.gov/OPUS/about.html#discussion.

NOAA. (2010). Remote sensing for coastal management. Retrieved May 1, 2010, from http://www.csc.noaa.gov/crs/rs_apps/sensors/lidar.htm.

Penn State Geography. (2010). Lesson 1: LiDAR sensor design. Retrieved October 26, 2010, from https://www.e-education.psu.edu/lidar/l1_p7.html.

Pfeifer, N. and C. Briese (2007). Geometrical aspects of Airborne Laser Scanning and Terrestrial Laser Scanning. International Archives of Photogrammetry, Remote Sensing and Spatial Information Sciences 36(3/W52): 311-319.

Popescu, S. C. (2010). TreeVaW, tree variable window. Retrieved December 11, 2010, from http://ssl.tamu.edu/personnel/s_popescu/TreeVaW/download.htm.

Popescu, S. C., H. W. Randolph and A. S. John (2004). Fusion of small-footprint LiDAR and multispectral data to estimate plot- level volume and biomass in deciduous and pine forests in Virginia, USA. Forest Science 50: 551-565.

Popescu, S. C. and R. H. Wynne (2004). Seeing the trees in the forest: using LiDAR and multispectral data fusion with local filtering and variable window size for estimating tree height. Photogrammetric Engineering and Remote Sensing 70(5): 589-604.

Popescu, S. C., R. H. Wynne and R. F. Nelson (2002). Estimating plot-level tree heights with LiDAR: local filtering with a canopy-height based variable window size. Computers and Electronics in Agriculture 37: 71-95.

Rahman, M. Z. A. and B. Gorte. (2007). Individual tree detection based on densities of high points of high resolution airborne LiDAR. Retrieved March 1, 2010, from http://homepages.ucalgary.ca/~gjhay/geobia/Aug18/GEOBIA%20Themes/__Theme16/6790_Rahman_Proc.pdf.

Ramano, M. E. (2004). Innovation in LiDAR processing technology. Photogrammetric Engineering and Remote Sensing 70: 1202-1206.

Ramsey, F. L. and D. W. Schafer (2002). The statistical sleuth: a course in methods of data analysis. Pacific Grove, CA, Thompson Learning.

Rapp, V. (2005). Monitoring forests at the speed of light. P. N. R. Station. Portland, OR, USDA Forest Service. December 2005**:** 12.

Reutebuch, S. E., H.-E. Andersen and R. J. McGaughey (2005). Light Detection and Ranging (LiDAR): an emerging tool for multiple resource inventory. Journal of Forestry 103: 286-292.

Reutebuch, S. E., R. J. McGaughey, H.-E. Andersen and W. W. Carson (2003). Accuracy of a high-resolution LiDAR terrain model under a conifer forest canopy. Canadian Journal of Remote Sensing 29(5): 527-535.

SAF. (2008). The dictionary of forestry. Retrieved August 29, 2010, from http://dictionaryofforestry.org/.

Saint Clair, J. B. (1993). Family differences in equations for predicting biomass and leaf area in Douglas-fir (Pseudotsuga menziesii var. menziesii). Forest Science 39(4): 743-756.

Scott, J. H. and E. D. Reinhardt (2001). Assessing crown fire potential by linking models of surface and crown fire behavior. Fort Colling, CO, US Department of Agriculture Forest Service, Rocky Mountain Research Station. Research Paper RMRS-RP-29**:** 66.

Sessa, R. (2009). Assessment of the status of the development of the standards for the terrestrial essential climate variables: biomass. G. T. O. System. Rome, Italy. Version 10**:** 1-18.

Smith, W. B. (2002). Forest inventory and analysis: a national inventory and monitoring program. Environmental Pollution 116: 233-242.

Solomon, S., D. Quin, M. Manning, R. B. Alley, T. Berntsen, N. L. Bindoff, Z. Chen, A. Chidthaisong, J. M. Gregory, G. C. Hegerl, M. Heimann, B. Hewitson, B. J. Hoskins, F. Joos, J. Jouzel, V. Kattsov, U. Lohmann, T. Matsuno, M. Molena, N. Nicholls, J. Overpeck, G. Raga, V. Ramaswamy, J. Ren, M. Rusticucci, R. Somerville, T. F. Stocker, P. Whetton, R. A. Wood and D. Wratt (2007). Technical summary. in: climate change 2007: the physical science basis. contribution of Working Group I to the fourth assessment report of the Intergovernmental Panel on Climate Change. C. U. Press. Cambridge, United Kingdom

New York, New York.

Su, J. and E. Bork (2006). Influence of vegetation, slope, and LiDAR sampling angle on DEM accuracy. Photogrammetric Engineering and Remote Sensing 72(11): 1265-1274.

Tappeiner II, J. C., D. A. Maguire and T. B. Harrington (2007). Silviculture and ecology of western U.S. forests. Corvallis, OR, Oregon State University Press.

Trimble (2006a). TerraSync software reference manual. T. N. Limited. Westminster, CO. Version 2.60**:** 1-248.

Trimble (2007). Data sheet: GeoXT handheld datasheet. Westminster, CO, Trimble**:** 1-2.

Trimble (2008). GPS Pathfinder Office help, Trimble Navigation Limited.

Trimble (2009a). Data sheet: Trimble GeoXH. Westminster, Trimble Navigation Limited**:** 1-2.

Trimble (2009b). Data sheet: GPS Pathfinder ProXH receiver. Westminster, Trimble Navigation Limited**:** 1-2.

UNFCC. (2010). Kyoto Protocol. Retrieved December 26, 2010, from http://unfccc.int/kyoto-protocol/items/2830.php.

USDAFS. (2008). Introduction to FUSION launch page. Retrieved 1-15, 2008, 2008, from www.fs.fed.us/eng/rsac/fusion/index.html.

USGS. (2009). Experimental Advanced Airborne Research Lidar (EAARL). Retrieved August 23, 2010, from http://ngom.usgs.gov/dsp/tech/eaarl/index.html.

Van Sickle, J. (2008). GPS for land surveyors. Boca Raton, CRC Press, Taylor & Francis Group.

Watershed Sciences (2008). LiDAR remote sensing data collection: McDonald-Dunn Research Forest. Corvallis, Oregon, Watershed Sciences Inc.**:** 20.

Williams, M. S. and H. T. Schreuder (2000). Guidelines for choosing volume equations in the presence of measurement error in height. Canadian Journal of Forest Research 30(2): 306-310.

Wing, M. G., A. Eklund and J. Sessions (2010). Applying LiDAR technology for tree measurements in burned landscapes. International Journal of Wildland Fire 19: 1-11.

Wing, M. G., D. Solmie and L. Kellogg (2004). Comparing digital range finders for forestry applications. Journal of Forestry 102: 16-20.

Zhou, X. and M. A. Hemstrom (2009). Estimating aboveground tree biomass on forest land in the Pacific Northwest: a comparison of approaches, United States Department of Agriculture**:** 1-18.

CHAPTER 5 -- CONCLUSION

The goal of this dissertation was to assess the ability of discrete return LiDAR to estimate forest biomass on a by feature (trees and shrubs) basis compared to estimated results obtained by traditional field measurement in the Pacific Northwest region of the United States. The key parameter for estimating forest biomass was tree height, which was used with regional allometric equations. Three computer software programs capable of delineating individual trees from LiDAR data were compared, one of which uses raw point clouds to manually delineate trees (FUSION), and two others which rely on a canopy height model (CHM) (TreeVaW and watershed segmentation). The majority of the field data were collected using mapping grade global positioning system (GPS) with redundant sampling by total station survey. Two field collection periods occurred, one during summer of 2008 and the other in winter 2009, both during one growing season. LiDAR data were collected April 2, 2008. Three research components were investigated to obtain the results. These components included the assessment of mapping grade GPS accuracy under forest canopy compared with traditional survey methods using a total station: analysis of LiDAR digital elevation model (DEM) accuracy compared with LiDAR and GPS derived DEMS; and finally a comparison of LiDAR tree delineation, height measurement and

biomass estimation, as compared to estimates derived from traditional field measurements.

Chapter 2 compared mapping grade GPS accuracy under forest canopy to positions obtained by total station traverse from control survey positions obtained under open sky using a survey-grade GPS. Results indicated that the greatest positional GPS error was associated with differentially corrected combination of coarse acquisition (C/A) code and dual frequency carrier processing, followed by raw, uncorrected data files and the least amount of error was associated with C/A code only postprocessing. These results indicate that in similar forest canopy conditions, using C/A code only postprocessing will achieve higher accuracy results than either raw, autonomous GPS or dual frequency carrier phase processing. These results were determined to be theoretically important when considering GPS collection under forest canopy because tree stems have such an impact on the dual frequency carrier signal and unlike carrier phase processing of GPS data collected in the open, differential correction of dual frequency carrier signals does not improve the accuracy. It appears that under forest canopy, mapping grade GPS users should use either postprocessed C/A code data collection or even autonomous C/A code over dual frequency GPS collection. The most important systematic error that accounts for the increased error with dual frequency carrier phase GPS is discontinuity in the signal caused by cycle slips, which result from tree stems and canopy temporarily blocking signals as each satellite moves in relation to the GPS receiver and the forest.

The key parameter used for estimating forest biomass with LiDAR is tree height. Since tree heights are based on elevations above ground, it is important to assess the accuracy of the digital elevation model (DEM) used for the tree base elevation. In Chapter 3 we used three methods for comparing elevations: 1) discrete point to discrete point, 2) discrete point to DEM, and 3) DEM to DEM. The discrete point to discrete point method compared the ground surveyed elevations from both total station and GPS to the closest discrete LiDAR point elevations. The discrete point to DEM method compared the ground surveyed points collected with total station and GPS to the vendor provided LiDAR DEM. The DEM to DEM method compared ArcGIS derived DEMs to the vendor provided DEM. Additional comparisons included total station derived DEM to GPS derived DEM and the effect of distance on elevation differences between ground surveyed points to the closest LiDAR elevation point. Three field survey methods of elevation data collection were compared to LiDAR elevations. The field survey methods included trigonometric leveling by total station, mapping grade GPS dual frequency carrier phase and C/A code combination, and mapping grade GPS using only C/A code processing. The LiDAR data used in the comparison included ground point clouds and a DEM provided by the vendor. Of the survey methods used in the study, the most accurate method for collecting vertical coordinates is trigonometric leveling. Results of GPS elevation comparisons were expectedly poor under canopy, however better than expected results were achieved in the open. The most accurate LiDAR elevations were obtained when comparing the

closest discrete LiDAR elevation point to the nearest total station elevation, however the most relevant for this study was the LiDAR DEM elevations compared to discrete total station elevations at the same horizontal location. This elevation comparison was the most relevant because tree heights were measured from the discrete locations relative to the LiDAR DEM. If LiDAR tree height measurements are in error, we must be able to determine whether it is due to the DEM or miscalculation of the tree apex height for accurate error assessment. The average ME, SD, and RMSE under forest canopy cover comparing total station elevations to the LiDAR DEM was -0.42 m, 0.39 m, and 0.57 m, respectively. These average accuracy metrics are surprisingly good considering that five hectare sized plots within a range of canopy and environmental conditions are considered. All total station plots included Douglas-fir canopy within a mix of dense, young, and even aged stands on relatively flat slopes, mature stands on very steep slopes, and uneven aged stands with various canopy openings. The lowest ME that we found on a single plot with canopy cover was -0.06 m (SD 0.37 m) and -0.09 m (SD 0.41 m) in a total station to LiDAR point and total station to LiDAR DEM comparisons, respectively.

This dissertation research culminates in Chapter 4 with LiDAR forest biomass estimations for tree data collected in the Pacific Northwest region of the United States. Individual tree biomass estimations were performed using tree heights modeled from discrete return LiDAR. Individual tree biomass was then summed to estimate biomass per hectare. The LiDAR biomass estimations were compared to biomass from field-

measured trees, which were also summed to estimate biomass per hectare. Total above ground biomass of field-measured trees were based on regional allometric equations by species. The LiDAR analysis was based only on point cloud height and pattern or on canopy height models (CHM) derived from the point cloud. No attempt was made to differentiate species either by LiDAR intensity values or through integrated use of other remotely sensed imagery. Thus, the LiDAR biomass estimations were based solely on two size classes of Douglas-fir (*Pseudotsuga menziesii*) because it is the dominant tree species in the study area. To assess the accuracy of LiDAR biomass estimation, two key components were analyzed including stem count and stem height, and for a more complete analysis a comparison of three computer software programs used to delineate and measure trees from LiDAR was completed. The software programs were FUSION, TreeVaW, and watershed segmentation. To delineate trees, FUSION utilizes the LiDAR point cloud, whereas TreeVaW and watershed segmentation use a CHM. Based only on tree counts, watershed segmentation performed the best followed by TreeVaW and FUSION with overall percentages of field-measured tree counts equaling 93%, 59%, and 44%, respectively. Similar results were achieved when pairing trees from each method to ground measured trees. Watershed segmentation performed far better in clearcut plots, but overall difficulty in delineating small trees in clearcut plots indicated that missing small trees with LiDAR is not merely a result of overstory obscuration, but also a factor of tree size and LiDAR pulse density. Three comparisons were used to analyze the accuracy of

LiDAR to field-measured tree heights. The first comparison was in even age, uneven age, and old growth plots and used only trees that could be positively paired with total station spatial location and laser range finder height field-measured trees. The second comparison was on a clearcut plot where trees were matched with GPS spatial location and height pole field-measured trees. The third analysis evaluated average heights by plot. In the total station to LiDAR comparison, three plots had mean height errors of approximately half a meter. The greatest error in one plot was a mean of almost three meters shorter than field-measured averages. The most accurate mean height difference was only 0.06 meters shorter in LiDAR than field-measured. The biomass analysis included comparisons of feature totals in each plot, mean biomass per feature in each plot, and total biomass by plot for each extraction method. Compared to field-measured biomass overall FUSION and TreeVaW underestimated by 25 and 31% respectively, and watershed segmentation overestimated by approximately 10%. LiDAR biomass underestimation occurred in 66% and overestimation occurred in 34% of the plot comparisons.

Future Research

For accurate above ground woody biomass estimation to occur using LiDAR, all or most of the forest must be delineated and measured. The fact that many understory trees are not detected using LiDAR indicates three data related problems. If detection of all the woody vegetation is desired from LiDAR data, a CHM must be avoided because all points under the primary canopy will be interpolated out of the dataset. To

detect all trees using the LiDAR point cloud, research should be conducted using a higher pulse rate than used in this study. A higher pulse rate would enable better penetration of forest with complex multidimensional canopy structure, and it would enable more detailed structural detection of small trees and shrubs. The software program FUSION might be a good program for researching a higher pulse rate because the program allows for a manual human interface. However if a higher pulse rate does improve understory stem detection, an automated approach is necessary for large scale vegetation delineation and biomass estimation. Further research is encouraged in the use of an integrated approach combining LiDAR with multispectral remote sensors, and acquiring multispectral imagery simultaneously with LiDAR is encouraged for an integrated approach. Finally, we know that electromagnetic near-infrared imagery provide excellent vegetation information, thus it is likely that near-infrared LiDAR as used in this research also has the potential vegetation analysis. In this study, it is believed that the near-infrared returns may have helped differentiate species, certainly differentiate conifer from broadleaf, thus allowing further refinement of biomass estimation. We plan to further research LiDAR intensity potential.

Lessons Learned

The most important lesson learned from this research is that if asked for advice on a field data collection method for similar purposes, I would avoid using GPS under forest canopy for robust data collection, unless specifically researching GPS. Due to the many variables discussed in Chapter 2 that effect the reception of accurate GPS

signals by the GPS receiver, e.g. PDOP, elevation mask, cycle slip etc, time required to complete a survey is increased, dramatically at times. On some days field collection using GPS was reduced to 30% of what was surveyed using a total station. When conducting the control survey work, the survey grade GPS was useless until we could find an open area adequate enough to receive a constant signal.

With respect to LiDAR, as previously discussed, increased pulse density would likely improve the resolution of biomass estimation however software programs that utilize the LiDAR point cloud versus the CHM must be used if a more complete model of the three dimensional forest structure is desired. While conducting the ground survey, we often wondered what details of the forest LiDAR was capable of detecting. One biological detail noticed was many large squirrel nests. We recorded these nests during the field survey and discovered that they were not detectible in the LiDAR data point cloud provided in the specifications for this research. Again, higher pulse rate may provide for information at this detail. On the other hand many logs were detected indicating that a higher fidelity of differentiating ground from objects close to the ground may be achieved than previously believed.

Summary

Although many before have researched the application of LiDAR in forest inventory, this research has answered the call for further research. No other LiDAR forest research is known to have accomplished as robust a ground survey of plots. We have added insight to GPS data collection. The LiDAR results not only add

information into what we can see in the forest and the accuracy of the ground elevation and tree height measurements, but critical information on details of forest structure that LiDAR misses has also been provided. These results are important for the forestry community interested in biomass and fuels information, and for those seeking to improve LiDAR in forest inventory applications. The results of this dissertation provide further insight into determining the utility of LiDAR for forest inventory versus traditional ground measurements. Although varying results were achieved by stand treatment type (even age, uneven age, clearcut and old growth) and computer software delineation method (FUSION, TreeVaW and watershed segmentation), promise in individual tree measurement and biomass estimations warrants the continued pursuit of LiDAR forest inventory applications.

Questions remain as to why such differences exists in the numbers and heights of trees detected by each software program, especially between TreeVaW and watershed segmentation since they both use a CHM, and this warrants further investigation. The ground elevation discrepancy between those determined by trigonometric leveling compared to the LiDAR also warrants further investigation. The cause of the discrepancy is likely a result two contributing factors: 1) the proprietary software used to differentiate ground from above ground features; and 2) analyst quality assurance in differentiating ground from above ground LiDAR point returns. The analyst caused discrepancy may be remedied through further training however the discrepancies associated with proprietary software can only be researched by those holding

proprietary rights. In either case research, training and improvements are recommended for the advancement of LiDAR forestry applications.

Light Detection and Ranging (LiDAR)
What we can and cannot see in the forest for the trees

BIBLIOGRAPHY

AFPA (2001). Status report on the US Forest Service Forest Inventory and Analysis Program: Update to the findings of the 1998 Blue Ribbon Panel. Washington, D.C., American Forest and Paper Association.

Aguilar, F. J. and J. P. Mills (2008). Accuracy assessment of LiDAR-derived digital elevation models. The Photogrammetric Record 23(122): 148-169.

Andersen, H.-E. (2009). Using Airborne Light Detection and Ranging (LIDAR) to characterize forest stand condition on the Kenai Peninsula of Alaska. Western Journal of Applied Forestry 24: 95-102.

Andersen, H.-E., T. Clarkin, K. Winterberger and J. Strunk (2009). An accuracy assessment of positions obtained using survey- and recreational-grade Global Positioning System receivers across a range of forest conditions within the Tanana Valley of interior Alaska. Western Journal of Applied Forestry 24: 128-136.

Andersen, H.-E., R. J. McGaughey and S. E. Reutebuch (2005). Estimating forest canopy fuel parameters using LiDAR data. Remote Sensing of Environment 94(4): 441-449.

Andersen, H.-E., S. E. Reutebuch and R. J. McGaughey (2006). A rigorous assessment of tree height measurements obtained using airborne LiDAR and conventional field methods. Canadian Journal of Remote Sensing 32(5): 355-366.

Anderson, E. S., J. A. Thompson, D. A. Crouse and R. E. Austin (2006). Horizontal resolution and data density effects on remotely sensed LIDAR-based DEM. Geoderma 132(3-4): 406-415.

ASPRS. (2009). Common LiDAR data exchange format - .LAS industry initiative. Retrieved October 5, 2010, from www.asprs.org/society/committees/lidar/lidar_format.html.

Barker, T., I. Bashmakov, L. Bernstein, J. E. Bogner, P. Bosch, D. Rutu, D. Ogunlade, B. S. Fisher, S. Gupta, K. Halsnaes, B. Heij, S. Kahn, S. Kobayashi, M. D. Levine, D. L. Martino, O. Masera, B. Metz, L. Meyer, G.-J. Nabuurs, A. Najam, N. Nebojsa, H.-H. Rogner, J. Roy, J. Sathaye, R. Schock, P. Shukla, R. E. H. Sims, P. Smith, D. A. Tirpak, D. Urge-Vorsatz and D. Zhou (2007). Technical summary. in: Climate Change 2007: Mitigation. Contribution of Working Group III to the Fourth Assessment
Report of the Intergovernmental Panel on Climate Change. Cambridge, United Kingdom and New York, NY, USA.

Bechtold, W. A. and P. L. Patterson (2005). The enhanced Forest Inventory and Analysis program, national sampling design and estimation procedures. General Technical Report. Ashville, NC, U.S. Department of Agriculture, Forest Service, Southern Research Station. SRS-80**:** 85.

Blewitt, G. and G. Taylor (2002). Mapping Dilution of Precision (MDOP) and map-matched GPS. International Journal of Geographical Information Science 16(1): 55 - 67.

Bolstad, P., A. Jenks, J. Berkin, K. Horne and H. Reading William (2005). A Comparison of autonomous, WAAS, real-time, and post-processed Global Positioning Systems (GPS) accuracies in northern forests. Northern Journal of Applied Forestry 22: 5-11.

Bortolot, Z. J. and R. H. Wynne (2005). Estimating forest biomass using small footprint LiDAR data: An individual tree-based approach that incorporates training data. ISPRS Journal of Photogrammetry and Remote Sensing 59(6): 342-360.

Brandtberg, T., T. A. Warner, R. E. Landenberger and J. B. McGraw (2003). Detection and analysis of individual leaf-off tree crowns in small footprint, high sampling density lidar data from the eastern deciduous forest in North America. Remote Sensing of Environment 85(3): 290-303.

Carson, W. W. and S. E. Reutebuch (1997). A rigorous test of the accuracy of USGS digital elevation models in forested areas of Oregon and Washington. Surveying and cartography: ACSM/ASPRS Annual convention and exposition technical paper 1: 133-143.

Chaplot, V., F. Darboux, H. Bourennane, S. Leguédois, N. Silvera and K. Phachomphon (2006). Accuracy of interpolation techniques for the derivation of digital elevation models in relation to landform types and data density. Geomorphology 77(1-2): 126-141.

Chen, Q. (2007). Airborne LiDAR data processing and information extraction. Photogrammetric Engineering and Remote Sensing 73: 175-185.

Ciais, P., B. Moore, W. Steffen, M. Hood, S. Quengan, J. Cihlar, M. Raupach, S. Rasool, C. Doney, C. Heinze, C. Sabine, K. Hibbard, D. Schulze, M. Heimann, P. Chedin, P. Monfray, A. Watson, C. LeQuere, P. Tans, H. Dolman, R. Valentini, O. Arino, J. Townshend, G. Seufert, C. Field, T. Igrashi, C. Goodale, A. Nobre, G. Inoue, D. Crisp, D. Baldocchi, J. Tschirley, S. Denning, R. Cramer, R. Francey and D. Wickland (2010). Integrated global carbon observation theme: A strategy to realize a coordinated system of integrated global carbon cycle observations**:** 1-61.

Clark, R. L. and R. Lee (1998). Development of topographic maps for precision farming with kinematic GPS. Transactions of the ASAE 41(4): 909-916.

Coops, N., T. Hilker, M. Wulder, B. St-Onge, G. Newnham, A. Siggins and J. Trofymow (2007). Estimating canopy structure of Douglas-fir forest stands from discrete-return LiDAR. Trees - Structure and Function 21(3): 295-310.

Deckert, C. and P. V. Bolstad (1996). Forest canopy, terrain, and distance effects on Global Positioning System point accuracy. Photogrammetric Engineering and Remote Sensing 62(3): 317-321.

Dixon, R. K., R. A. Houghton, A. M. Solomon, M. C. Trexler and J. Wisniewski (1994). Carbon pools and flux of global forest ecosystems. Science 263: 185-190.

Dong, J., R. K. Kaufmann, R. B. Myneni, C. J. Tucker, P. E. Kauppi, J. Liski, W. Buermann, V. Alexeyev and M. K. Hughes (2003). Remote sensing estimates of boreal and temperate forest woody biomass: carbon pools, sources, and sinks. Remote Sensing of Environment 84(3): 393-410.

Dorren, L., B. Maier and F. Berger (2006). Assessing protection forest structure with Airborne Laser Scanning in steep mountainous terrain. Proceedings from Workshop on 3D Remote Sensing in Forestry, Vienna, Austria.

ESRI (2011). How Hot Spot Analysis: Getis-Ord Gi* (Spatial Statistics) works. ArcToolbox Help.

Evans, J. S., A. T. Hudak, R. Faux and A. M. S. Smith (2009). Discrete return LiDAR in natural resources: recommendations for project planning, data processing, and deliverables. Remote Sensing 1: 776-794.

Falkowski, M. J., A. M. S. Smith, P. E. Gessler, A. T. Hudak, L. A. Vierling and J. S. Evans (2008). The influence of conifer forest canopy cover on the accuracy of two individual tree measurement algorithms using LiDAR data. Canadian Journal of Remote Sensing 34(Suppl. 2): S1-S13.

Farid, A., D. C. Goodrich and S. Sorooshian (2006). Using airborne LiDAR to discern age classes of cottonwood trees in a riparian area. Western Journal of Applied Forestry 21(3): 149-158.

Fisher, P. F. and N. J. Tate (2006). Causes and consequences of error in digital elevation models. Progress in Physical Geography 30(4): 467-489.

Gatziolis, D. and H.-E. Andersen (2008). A guide to LiDAR data acquisition and processing for the forests of the Pacific Northwest**:** 1-32.

Gaveau, D. L. A. and R. A. Hill (2003). Quantifying canopy height underestimation by laser pulse penetration in small-footprint airborne laser scanning data. Canadian Journal of Remote Sensing 29(5): 650-657.

Goerndt, M. E. (2010). Comparison and analysis of small area estimation methods for improving estimates of selected forest attributes. Forest Engineering Resources and Management. Corvallis, OR, Oregon State University. Ph.D.**:** 149.

Goerndt, M. E., V. J. Monleon and H. Temesgen (2010). Relating forest attributes with area- and tree-based Light Detection and Ranging metrics for Western Oregon. Society of American Foresters.

Gomes Pereira, L. M. and L. L. F. Janssen (1999). Suitability of laser data for DTM generation: a case study in the context of road planning and design. ISPRS Journal of Photogrammetry and Remote Sensing 54(4): 244-253.

Grotefendt, R. A. and H. T. Schreuder (2006). A new FIA-type srategic inventory (NFI). Monitoring Science and Technology Symposium: Unifying Knowledge for Sustainability in the Western Hemisphere, Fort Collins, CO, U.S. Department of Agriculture, Forest Service, Rocky Mountain Research Station.

Hasegawa, H. and T. Yoshimura (2003). Application of dual-frequency GPS receivers for static surveying under tree canopies. Journal of Forest Research 8(2): 0103-0110.

Hodgson, M. E. and P. Bresnahan (2004). Accuracy of airborne LiDAR-derived elevation: empirical assessment and error budget. Photogrammetric Engineering and Remote Sensing 70(3): 331-339.

Hodgson, M. E., J. Jenson, G. Raber, J. Tullis, B. A. Davis, G. Thompson and K. Schuckman (2005). An evaluation of LiDAR-derived elevation and terrain slope in leaf-off condition. Photogrammetric Engineering and Remote Sensing 62: 415-433.

Hoen, H. F. and B. Solberg (1994). Potential and economic efficiency of carbon sequestration in forest biomass through silvicultural management. Forest Science 40: 429-451.

Hofmann-Wellenhof, B., H. Lichtenegger and J. Collins (2001). GPS theory and practice. New York, Springer-Verlag Wien.

Holmes, K. W., O. A. Chadwick and P. C. Kyriakidis (2000). Error in a USGS 30-meter digital elevation model and its impact on terrain modeling. Journal of Hydrology 233(1-4): 154-173.

Hudiburg, T., B. Law, D. P. Turner, J. Campbell, D. Donato and M. Duane (2009). Carbon dynamics of Oregon and Northern California forests and potential land-based carbon storage. Ecological Applications 19(1): 163-180.

Husch, B., C. I. Miller and T. Beers (1982). Forest mensuration. New York, John Wiley and Sons.

Hyyppa, J., H. Hyyppa, D. Leckie, F. Gougeon, X. Yu and M. Maltamo (2008). Review of methods of small-footprint Airborne Laser Scanning for extracting forest inventory data in boreal forests. International Journal of Remote Sensing 29(5): 1339-1366.

Hyyppa, J., H. Hyyppa, P. Litkey, X. Yu, H. Haggren, P. Ronnholm, U. Pyysalo, J. Pitkanen and M. Maltamo (2004). Algorithms and methods of Airborne Laser Scanning for forest measurements. International Archives of Photogrammetry, Remote Sensing and Spatial Information Sciences XXXVI(8/W2): 82-89.

Hyyppa, J., O. Kelle, M. Lehikoinen and M. Inkinen (2001). A segmentation-based method to retrieve stem volume estimates from 3-D tree height models

produced by laser scanners. Geoscience and Remote Sensing, IEEE Transactions on 39(5): 969-975.

Hyyppa, J., U. Pyysalo, H. Hyyppa and A. Samberg (2000). Elevation accuracy of laser scanning-derived digital terrain and target models in forest environment. In Proceedings of EARSeL-SIG Workshop LIDAR, Dresden, Germany, European Association of Remote Sensing Laboratores.

Jennings, S., N. Brown and D. Sheil (1999). Assessing forest canopies and understorey illumination: canopy closure, canopy cover and other measures. Forestry 72(1): 59-74.

Jensen, J. R., Ed. (1996). Introductory digital image processing. Prentice Hall Series in Geographic Information Science. Upper Saddle River, New Jersey, Prentice Hall.

Johnson, C. E. and C. C. Barton (2004). Where in the world are my field plots? Using GPS effectively in environmental field studies. Frontiers in Ecology and the Environment 2(9): 475-482.

Karsky, D. (2004). Comparing four methods of correcting GPS data: DGPS, WAAS, L-band, and postprocessing. Engineering Tech Tips, United States Department of Agriculture Forest Service 0471-3-2307-MTDC: 1-6.

Kato, A., L. M. Moskal, P. Schiess, M. E. Swanson, D. Calhoun and W. Stuetzle (2009). Capturing tree crown formation through implicit surface reconstruction using airborne LiDAR data. Remote Sensing of Environment 113(6): 1148-1162.

Keim, R. F., A. E. Skaugset and D. S. Bateman (1999). Digital terrain modeling of small stream channels with a total-station theodolite. Advances in Water Resources 23(1): 41-48.

Kini, A. U. and S. C. Popescu (2004). TreeVaW: a versatile tool for analyzing forest canopy LiDAR data - a preview with an eye towards future. ASPRS Images Decision: Remote Sensing Foundation for GIS Applications: 1-10.

Krabill, W. B., J. G. Collins, L. E. Link, R. N. Swift and M. L. Butler (1984). Airborne laser topographic mapping results. Photogrammetric Engineering and Remote Sensing 50: 685-694.

Kraus, K. and N. Pfeifer (1998). Determination of terrain models in wooded areas with Airborne Laser Scanner data. ISPRS Journal of Photogrammetry and Remote Sensing 53(4): 193-203.

Lahm, J. (2009). GeoXH vs. ProXH. C. Edson.

Law, B., D. Turner, J. Campbell, M. Lefsky, M. Guzy, O. Sun, S. Tuyl and W. Cohen (2006). Carbon fluxes across regions: observationoal constraints at multiple scales. Scaling and uncertainty analysis in ecology J. Wu, K. B. Jones, H. Li and O. L. Loucks, Springer Netherlands**:** 167-190.

Leckie, D., F. Gougeon, D. Hill, R. Quinn, L. Armstrong and R. Shreenan (2003). Combined high-density LiDAR and multispectral imagery for individual tree crown analysis. Canadian Journal of Remote Sensing 29(5): 633-649.

Lefsky, M. A., W. B. Cohen, S. A. Acker, G. G. Parker, T. A. Spies and D. Harding (1999a). LiDAR remote sensing of the canopy structure and biophysical properties of Douglas-fir western hemlock forests. Remote Sensing of Environment 70(3): 339-361.

Lefsky, M. A., W. B. Cohen, G. G. Parker and D. J. Harding (2002). LiDAR remote sensing for ecosystem studies. BioScience 52(1): 19-30.

Lefsky, M. A., D. Harding, W. B. Cohen, G. Parker and H. H. Shugart (1999b). Surface LiDAR remote sensing of basal area and biomass in deciduous forests of Eastern Maryland, USA. Remote Sensing of Environment 67(1): 83-98.

Lefsky, M. A., A. T. Hudak, W. B. Cohen and S. A. Acker (2005b). Geographic variability in lidar predictions of forest stand structure in the Pacific Northwest. Remote Sensing of Environment 95(4): 532-548.

Li, J., G. Taylor and D. B. Kidner (2005). Accuracy and reliability of map-matched GPS coordinates: the dependence on terrain model resolution and interpolation algorithm. Computers & Geosciences 31(2): 241-251.

Lim, K., P. Treitz, A. Groot and B. St.-Onge (2001). Estimation of individual tree heights using LiDAR remote sensing. Proceedings of the 23rd Annual Canadian Symposium on Remote Sensing. Quebec, Canada, CASI**:** 243-250.

Lim, K., P. Treitz, M. Wulder, B. St-Onge and M. Flood (2003). LiDAR remote sensing of forest structure. Progress in Physical Geography 27(1): 88-106.

Liu, X. (2008). Airborne LiDAR for DEM generation: some critical issues. Progress in Physical Geography 32(1): 31-49.

Lovell, J. L., D. L. B. Jupp, G. J. Newnham, N. C. Coops and D. S. Culvenor (2005). Simulation study for finding optimal lidar acquisition parameters for forest height retrieval. Forest Ecology and Management 214(1-3): 398-412.

Lucas, R. M., A. C. Lee and P. J. Bunting (2008). Retrieving forest biomass through integration of CASI and LiDAR data. International Journal of Remote Sensing 29(5): 1553-1577.

Luccio, M. (2008). Beyond terrain models: LiDAR enters the geospatial mainstream. Retrieved May 1, 2010, from http://www.imagingnotes.com/go/article_free.php?mp_id=204.

Luyssaert, S., E. D. Schulze, A. Borner, A. Knohl, D. Hessenmoller, B. E. Law, P. Ciais and J. Grace (2008). Old-growth forests as global carbon sinks. Nature 455(7210): 213-215.

Maraseni, T. N., G. Cockfield, A. Apan and N. Mather (2005). Estimation of shrub biomass: development and evaluation of allometric models leading to innovative teaching methods. International Journal of Business & Management

Education Special Issue: Postgraduate Research in Innovative Methods of Teaching and Learning: 17-32.

McGaughey, R. (2007). FUSION/LDV: Software for LIDAR Data Analysis and Visualization, United States Department of Agriculture Forest Service, Pacific Northwest Research Station**:** Users Manual.

McGaughey, R. J., W. W. Carson and S. E. Reutebuch (2004). Direct measurement of individual tree characteristics from LiDAR data. Proceedings of the 2004 Annual ASPRS Conference.

McRoberts, R. E., W. A. Bechtold, P. L. Patterson, C. T. Scott and G. A. Reams (2005). The enhanced forest inventory and analysis program of the USDA Forest Service: historical perspective and announcement of statistical documentation. Journal of Forestry 103(6): 304-308.

Means, J. E. (2000). Comparison of large-footprint and small-footprint lidar systems: design, capabilities, and uses. Second International Conference on Geospatial Information in Agriculture and Forestry, Lake Buena Vista, Florida.

Means, J. E., S. A. Acker, B. J. Fitt, M. Renslow, L. Emerson and C. J. Hendrix (2000). Predicting forest stand characteristics with Airborn Scanning LiDAR. Photogrammetric Engineering and Remote Sensing 66(11): 1367-1371.

Means, J. E., S. A. Acker, D. J. Harding, J. B. Blair, M. A. Lefsky, W. B. Cohen, M. E. Harmon and W. A. McKee (1999). Use of large-footprint Scanning Airborne LiDAR to estimate forest stand characteristics in the Western Cascades of Oregon. Remote Sensing of Environment 67(3): 298-308.

Means, J. E., H. A. Hanson, G. J. Koerper, P. B. Alaback and M. W. Klopsch (1994). Software for computing plant biomass-BIOPAK users guide. Portland, OR, United States Department of Agriculture Forest Service**:** 194.

Meyer, T. H., C. R. Ferguson, J. E. Bean and J. M. Naismith (2002). The effect of broadleaf canopies on survey-grade horizontal GPS/GLONASS measurements. Surveying and Land Information Science 62(4): 215-224.

Næsset, E. and K.-O. Bjerknes (2001). Estimating tree heights and number of stems in young forest stands using airborne laser scanner data. Remote Sensing of Environment 78(3): 328-340.

Næsset, E., T. Gobakken, J. Holmgren, H. Hyyppä, J. Hyyppä, M. Maltamo, M. Nilsson, H. Olsson, Å. Persson and U. Söderman (2004). Laser scanning of forest resources: the nordic experience. Scandinavian Journal of Forest Research 19(6): 482-499.

Næsset, E. and T. Økland (2002). Estimating tree height and tree crown properties using Airborne Scanning Laser in a boreal nature reserve. Remote Sensing of Environment 79(1): 105-115.

Naidu, S. L., E. H. Delucia and R. B. Thomas (1998). Contrasting patterns of biomass allocation in dominant and suppressed loblolly pine. Canadian Journal of Forest Research 28(8): 1116-1124.

Nelson, R., R. Swift and W. Krabill (1988). Using airborne lasers to estimate forest canopy and stand characteristics. Journal of Forestry 86: 31-38.

NGS. (2009). What is OPUS? Retrieved March 17, 2010, from http://www.ngs.noaa.gov/OPUS/about.html#discussion.

NGS. (2010). The NGS geoid page. Retrieved May 14, 2010, from http://www.ngs.noaa.gov/GEOID/.

NOAA. (2010). Remote sensing for coastal management. Retrieved May 1, 2010, from http://www.csc.noaa.gov/crs/rs_apps/sensors/lidar.htm.

Penn State Geography. (2010). Lesson 1: LiDAR sensor design. Retrieved October 26, 2010, from https://www.e-education.psu.edu/lidar/l1_p7.html.

Pfeifer, N. and C. Briese (2007). Geometrical aspects of Airborne Laser Scanning and Terrestrial Laser Scanning. International Archives of Photogrammetry, Remote Sensing and Spatial Information Sciences 36(3/W52): 311-319.

Piedallu, C. and J.-C. Gegout (2005). Effects of forest environment and survey protocol on GPS accuracy. Photogrammetric Engineering and Remote Sensing 71(9): 1071-1078.

Popescu, S. C. (2007). Estimating biomass of individual pine trees using airborne LiDAR. Biomass and Bioenergy 31(9): 646-655.

Popescu, S. C. (2010). TreeVaW, tree variable window. Retrieved December 11, 2010, from http://ssl.tamu.edu/personnel/s_popescu/TreeVaW/download.htm.

Popescu, S. C., H. W. Randolph and A. S. John (2004). Fusion of small-footprint LiDAR and multispectral data to estimate plot- level volume and biomass in deciduous and pine forests in Virginia, USA. Forest Science 50: 551-565.

Popescu, S. C. and R. H. Wynne (2004). Seeing the trees in the forest: using LiDAR and multispectral data fusion with local filtering and variable window size for estimating tree height. Photogrammetric Engineering and Remote Sensing 70(5): 589-604.

Popescu, S. C., R. H. Wynne and R. F. Nelson (2002). Estimating plot-level tree heights with LiDAR: local filtering with a canopy-height based variable window size. Computers and Electronics in Agriculture 37: 71-95.

Rahman, M. Z. A. and B. Gorte. (2007). Individual tree detection based on densities of high points of high resolution airborne LiDAR. Retrieved March 1, 2010, from http://homepages.ucalgary.ca/~gjhay/geobia/Aug18/GEOBIA%20Themes/__Theme16/6790_Rahman_Proc.pdf.

Ramano, M. E. (2004). Innovation in LiDAR processing technology. Photogrammetric Engineering and Remote Sensing 70: 1202-1206.

Ramsey, F. L. and D. W. Schafer (2002). The statistical sleuth: a course in methods of data analysis. Pacific Grove, CA, Thompson Learning.

Rapp, V. (2005). Monitoring forests at the speed of light. P. N. R. Station. Portland, OR, USDA Forest Service. December 2005**:** 12.

Renslow, M., P. Greenfield and T. Guay (2000). Evaluation of multi-return LiDAR for forestry applications, US Department of Agriculture, Forest Service-Engineering, Remote Sensing Applications Center. RSAC-2060/4180-LSP-001-RPT1.

Reutebuch, S. E., H.-E. Andersen and R. J. McGaughey (2005). Light Detection and Ranging (LiDAR): an emerging tool for multiple resource inventory. Journal of Forestry 103: 286-292.

Reutebuch, S. E., R. J. McGaughey, H.-E. Andersen and W. W. Carson (2003). Accuracy of a high-resolution LiDAR terrain model under a conifer forest canopy. Canadian Journal of Remote Sensing 29(5): 527-535.

SAF. (2008). The dictionary of forestry. Retrieved August 29, 2010, from http://dictionaryofforestry.org/.

Saint Clair, J. B. (1993). Family differences in equations for predicting biomass and leaf area in Douglas-fir (Pseudotsuga menziesii var. menziesii). Forest Science 39(4): 743-756.

Scott, J. H. and E. D. Reinhardt (2001). Assessing crown fire potential by linking models of surface and crown fire behavior. Fort Colling, CO, US Department of Agriculture Forest Service, Rocky Mountain Research Station. Research Paper RMRS-RP-29**:** 66.

Sessa, R. (2009). Assessment of the status of the development of the standards for the terrestrial essential climate variables: biomass. G. T. O. System. Rome, Italy. Version 10**:** 1-18.

Sigrist, P., P. Coppin and M. Hermy (1999). Impact of forest canopy on quality and accuracy of GPS measurements. International Journal of Remote Sensing 20(18): 3595-3610.

Smith, W. B. (2002). Forest inventory and analysis: a national inventory and monitoring program. Environmental Pollution 116: 233-242.

Solomon, S., D. Quin, M. Manning, R. B. Alley, T. Berntsen, N. L. Bindoff, Z. Chen, A. Chidthaisong, J. M. Gregory, G. C. Hegerl, M. Heimann, B. Hewitson, B. J. Hoskins, F. Joos, J. Jouzel, V. Kattsov, U. Lohmann, T. Matsuno, M. Molena, N. Nicholls, J. Overpeck, G. Raga, V. Ramaswamy, J. Ren, M. Rusticucci, R. Somerville, T. F. Stocker, P. Whetton, R. A. Wood and D. Wratt (2007). Technical summary. in: climate change 2007: the physical science basis. contribution of Working Group I to the fourth assessment report of the Intergovernmental Panel on Climate Change. C. U. Press. Cambridge, United Kingdom

New York, New York.

Su, J. and E. Bork (2006). Influence of vegetation, slope, and LiDAR sampling angle on DEM accuracy. Photogrammetric Engineering and Remote Sensing 72(11): 1265-1274.

Tappeiner II, J. C., D. A. Maguire and T. B. Harrington (2007). Silviculture and ecology of western U.S. forests. Corvallis, OR, Oregon State University Press.

Taylor, G., G. Blewitt, D. Steup, S. Corbett and A. Car (2001). Road reduction filtering for GPS-GIS navigation. Transactions in GIS 5(3): 193.

Trimble (1995-2008). GPS Pathfinder Office Help, Trimble Navigation Limited.

Trimble. (2005). Data sheet: H-Star technology explained. Retrieved February, 2009, from http://trl.trimble.com/docushare/dsweb/Get/Document-224437/022501-071_H-Star%20technology%20explained_0805.pdf.

Trimble (2006-2009). GPS Pathfinder ProXH Receiver Datasheet. Westminster, Trimble Navigation Limited**:** 1-2.

Trimble (2006a). TerraSync software reference manual. T. N. Limited. Westminster, CO. Version 2.60**:** 1-248.

Trimble (2006b). Data sheet: GPS Pathfinder ProXH receiver. Trimble. Westminster, CO.

Trimble (2007). Data sheet: GeoXT handheld datasheet. Westminster, CO, Trimble**:** 1-2.

Trimble (2008). GPS Pathfinder Office help, Trimble Navigation Limited.

Trimble (2008-2009). Trimble GeoXH Datasheet. Westminster, Trimble Navigation Limited**:** 1-2.

Trimble (2009a). Data sheet: Trimble GeoXH. Westminster, Trimble Navigation Limited**:** 1-2.

Trimble (2009b). Data sheet: GPS Pathfinder ProXH receiver. Westminster, Trimble Navigation Limited**:** 1-2.

UNFCC. (2010). Kyoto Protocol. Retrieved December 26, 2010, from http://unfccc.int/kyoto-protocol/items/2830.php.

USDAFS. (1998). US Forest Service post-fire conditions glossary. Retrieved August 25, 2010, from http://www.fs.fed.us/postfirevegcondition/glossary.shtml.

USDAFS. (2008). Introduction to FUSION launch page. Retrieved 1-15, 2008, 2008, from www.fs.fed.us/eng/rsac/fusion/index.html.

USGS. (2009). Experimental Advanced Airborne Research Lidar (EAARL). Retrieved August 23, 2010, from http://ngom.usgs.gov/dsp/tech/eaarl/index.html.

Van Sickle, J. (2008). GPS for land surveyors. Boca Raton, CRC Press, Taylor & Francis Group.

Vanicek, P. (1990). Vertical datum and NAVD 88. Retrieved May 14, 2010, from http://www.ngs.noaa.gov/web/about_ngs/history/Vanicek1.pdf.

Watershed Sciences (2008). LiDAR remote sensing data collection: McDonald-Dunn Research Forest. Corvallis, Oregon, Watershed Sciences Inc.**:** 20.

Williams, M. S. and H. T. Schreuder (2000). Guidelines for choosing volume equations in the presence of measurement error in height. Canadian Journal of Forest Research 30(2): 306-310.

Wing, M. G. (2008). Keeping Pace with Global Positioning System technology in the forest. Journal of Forestry 106: 332-338.

Wing, M. G. and A. Eklund (2007). Elevation measurement capabilities of consumer-grade Global Positioning System (GPS) receivers. Journal of Forestry 105: 91-94.

Wing, M. G., A. Eklund, S. John and K. Richard (2008). Horizontal measurement performance of five mapping-grade Global Positioning System receiver configurations in several forested settings. Western Journal of Applied Forestry 23: 166-171.

Wing, M. G., A. Eklund and L. D. Kellogg (2005). Consumer-grade Global Positioning System (GPS) accuracy and reliability. Journal of Forestry 103: 169-173.

Wing, M. G., A. Eklund and J. Sessions (2010). Applying LiDAR technology for tree measurements in burned landscapes. International Journal of Wildland Fire 19: 1-11.

Wing, M. G. and R. Karsky (2006). Standard and real-time accuracy and reliability of a mapping-grade GPS in a coniferous western Oregon forest. Western Journal of Applied Forestry 21: 222-227.

Wing, M. G., D. Solmie and L. Kellogg (2004). Comparing digital range finders for forestry applications. Journal of Forestry 102: 16-20.

Wolf, P. R. and C. D. Ghilani (2002). Elementary surveying an introduction to geomatics. Upper Saddle River, New Jersey, Prentice Hall.

Yang, Q., T. G. Van Niel, T. R. McVicar, M. F. Hutchinson and L. Li (2005). Developing a Digital Elevation Model using ANUDEM for the course sandy hilly catchments of the Loess Plateau, China. Canberra, Australia, CSIRO Land and Water**:** 82.

Yao, H. and R. L. Clark (2000). Evaluation of sub-meter and 2 to 5 meter accuracy GPS receivers to develop Digital Elevation Models. Precision Agriculture 2(2): 189-200.

Yoshimura, T. and H. Hasegawa (2003). Comparing the precision and accuracy of GPS positioning in forested areas. Journal of Forest Research 8(3): 147-152.

Zengin, H. and A. Yeşil (2006). Comparing the performances of real-time kinematic GPS and a handheld GPS receiver under forest cover. Turkish Journal of Agriculture & Forestry 30(2): 101-110.

Zhang, Z., K. Zhang, Y. Deng and C. Luo (2005). Research on precise trigonometric leveling in place of first order leveling. Geo-spatial Information Science (Quarterly) 8(4): 235-239.

Zheng, J., Y. Wang and N. L. Nihan (2005). Quantitative evaluation of GPS performance under forest canopies. IEEE Proceedings of Networking, Sensing and Control: 777-782.

Zhou, X. and M. A. Hemstrom (2009). Estimating aboveground tree biomass on forest land in the Pacific Northwest: a comparison of approaches, United States Department of Agriculture**:** 1-18.

APPENDIX

Appendix A-1. Tree species count by plot.

Plot	Plot Statistics	BM	CH	CB	CP	CW	DF	GF	HW	HY	MA	OS	OW	OG	PD	SF	PY	PP
	Total Count						690						1					
C20																		
	Height						1.00						0.35					
	Crown Width						0.56						2.30					
	>= 0.13 m Count												1					
	DBH (m)												0.14					
	< 0.13 m Count						690											
	AGL (m)						0.20											
C27	Total Count	9					556											
	Height	2.28					1.01											
	Crown Width	2.48					0.57											
	>= 0.13 m Count																	
	DBH (m)																	
	< 0.13 m Count	9					556											
	AGL (m)	0.06					0.03											
C61	Total Count	11				1	467	17										35
	Height	17.45				44.45	1.22	1.28										1.24
	Crown Width	5.46				28.10	0.78	0.79										0.90
	>= 0.13 m Count	11				1												
	DBH (m)	0.31				1.43												
	< 0.13 m Count						467	17										35
	AGL (m)						0.03	0.07										0.18

Appendix A-1. Tree species statistics by plot (continued).

Plot	Plot Statistics	RE	VM	O	Plot Total	Conifer Total	Broadleaf Total
	Total Count				691	690	1
C20							
	Height						
	Crown Width						
	>= 0.13 m Count						
	DBH (m)						
	< 0.13 m Count						
	AGL (m)						
C27	Total Count				565	556	9
	Height						
	Crown Width						
	>= 0.13 m Count						
	DBH (m)						
	< 0.13 m Count						
	AGL (m)						
C61	Total Count			3	534	519	15
	Height			1.33			
	Crown Width			0.88			
	>= 0.13 m Count						
	DBH (m)						
	< 0.13 m Count			3			
	AGL (m)			0.04			

Species Abbreviation

BM - Bigleaf Maple (*Acer macrophyllum)*
CH- California Hazel (*Corylus cornuta*)
CB - cascara Buckthorn (*Rhamnus purshiana*)
CP - cherry (*Prunus spp.*)
CW - black cottonwood (*Populus trichocarpa*)
DF - Douglas-Fir (*Pseudotsuga menziesii*)
GF - grand fir (*Abies grandis*)
HT - hawthorne (*Crataegus spp.*)
HY - holly (*Ilex spp.)*
MA - madrone (*Arbutus spp.*)
OS - oceanspray (*Holodiscus discolor*)
OW - Oregon white oak (*Quercus garryana*)
OG - Oregon grape (*Berberis aquifolium*)
PD - Pacific dogwood (*Cornus nuttalii*)
SF - Pacific silver fir (*Abies amabilis*)
PY - Pacific yew (*Taxus brevifolia*)
PP - ponderosa pine (*Pinus ponderosa*)
RE - red elderberry (*Sambucus racemosa*)
VM - vine maple (*Acer circinatum*)
O - other

Appendix A-1. Tree species statistics by plot (continued).

Plot	Plot Statistics	BM	CH	CB	CP	CW	DF	GF	HW	HY	MA	OS	OW	OG	PD	SF	PY	PP
C110	Total Count	9	1				500	41					1	6				14
	Height	6.17	2.11				2.14	1.06					2.24	5.65				1.58
	Crown Width	1.93	1.29				1.09	0.82					0.86	3.86				0.89
	>= 0.13 m Count	3					2											
	DBH (m)	0.15					0.18											
	< 0.13 m Count	6	1				498	41					1	6				14
	AGL (m)	0.08	0.03				0.13	0.03					0.06	0.08				0.05
E200	Total Count	10	3	53	92		763	12	5		1			3				
	Height	8.43	6.61	9.05	8.14		13.64	3.51	5.68		13.30			3.06				
	Crown Width	4.03	2.80	3.42	3.11		5.35	1.76	3.55		5.84			3.09				
	>= 0.13 m Count	1		3	1		736	2										
	DBH (m)	0.13		0.14	0.14		0.20	0.16										
	< 0.13 m Count	9	3	50	91		27	10	5		1			3				
	AGL (m)	0.08	0.07	0.08	0.07		0.11	0.02	0.06		0.10			0.07				
E412	Total Count	2					901	16					2		1	7		
	Height	4.47					6.64	2.89					11.84		3.99	3.91		
	Crown Width	3.70					3.78	1.60					5.24		2.00	2.41		
	>= 0.13 m Count						78						1			1		
	DBH (m)						0.14						0.48			0.17		
	< 0.13 m Count	2					823	16					1		1	6		
	AGL (m)	0.06					0.11	0.04					0.06		0.06	0.07		

Appendix A-1. Tree species statistics by plot (continued).

Plot	Plot Statistics	RE	VM	O	Plot Total	Conifer Total	Broadleaf Total
C110	Total Count			3	575	555	20
	Height						
	Crown Width						
	>= 0.13 m Count						
	DBH (m)						
	< 0.13 m Count			3			
	AGL (m)						
E200	Total Count		2	2	946	775	171
	Height		5.48	5.85			
	Crown Width		3.39	4.02			
	>= 0.13 m Count						
	DBH (m)						
	< 0.13 m Count		2	2			
	AGL (m)		0.05	0.03			
E412	Total Count				929	924	5
	Height						
	Crown Width						
	>= 0.13 m Count						
	DBH (m)						
	< 0.13 m Count						
	AGL (m)						

Species Abbreviation

BM - Bigleaf Maple (*Acer macrophyllum)*
CH- California Hazel (*Corylus cornuta*)
CB - cascara Buckthorn (*Rhamnus purshiana*)
CP - cherry (*Prunus spp*.)
CW - black cottonwood (*Populus trichocarpa*)
DF - Douglas-Fir (*Pseudotsuga menziesii*)
GF - grand fir (*Abies grandis*)
HT - hawthorne (*Crataegus spp.*)
HY - holly (*Ilex spp.)*
MA - madrone (*Arbutus spp.*)
OS - oceanspray (*Holodiscus discolor*)
OW - Oregon white oak (*Quercus garryana*)
OG - Oregon grape (*Berberis aquifolium*)
PD - Pacific dogwood (*Cornus nuttalii*)
SF - Pacific silver fir (*Abies amabilis*)
PY - Pacific yew (*Taxus brevifolia*)
PP - ponderosa pine (*Pinus ponderosa*)
RE - red elderberry (*Sambucus racemosa*)
VM - vine maple (*Acer circinatum*)
O - other

Appendix A-1. Tree species statistics by plot (continued).

Plot	Plot Statistics	BM	CH	CB	CP	CW	DF	GF	HW	HY	MA	OS	OW	OG	PD	SF	PY	PP
	Total Count	124	3		3		120	111					1					
O16																		
	Height	15.92	7.48		7.58		27.48	13.41					7.53					
	Crown Width	9.13	6.31		6.41		8.08	5.35					6.49					
	>= 0.13 m Count	89					88	64										
	DBH (m)	0.32					0.66	0.27										
	< 0.13 m Count	35	3		3		32	47					1					
	AGL (m)	0.11	0.08		0.10		0.08	0.09					0.14					
O69	Total Count	67					87	82							1		20	
	Height	13.78					40.27	8.02							4.20		7.03	
	Crown Width	10.15					10.38	4.14							6.97		4.66	
	>= 0.13 m Count	51					84	32							1		14	
	DBH (m)	0.31					0.81	0.21							0.13		0.20	
	< 0.13 m Count	16					3	50									6	
	AGL (m)	0.09					0.08	0.08									0.09	
U8	Total Count	92					205	57		6			3					
	Height	15.16					24.08	3.25		3.42			14.13					
	Crown Width	8.85					7.21	2.07		1.82			2.63					
	>= 0.13 m Count	70					118	3					3					
	DBH (m)	0.27					0.61	0.17					0.17					
	< 0.13 m Count	22					87	54		6								
	AGL (m)	0.09					0.03	0.03		0.04								

Appendix A-1. Tree species statistics by plot (continued).

Plot	Plot Statistics	RE	VM	O	Plot Total	Conifer Total	Broadleaf Total
	Total Count		1		363	231	132
O16							
	Height		6.01				
	Crown Width		5.02				
	>= 0.13 m Count						
	DBH (m)						
	< 0.13 m Count		1				
	AGL (m)		0.08				
O69	Total Count				257	189	68
	Height						
	Crown Width						
	>= 0.13 m Count						
	DBH (m)						
	< 0.13 m Count						
	AGL (m)						
U8	Total Count			4	367	262	105
	Height			6.08			
	Crown Width			3.03			
	>= 0.13 m Count						
	DBH (m)						
	< 0.13 m Count			4			
	AGL (m)			0.07			

Species Abbreviation

BM - Bigleaf Maple (*Acer macrophyll*
CH- California Hazel (*Corylus cornut*
CB - cascara Buckthorn (*Rhamnus pur*
CP - cherry (*Prunus spp.*)
CW - black cottonwood (*Populus trich*
DF - Douglas-Fir (*Pseudotsuga menzi*
GF - grand fir (*Abies grandis*)
HT - hawthorne (*Crataegus spp.*)
HY - holly (*Ilex spp.)*
MA - madrone (*Arbutus spp.*)
OS - oceanspray (*Holodiscus discolor*)
OW - Oregon white oak (*Quercus gar*
OG - Oregon grape (*Berberis aquifoli*
PD - Pacific dogwood (*Cornus nuttali*
SF - Pacific silver fir (*Abies amabilis*)
PY - Pacific yew (*Taxus brevifolia*)
PP - ponderosa pine (*Pinus ponderosa*
RE - red elderberry (*Sambucus racem*
VM - vine maple (*Acer circinatum*)
O - other

Appendix A-1. Tree species statistics by plot (continued).

Plot	Plot Statistics	BM	CH	CB	CP	CW	DF	GF	HW	HY	MA	OS	OW	OG	PD	SF	PY	PP
	Total Count	23	1	4	4		298	164			2		1					
U13																		
	Height	15.03	3.62	3.60	10.10		8.42	2.88			3.50		2.34					
	Crown Width	7.44	3.42	2.47	5.46		3.68	2.22			1.56		1.18					
	>= 0.13 m Count	14			1		40	5										
	DBH (m)	0.47			0.30		0.81	0.22										
	< 0.13 m Count	9	1	4	3		258	159			2		1					
	AGL (m)	0.10	0.04	0.04	0.10		0.06	0.06			0.09		0.04					
U56	Total Count	24		19	148		658	376	1		7	3				1		
	Height	7.34		3.96	4.75		9.95	1.99	2.73		2.36	3.81				5.45		
	Crown Width	4.41		2.29	1.91		3.28	1.41	0.83		1.02	2.12				3.79		
	>= 0.13 m Count	4					129	1										
	DBH (m)	0.25					0.48	0.16										
	< 0.13 m Count	20		19	148		529	375	1		7	3				1		
	AGL (m)	0.06		0.04	0.04		0.05	0.03	0.02		0.03	0.03				0.08		
	Study Count	371	8	76	247	1	5245	876	6	6	10	3	9	9	2	8	20	49

Appendix A-1. Tree species statistics by plot (continued).

Plot	Plot Statistics	RE	VM	O	Plot Total	Conifer Total	Broadleaf Total
U13	Total Count			1	498	462	36
	Height			7.28			
	Crown Width			5.15			
	>= 0.13 m Count						
	DBH (m)						
	< 0.13 m Count			1			
	AGL (m)			0.15			
U56	Total Count	6	7	5	1255	1035	220
	Height	4.94	3.76	4.05			
	Crown Width	2.65	2.00	1.75			
	>= 0.13 m Count						
	DBH (m)						
	< 0.13 m Count	6	7	5			
	AGL (m)	0.04	0.04	0.03			
	Study Count	6	10	18	6980	6198	782

Species Abbreviation

BM - Bigleaf Maple (*Acer macrophyllum)*
CH- California Hazel (*Corylus cornuta*)
CB - cascara Buckthorn (*Rhamnus purshiana*)
CP - cherry (*Prunus spp.*)
CW - black cottonwood (*Populus trichocarpa*)
DF - Douglas-Fir (*Pseudotsuga menziesii*)
GF - grand fir (*Abies grandis*)
HT - hawthorne (*Crataegus spp.*)
HY - holly (*Ilex spp.)*
MA - madrone (*Arbutus spp.*)
OS - oceanspray (*Holodiscus discolor*)
OW - Oregon white oak (*Quercus garryana*)
OG - Oregon grape (*Berberis aquifolium*)
PD - Pacific dogwood (*Cornus nuttalii*)
SF - Pacific silver fir (*Abies amabilis*)
PY - Pacific yew (*Taxus brevifolia*)
PP - ponderosa pine (*Pinus ponderosa*)
RE - red elderberry (*Sambucus racemosa*)
VM - vine maple (*Acer circinatum*)
O - other

Appendix A-2. Shrub species statistics by plot.

Plot	Statistic	BM	CB	CH	CP	DF	HY	MA	MM	OS	OG	OW	PD	RE	SW	SB	VM	O	Total
C20	Count	4		4															8
	Mean Height	3.27		3.65															
	Mean Crown	4.75		3.50															
C27	Count	12																3	15
	Mean Height	3.42																2.38	
	Mean Crown	3.12																2.6	
C61	Count	0																	0
	Mean Height																		
	Mean Crown																		
C110	Count	49				1			1		63				2	1		1	118
	Mean Height	3.38				2.07			2.52		2.13				1.91	3.05		2.57	
	Mean Crown	2.61				2.13			2.27		1.65				2.64	2.08		2.4	
E200	Count	13		23	8		8										2	2	56
	Mean Height	3.54		5.26	5.67		3.31										6.38	5.4	
	Mean Crown	2.99		3.27	4.12		3.42										3.96	2.97	
E412	Count	8		32						9		4					4		57
	Mean Height	3.19		3.81						3.00		2.10					2.80		
	Mean Crown	2.34		3.89						3.93		1.85					3.00		

Appendix A-2. Shrub species statistics by plot (continued).

Plot	Statistic	BM	CB	CH	CP	DF	HY	MA	MM	OS	OG	OW	PD	RE	SW	SB	VM	O	Total
O16	Count	8		126	6														140
	Mean Height	4.29		4.93	5.88														
	Mean Crown	4.93		5.7	5.54														
O69	Count	4								33			6					2	45
	Mean Height	5.38								3.41			3.41					2.8	
	Mean Crown	5.15								4.07			6.73					3.65	
U8	Count	4		134				1		3							6	5	153
	Mean Height	3.31		4.02				2.50		3.83							4.05	3.44	
	Mean Crown	4.68		4.94				1.35		3.73							8.35	5.91	
U13	Count	6		40							1								47
	Mean Height	3.81		3.82							3.6								
	Mean Crown	3.25		3.85							2.58								
U56	Count	2	2	22	3		1			28		1		12				1	72
	Mean Height	4.47	2.79	2.88	3.4		1.2			3.38		3.73		4.07				3.92	
	Mean Crown	2.81	1.44	3.19	2.05		1.34			2.49		2.33		2.46				2.16	
	Total Species	110	2	381	17	1	9	1	1	73	64	5	6	12	2	1	12	14	711

Species abbreviations

BM - Bigleaf Maple (*Acer macrophyllum)*
CB - cascara Buckthorn (*Rhamnus purshiana*)
CH- California Hazel (*Corylus cornuta*)
CP - cherry (*Prunus spp.*)
DF - Douglas-Fir (*Pseudotsuga menziesii*)
HY - holly (*Ilex spp.)*
MA - madrone (*Arbutus spp.*)
MM - mountain mahogany (*Cercocarpus*)
OS - oceanspray (*Holodiscus discolor*)
OW - Oregon white oak (*Quercus garryana*)
OG - Oregon grape (*Berberis aquifolium*)
PD - Pacific dogwood (*Cornus nuttalii*)
RE - red elderberry (*Sambucus racemosa*)
SB - snowberry (*Symphoricarpos albus*)
SW – Scouler's willow (*Salix scouleriana*)
VM – vine maple (*Acer circinatum*)
O – other